Long range energy efficient wireless sensor system

Purković, Dalibor

Doctoral thesis / Disertacija

2019

Degree Grantor / Ustanova koja je dodijelila akademski / stručni stupanj: **University of Zagreb, Faculty of Electrical Engineering and Computing / Sveučilište u Zagrebu, Fakultet elektrotehnike i računarstva**

Permanent link / Trajna poveznica: https://urn.nsk.hr/urn:nbn:hr:168:569556

Rights / Prava: In copyright/Zaštićeno autorskim pravom.

Download date / Datum preuzimanja: **2024-07-20**

University of Zagreb

FACULTY OF ELECTRICAL ENGINEERING AND COMPUTING

Dalibor Purković

LONG RANGE ENERGY EFFICIENT WIRELESS SENSOR SYSTEM

DOCTORAL THESIS

Zagreb, 2019

University of Zagreb

FACULTY OF ELECTRICAL ENGINEERING AND COMPUTING

Dalibor Purković

LONG RANGE ENERGY EFFICIENT WIRELESS SENSOR SYSTEM

DOCTORAL THESIS

Supervisor:
Professor Zvonimir Šipuš, Ph.D.

Zagreb, 2019

Sveučilište u Zagrebu

FAKULTET ELEKTROTEHNIKE I RAČUNARSTVA

Dalibor Purković

ENERGETSKI UČINKOVIT BEŽIČNI SENZORSKI SUSTAV VELIKOGA DOMETA

DOKTORSKI RAD

Mentor:
Prof. dr. sc. Zvonimir Šipuš

Zagreb, 2019.

This Doctoral thesis is made at the University of Zagreb, Faculty of electrical engineering and computing, Department of Wireless Communications and at EnOcean GmbH.

Supervisor: Professor Zvonimir Šipuš, Ph.D.

This doctoral thesis has: 177 pages

Doctoral Thesis No.:_____

ABOUT THE SUPERVISOR

Zvonimir Šipuš was born in Zagreb, Croatia, in 1964. He received both the B.Sc. and M.Sc. degrees in electrical engineering from the University of Zagreb, Croatia, in 1988 and 1991, respectively. He then gained his Ph.D. degree in electrical engineering from Chalmers University of Technology, Gothenburg, Sweden, in 1997.

From 1988 to 1993, he worked at Ruđer Bošković Institute, Zagreb, Croatia, as a research assistant, involved in the development of detectors for explosive gases. In 1994, he joined the Antenna Group at Chalmers University of Technology, where he was involved in research projects concerning conformal antennas and soft and hard surfaces. In 1997, he joined the Faculty of Electrical Engineering and Computing at the University of Zagreb, where he is currently a professor. From 1999 to 2005, he was also an adjunct researcher in the Department of Electromagnetics, at Chalmers University of Technology. Since 2006, he has been engaged in teaching in the European Doctoral School of Antennas (ESoA). His current research interests include analysis and design of electromagnetic structures with application to antennas, microwaves, and optical communication and sensor systems. He is the author or co-author of more than 60 papers published in scientific journals.

Professor Šipuš received the annual national science award in 2006 for his research in conformal antennas and periodic structures.

O MENTORU

Zvonimir Šipuš rođen je 12. ožujka 1964. godine u Zagrebu. Diplomirao je i magistrirao na Elektrotehničkom fakultetu u Zagrebu 1988. godine, odnosno 1991. godine, a doktorirao je 1997. godine na Chalmers University of Technology u Göteborgu u Švedskoj.

Od prosinca 1988. godine do srpnja 1993. godine radio je na Institutu Ruđer Bošković u Zagrebu u laboratoriju za poluvodiče. Sudjelovao je u razvoju uređaja za mjerenje koncentracije eksplozivnih plinova zasnovanih na poluvodičkim senzorima. Od kolovoza 1993. godine radi na Zavodu za radiokomunikacije na Fakultetu elektrotehnike i računarstva u u Zagrebu, gdje je i danas prisutan u svojstvu redovitog profesora. Od rujna 1994. godine do listopada 1997. godine bio je na znanstvenom usavršavanju na Department of Microwave Technology, Chalmers University of Technology u Göteborgu u Švedskoj, gdje je bio doktorski student. Na istom je sveučilištu na jesen 1999. godine izabran u zvanje gostujući

istraživač (Adjunct Researcher) i tu je aktivnost obavljao do 2005. godine. Od 2006. godine predaje i u Europskoj doktorskoj školi antena (European School of Antennas).

Znanstvenoistraživačka djelatnost Zvonimira Šipuša vezana je uz analizu mikrovalnih antena i antenskih nizova, uz numeričke metode u elektromagnetizmu te uz svjetlovodne komunikacijske i senzorske sustave. Autor je ili koautor više od 60 znanstvenih radova objavljenih u znanstvenim časopisima.

Zvonimir Šipuš dobitnik je državne godišnje nagrade za znanost za 2006. godinu, za istraživanja konformnih antenskih i periodičnih struktura.

ACKNOWLEDGEMENTS

ZAHVALA

Želio bih zahvaliti firmi EnOcean GmbH na svoj podršci pri izradi ove doktorske disertacije. Veliko hvala mojim EnOcean kolegama, a posebno svima onima koji su bili uključeni u „Orca" projekt.

Posvećujem ovu doktorsku disertaciju svojim roditeljima: majci Mari i ocu Bori. Iako smo često bili razdvojeni, uvijek sam znao da mogu računati i osloniti se na vas, te da ste tu za mene. Svi imamo taj jedan život, a vi ste svoje živote nesebično odlučili posvetiti mojoj svjetlijoj budućnosti, žrtvujući se pri tome i naporno radeći iz dana u dan. Da su vas vaši roditelji podupirali na način na koji ste vi to činili za mene, ne sumnjam da biste danas oboje imali doktorske titule. U mojim očima vi ih već imate.

Mama Maro, ti si je zaslužila kao najbrižnija i najsrdačnija osoba koju poznajem. Unatoč svemu što si prošla u životu, zbog svog neslomljivog duha ostala si uvijek pozitivna i optimistična. To je i mene definiralo kao osobu i usadilo način kako trebam pristupati životu. Hvala ti na tome, i hvala ti na svim tvojim postovima i molitvama za mene.

Tata Boro, ti si je zaslužio jer si preživio rat, kako bih ja mogao imati oca u životu. Kao i mamu, život te također odveo u inozemstvo i u nepoznato. Ali opet, ti si bio neustrašiv, radio si naporno razne teške poslove kako bi nas zbrinuo. Pri tome si uvijek nesebično davao sve od sebe i u najboljem interesu za našu obitelj.

Na kraju veliko hvala i mojoj starijoj sestri Valentini. Kad je trebalo, bila si mi oboje, i majka i otac. Tvoja briga za mene i savjeti koje si mi davala imali su uvijek pozitivan učinak na moj život i zadržali su me na pravom putu.

Bog nas sve blagoslovio!

ABSTRACT

Energy consumption has become one of the main parameters in evaluating sensor systems in the IoT market. The long range sensor systems which are discussed in this dissertation are not an exception. Their application in the outdoor environment makes them an ideal candidate for combining energy harvesting mechanisms with low power features. As it is discovered, using just the low power electric components is not enough to ensure energy efficiency. Techniques and mechanisms for harvesting and saving energy had to be investigated and developed in order to successfully realize an energy efficient sensor system. The approach used was to build an entire sensor system from scratch, with careful selection of the main hardware components, and a deeper analysis of their behaviour and energy consumption for different temperatures, humidity and supply voltages. The concept of having one developed Printed Circuit Board (PCB), which is used in both the transmitter and receiver side, resulted in the development of two different modules which share same hardware components. Based on the required application, these modules can be assembled as either a *Sensor module* or a *Data logger module*.

Furthermore, a unique, low power, energy efficient communication protocol is developed and described. A communication protocol optimizes the way the information is collected from the environment, packed and transmitted over long distances with minimum needed energy. It is designed specifically for energy constrained sensor modules which rely on energy harvesting. Gathered information is transmitted in a form of two different packet types called *Teach-in* and *Data telegrams*, respectively. A detailed structure of these packets and the energy required for transmission is explained together with a deeper analysis of the protocol's physical layer (PHY). In addition, big potential of the developed sensor system for mass market is demonstrated, as a result of the many proposed solutions that have been tested and implemented in fully developed functioning prototypes already running in different field installations.

Keywords: *sensor module, data logger module, low power, long range, wireless communication, energy harvesting, supercapacitor, teach-in telegram, data telegram, unidirectional communication, bidirectional communication, communication protocol, LPWAN.*

Energetski učinkovit bežični senzorski sustav velikoga dometa

Uvod

Potrošnja energije jedan je od osnovnih evaluacijskih parametara senzorskih sustava u svijetu Interneta stvari (engl. IoT). Senzorski sustavi velikoga dometa analizirani u ovoj disertaciji nisu iznimka. Njihova primjena u vanjskim uvjetima u okolišu te niska potrošnja čini ih idealnim kandidatima za integraciju mehanizama prikupljanja energije iz okoliša (engl. energy harvesting).

Ustanovljeno je da samo korištenje elektroničkih komponenata niske potrošnje neće rezultirati senzorskim sustavom koji je potpuno energetski učinkovit. Stoga je bilo potrebno istražiti i razviti dodatne tehnike i mehanizme za učinkovito prikupljanje energije iz okoliša te njezinu pohranu u samom senzorskom sustavu. Kako bi se to omogućilo, čitav senzorski sustav je razvijen od „nule", s pomno biranim hardverskim komponentama i dubljom analizom ponašanja tih komponenti. Pri tome je prvenstveno analizirana potrošnja energije izabranih komponenata u uvjetima različite temperature, relativne vlažnosti zraka te napona napajanja.

Koncept jednog dizajna tiskane pločice (engl. PCB) koja se koristi za realizaciju predajnika, ali i prijemnika, rezultirao je razvojem dvaju različitih modula koji dijele iste hardverske komponente. Ovisno o primjeni i montiranim komponentama, ovi moduli mogu biti sastavljeni kao *Senzorski modul (engl. Sensor module)* ili *Modul za pohranu podataka (engl. Data logger module)*.

Dodatno je razvijen i predstavljen jedinstven, energetski učinkovit komunikacijski protokol. Ovaj protokol optimizira način na koji je mjerena veličina prikupljena iz okoliša zapakirana u podatkovni paket i poslana preko velikih udaljenosti s minimalnom potrošenom energijom. Razvijeni protokol prvenstveno je namijenjen senzorskim sustavima s ograničenom pohranjenom energijom koji se pri svom radu oslanjaju na prikupljanje energije iz okoliša. Procesirana mjerena veličina šalje se u obliku dviju vrsta podatkovnih paketa nazvanih *Teach-in* i *Data* telegrami. Također, dana je detaljna struktura ovih podatkovnih paketa te je određena minimalna energija potrebna za njihovo slanje bežičnim putem. Provedena je i dublja analiza fizičkog sloja razvijenog komunikacijskog protokola te su definirani temeljni parametri bežičnog prijenosa informacija kao što su vrsta modulacije prijenosnog signala, brzina prijenosa podataka, snaga odašiljanja i sl.

Također je demonstriran i veliki tržišni potencijal razvijenog senzorskog sustava, što je rezultat mnogih provedenih testiranja na prototipovima instaliranim u realnim, vanjskim radnim uvjetima. Iako prvenstveno namijenjen za primjenu u poljoprivredi, razvijeni senzorski sustav uspješno je testiran i u području pametnih gradova (engl. Smart cities), i to u državama kao što su Njemačka i Japan. Područja primjene, dakle, variraju od nadzora parametara zraka i tla pri uzgoju poljoprivrednih kultura u staklenicima i na otvorenim poljima, do nadzora razine vodostaja rijeka ili zauzeća parkirnih mjesta u gradovima.

Pregled poglavlja

Ova doktorska disertacija, osim ovog proširenog sažetka, sadrži još i sažetak na engleskom jeziku, pet temeljnih poglavlja, zaključak s opisom budućeg rada, reference te životopis doktoranda na engleskom i hrvatskom jeziku. Pet temeljnih poglavlja redoslijedom kako su napisana donose sljedeće:

Poglavlje 1 „Uvod" (engl. „Introduction") započinje s pregledom postojećih senzorskih rješenja u domeni sustava male potrošnje energije razvijenih u posljednjih 15 godina. Pregled uključuje analizu prototipova razvijenih unutar akademske zajednice, ali i analizu komercijalnih rješenja dostupnih na tržištu poput LoRa i Sigfox tehnologije. Pažljivo su analizirana ograničenja postojećih rješenja, utvrđena su moguća poboljšanja, a rezultati analize korišteni su kao smjernica tijekom razvoja vlastitog senzorskog sustava na kojemu je i zasnovana ova doktorska disertacija. U ovom poglavlju utvrđene su smjernice kako bi trebao izgledati novorazvijeni senzorski sustav. Tvorit će ga jedinstvena hardverska platforma, koja će se ovisno o sastavljenim komponentama i programiranom softveru ponašati kao senzorski modul, odnosno kao modul za pohranu podataka (prijemnik). Definirano je kako će se za spremnik energije umjesto baterije koristiti superkondenzator, punjen solarnom energijom pomoću male, kompaktne solarne ćelije integrirane unutar samog kućišta senzorskog modula. Utvrđeno je i kako je potrebno pristupiti razvoju vlastitog komunikacijskog protokola, a sve u svrhu optimizacije potrošnje energije senzorskog sustava prilikom prikupljanja i procesiranja informacije iz okoliša, te njezinog slanja bežičnim putem. Neki od temeljnih parametara pri analizi učinkovitosti senzorskih modula za primjenu u mrežama male snage i široke pokrivenosti (engl. LPWAN - Low Power Wide Area Networks) su:

- potrošnja energije senzorskog modula u stanju spavanja (engl. Sleep mode)
- potrošnja energije prilikom odašiljanja podataka (engl. Tx mode)

- potrošnja energije prilikom prijema podataka (engl. Rx mode)
- osjetljivost prijemnika
- ostvareni domet pri prijenosu podataka

Ovih pet parametara provlače se kroz sva poglavlja disertacije i osnovno su mjerilo pri usporedbi realiziranog senzorskog sustava s postojećim rješenjima.

Poglavlje 2 „Arhitektura senzorskog sustava" (engl. „Sensor system architecture") započinje s hardverskim blok dijagramom senzorskog modula. U potpoglavljima koji slijede opisane su sve glavne hardverske komponente koje se nalaze u blok-dijagramu. Detaljno je opisano realizirano sklopovlje za zaštitu superkondenzatora od prenapona i prepražnjenja. Dan je izvorni shematski prikaz sklopovlja s jasno naznačenim tipovima upotrijebljenih elektroničkih komponenti. Prikazan je tok električne struje od solarne ćelije, preko superkondenzatora prema mikrokontroleru i ostalom sklopovlju. S obzirom da je senzorski sustav predviđen za rad u vanjskom okolišu, analizirana je potrošnja energije pojedinih komponenata pri različitim temperaturama. Posebno potpoglavlje posvećeno je analizi superkondenzatora kao spremnika energije te su navedene sve njegove prednosti i nedostaci u usporedbi s različitim vrstama baterija kao spremnika energije. Kao sastavni dio 2. poglavlja analizirane su i ostale temeljne komponente senzorskog sustava kao što su primijenjeni mikrokontroler, radio čip, dodatni memorijski čip te temperaturno-kompenzirani kristal kvarca. Nakon opisa sučelja senzorskog modula prikazana je arhitektura modula za pohranu podataka (ujedno i prijemnika) i objašnjene su najbitnije razlike između ovih dviju hardverskih platformi. Tako je vidljivo da je modul za pohranu podataka, iako temeljen na istoj tiskanoj pločici kao i senzorski modul, realiziran s gotovo 50% manje elektroničkih komponenti. Pri kraju poglavlja prikazan je i pregled testiranih vanjskih antena korištenih pri realizaciji senzorskog sustava.

Poglavlje 3 „Protokol za energetski učinkovitu komunikaciju" (engl. „Energy efficient communication protocol") sadrži detaljan opis razvijenog komunikacijskog protokola. Opis započinje s definicijom parametara fizičkog sloja koji su izabrani na temelju mnogih provedenih testova, a koji će pozicionirati senzorski sustav u domenu niske potrošnje i dalekometnog prijenosa informacije. Naglasak je stavljen na analizu osjetljivosti prijemnika kao temeljnog parametra pri postizanju dalekometnosti. Poglavlje, nadalje, sadrži opis podržanih načina komunikacije, a to su jednosmjerna i dvosmjerna komunikacija te njihov utjecaj na utrošak energije senzorskog modula. Analizirane su prednosti i nedostaci svakog

načina rada, grafički su prikazani odnosi u potrošnji energije jednog, odnosno drugog načina rada. Definirano je i maksimalno operativno vrijeme senzorskog modula u slučaju ne-mogućnosti žetve energije iz okoliša. Nakon toga detaljno je opisana struktura podatkovnih paketa (telegrama) te su prikazani primjeri kodiranja same informacije sadržane u pojedinim telegramima. Objašnjeni su i dodatni integrirani mehanizmi u sklopu samog komunikacijskog protokola kao što su; detekcija okupiranosti radio kanala (engl. Clear channel assessment), ulančavanje telegrama (engl. Radio telegram chaining) te prosljeđivanje već primljenih telegrama (engl. Radio telegram repeating).

Poglavlje 4 „Operativni dijagram toka i algoritam upravljanja potrošnjom energije" (engl. „Operation flowchart and energy usage control algorithm") analizira programiranu hardversku platformu i energetsku učinkovitost komunikacijskog protokola. Dijagram toka i algoritam za upravljanje prikazani su kroz izvođenje jednog potpunog ciklusa „buđenja" senzorskog sustava. Prikazana je potrošnja energije svakog radnog stanja dobivena prvotno procjenama, a potom i mjerenjima. Mnoštvo oscilograma snimljenih izravno sa zaslona osciloskopa jasno prikazuje dinamički raspon u potrošnji energije i pripadajuću električnu struju koja se crpi iz superkondenzatora. Posebno izazovno bilo je mjerenje električne struje koja varira ovisno o radnom stanju te se kreće u rasponu od manje od jednog mikroampera do stotinu miliampera (promjena reda veličine 100 000 puta).

Poglavlje 5 „Eksperimentalni rezultati" (engl. „Experimental results") donosi eksperimentalne rezultate prikupljene pri rada razvijenog senzorskog sustava u različitim ispitnim okolinama u Njemačkoj i Japanu. Učinkovitost razvijenog senzorskog sustava verificirana je na temelju njegovih dalekometnih prijenosnih mogućnosti, potvrđene niske potrošnje energije i postignute energetske neovisnosti temeljene na principu sakupljanja energije iz okoliša (engl. Energy harvesting) pomoću male solarne ćelije. To su ujedno i tri temeljna testa pri verifikaciji funkcionalnosti senzorskog sustava. Jedno od potpoglavlja donosi i pregled palete razvijenih senzora, kompatibilnih sa senzorskim modulom. Pri tome su pojedini senzori posebno razvijani paralelno sa senzorskim modulom, dok su drugi već bili komercijalno dostupni, ali su također naknadno prilagođeni kako bi bili kompatibilni. Neki od predstavljenih senzora su: analogni senzor za mjerenje temperature i relativne vlažnosti zraka, analogni senzor za mjerenje temperature i vlažnosti tla, digitalni senzor osvijetljenosti plohe, ultrazvučni senzor i sl. Zbog mnoštva slika koje prikazuju razvijeni senzorski sustav instaliran u različitim okolinama i u različitim primjenama, poglavlje 5 istodobno služi i kao „grafički"

zaključak. Potvrda je to i praktičnosti i primjenjivosti ove doktorske disertacije jer su u ovom poglavlju demonstrirane sve mogućnosti razvijenog senzorskog sustava u stvarnom okruženju.

Poglavlje „Zaključak" (engl. „Conclusions") osim što predstavlja svojevrstan sažetak ukupnog rada, sumira i donesene zaključke i daje prijedloge za budući rad i eventualna poboljšanja samog senzorskog sustava. Neki od temeljnih postulata iskazanih u zaključku su da se odabrani superkondenzator pokazao kao vrlo kvalitetan i pouzdan spremnik energije koji jamči dugovječnost u radu senzorskog modula i njegovu konstantnu opskrbu energijom. Na pravi način korišteni mikrokontroler i radio čip, spretno integrirani na tiskanoj pločici uz iskorištavanje svih dostupnih niskoenergetskih karakteristika, omogućili su nisku potrošnju čitavog senzorskog sustava. Doda li se tome i jedinstveni, posebno za ovu svrhu razvijeni komunikacijski protokol s različitim podržanim komunikacijskim modovima, niska potrošnja i daleki domet razvijenog senzorskog sustava su zajamčeni.

Daljnja unapređenja senzorskog sustava temeljila bi se prvenstveno na proširenju palete kompatibilnih senzora čime bi se automatski proširilo i područje primjene samog senzorskog sustava. Težilo bi se generičkom senzorskom sučelju, koje bi sa senzorima komuniciralo putem digitalnih I^2C linija čime bi i svi budući senzori postali digitalni. To bi naravno uključivalo dodatan, jednostavniji mikrokontroler na strani senzora, koji bi funkcionirao kao posrednik između senzorskog modula i priključenog vanjskog senzora uz jasno definiranu listu naredbi u obliku generičkog senzorskog protokola namijenjenog upravo ovom sučelju.

Postignuća i znanstveni doprinosi

Istraživački rezultati ove doktorske disertacije uspješno su sažeti i objavljeni u renomiranom međunarodnom časopisu (*IEEE Sensors Journal*) indeksiranom u bazi Current Contents te u dva rada prezentirana na međunarodnim konferencijama. Na temelju provedenih istraživanja primjenjivosti superkondenzatora kao spremnika energije u senzorskim sustavima niske potrošnje, napisano je i objavljeno poglavlje u knjizi naslova „*Supercapacitors as Guarantors for Energy Sustainability in Low-Power Energy Harvesting Sensor Modules,*" (DOI: 10.5772/intechopen.88007).

Realizacijom ove disertacije postignuti su sljedeći originalni znanstveni doprinosi:

1. Energetski učinkovit komunikacijski protokol i njegova implementacija u bežičnim senzorskim sustavima.
2. Algoritam za upravljanje potrošnjom energije senzorskog modula zasnovanog na solarnoj ćeliji i superkondenzatoru.
3. Energetski neovisan bežični senzorski sustav velikoga dometa s implementiranim komunikacijskim protokolom i algoritmom za upravljanje potrošnjom energije.

Osim znanstvenih postignuća razvijeni senzorski sustav prepoznat je i od strane industrije. Razvijeni prototipovi pokazali su se uspješnim u radu na različitim terenskim instalacijama u Japanu. Razvijeni senzorski sustav prošao je sva potrebna certificiranja u ovlaštenom laboratoriju i ušao u fazu serijske proizvodnje te se trenutno distribuira na području Japana.

Ključne riječi: *senzorski modul, modul za pohranu podataka, niska potrošnja, veliki domet, bežična komunikacija, prikupljanje energije iz okoliša, superkondenzator, telegrami, jednosmjerna komunikacija, dvosmjerna komunikacija, komunikacijski protokol, LPWAN*

CONTENTS

1. INTRODUCTION

In the last decade, Low Power Wide Area Networks (LPWAN) have become a very popular research topic, and with every new research, new application fields are introduced [1], [2]. The majority of research currently available defines some basic parameters and requests on LPWAN: easy installation, low price, minimum maintenance, small surface of nodes in the network and low energy consumption [1], [2], [3]. Low energy consumption of each node in the LPWAN will allow long term operation and data collection from the environment without disruption. Current research aims to confirm the concept of low power sensor nodes equipped with batteries and their ability to communicate over some of the standardised protocols like IEEE-802.15.4, Bluetooth, ZigBee, LoRaWAN and adequate off the shelf receivers [1], [4], [5], [6]. Standardised protocols also require the use of standardised frequencies and thus the acceptance of the associated limitations [1], [7]. Limitations do not just stem from the standardised protocols but also from the inadequate hardware.

Developing actual low power systems require strong attention to detail; every hardware component must be carefully selected and any unnecessary loss of energy needs to be identified and eliminated. Any component which is not used at a certain stage of the system operation process should not consume any energy and in the ideal case should be completely disconnected from the power supply [8]. Energy storage and its control is the starting point when developing low power sensor system. Battery behaviour over a longer operation time is well known; with every charge cycle it will use a fraction less of its nominal capacity. Also, voltage will be stable until a certain point during operation and then it will drop without possibility to retrieve initial values [9], [10]. Due to these reasons, experiments have been conducted that use a supercapacitor as the main energy storage element instead of batteries [8], [10], [11]. The microcontroller and radio chip are the main energy consumers in the low power sensor system. Their type and the way have they are controlled determines characteristics of the entire sensor system and defines main limitations in every operating aspect. Surrounding these main building blocks, a communication protocol is then integrated. The specially developed energy efficient communication protocol described in this thesis is intended to be used in the upper part of the unlicensed sub-GHz frequency band. This is where the best signal propagation characteristics can be obtained [1], with optimal transmit power not exceeding 25 mW. Latest LPWAN solutions [1] rely on the use and integration of new, or the existing mobile base stations as a part of the network architecture, especially when

ensuring longer range and low power consumption of the end nodes [7]. This approach has limitations in isolated areas like, fields, farms, forests and areas where the mobile base stations coverage is poor. Moreover, building completely new network infrastructure required by solutions presented in [7] is extremely expensive. The solution presented in this thesis combats the aforementioned conditions; it offers end to end communication between the nodes, and easy deployment without the need for existing or new infrastructure in the form of mobile base stations, etc.

1.1.   *Overview of the existing sensor system solutions*

LPWAN is a current research topic, going along with the growth and popularity of the Internet of things (IoT). The main focus is on the core element behind each of these aspects; i.e. the sensor node. A sensor node as an independent unit, or part of a LPWAN that performs many tasks. It can harvest energy, give power to attached sensors, collect and process data from these sensors and transmit it through the air, while sustaining its own power management [8]. Application fields of the IoT world are constantly expanding and with it, researched sensor platforms. The focus of this thesis is on outdoor sensor modules, with energy harvesting capabilities and tendency for long range transmission. Therefore, the overview of sensor systems with similar capabilities is provided in this chapter.

An example of sensor platform that uses the microcontroller and radio chip from the same family as the sensor system described in this thesis, is the Trio sensor module [12]. The Trio combines three different printed circuit boards (PCBs). It uses an off-the-shelf Telos wireless sensor module, which utilises a MSP430F1611 microcontroller and a CC2420 radio chip, both from Texas Instruments [13]. There is also a separate circuit board module which contains sensors, and an additional module with the solar cell charging system for a small solar cell. These three different platforms are originally intended for different applications. Therefore, by combining these into one sensor module, energy efficiency will be lost throughout the process.

The authors of Trio confirmed this in their article by stating the following: "*Our testbed can be operated at 100% duty-cycle during only a few hours in the middle of day when direct sunlight is present. However, a duty-cycle ranging from 20% to 40%, depending on the time of year, allows continuous operation. This availability limitation stems from several factors: our own limited appreciation for subtleties of solar energy harvesting, the high power draw and lack of a low-power TinyOS MAC layer for the CC2420 radio, and several oversights in*

the design of the Prometheus solar energy harvesting system." [12].

The quoted statement was taken as a motivation in this thesis, to prove that energy harvesting is a suitable choice for the low power sensor modules. Although, the approach should include building the module from scratch, preferably on one PCB, with carefully selected components and with a dedicated communication protocol to run the whole sensor system.

As a part of the IoT, there are many different communication technologies used in a variety of sensors; Bluetooth, Bluetooth Low Energy (BLE), ZigBee, WiFi, LoRa, Sigfox… [1], [14], [15], [16]. Depending on the chosen communication technology, operating frequency bands vary from 2.4 GHz frequency band (BLE, ZigBee, WiFi) to sub-1 GHz band (Sigfox, LoRa) [7], [17]. It is known from the radio signal propagation characteristics [1], that transmitting on higher frequencies will decrease the achieved range. This is why a sub-1 GHz frequency band is always a better choice than a 2.4 GHz band in terms of the possible achieved range. The authors in [18] built a sensor module for measuring soil moisture and soil temperature and it is intended for scheduling irrigation of the crops. It uses an operating frequency of 2.4 GHz. During crop growth, transmission signal degradation occurs, and the achieved transmission range in the line-of-sight is only 800 meters [18]. To obtain an accurate comparison of the long range capabilities of the developed sensor module in this thesis, articles such as [2] or [19] are taken as the long range sensor system references. Sensor modules described in these articles use the sub-1 GHz frequency band and the communication technologies LoRa and Sigfox, which are already developed and present on the market, and intended for truly long range operation.

Authors in [2] and [5] give a good overview of the existing LPWAN technologies and introduce the main measuring parameters for quantifying LPWAN modules:

- power consumption in the sleep mode
- power consumption in the transmit (Tx) mode
- power consumption in the receive (Rx) mode
- receiver sensitivity
- achievable transmission range

Following these parameters, this thesis compares the developed sensor module with the commercial low power, long range modules based on the technologies like LoRa [6] and Sigfox [7], and other meaningful prototypes, like the Trio sensing platform [12].

Depending on the radio module and the communication technology used, the sensor module consumption will vary. The authors in [15] present a sensor module based on the WSN802G Wi-Fi radio module. The current consumption for this module in Tx mode reaches 200 mA and in Rx mode around 150 mA. Compared to the other LPWAN technologies mentioned above and overviewed in [5], this current consumption is around 5 and 10 times higher respectively. A sleep mode current of 7.5 µA is reported in [15], while authors in [18] measured a 150 µA current in sleep mode. It will be clear throughout this thesis that sleep current is one of the parameters which can be reduced to as low as 1 µA. Sleep current is a significant contributor to energy saving if the operation flowchart of the sensor module is designed properly. The reason for this is that the majority of the operating time (up to 99%) the sensor module spends in sleep mode [8], [20].

Last but not least, the majority of the referenced sensor modules in this introduction rely on batteries as the main power supply. Problems with batteries are well known [9], [11] and thus research is now directed towards finding energy storage alternatives to be used in low power sensor modules. A good alternative is supercapacitors. The advantages of the supercapacitors are also recognized by authors of [10]. Some of these include, very high rates of charge and discharge, little degradation of capacity over hundreds of thousands of cycles, low toxicity of materials used, high cycle efficiency (95% or more). Authors of [11] highlight the use of a supercapacitor instead of a battery to secure long term operation. This is described as the main advantage of their wireless sensor node. One of the disadvantages of supercapacitors, besides currently higher price, is that their energy density today is still less than in batteries by an order of magnitude [11]. Since a supercapacitor is usually used in conjunction with a suitable solar cell, this lower energy density drawback is overcome. In [9], the book entitled "Energy harvesting for Autonomous Systems", also outlines many advantages of supercapacitors, when used in an energy harvesting systems compared to the different types of batteries. A detailed comparison between these two technologies is given in the Chapter 2.1.2 of this thesis as well.

1.2. *Design of low-power sensor solutions: motivation and main focus*

A step further is made in today's ubiquitous Internet of Things (IoT) development by developing a battery free and energy independent sensor module. These modules can gather different environmental parameters and transfer them over longer distances. The main goal is to develop a robust outdoor monitoring system with compact dimensions whose application

varies depending on the attached external sensors: from agriculture, structural monitoring, air quality monitoring, parking spaces occupancy, etc. Since the sensor system is intended primarily for outdoor applications, the focus is set on solar energy harvesting. The exception is that the solar cell size needs to be compact enough to allow integration inside the sensor module's firmly closed housing. In addition, the housing must be sufficiently resistant to protect the PCB inside from any environmental influence. Harvested energy will be directly used to power the energy store which will not be a rechargeable battery but rather a supercapacitor. This is a component which can truly secure long life of the sensor module without the need for maintenance or energy storage replacement. The operation flow chart and the complete wake up cycle needs to be designed in a way that all the advantages and low power features of the microcontroller and radio chip are exploited. Different types of existing sensors should be easily adapted to the developed sensor module, thus allowing different applications.

Combining all these ideas with a proven RF (radio frequency) design makes it possible to counter what are normally two opposite requests: long range and low power consumption. Therefore, this thesis should also serve as the summarised guidelines for the development of low power sensor modules, obtained through theory and many experimental results.

The solutions provided in this thesis allow the scientific community to overcome the current limitations which many research papers address when discussing low power sensor systems. These limitation include inadequate communication protocol, none optimized energy consumption and limited operation time, use of batteries, etc.

At the same time development is also market oriented, and how it compares with the similar low power, long range solutions already on the market. This is why different radio norms, and the performance and design limitations they introduce are considered.

1.2.1. Unique hardware platform

Adopting on the market currently available and finished modules, and attempting to combine them into one system, will never result in optimal performance, or give a truly low power system. Therefore, the developed sensor system described in this thesis is built from scratch. The hardware platform is unique as there is only one PCB (Printed Circuit Board) developed, which can be used as a sensor module as well as the data logger module (receiver). For which module the PCB will be used, depends on the parts assembled and the programmed firmware. If the PCB is used as a sensor module, 113 components need to be assembled on

the PCB. However when it is used as a data logger module, only 55 components need to be assembled (49%). The main electronic components (microcontroller, radio chip, crystals, flash memory, voltage limiters and supercapacitor) were carefully selected from many available. Then a completely new protocol was developed around this cluster of components. This allows optimal operation of the sensor system regarding energy consumption, and at the same time allowing long range transmissions.

The following main components are the integral parts of the developed sensor module:

- *Microcontroller – Texas Instruments MSP430FR5949* [21]

- *Radio chip – Texas Instruments CC1120* [22]

- *Flash memory – Adesto AT45DB321E* [23]

- *Step-up converter – Texas Instruments TLV61220* [24]

- *Quartz crystal – 32.767 kHz Seiko SSP- T7-F* [25]

- *Voltage detectors – Ablic S-1009 Series* [26]

- *Supercapacitor – Taiyo Yuden LIC1235RS3R8406 (40 Farad)* [27]

A detailed description of the developed hardware platform is provided in the Chapter 2.

1.2.2. Energy harvesting as a must have

Energy harvesting systems operate by transforming environmental energy (light, heat, mechanical movement…) into useful electrical charge and therefor into electrical energy. The smaller the scale of the energy harvester the smaller the amount of harvested electrical charge and useful electrical energy. This supports the concept that the energy balance should be preserved [9], [28]. This implies that the initial available energy plus the energy harvested during operation time should always be greater than or equal to the consumed energy. With the primary intention of the sensor system to be for outdoor monitoring, the solar cell poses as a logical energy harvester. The developed sensor module uses a small solar cell (dimensions only 74.5 mm x 48.0 mm) to continuously harvest energy from incident light. This energy is then stored in the supercapacitor and used to power the microcontroller, the radio chip and attached sensors, for data processing and data transmission over long distances (3 km and more). A small solar cell also lowers the cost of the sensor module as well as allowing an easier and cheaper installation. The chosen dimensions allow solar cell integration inside a compact housing and tests show that full recharge of the sensor module is ensured within 1 hour in normal bright day conditions (around 70 000 lux). Even in low light conditions or an

indoor environment with 1 000 lux allows wake up of the sensor system and slow continuous recharge.

The selected solar cell is made from amorphous silicon (ASI3O-04 from Budasol) and it has a V_{OC} (*Open Circuit Voltage*) of up to 6.4 V, V_{MPP} (*Maximum Power Point Voltage*) = 4.8 V, I_{MPP} (*Maximum Power Point Current*) = 31 mA, and I_{SC} (*Short Circuit Current*) = 41 mA. All the values shown are obtained under standard test conditions (STC). STC is an industry-wide standard to indicate the performance of a solar cell and specifies that the measurements are done at a cell temperature of 25°C and an irradiance of 1000 W/m^2 with an air mass 1.5 (AM1.5) spectrum [29]. Since the V_{MPP} of the selected solar cell is 4.8 V, an additional circuitry is required between the solar cell and supercapacitor to prevent overcharge of the supercapacitor and ensure that its voltage does not exceed the defined maximum 3.8 V. To further characterise the selected solar cell behaviour, an experiment with 300 solar cells of the same type was conducted. These solar cells were illuminated with a very low light intensity of only 1000 lux. A voltage generator (with 3.6 V output) which can sink current was used as the load. The maximum charge current observed in the experiment at 1000 lux was 0.3 mA. This current is sufficient to charge the supercapacitor e.g. from 2.3 V to 2.5 V within 1 hour. The 2.5 V is set as the minimum defined voltage needed to operate the sensor module. This value is based on the supercapacitor's minimum operating voltage of 2.2 V and the electrical characteristics of the undevoltage protection circuitry (Chapter 2.1.1.4).

Since the solar cell is the main harvesting mechanism, the sensor module needs to be able to operate during periods of low light or complete darkness. The minimum requirement is to withstand at least a 15 hour overnight period and maintain continuous normal operation during the night. Sensor systems with some typical non-rechargeable batteries have an overall minimum operation time of minimum two years and the dark time operation as a parameter is in this case irrelevant [5], [20]. By using the supercapacitor with daily discharge and recharge cycles, the dark time operation is an important parameter. The developed sensor module can reach up to 30 days of dark time operation depending on the wake up interval, attached sensors type and communication mode selected. Some attached sensors are more energy consuming than the others, with the peak currents varying from 1 mA to 100 mA. The sensor measurements are performed very fast, with the tested sensors active operation time varies from 100 ms to 600 ms. This contribution of the sensor measurement time to the overall energy consumption is still quite low at around 3%. With some sensors, developed especially

for the sensor module, such as the digital illuminance sensor, this percentage even drops to 1%.

The main influence on dark time operation, besides radio transmission, is the sensor module's wake up interval, together with the energy consumption in the deep sleep mode. The lowest supported wake up interval is 2 minute ± 30 seconds while standard default value is 15 minutes ± 30 seconds.

In Chapter 5 results from different outdoor field tests are given. These prove that the solar energy harvesting with a compact solar cell, without any issues maintains 100% of the supply energy of the sensor module, observed through a 1 year period.

1.2.3. Custom-made communication protocol

Using solely low power electric components is not enough to ensure energy efficiency. Special techniques and mechanisms for harvesting and saving energy must be introduced. The microcontroller initialisation, peripherals handling, control of external sensors, and data transmission over the air, are all actions that require strictly defined behaviour. Therefore, specially for this sensor system, unique communication protocol and its supporting algorithm have been developed. Since the hardware platform is in its essence, designed as low power, the supporting communication protocol needs to also be energy efficient. The described protocol in this thesis optimises the way in which information is collected from the environment, packed and transmitted over longer distances using minimum consumed energy (around 90 mWs). It is specially designed for energy constrained sensor modules which rely on energy harvesting. The gathered information is transmitted in a form of two different packet types called *Teach-in* and *Data* telegrams, respectively. A detailed structure of these packets is described in Chapter 3.4 of this thesis. Keeping energy efficiency in mind two different communication modes are developed, *Unidirectional* and *Bidirectional*. This option allows up to 30% energy saving depending on the application of a sensor module. The developed protocol should not only be observed through the packet format and physical layer, but also through its communication modes, and processing of data collected from the attached sensor. In addition, through the concept of teach-in and data telegrams, repeater functionality, integrated additional features, and examples of data coding and integrated status and error codes.

1.3.   Structure of the thesis

This thesis is organised in 5 main chapters. Since the essential idea was to physically develop a sensor system, chapters are organised in a way which reflects typical product development.

INTRODUCTION provides an overview of some of the existing sensor system solutions in the low power domain, developed within last 15 years. Research includes developed prototypes analysis, as well as commercial market solutions. Limitations of the existing solutions and the possible improvements are carefully analysed and used as motivation during the development. Outcomes of the research phase practically defined the appearance of the developed sensor system in this thesis. It was clear that the unique sensor platform had to be built from scratch. Ideally, this would consists of one PCB which can be used for the sensor module and as well as for the data logger module. The sensor module will be an energy harvesting device, powered by solar energy stored in the supercapacitor. The best way to achieve low power and long range operation is to utilise a custom communication protocol, which will also propel hardware design in this direction.

Chapter 2 displays the hardware block diagram of the sensor module. Within the subchapters, all the main hardware components used, relating to the block diagram, are described. Important tests carried out with individual components are described in the Chapter 2 as well. Following the description of the main sensor module interfaces, the architecture of the data logger module is shown and the main differences between the hardware platforms are explained. Concluding Chapter 2, the final PCB designs of the developed and assembled modules are shown.

Chapter 3 is the central part of this thesis and the most comprehensive chapter. It provides a detailed description of the developed communication protocol. It first defines the physical layer parameters, whose selection is supported by many tests performed. Following this, a description of supported communication modes is given. Their influence on the energy consumption of the sensor module, together with the analysed advantages and disadvantages of each mode is discussed. Subchapter 3.4 gives a detailed description of packet structure, together with the telegram coding approach. Examples of the telegrams sent when different types of sensors are connected to the sensor module are provided. Additionally implemented mechanisms such as telegram repeating, telegram chaining, status and error codes are also described in the Chapter 3.

Chapter 4 analyses the programmed hardware platform and the energy efficiency of the communication protocol. The operation flowchart and running algorithm are explained through the execution of one complete wake-up cycle. The energy consumption of each operation state, obtained through estimations and measurements, is given.

In Chapter 5, experimental results gathered from different field test sites in Germany and Japan are shown. The performance of the developed sensor system is verified, based on its long range transmission capabilities, power consumption and the achieved energy independency through the use of energy harvesting. A variety of outdoor applications based on the different types of connected sensors are verified and demonstrated in this chapter as well. Chapter 5 serves as a "graphical" conclusion and the highlight of this thesis. This is because, it demonstrates all the capabilities of the developed sensor system in the real outdoor environment. It also confirms the success of the initial hypothesis and the motivation set in the introduction of this thesis.

Finally, a summary of the work done, next steps, lessons learned and future improvements are presented in the CONCLUSIONS chapter.

2. SENSOR SYSTEM ARCHITECTURE

The sensor system architecture which is in the scope of this thesis is shown in Figure 2.1.
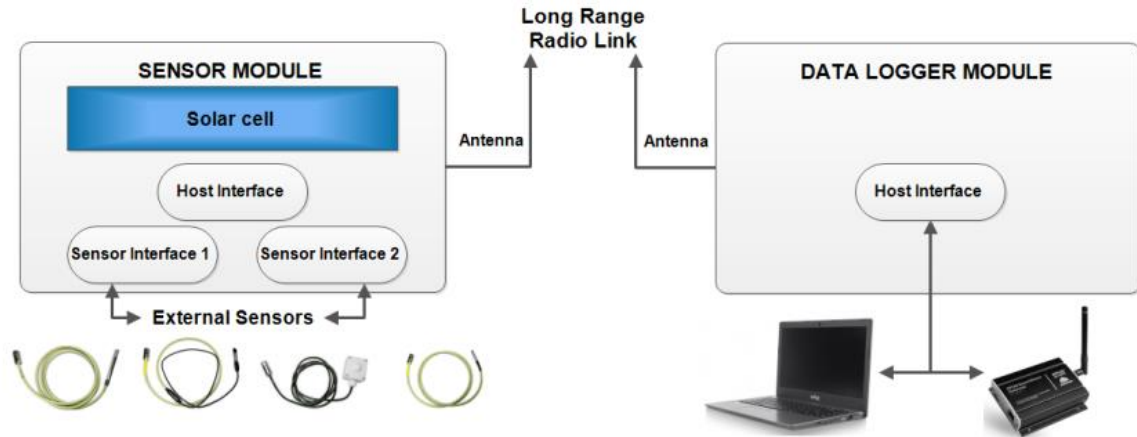

Figure 2.1. The sensor system architecture described in this thesis.

The key elements which form the depicted sensor system are the sensor module and the data logger module. A detailed description of these elements is provided in this chapter.

A variety of external sensors can be connected to the sensor module, some of which are specially developed to be included in this thesis. On the other side of the communication channel, data received by the data logger module can be visualised either on a computer or through the use of a gateway. This gateway further forwards the data to the cloud.

2.1. Sensor module hardware architecture

In Figure 2.2 the sensor module hardware block diagram is shown. The main hardware components and their interconnections can be seen, together with the predefined supply voltages and the quartz crystal frequency. Each of the components depicted in the block diagram is described in greater detail in the following subchapters.
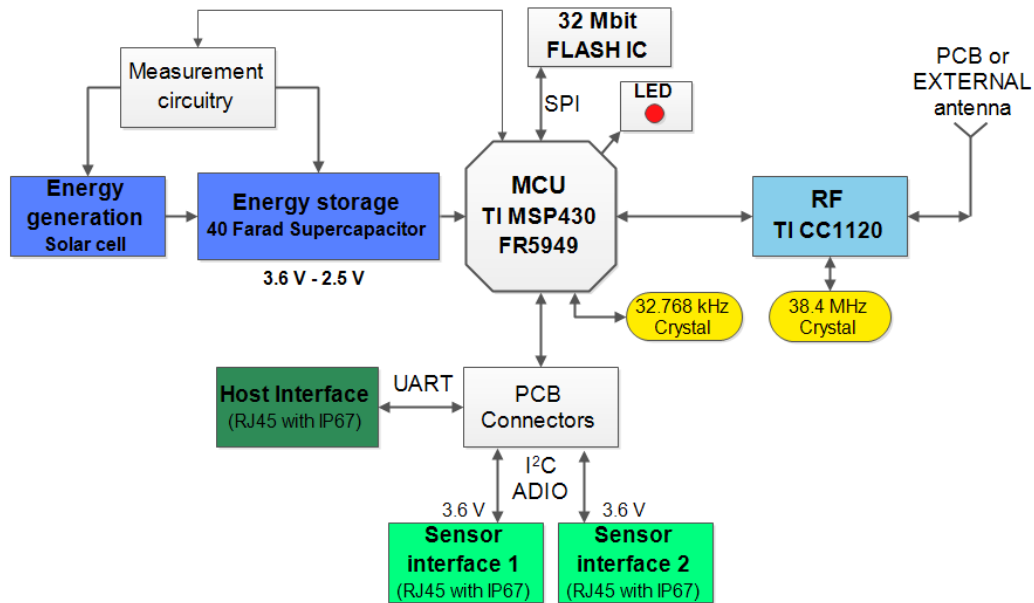
Figure 2.2. Block diagram of the sensor module.

2.1.1. Energy management circuitry

Starting from the left side in the above diagram, the energy management section is depicted. Energy harvested from the solar cell (with dimensions only 74.5 mm x 48.0 mm) is transferred directly to the supercapacitor (in our case 40 F). As it can be seen in the schematic in Figure 2.3 and Figure 2.4, only one diode D7 and the p-channel MOSFET (pMOS) transistor T1 (BSS84) are present on the electrical current path. The role of the transistor is to continuously disconnect the supercapacitor from the solar cell should the voltage begin to exceed 3.6 V. To detect the voltage of the supercapacitor and to control the switching pMOS T1, an Ablic S-1009 Series voltage level detector is used [26]. The same type of component is utilised as the supercapacitor discharge protection (Figure 2.5), only with a lower voltage threshold (2.3 V) and reversed operation as it is described in Chapter 2.1.1.4. Since both components use CMOS architecture, they consume very low values of current, around 300 nA [26]. This low consumption is especially important in the undervoltage protection circuitry since it will minimise energy loss due to the constant supercapacitor voltage monitoring as shown in Figure 2.5. In the overvoltage protection circuitry, energy consumed by the components is compensated with the charge current from the solar cell.
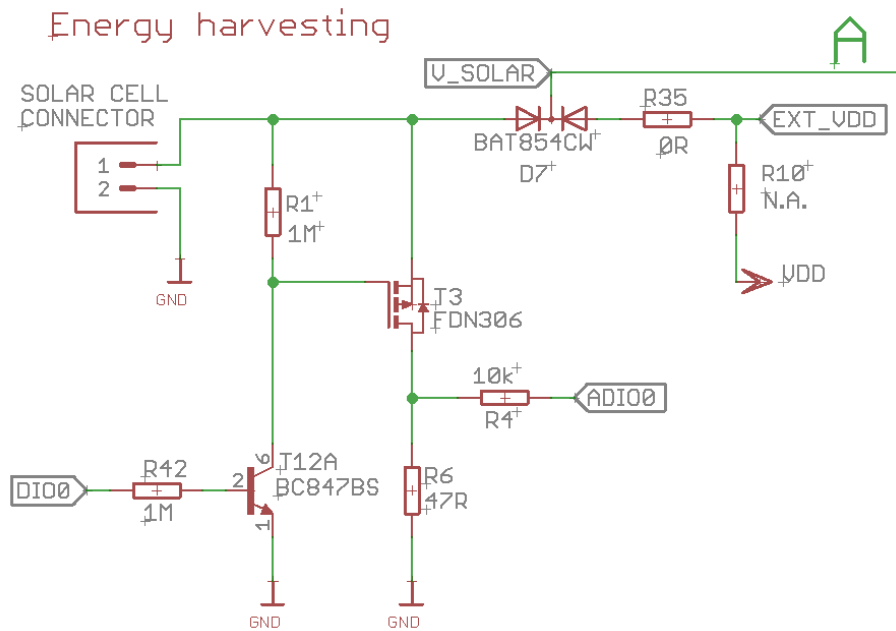
Figure 2.3. The solar cell connector together with the circuitry for charging current measurements, and an electrical path towards overvoltage protection and the supercapacitor (marked with A).

Additional circuitry, which can be seen in the figure above, is used for a solar cell charge current measurement. This is one of the parameters which is always transmitted as part of the standard data telegram (Chapter 3.4.2.1). To measure solar cell charge current, pin DIO0 set as digital output, is pulled high by the microcontroller (MCU). The electrical current from the solar cell flows through the transistor T3 and the resistor R6 and creates a voltage drop across the resistor. This voltage drop is measured by a 12-bit analog-to-digital converter (ADC) of the microcontroller. From this value, the solar cell charge current available in that moment is calculated. During measurement, the rest of the circuitry is disconnected again via the transistor T1, which is also controlled by the digital output pin DIO0 (Figure 2.4). This is done so all of the solar cell current passes through the resistor R6. The chosen value of R6 takes into the account the maximum possible solar cell current (short circuit current $I_{SC} = 41$ mA). Thus, limiting the maximum input voltage of the ADC to below 2.4 V. This is close to the sensor module's minimum operating voltage of 2.5 V. This circuitry could also be used to indirectly determine the approximate ambient illuminance. This could be done from knowing the solar cell incident light intensity characteristics and combining it with the measured electrical current. This could be observed in this case, as the approximate solar cell short circuit current is known at the given moment [30].
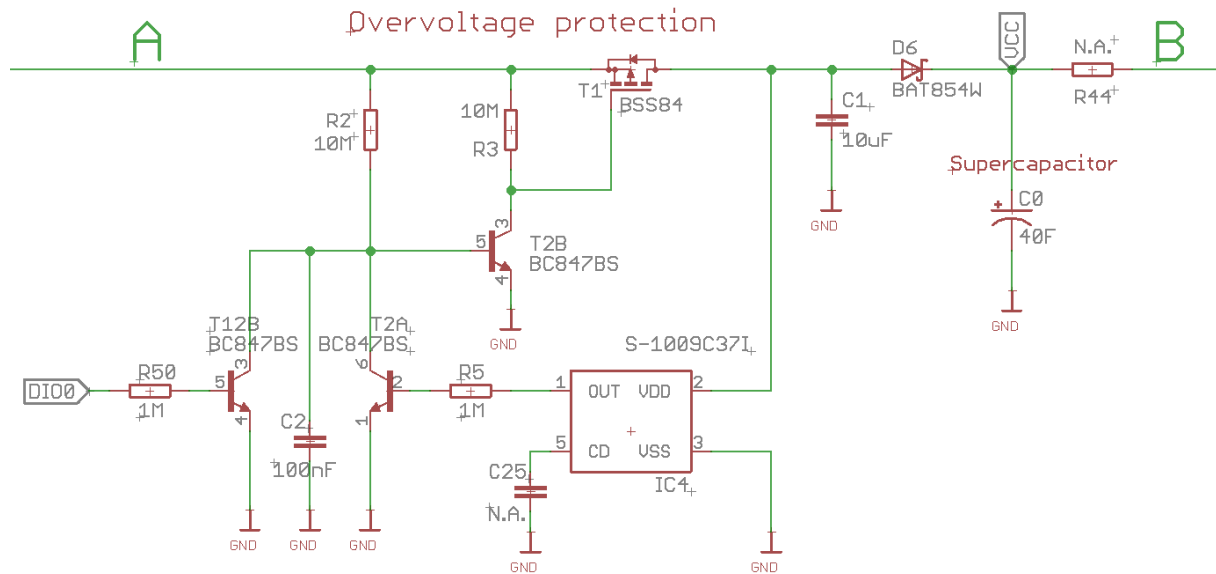
Figure 2.4. Supercapacitor overvoltage protection circuitry.

The input to the IC4 is the voltage from the 10 µF capacitor C1 and this voltage is constantly monitored. Based on the voltage level of the capacitor C1, supercapacitor C0 voltage level is determined. The chosen chip has a detection voltage of 3.7 V ± 0.5%. If the voltage of the capacitor C1 rises above this threshold, pin 1 of IC4 will go high. Additionally, by means of the combination of transistors T2A, T2B and T1, capacitor C1 together with the supercapacitor C0 will be disconnected from the solar cell. Between capacitor C1 and the supercapacitor C0, a Schottky diode D6 is placed. This minimises the reverse electrical current flow from the supercapacitor towards the solar cell and the rest of the overvoltage protection circuitry. This ultimately prevents discharge of the supercapacitor in the unwanted direction. The forward voltage of the diode D6 (Table 2.2) has to be very low in order to not affect too much the charge voltage of the supercapacitor. The maximum charge current coming from the chosen solar cell is around 40 mA. For this current, the measured voltage drop across the diode D6 is around 360 mV. IC4 also has a voltage hysteresis of 5%, allowing the voltage on C1 to rise to a maximum of 4 V. However, due to the diode D6, the measured voltage on the supercapacitor does not exceed 3.65 V.

When an external sensor is connected, the electrical current path between the V_{CC} (Figure 2.4) and V_{DD1} (Figure 2.5) is closed. The microcontroller will be supplied if the voltage of the supercapacitor is above 2.4 V. During the tests, an external sensor connection was simulated by populating the resistor R44 (Figure 2.4) which, by default, is not assembled on the PCB.

The undervoltage protection chip (IC6) and its voltage hysteresis of around 5%, set the minimum needed voltage of the supercapacitor to 2.4 V. The 470 µF capacitor C27 as part of the undervoltage protection circuitry, is used to smoothen transient current, which occurs upon sensor connection. It is also used to compensate the voltage drops across the sensor cable.
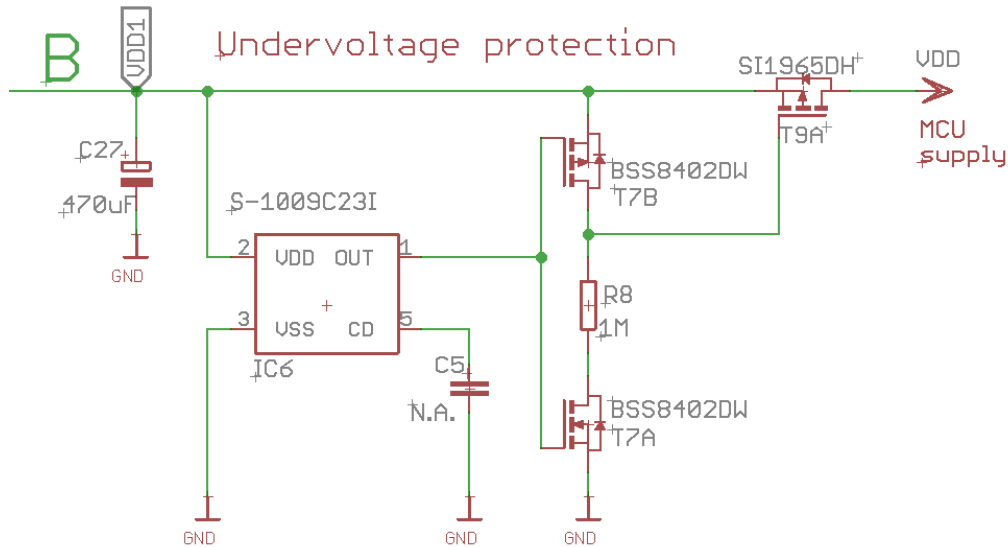
Figure 2.5. Supercapacitor undervoltage protection circuitry and an electrical path towards the microcontroller (MCU supply).

2.1.1.1. Overvoltage protection circuitry measurements

To analyse and measure the behaviour of the overvoltage protection chip shown in Figure 2.4, a test setup with the four measurement points have been set to observe four different voltages as seen in Figure 2.6.

Four 10 MΩ probes of the oscilloscope are connected to each of the test points and the following voltages are investigated (marked with different colours as in Figure 2.7):

1. **V_{INPUT} (CH4)** is the voltage from the solar cell.

2. **V_{DD_CHIP} (CH2)** is the voltage of the capacitor C1 and the voltage on the VDD pin of IC4 (S-1009C36I).

3. **V_{OUT_CHIP} (CH1)** is the voltage on the output pin of IC4.

4. **V_{CC} (CH3)** is the voltage on the cathode of D6 (voltage of the supercapacitor in normal use case).

During this test, a supercapacitor (C0 in the Figure 2.6) was not connected due to its high capacity (40 F). This would drastically prolong the measurement time especially during charge and the discharge procedure. Capacitor C1 was sufficient to test the behaviour of the energy management circuitry.
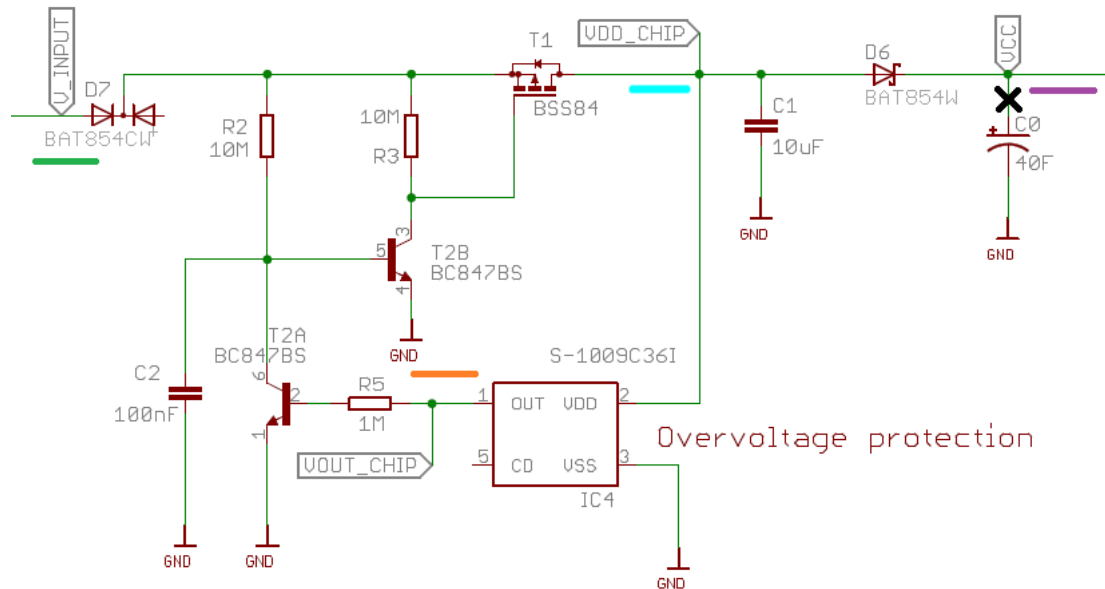

Figure 2.6. Overvoltage protection circuitry with the marked measurement points.

The initial values of all four voltage readings are shown in Figure 2.7. In the same figure it is observed that the output of pin 1 of IC4 (detection voltage 3.6 V ± 0.5%) is low, even when the mean voltage on the V_{DD} pin is 3.81 V. The mean voltage is used due to the constant switching of the transistor T1, which as a consequence produces a certain amount of ripple in the DC voltage at the capacitor C1. Thus, resulting in a sawtooth voltage waveform. This ripple is also measured at CH2 and is expressed as the peak-to-peak voltage in the oscillograms in Figure 2.7 to Figure 2.10. Therefore, in order to express the maximum possible voltage on capacitor C1, the measured mean value plus half of the peak-to-peak voltage can be taken. The ripple voltage here does not represent a problem since it will be further smoothed and minimised by the 40 F supercapacitor.

When the input voltage (V_INPUT) is increased by another 100 mV, IC4 reacts and its output pin becomes high as seen in the Figure 2.8. When the input voltage (CH4) is increased further, the voltage on the capacitor C1 remained stable. A change in the input voltage by 1 V causes a very small voltage difference (70 mV) in the capacitor C1 (CH3). Figure 2.9 and Figure 2.10 demonstrate very good behaviour of the overvoltage protection chip even for input voltages above 8 V (CH4). The absolute maximum, according to the data sheet, is 12 V

on the V_{DD} pin of the IC4 [26]. For 8.23 V input of the overvoltage protection circuitry, the absolute maximum value of the voltage V_{CC}, which would be present on the supercapacitor (CH3), is 4.05 V. This voltage is a result of the measured mean value of 3.75 V, to which half of the peak-to-peak voltage measured on the capacitor C1 is added. In this extreme case, the voltage level would be above the supercapacitor's maximum allowed voltage of 3.8 V. However, as mentioned earlier, with the soldered 40 F supercapacitor, a ripple voltage decreases 90%. In addition, the selected solar cell, when under load, it cannot produce voltages above 5.5 V.
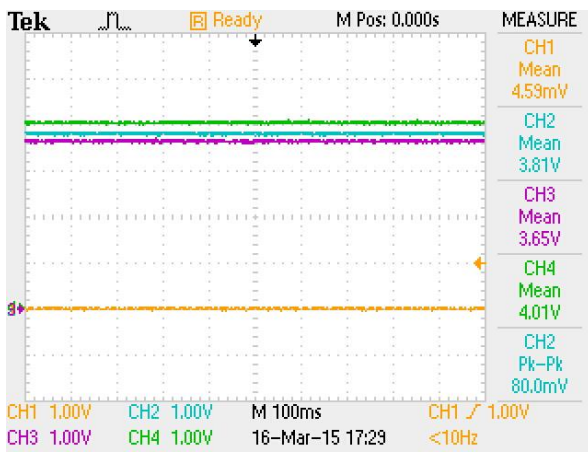

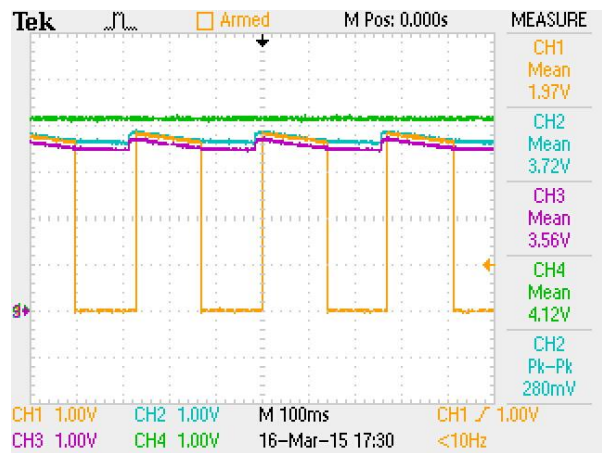Figure 2.7. All 4 observed voltages when the output pin of the S-1009C36I is low.

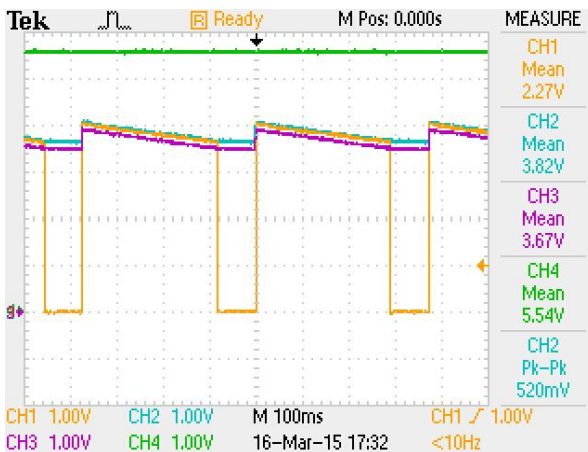Figure 2.8. Observed voltages when the S-1009C36I becomes active.

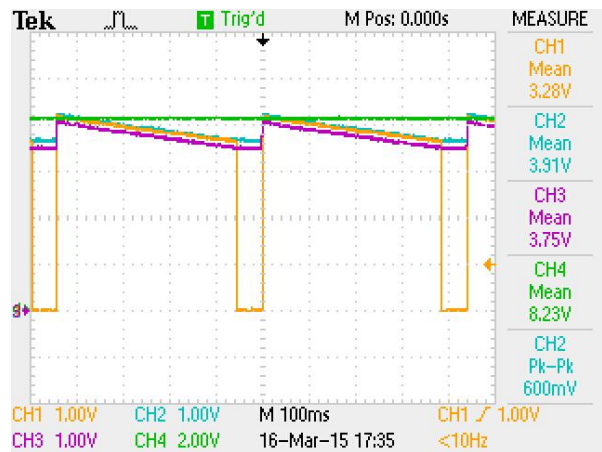Figure 2.9. Observed voltages for the increased input voltage (CH4) of 5.54 V.

Figure 2.10. Observed voltages for input voltage (CH4) increase to 8.23 V (Vertical scale set to 2.00 V/div).

2.1.1.2. Overvoltage protection circuitry behaviour at different temperatures

Since the sensor module is primarily intended for outdoor installation and use, temperature variations will influence the IC4 detection threshold.

Table 2.1 shows V_{CC} voltage, present at the capacitor C0 (channel CH3 in the Figure 2.6), for an input voltage of 4 V, which corresponds to an average value generated by the solar cell.

Table 2.1. Measured voltages after the diode D6 at different temperatures.

Temperature [°C]	$V_{\_INPUT}$ [V]	V_{CC} [V]
- 20	4.09	3.64
+ 25	4.08	3.64
+ 60	4.05	3.68

The results in the Table 2.1 are obtained with IC4, which has a defined voltage detection threshold of 3.7 V ± 0.5%. It can be seen that the voltage on supercapacitor C0 would rise above 3.6 V, and that the temperature influence is very small. Depending on what supply voltage is desired for the microcontroller, an overvoltage protection chip with a different threshold can be selected. In this case, a supply voltage between 3.6 V and 3.7 V is acceptable and therefore IC4 with a 3.7 V threshold is selected. As the voltage of the supercapacitor also depends on the diode D6, it is important to measure the voltage drop across the diode, for different currents. In the Table 2.2, different diode forward voltages are compared. The comparison is done for different values of forward current applied. A comparison of the measured values (at 25 °C), with the values from the data sheets of diodes BAT854 and BAS70 respectively, is performed. The reverse current of both diodes is very low. At 3.6 V the measured reverse current is less than 0.1 µA for both diodes. It is important that this value is as low as possible, as it contribute to the leakage current of the supercapacitor. At the beginning of the sensor module development, different type of Schottky diode (BAS70-70-F) was investigated. The outcome of this investigation is summarised in Table 2.2.

The diode BAS70-70-F compared to the diode BAT854W, for the same applied forward current I_F values, measures from 1.5 to 3.3 times higher forward voltage drop. This is why a diode BAT854W is ultimately selected in the final hardware design.

Table 2.2. Typical forward voltage drops across the two tested different diodes BAT854W from Nexperia and BAS70 from Diodes Incorporated respectively. Due to the lower forward voltage, Diode BAT854W is selected as diode D6 in the final hardware design.

Forward current I_F [mA]	Forward voltage data sheet [mV] BAT854	Forward voltage data sheet [mV] BAS70	Forward voltage measured [mV] BAT854	Forward voltage measured [mV] BAS70
0.1	200	300	189	286
1	260	400	252	377
10	340	700	318	674
30	420	1100	359	1000
100	550	>1600	439	1450

2.1.1.3. Current consumption of the overvoltage protection chip

The current consumption of the overvoltage protection chip S-1009C37I is not considered a limiting factor since this chip is directly powered by the solar cell. However, the same type of chip, with a different voltage threshold, is also used as the undervoltage protection. Then small energy consumption of this type of chip becomes significant factor. Table 2.3 presents current consumption of IC4 chip at different voltages on its input pin. At this pin, the output voltage of the solar cell, lowered by the voltage drop across the diode D7 and the transistor T1 is usually present (Figure 2.6).

Table 2.3. Measured current consumption of the S-1009C37.

V_{DD_CHIP} [V]	1.6	2.6	3.6	4.6	5.6	6.6
Current consumption of the S-1009C37 [µA]	0.54	0.82	1.15	3.45	3.70	3.8

2.1.1.4. Undervoltage protection circuitry measurements

Commencing this chapter, Figure 2.5 presents supercapacitor undervoltage protection circuitry. This same circuitry, however without the 470 µF capacitor C27, is also used during this test. As seen in Figure 2.11 three measurements points are set. Using the same oscilloscope and probe settings as in the tests described in Chapter 2.1.1.1, three different voltages have been monitored:

1. **V_{DD1} (CH2)** is the voltage on the VDD pin of S-1009C23I (this is also the output voltage from the supercapacitor).

2. **V_{OUT_CHIP} (CH1)** is the voltage on the output pin of S-1009C23I.

3. **V_{DD} (CH3)** is the main supply voltage to the rest of the sensor module circuitry.

During tests of the undervoltage protection circuitry functionality, V_{DD1} voltage was increased from 1.85 V up to 3.8 V (Figure 2.12 to Figure 2.15). The voltage on the output pin of IC6 was observed, together with the main supply voltage $V_{DD,}$ used to supply the microcontroller and the rest of the circuitry.
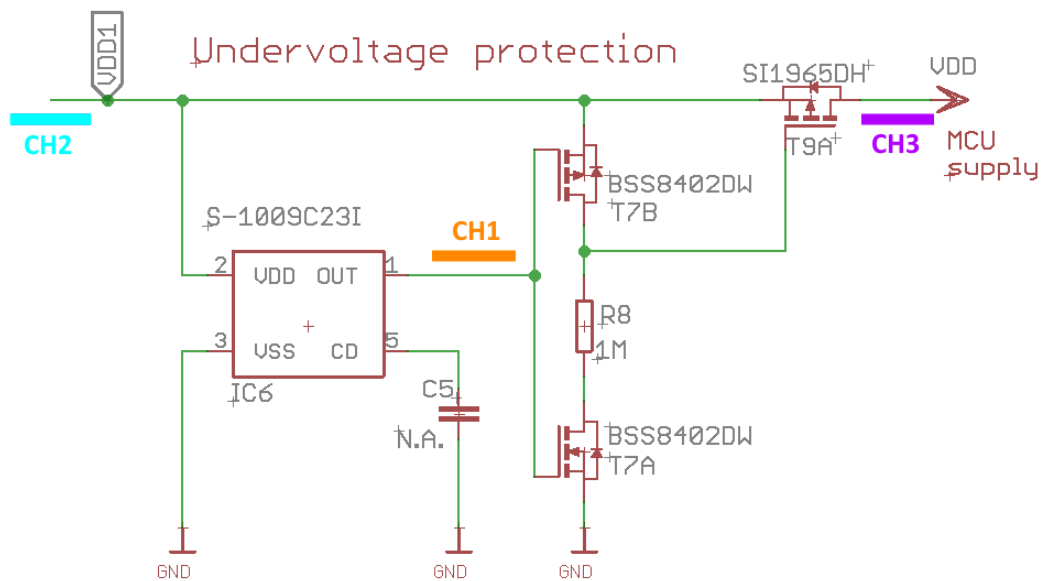
Figure 2.11. Supercapacitor undervoltage protection circuitry with S-1009C23I.

Figure 2.12 and Figure 2.13, imply that the undervoltage protection chip is active low, i.e. the voltage level on the output pin 1 is 0 V. This occurs when the V_{DD1} voltage on the input pin 2 of IC6 is below its threshold. The voltage threshold of IC6 (S1009C23I) is 2.3 V ± 120 mV. With the measured voltage of 0 V at the CH1, the supply voltage is not connected to the rest of the circuitry. This is because, in this case, the pMOS transistor T9A behaves as an open switch. When the input voltage (V_{DD1}) is further increased, the undervoltage protection chip changes the voltage level of its output pin, pulling it to high (V_{DD1}). As seen in Figure 2.14 this is true for 2.51 V ± 100 mV at the input (V_{DD1}). At this point, the microcontroller and the rest of the sensor module circuitry is supplied with voltage (CH3 in Figure 2.15).
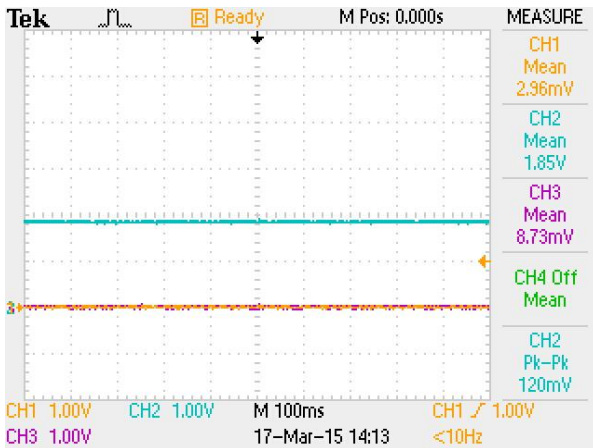
Figure 2.12. Input voltage V_{DD1} at 1.85 V for which V_{OUT_CHIP} and V_{DD} are low (< 10 mV).
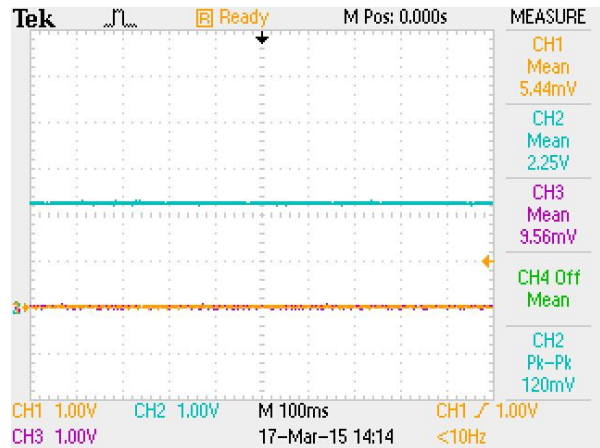
Figure 2.13. Input voltage (V_{DD1}) at 2.25 V for which V_{OUT_CHIP} and V_{DD} remain low (< 10 mV).
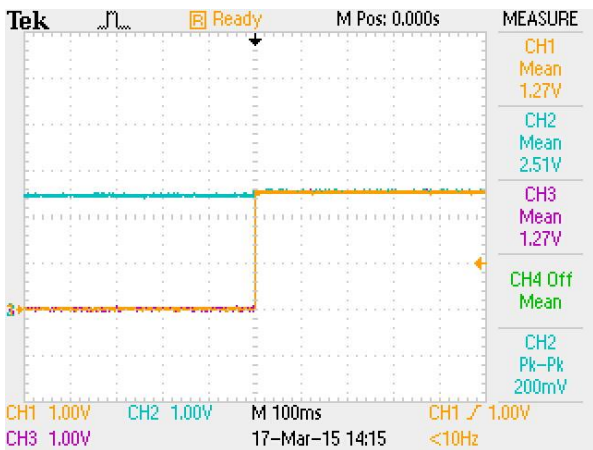
Figure 2.14. Input voltage V_{DD1} at 2.51 V for which the undervoltage protection "turns OFF" and connects the V_{DD} to the supercapacitor. V_{DD} and V_{OUT_CHIP} become high.
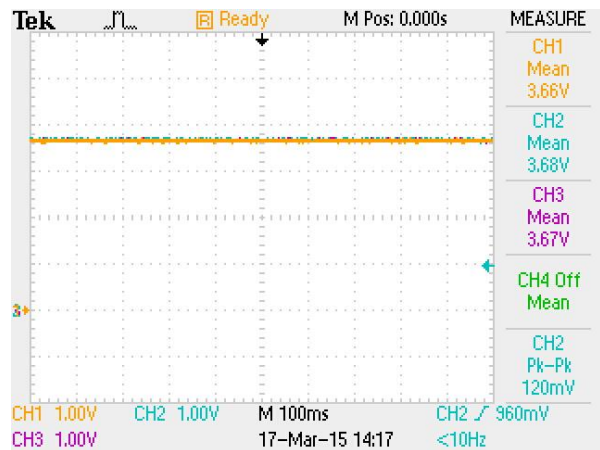
Figure 2.15. Further increase of the Input voltage V_{DD1} to the standard supercapacitor's operation voltage level.

If the input voltage (CH2) returns to the level below 2.5 V, the undervoltage protection chip will "turn ON" again. This implies that the output voltage on pin 1 will be low. This will occur at approximately 2.41 V input of the IC6 (pin 2, CH2).

Comparing Figure 2.14 with the Figure 2.16 it is evident that the S1009C23I has a certain voltage hysteresis of approximately 100 mV. This hysteresis needs to be taken into consideration when defining sensor module wake up voltage. Based on the above described IC6 chip behaviour, in the sensor module firmware this wake up voltage is set to a minimum 2.5 V.
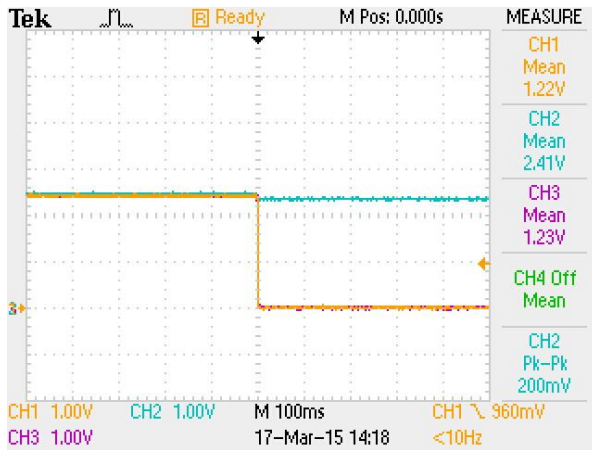
Figure 2.16. The moment when the undervoltage protection "turns ON" again and disconnects V_{DD} from the supercapacitor.
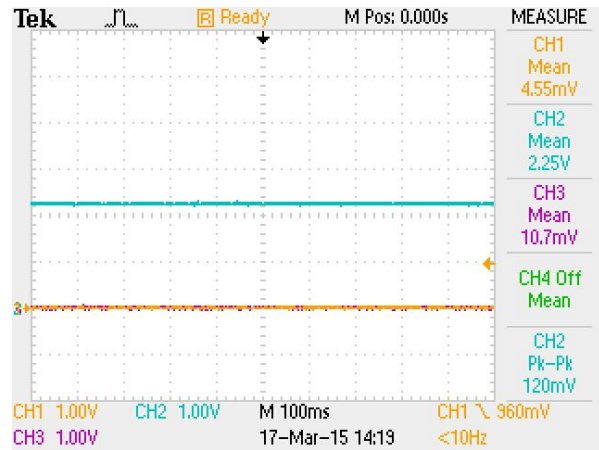
Figure 2.17. Further lowering of input voltage V_{DD1} to 2.25 V. Undervoltage protection remains active and keeps V_{DD} disconnected from the supercapacitor. V_{OUT_CHIP} and V_{DD} are low (< 10 mV).

2.1.1.5. Current consumption of the undervoltage protection chip

Since the undervoltage protection chip is supplied directly from the supercapacitor, its current consumption is very important, and should be as low as possible.

Table 2.4 summarises the measured current consumption for two different undervoltage protection chips, with respect to different supercapacitor voltages. As an alternative to the Ablic S1009C23I chip, another voltage monitoring chip, Rohm BU4923G-TR was tested. As it can be seen in Table 2.4 Ablic chip values are quite low and comparable to the data sheet values (0.42 µA typical and 0.90 µA maximum, for detection voltage VDET between 2.3 V and 3.6 V) [26].

A Rohm chip has between 38% and 200% higher current consumption (depending on the supply voltage) in comparison with the Ablic chip.

Special consideration must be taken when aiming for the lowest possible current consumption of the sensor module and deciding on the alternative voltage regulators. This is because undervoltage protection circuitry is constantly powered directly from the supercapacitor.

Table 2.4. Current consumption of two different voltage regulators used in the undervoltage protection circuitry.

V_{DD1} voltage [V]	1.8	2.2	2.6	3.0	3.6	4.0
Current consumption S1009-C23I [µA]	0.36	0.42	0.46	0.5	0.54	0.57
Current consumption BU4923G-TR [µA]	0.50	0.56	1.18	1.33	1.58	1.73

2.1.2. Supercapacitor as an energy storage

One of the novelties in the energy management of the developed sensor module is the use of the supercapacitor instead of a battery. The traditional approach in sensor module development relied on different types of battery [15], [18]. Compared to supercapacitors, batteries have many limitations when used in the outdoor sensor modules. During each transmission, current peaks in the developed sensor module are around 40 mA. This is a serious disadvantage when utilising batteries as they are very sensitive to current peaks. Current peaks above 30 mA limit their life cycle [1], [9], and batteries already have a lower life cycle, highly dependent on the number of charge/discharge cycles. E.g. the lithium-ion battery whose characteristics are shown in Figure 2.18 can be recharged from 4000 to 7000 times. This depends whether the previous discharge levels were less or greater than 50% respectively. After a certain period of time batteries lose their capacity and their nominal operating voltage gets degraded, and they need to be replaced [9]. On the other hand, a supercapacitor can be charged and discharged virtually an unlimited number of times. Due to this, information concerning supercapacitor life cycle is not usually in their specification. For example, for the used supercapacitor, the only information available regarding its life cycle, is that after 10 000 charge/discharge cycles the supercapacitor will still maintain a minimum 70% of the initially specified capacitance [27]. Figure 2.18 displays typical battery discharge curve. After full charge and start of operation there is an initial voltage drop, after which the battery voltage is then stable. At a point towards the end of the lifecycle, another voltage drop will occur. The battery supply voltage will be below nominal voltage, and the battery will require replacement. Within the same figure, one can also see another disadvantage of batteries, the huge battery capacity temperature dependency (especially at negative temperatures).
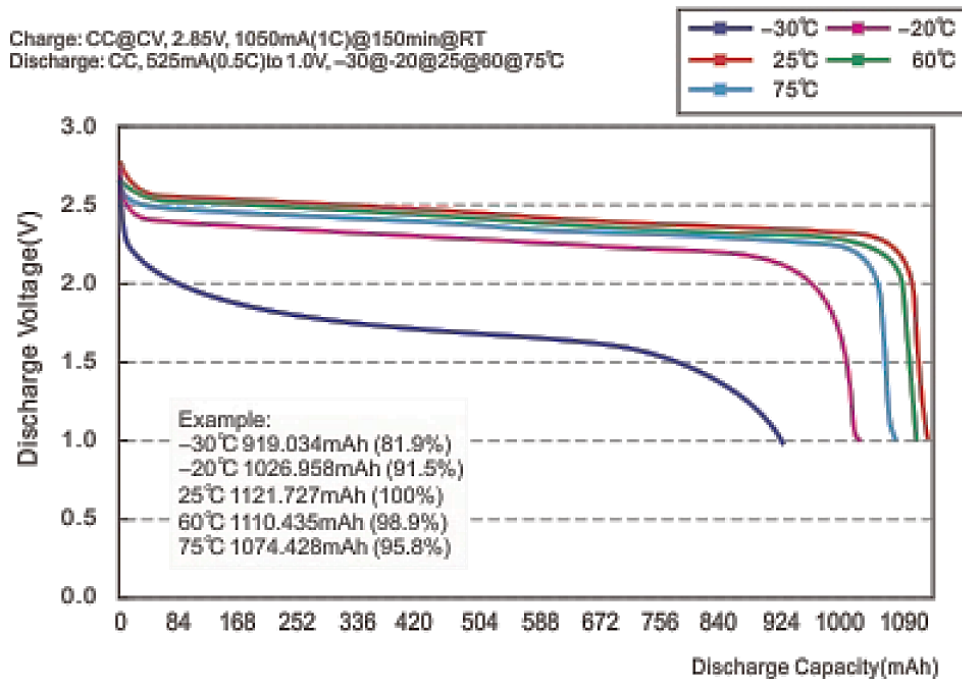
Figure 2.18. Discharge temperature characteristics of the lithium-ion rechargeable battery Huahui HTC0407 with the life cycle between 4000 and 7000 times [31].

Supercapacitors, on the other hand, do not have any special charging requests, expect ensuring that the maximum defined voltage is not exceeded, or that the minimum operating voltage is not reached. The supercapacitors have a low ESR (Equivalent Series Resistance), typically below 100 mΩ. This reduces internal losses during charge and discharge cycles, thus allowing them to handle current surges without the output voltage dropping significantly [9].

Different types of energy storage have been investigated. A comparison is displayed in Table 2.5. Besides internal impedance, leakage current is the most important criteria when selecting energy storage for a low power sensor module.

Table 2.5. Comparison of different technologies used for energy storage.

Type	Technology	Voltage	Capacity	Measured Impedance	Self-discharge	Comments
ML2430	Manganese Lithium	3.1 V	100 mAh	≈ 13 Ω	2% / year	Measured 0.2V voltage drop at 40 mA.
VL2320	Manganese Lithium	3.1 V	30 mAh	≈ 30 Ω	< 2% / year	Too high impedance.
MS920SE	Manganese	3.1 V	11 mAh	≈ 35 Ω	2% / year	Too high

	Lithium					impedance.
LIR1220	Lithium-Ion	3.6 V	8 mAh	< 2 Ω	7% / month	Self-discharge values from < 2% / year to 7% / month
CP1624	Lithium-Ion	3.6 V	50 mAh	< 1 Ω	20% / year	20% self-discharge per year is equivalent to steady 1μA

Based on the Table 2.5 and Figure 2.19 it is obvious that the energy storage with lithium-ion technology is the most promising for use in the low power sensor modules. Figure 2.19 demonstrates why some types of energy storage should be avoided in energy harvesting devices. The generated electrical current from a small solar cell (photo current) is shown in the same figure, assuming a worst case scenario with indoor conditions (solar cell illuminated 4 h with only 500 lux per day). It can be seen that this harvested photo current would be completely consumed by the leakage current of e.g. NiCad based energy storage device.

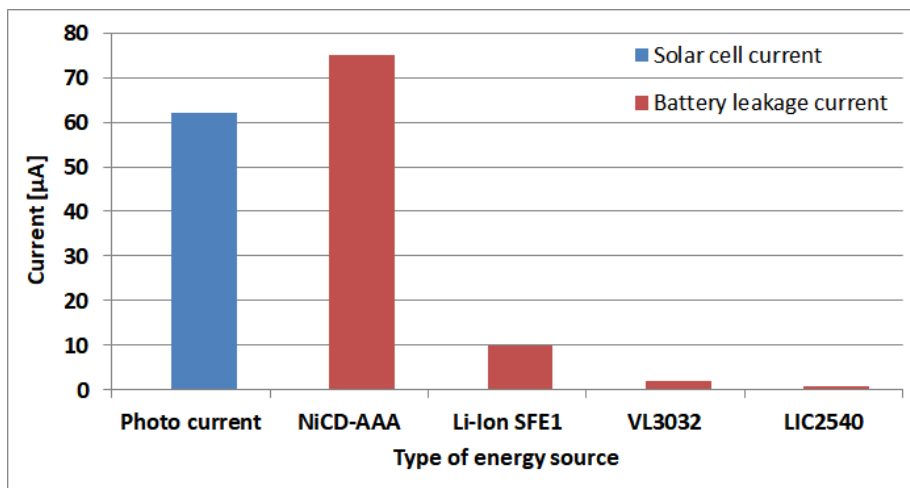*Figure 2.19. Measured leakage currents of different energy storage and comparison with a generated photo current from a small solar cell.*

Generally, only a low impedance energy storage with minimum leakage current and sufficient capacity, is able to deliver the required energy to power-up sensors and transmit data over longer period of time. Due to limitations mentioned above, the tested batteries are

unacceptable energy storage solution. Therefore, an alternative is found with capacitor-like characteristics.

A lithium-ion supercapacitor LIC1235RS3R8406 from Taiyo Yuden is selected as the main energy storage and it became the "heart" of the developed sensor module. Lithium-ion capacitors are hybrid capacitors, featuring the best characteristics of both EDLC (Electrical Double Layer Capacitors) and Lithium-Ion Secondary Batteries (LIB). Some of these characteristics are shown in Table 2.6 [27].

Table 2.6. Main characteristics of the LIC1235RS3R8406 [27].

	Items		Specifications
1	Operating Temperature Range (°C)		-30 ~ +85
2	Upper limit Voltage (V)		3.8
3	Lower limit Voltage(V)		2.2
4	Initial Characteristics	Capacitance	36-44F
		DCR	Under 125mΩ
5	Soldering Heat Resistance	Capacitance	Within initial spec
		DCR	Within initial spec

Figure 2.20 shows self-discharge property of the two different capacitor types. The cylinder type Lithium-Ion Capacitor (LIC) has a 40 F capacity, when charged for 24 hours with 3.8 V, at a temperature of 25 ºC. The other is a symmetrical type EDLC whose capacitance is similar to that of the lithium-ion capacitor. As seen here, the symmetrical type EDLC has a large self-discharge. After a month at 25 ºC, its operating voltage lowered to 80% of the initial voltage. In contrast, the LIC displays far better self-discharge behaviour. At 25 ºC it can maintain a voltage higher than 3.7 V, even 100 days since fully recharged [32]. Two additional self-discharge properties of the LIC, at two different temperatures are shown in Figure 2.21 (capacity is 200 F). As it can been seen, at 60 °C after 4000 hours, the supercapacitor maintains close to 90% of its initial voltage. At 25 °C it behaves even better, preserving 96% of the initial voltage.

The voltage retention behaviour of the lithium-ion capacitors is shown in Figure 2.22. After 22 000 hours, at 25 °C this 100 F supercapacitor maintained 92% of the initial voltage [32].

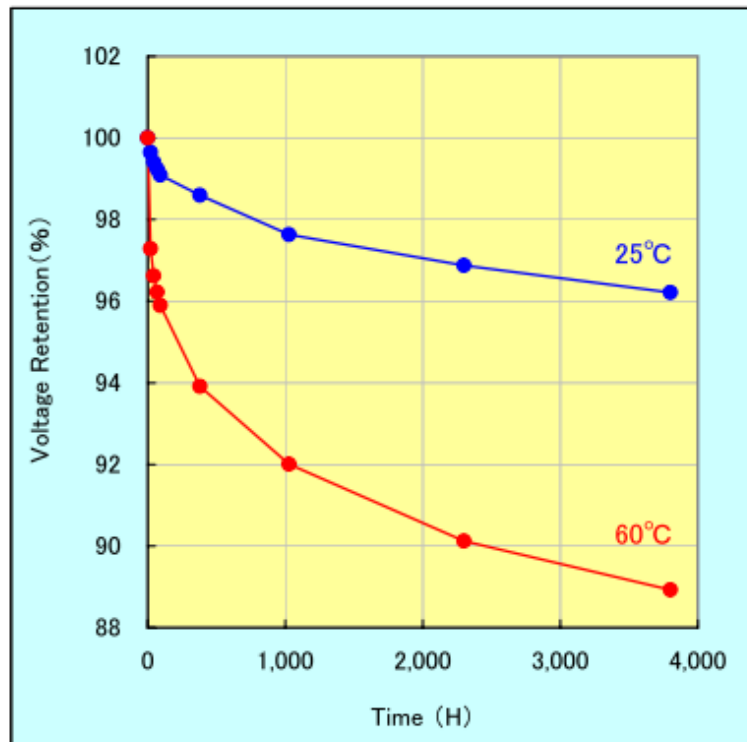*Figure 2.20. Self-discharge property of the cylinder type LIC with 40 F vs. EDLC with a similar capacitance [32].*

Figure 2.21. Self-discharge characteristic of the 200 F (50 mΩ) Taiyo Yuden lithium-ion capacitor for two different temperatures [32].

27

Model : LIC1840R 3R8107
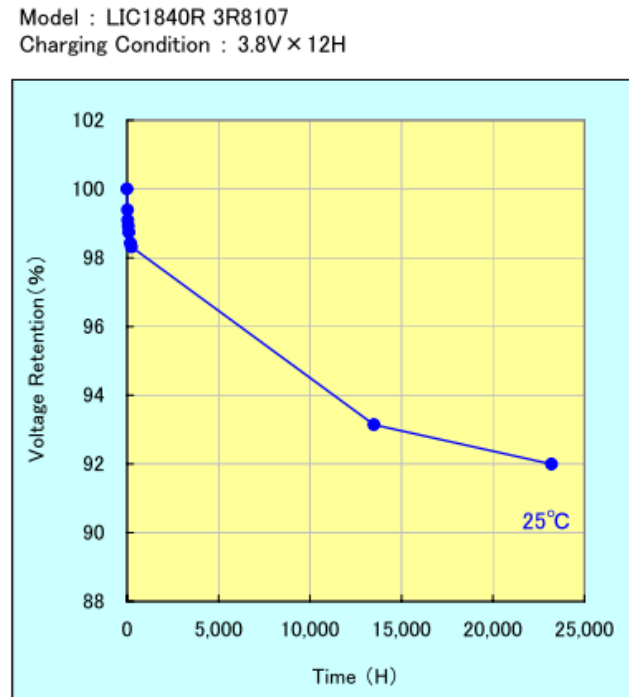Charging Condition : 3.8V × 12H

Figure 2.22. Self-discharge characteristic of the 100 F (100 mΩ) Taiyo Yuden lithium-ion capacitor at 25 ℃
[32].

The selected supercapacitor has a capacity of 40 F and this value is in the first order price compromise, compared to the 100 F and 200 F versions. On the other hand, a larger capacitance is not needed since the consumption of the developed sensor module is optimised and long term operation is secured. With the development of more energy consuming sensors, a supercapacitor with a higher capacity could be considered. The supercapacitor is still the most expensive component on the sensor module PCB, contributing with 20% of the overall costs of the assembled PCB.

Since the developed sensor module will be primarily used outdoors, it is of great interest to define the supercapacitor's leakage current over a larger temperature span. The recorded measurements show that during a bright and sunny day, the temperature inside the sensor module housing can reach close to +70 °C with direct sunlight (Figure 2.23). A high temperature can have several negative effects on the supercapacitor behaviour: the internal direct current resistance (DCR) increases, the equivalent series resistance (ESR) increases and the capacitance decreases [32]. Taking the aforementioned into consideration, the supercapacitor's leakage current over different temperatures has been measured and displayed in Table 2.7 and Figure 2.24.

Figure 2.23. Measuring temperature inside a sensor module housing. The two channels of the thermometer (yellow device) are measuring the temperature of the solar cell (52.3 °C) and supercapacitor (50.1 °C) respectively. Outside temperature was 30 °C.

Table 2.7. Supercapacitor's leakage current measured over different temperatures, for two different voltages of the supercapacitor [8].

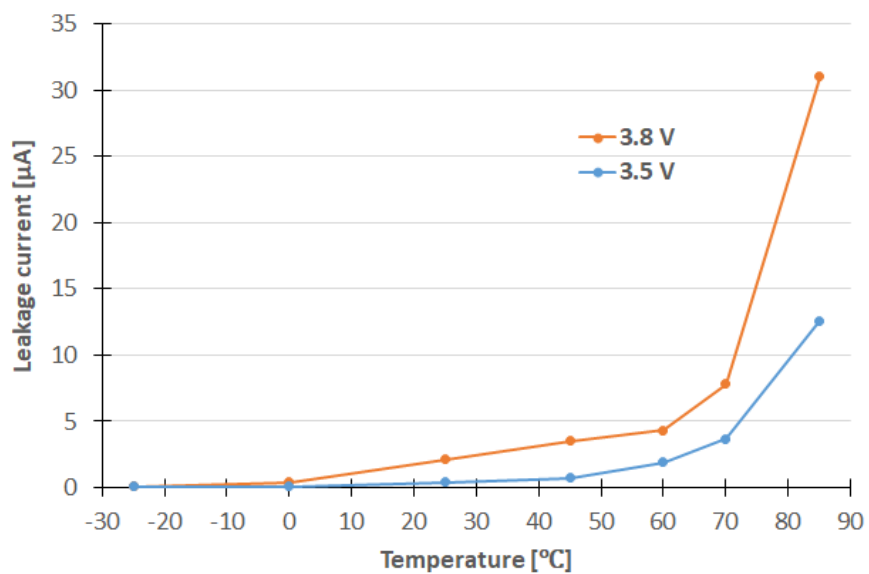| Temperature [°C]		85	70	60	45	25	0	-25
Leakage current after 8h [μA]	3.8 V	31.0	7.8	4.3	3.5	2.1	0.4	< 0.1
	3.5 V	12.6	3.7	1.9	0.7	0.4	< 0.1	< 0.1

Figure 2.24. Supercapacitor's leakage current values over different temperature for different voltage levels. This is graphical representation of the results from the Table 2.7.

Measurements are taken for two different voltages of the supercapacitor; 3.8 V as the maximum usable voltage, and 3.5 V as the voltage just below maximum operating voltage. The voltage of the supercapacitor was kept constant, while the temperature was altered every 8 hours. During the last 1000 seconds of each cycle, the leakage current (current drained by the supercapacitor from the power source) was measured every 10 seconds and an average was calculated. As it can be seen in Table 2.7 and Figure 2.24, a drastic increase in the supercapacitor's leakage current is observed at +85 °C, compared to 25 °C or lower.

The supercapacitor's leakage current contributes to 40% (at 25 °C) of the sensor module's overall current consumption during deep sleep mode. Therefore it must be considered when estimating dark run time operation.

To measure the real use case behaviour of the supercapacitor and obtain its realistic leakage current, an additional 100 hours test is conducted. Charge and discharge cycles remaining within the supercapacitor's defined operating voltage range (from 2.2 V to 3.8 V) have been executed. This was done using an automated test created with LabVIEW as it can be seen in Figure 2.25. For 5 hours at room temperature, 3.8 V supply voltage was applied to the supercapacitor with the maximum current limit of 50 mA. The voltage on the supercapacitor and the charge current was recorded at 10 second intervals. After 5 hours, the applied voltage was changed from 3.8 V to 2.2 V. The discharge of the supercapacitor then started through the power source with the capability to sink current (sink current limit set to 50 mA). This was repeated 7 times. The applied charge to the supercapacitor was also calculated, and is shown by the green line in Figure 2.25.

After 7 charge/discharge cycles, a constant 3.8 V was applied to the supercapacitor for the next 30 hours and the leakage current was measured during this period.

From Figure 2.26, the average value of the supercapacitor leakage current is 5 µA. Due to this, the supercapacitor only lost 100 mAs or 0.156% of its capacity during 5.5 hours.
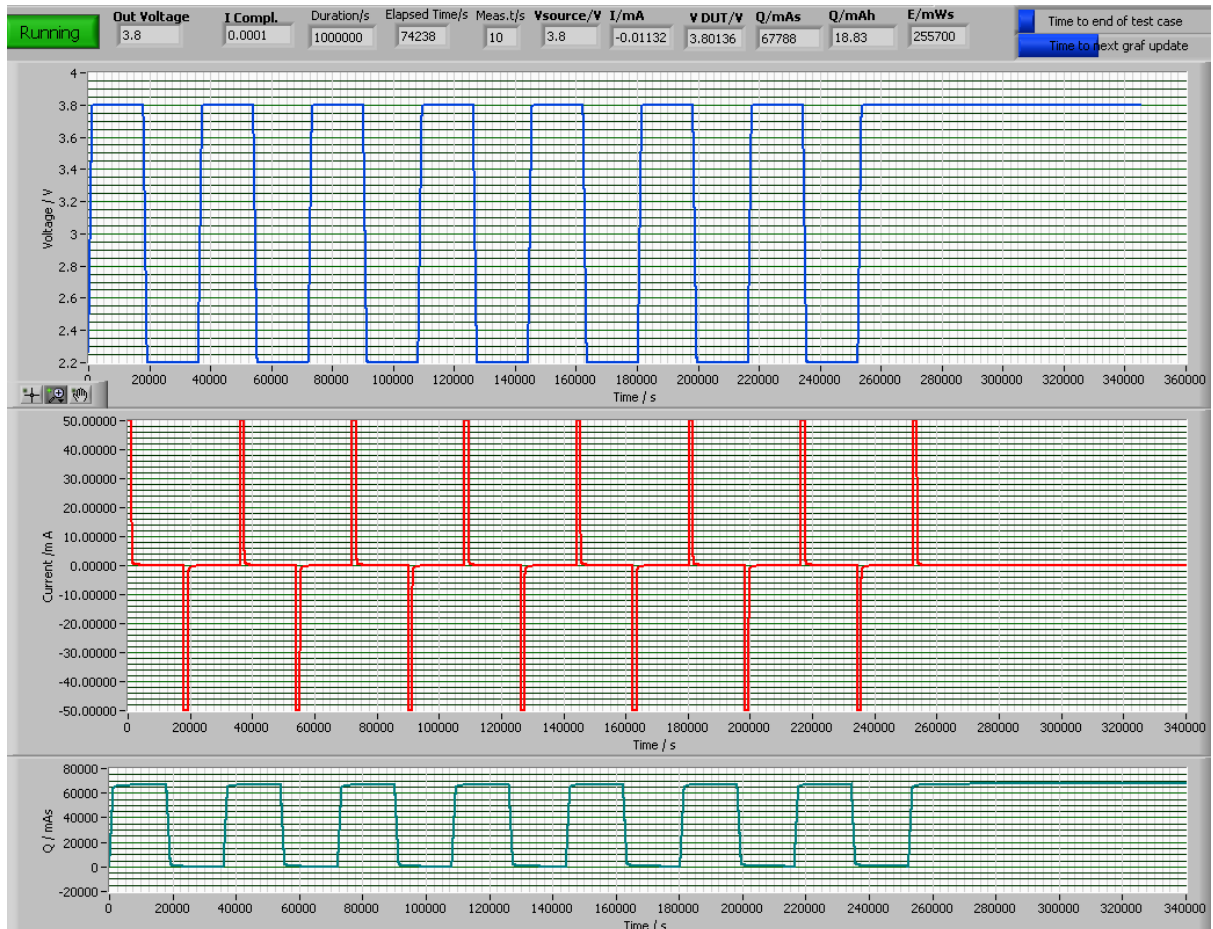
Figure 2.25. Cycles of charge and discharge of supercapacitor. The blue, red and green lines represent the applied voltage, current drawn and available charge respectively.
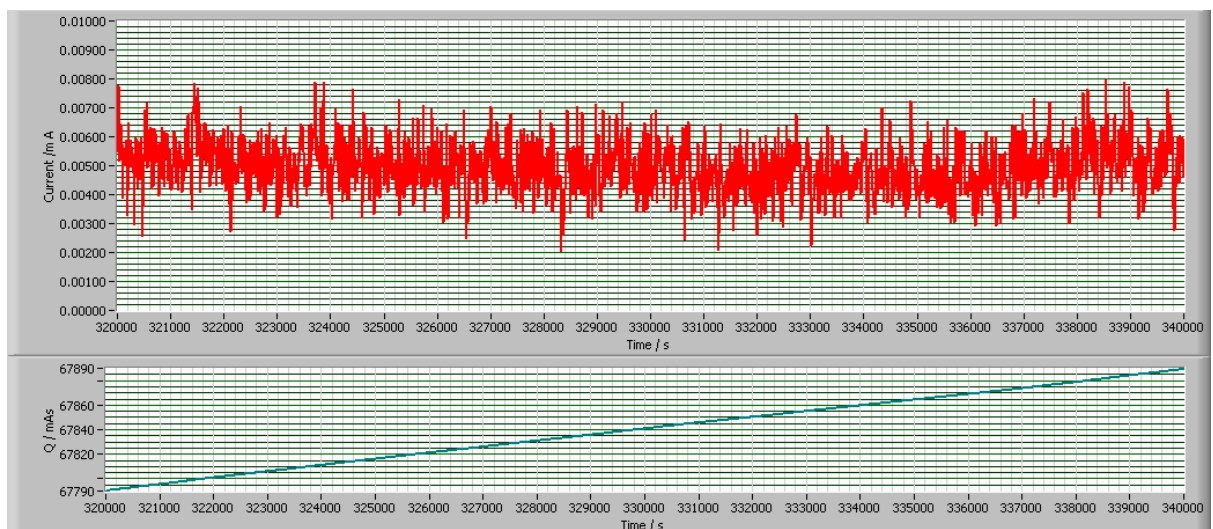

Figure 2.26. Supercapacitor leakage current (red line) after 100 hour test. Fluctuations in measurement values arise due to the limited precision of the measurement equipment and noise. The green line depicts lost charge due to leakage current over a 5.5 hour period of time.

31

Since the recommended maximum operating voltage of most microcontrollers and radio chips is 3.6 V, the supercapacitor comes from suppliers already charged to 3.6 V ± 100 mV. It is then soldered on the sensor module PCB and put into operation.

Based on the low leakage current of the supercapacitor, determined in the tests above, it is to be expected that the sensor module will conserve its energy when not in use for a longer period of time. The results displayed in Figure 2.27 confirm this assumption. The voltage of the supercapacitor is measured on 10 sensor module PCBs assembled almost 3 years ago (Week 29, 2016). These PCBs were then stored and not used. The initial voltage when these samples were first produced is represented by the red dots in Figure 2.27. In March 2019, the supercapacitor voltage of these 10 samples is measured again and these results are displayed by the blue dots in the same figure. As it can be seen, all 10 supercapacitors lost a similar amount of charge due to their leakage current. However, the measured voltage levels are still significantly high. This suggests that when connecting a sensor to these sensor modules today, they would operate normally. In addition to this, as soon as the solar cell is connected, these supercapacitors would begin to recharge to initial voltage levels.
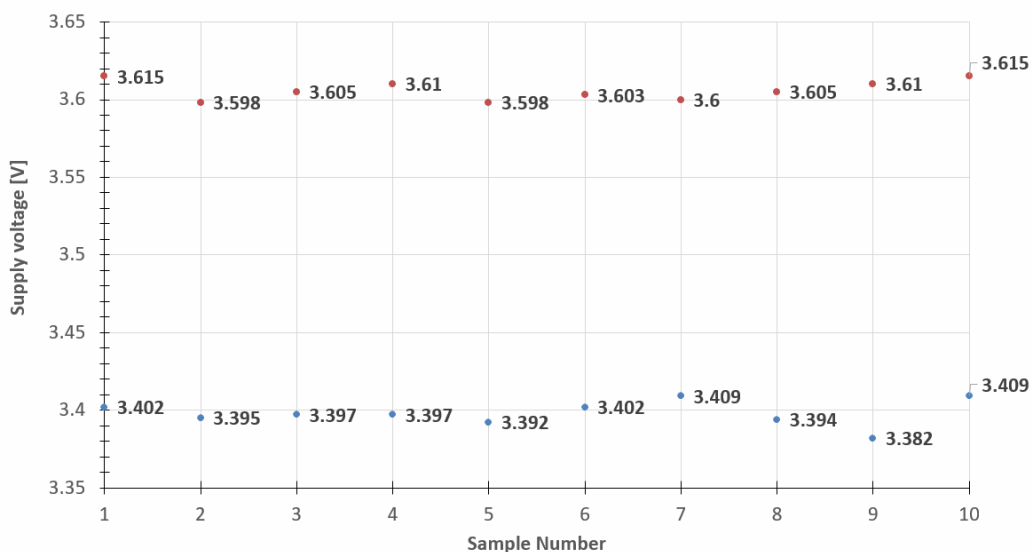
Figure 2.27. Measured voltage of the supercapacitors soldered on the developed sensor module PCBs at the assembly (red dots) and after 3 years of no usage (blue dots).

2.1.3. Microcontroller with FRAM

The selected microcontroller is the low power MSP430FR5949 from Texas Instruments. It has 64 KB of uniquely embedded, ultra-low-power Ferroelectric Random Access Memory (FRAM). FRAM technology combines the speed, flexibility, and endurance of SRAM (Static

RAM) with the stability and reliability of flash, but at much lower power [21]. Fast accessible FRAM memory instead of EEPROM (Electrically Erasable Programmable Read-Only Memory) ensures very low power consumption [33]. Figure 2.28 shows FRAM advantages over EEPROM.
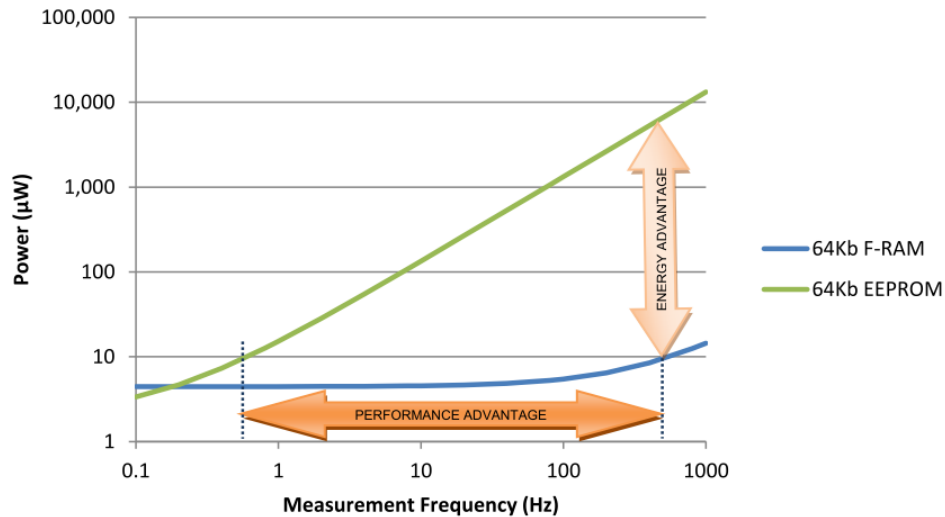
Figure 2.28. Power consumption comparisons between FRAM and EEPROM during a 1 byte data write [33].

Besides FRAM, the chosen microcontroller supports different low power operation modes, of which, 3 different are used in the developed sensor module:

- **Active mode** with typical current consumption of 103 µA/MHz
- **Standby mode - LPM3** with typical current consumption of 0.4 µA
- **RTC (Real time clock) only mode - LPM3.5** with typical current consumption of 0.25 µA

RTC only mode is also known as deep sleep mode and the microcontroller spends 90% of its operating time in this mode. Depending on the supply voltage, the current consumption in each mode can vary. The data sheet defines current consumption values shown above for 3.0 V supply voltage [21]. However, the microcontroller in the developed sensor module is supplied with a voltage varying from 3.6 V to 2.5 V. Figure 2.29 depicts the current consumption of the entire sensor module when the microcontroller is in deep sleep mode. Besides microcontroller consumption, around 300 nA of current is consumed by the 32.768 kHz external quartz crystal attached to the microcontroller, and an additional 350 nA by the previously mentioned undervoltage detector chip. This is also displayed on the graph. All

other components present in the block diagram in Figure 2.2 are disconnected from the supply voltage to minimize energy consumption.

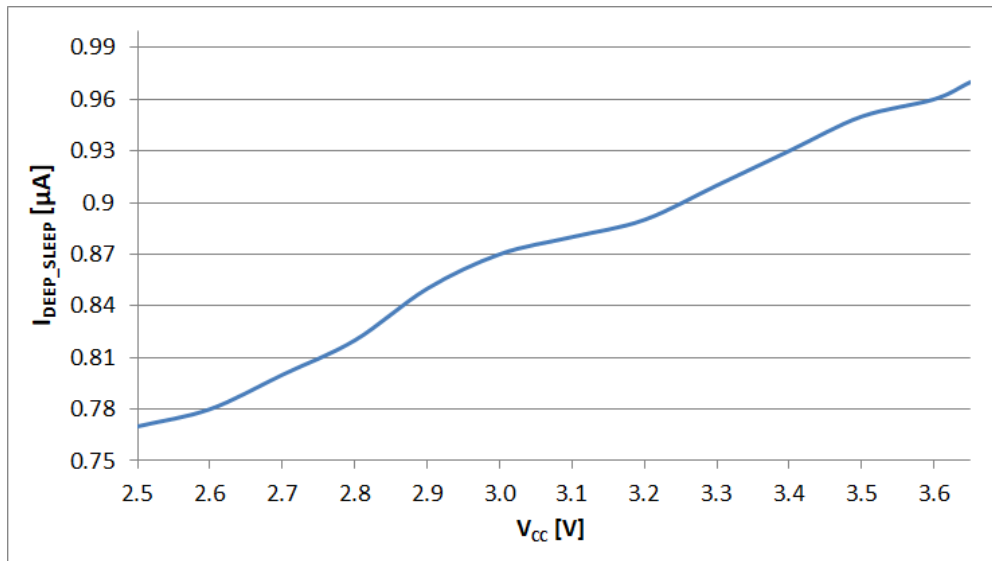*Figure 2.29. Current consumption of the sensor module in deep sleep mode. The current consumption is measured indirectly, as a voltage drop over a 10 kΩ (± 1%) resistor at different voltages of the supercapacitor.*

The achieved power consumption of the developed sensor module at 3.6 V when in the deep sleep mode is 3.46 μW. This is around 20% less compared to 4.32 μW consumed by other commercially available platforms, such as Sigfox and LoRa based modules [5].

The selected microcontroller also supports internal measurement of the supply voltage and this feature is used as standard part of the sensor module's control algorithm (Chapter 4). By using the available internal measurement of the supply voltage, no additional measurement circuitry is needed, thus no additional leakage current is present.

2.1.3.1. Low power oscillator

During deep sleep mode of the microcontroller, the time until the next wake up cycle must be measured. An external 32.768 kHz tuning fork quartz crystal, is implemented for this purpose. The Seiko SSP-T7-F with the load capacitance of 12.5 pF is used [25]. Since this component is always powered and running, its current consumption should be as low as possible. The measured constant current flow going into the crystal measures approximately 300 nA. A more expensive, low power version of this crystal (SSP-T7-FL) is also available and has been tested. It has a load capacitance of maximum 6.0 pF and drive level of only 0.01 μW, which is one tenth the standby power of general crystal resonators, including the above mentioned SSP-T7-F. The overall influence of this difference in current consumption in dark

run time operation is negligible. Therefore, the cheaper version is employed in the developed sensor module.

2.1.4. External Flash memory

The firmware and all configuration parameters are stored inside the microcontroller's FRAM memory. However, an additional flash memory is added to the developed PCB so each sent or received telegram can be stored and later read via the host interface when needed. The Adesto AT45DB321E, 32 Mbit data flash with a 2.3 V minimum supply voltage is used. Besides operating voltage ranging from 2.3 V to 3.6 V (which abides by the supply voltage limits provided by the supercapacitor), it also has low-power dissipation and a minimum endurance of 100 000 write/erase cycles per page [23].

The microcontroller communicates with this external flash memory chip via SPI (Serial Peripheral Interface) lines. Each telegram transmitted is stored in the external flash memory of the sensor module, and its 32 Mbit of memory allows storage of around 65 000 telegrams. Typically, with a 15 minute transmission cycle, the external flash memory is sufficient for almost two years of sent telegram storage. After the external flash is full, the oldest telegrams will be overwritten with the newly sent telegrams.

The Adesto chip has a defined ultra-deep sleep consumption of only 400 nA [23]. However, to further minimise the deep sleep power consumption of the sensor module, this component is also completely disconnected from the supply voltage when not in use.

Since the same SPI lines are shared by the flash memory chip and the radio chip, care has to be taken that both components are powered simultaneously. Otherwise, one of the components may become powered via SPI lines, which will result in increased power consumption.

2.1.5. Radio chip for Sub-GHz frequency band

The selected radio chip is the CC1120, high performance sub-1 GHz transceiver for narrowband systems from Texas Instruments [22].

The following parameters led to the selection of this radio chip for the developed sensor system:

- Excellent receiver sensitivity of -123 dBm at 1.2 kbps.
- Very low phase noise of -111 dBc/Hz at 10-kHz offset.
- Wide supply voltage range from 2.0 V to 3.6 V.

- Low current consumption. In Rx mode peak current is 22 mA, and in Tx mode with +14 dBm output power, it is 45 mA.

- Compliant with European, American and Japanese radio norms.

- Operates in sub-1 GHz frequency band (820-960 MHz of interest).

- Automatic Clear Channel Assessment (CCA) for Listen-Before-Talk (LBT) systems.

- Digital Receive Signal Strength Indicator (RSSI) measurement.

Although the CC1120 supports a low power mode, whenever is not in use it is completely shut down by the microcontroller and disconnected from the supply voltage. The radio chip and microcontroller communicate via SPI lines and GPIO pins, which are used for interrupt detection from the radio chip. Around 60 different signals can be output on the 3 GPIOs coming from the radio chip [34]. The interrupts received from the radio chip inform the microcontroller about a variety of events. Some of these include the following; the crystal is stable and the radio chip is ready for operation, telegram transmission is complete, the radio channel is busy, etc.

In the environment of the radio chip, an RF front end filter has to be built between the antenna and the input to radio chip's Low Noise Amplifier (LNA). To obtain maximum possible transfer of output power from the LNA to the antenna, and deliver a balanced feed line to the unbalanced antenna connector, two different designs for the RF front end filter have been investigated. In Figure 2.30 a discrete reference design from the CC1120 Evaluation board [35] with more passive components is shown, while Figure 2.31 depicts a design implementing only one impedance-matched integrated ceramic passive component, so known as Balun [36]. Balun is a specially designed component from Johanson Technology for Texas Instruments CC112x radio chips. For both solutions, the output power delivered to the matching circuitry of the antenna has been measured. Table 2.8 compares the efficiency of this radio power transfer for different radio chip power settings.
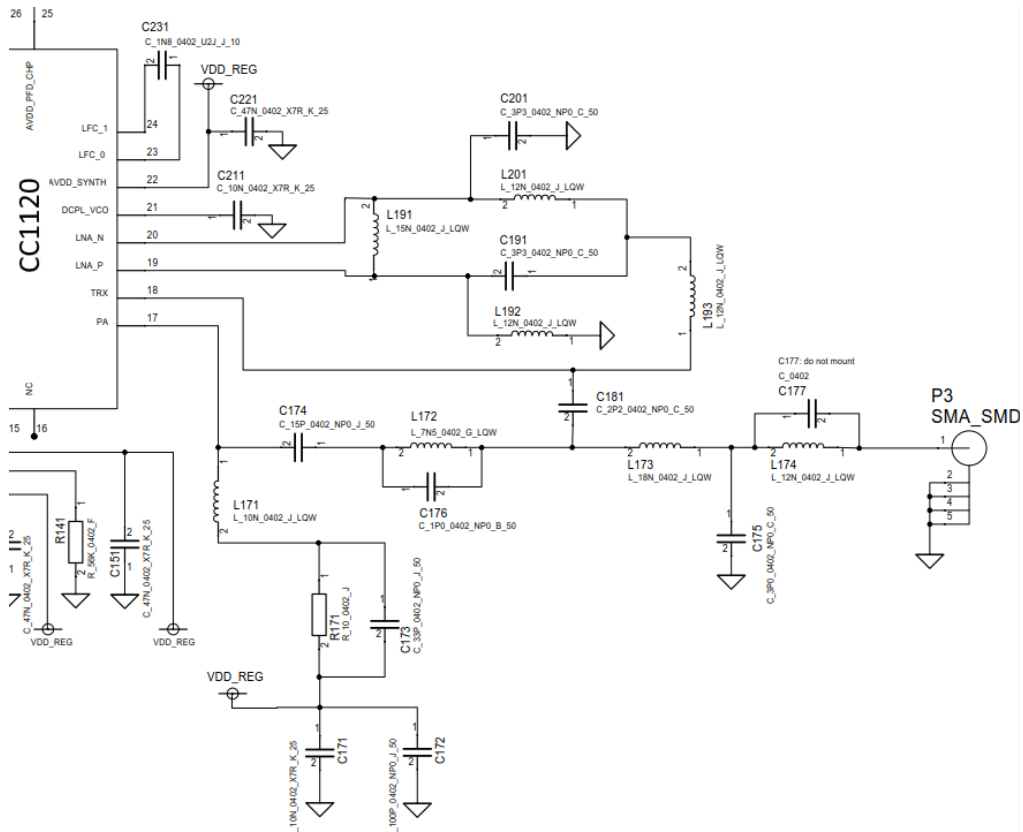
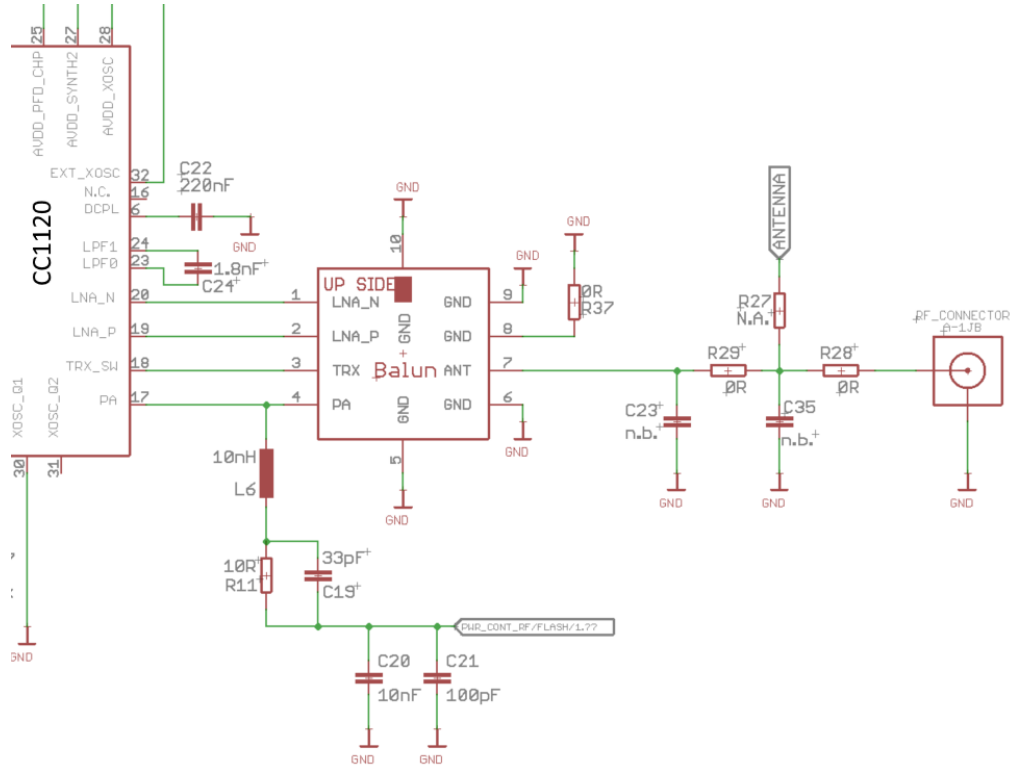*Figure 2.30. A discrete RF front end filter reference design. It consists of many passive components [35].*

Figure 2.31. RF front end filter design used in developed modules with only one impedance-matched component called Balun.

Table 2.8. Comparison of two different RF front end designs and their influence on the output power (Tx) measured at the RF connectors in Figure 2.30 and Figure 2.31 respectively.

Tx power setting of the CC1120 radio chip [dBm]	Output power of the EVA board reference design and 32 MHz crystal [dBm]	Output power of the sensor module board with Balun design and 38.4 MHz crystal [dBm]
0	-4.19	-4.15
+10	6.41	6.45
+14	11.50	11.53

During measurements, the transmission frequency of the tested continuous wave (CW) signal was set to 925 MHz. Two different TCXO (Temperature compensated crystal oscillator) values have been tested, 32 MHz and 38.4 MHz respectively. At the time of the test, the 38.4 MHz TCXO was already available and cheaper than the 32 MHz version. As seen in Table 2.8, there is no significant difference of the two crystal's performance. Due to this the 38.4 MHz crystal was implemented into the final design, despite not having the standard recommended value for the CC1120 radio chip. The RF front end filter design including Balun was also selected as a more efficient and "cleaner" solution. This selection considered both the occupied space and the number of components used, compared to the reference design with passive components. Further tests with the RF front end filter with the Balun were conducted. These tests involved the measurement of the test CW signal output power for different RF output power values set in the register PA_CFG2 of the radio chip [34]. During test, the radio chip was supplied with two different voltage levels; 3.6 V and 3.3 V. In addition, the measurements were conducted at two different transmit frequencies, 868 MHz and 925 MHz respectively. The obtained results are shown in Figure 2.32. The higher output power was measured at 868 MHz. The main reason for this is the electrical performance of the selected Balun [36]. Furthermore, at both frequencies the measured output power is 0.5 dB lower for 3.3 V compared to 3.6 V supply voltage. This is due to the performance of the power amplifier integrated into the radio chip [34].

From an energy consumption point of view, it is important to characterise the radio chip's current consumption and the measured peak currents in the Tx mode for different radio chip power settings and supply voltage levels. In addition to this, current consumption is as well compared for two different supply voltages, 3.6 V and 3.3 V, at the transmit frequency of 925

MHz. The obtained results are shown in Figure 2.33. The current consumption in Rx mode is constant with a value of approximately 25 mA.
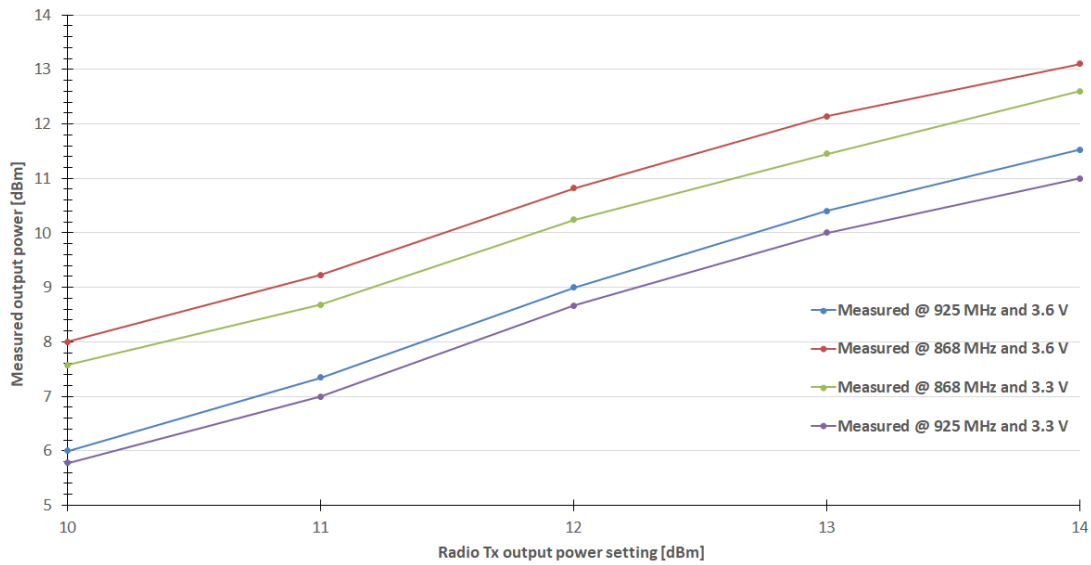
Figure 2.32. Measured sensor module output Tx power vs. output power value set in the radio chip register.
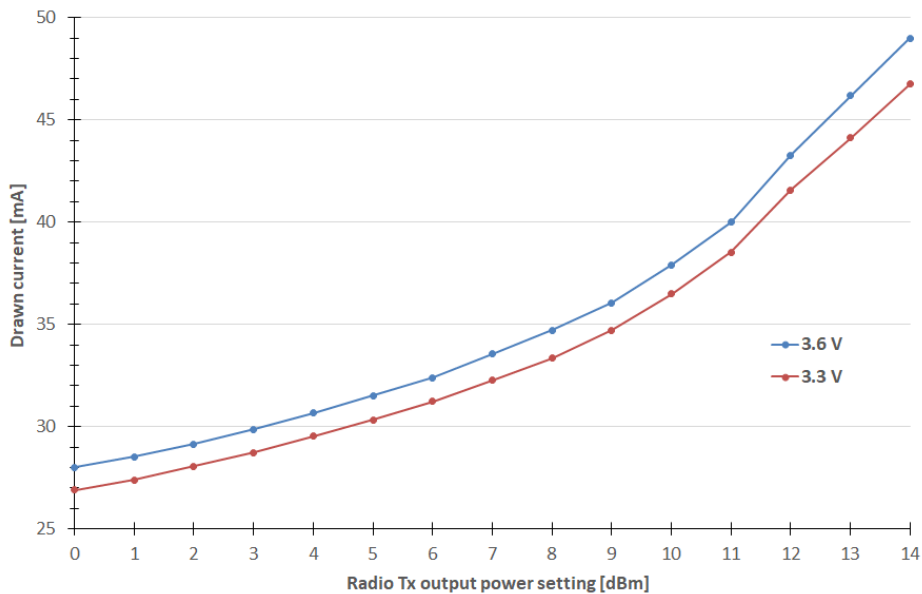
Figure 2.33. The electrical current drawn by a sensor module for different radio Tx output power level settings.

2.1.5.1.   Temperature compensated crystal oscillator (TCXO)

Since the developed sensor module will be primarily used outdoors, large potential variations in temperature will influence the stability of the crystal oscillator connected to the radio chip. Therefore, this influence should be as minimal as possible. This is why advantage should be given to a temperature-compensated crystal oscillator (TCXO) in front of different crystal types, e.g. simple packaged crystal oscillator (SPXO).

39

TCXOs have temperature-compensated circuits incorporated and are designed to have satisfactory temperature characteristics across a wide temperature range. Figure 2.34 displays an example of a temperature-compensated crystal oscillator before and after compensation [37].
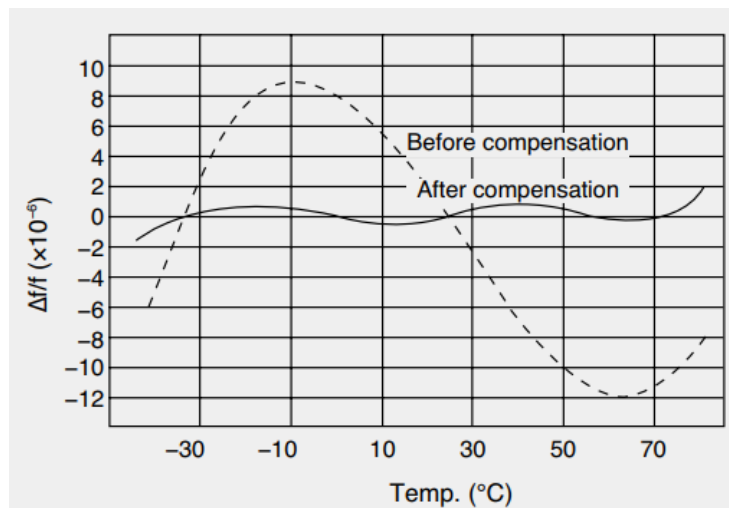
Figure 2.34. Example of the frequency-temperature characteristics of a temperature-compensated crystal oscillator [37].

Table 2.9 outlines some of the parameters of the TCXO used. These need to be taken into consideration when anticipating minimum life time of the developed modules.

Table 2.9. Main parameters of the Petermann-Technik TCXO utilised in the developed sensor and data logger module [38].

Parameter		min.	typ.	max.
Output type			Clipped sinewave	
Output load			10 kΩ | 10 pF (±10%)	
Supply voltage		-5%	1.8 V	+5%
Frequency			38.4 MHz	
Supply current				1.5 mA
Startup time				2.0 ms
Frequency Stability	Vs. temperature (-40…+85 °C)			±0.5 ppm
	Vs. load (load varies ±10%)			±0.1 ppm
	Vs. supply voltage (±5%)			±0.2 ppm
Frequency Tolerance	At 25°C after 2 reflows			±1.5 ppm
Aging per year				±1.0 ppm

From the table above, a further calculation of the total TCXO frequency error can be made. Upon doing this, one must also consider the following requirements:

- Module's centre frequency is calibrated in production.
- The calibration is carried out after a sufficient time has passed since the reflow process. This allows the TCXO to settle.
- The sensor module and data logger module may operate at completely different temperatures.
- The expected minimum life time of the developed module is 10 years.

The total frequency error after 10 years can be expressed as:

$$error_{total} = error_{temperature} + error_{load} + error_{supply} + 10 * error_{aging} \qquad (2.1)$$

With the values from Table 2.9, and by using (2.1), the maximum expected total frequency error of the developed sensor module after 10 years of operation in the field would be:

$$error_{total} = 0.5\ ppm + 0.1\ ppm + 0.2\ ppm + 10\ ppm = 10.8\ ppm$$

This calculated total frequency error needs to be taken into consideration when predicting the minimum needed receiver frequency filter bandwidth. This is because, it must be able to receive long range telegrams supported by the developed protocol (Chapter 3), even after 10 years of operation in the field.

In Figure 2.35, the measured frequency shift of the central frequency in 10 sensor modules has been shown. All 10 modules have been recalibrated and their central frequency set to 925 MHz, 3 years ago. During this time, the modules were in operation for approximately 1/3 of the time, and the remaining time they were stored and not in use. The main contributor to the central frequency shift is the frequency error, due to the crystal aging.

Upon comparison with the expected values from the crystal datasheet [38], the measured frequency shift values are much lower than those estimated and expected. For all tested modules, the frequency shift occurred towards the lower frequency values. An example of a -301 Hz central frequency shift after 3 years is depicted in Figure 2.36. This result is obtained from a calibrated sensor module (925 MHz) which was deployed after 3 years in storage. This module's central transmit frequency was measured again by transmitting a test CW signal.
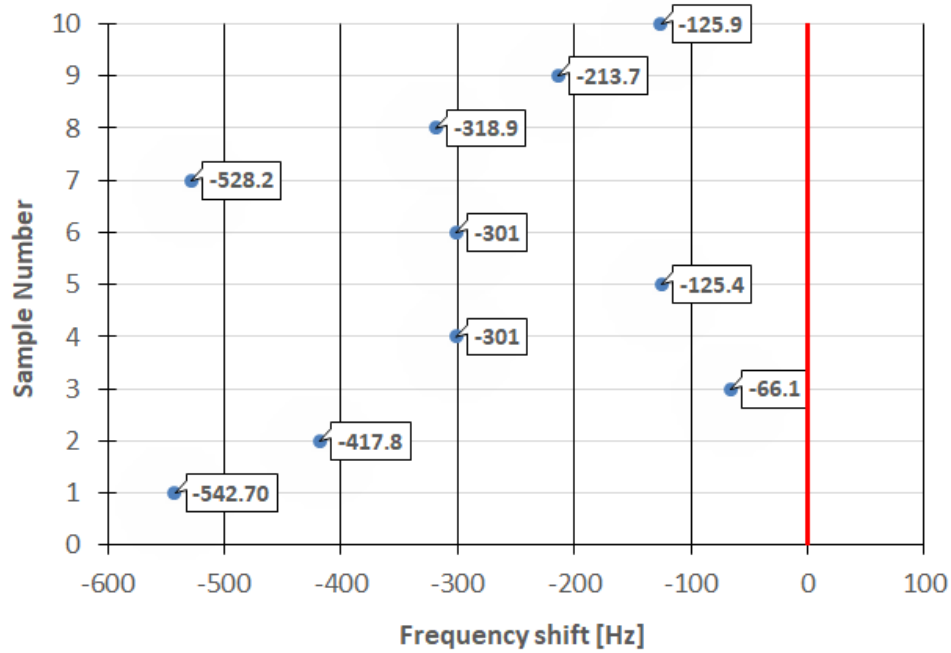
Figure 2.35. Central frequency shift of 10 sensor modules during a time period of 3 years. All 10 modules have been initially calibrated to 925 MHz. The reference 0 Hz frequency shift is represented by the red line.
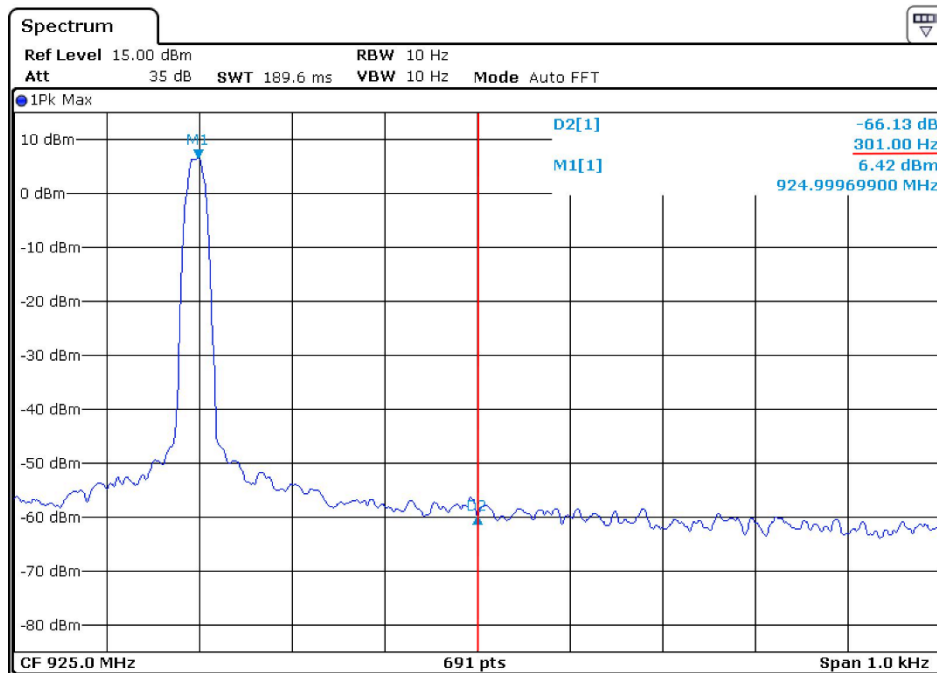
Figure 2.36. A sensor module's central transmit frequency shift due to the crystal tolerances. This data was obtained 3 years after the original sensor module assembly. -301 Hz shift from the initially calibrated 925 MHz has occurred during this time period.

2.1.6. Integrated PCB antenna and the connector for the external antenna

The developed PCB contains an integrated PCB slot antenna, and as well a 50 ohm connector for the external antenna. The output which is used is defined by placing a 0 ohm resistor in the place of the R27 or R28 as it can be seen in Figure 2.37.
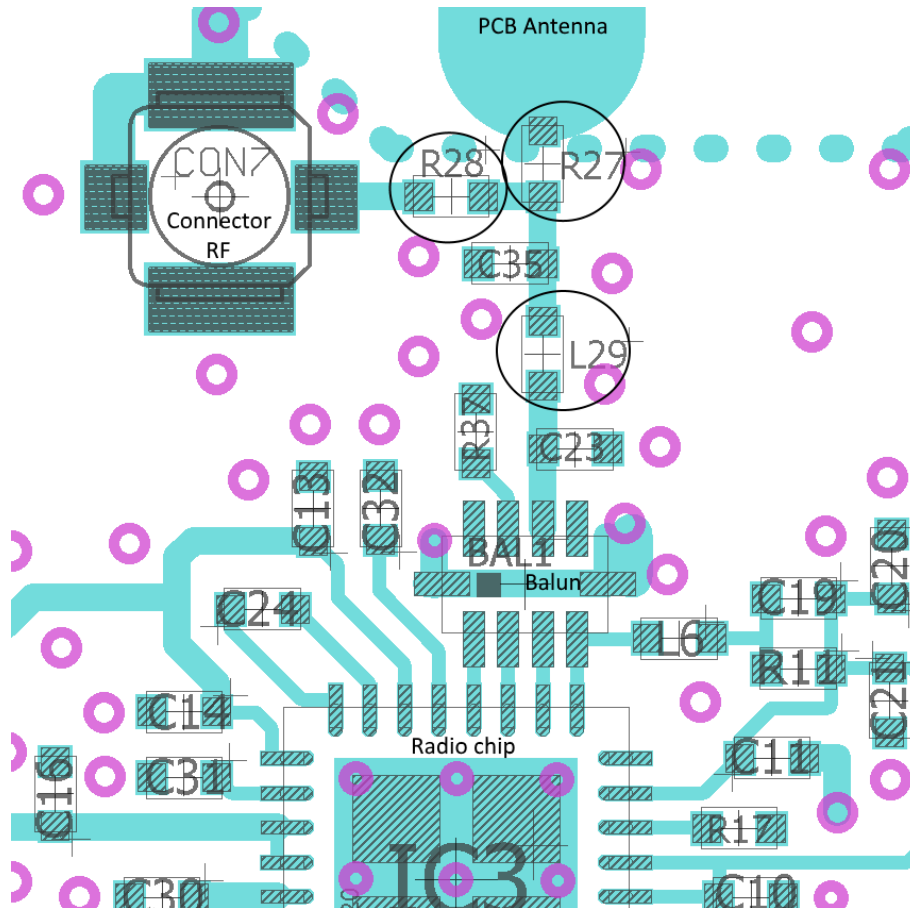
Figure 2.37. RF output stage of the radio chip with connection to the integrated PCB antenna (with 0 Ω resistor R27) or to the 50 ohm connector (with 0 Ω resistor R28).

Absence or placement of either resistor R27 or R28, directly connects the radio chip RF front end to the integrated slot antenna or the 50 ohm connector (CON7) respectively. When the external antenna is used and connected to CON7, passive components C35, L29 and C23 are used for the external antenna matching when needed. The same components can be populated with different values when the integrated PCB antenna is in use and antenna impedance matching is needed. Since the output of the Balun is designed to accept 50 ohm impedance (with a frequency band of 868 to 928 MHz) [36], no additional matching may be required if the integrated PCB antenna is properly designed. Figure 2.38 and Figure 2.39 show the output impedance and the magnitude of the S11 factor of the radio chip RF front end, as seen from

the connector CON7 in the Rx and Tx mode respectively. This data is taken without any external antenna or integrated PCB antenna connected. As it can be seen different matching component values should be used in the T_X and R_X mode. Since for the majority of time, the data logger module is used in the Rx mode as a receiver, it can have one set of values for matching components. Thus, the sensor module as a transmitter could have different matching components. Due to the fact that the modules can have reversed roles in the bidirectional communication mode (Chapter 3.3.2), perfect impedance matching is difficult to achieve. The measurements showed that the impedance in both Tx and Rx mode is close to 50 ohm in the desired frequency range (868 MHz to 925 MHz). Therefore, a compromise is made; CON7 is connected just with 0 ohm resistors to the RF front end. This solution functions sufficiently for connecting the integrated PCB antenna as well. This is evident from Figure 2.41 where the magnitude of the S11 factor of the integrated PCB antenna measured at the CON7 is shown. During this measurement the rest of the circuitry was disconnected by removing the inductor L29. The integrated PCB antenna is originally designed for this frequency.
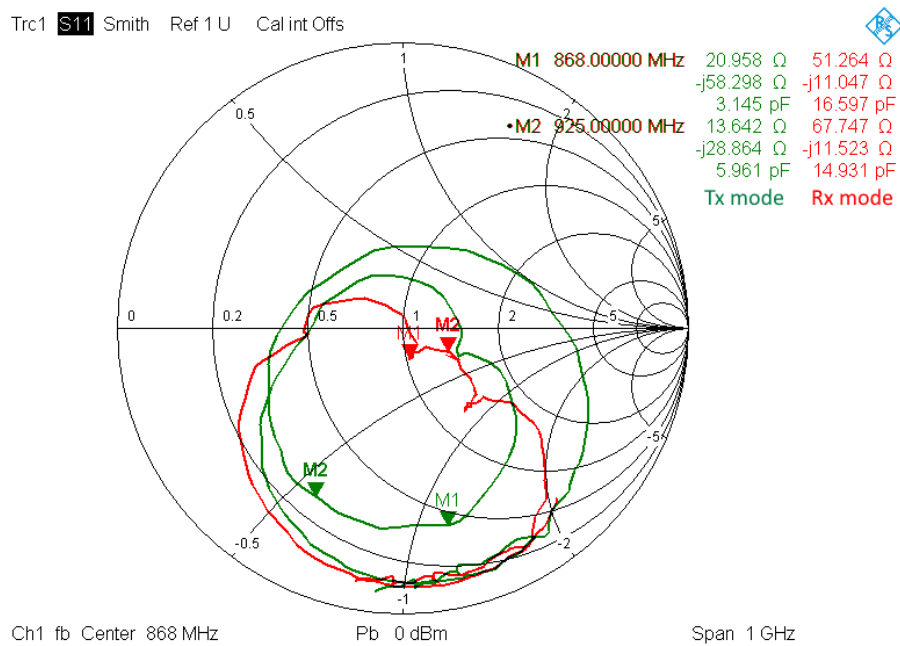
Figure 2.38. Output impedance in the Tx and Rx mode as seen from CON7 when the integrated PCB antenna is disconnected.
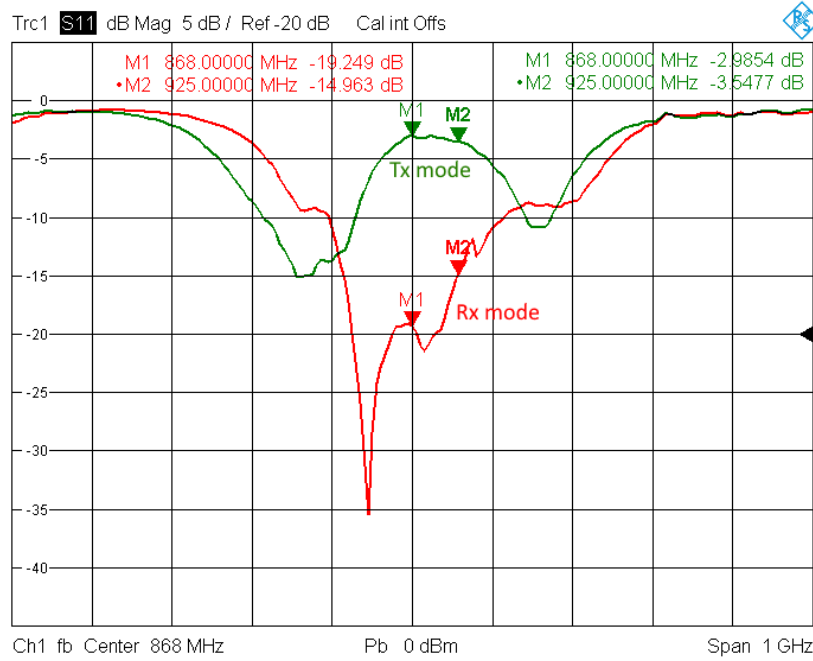
Figure 2.39. Magnitude of the S11 factor in the Tx and Rx mode as seen from CON7 when the integrated PCB antenna is disconnected.
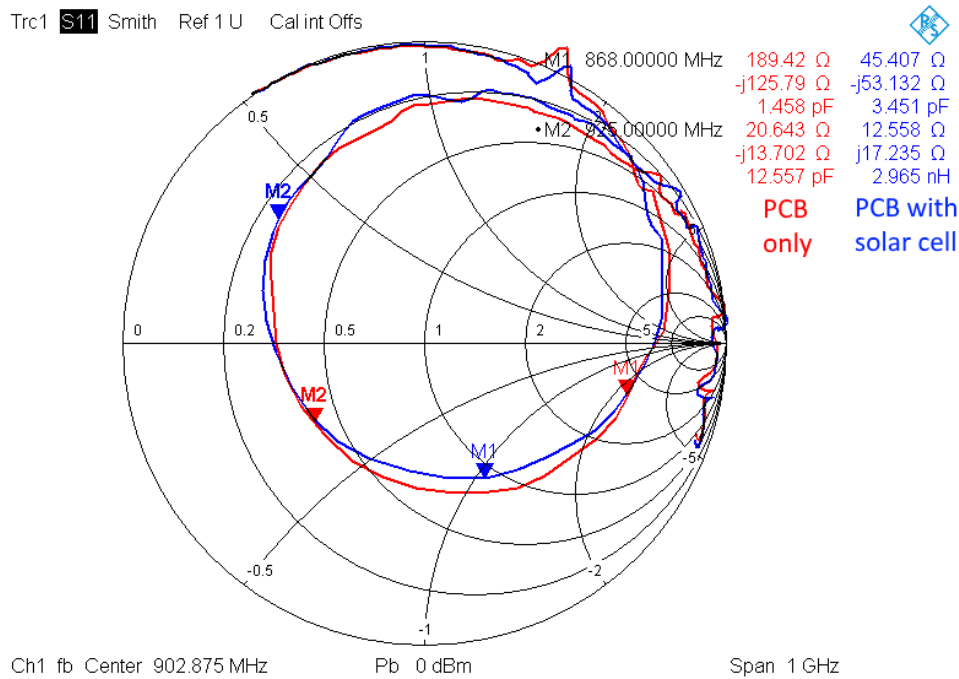
Figure 2.40. Impedance of the integrated PCB antenna measured from CON7. This is done when the rest of the circuitry is disconnected (by removing L29 in Figure 2.37). The measurements are done without a solar cell placed on the bottom side of the PCB (red line) and with the placed solar cell (blue line). The markers are placed at two different transmit frequencies, 868 MHz (M1) and 925 MHz (M2) respectively.
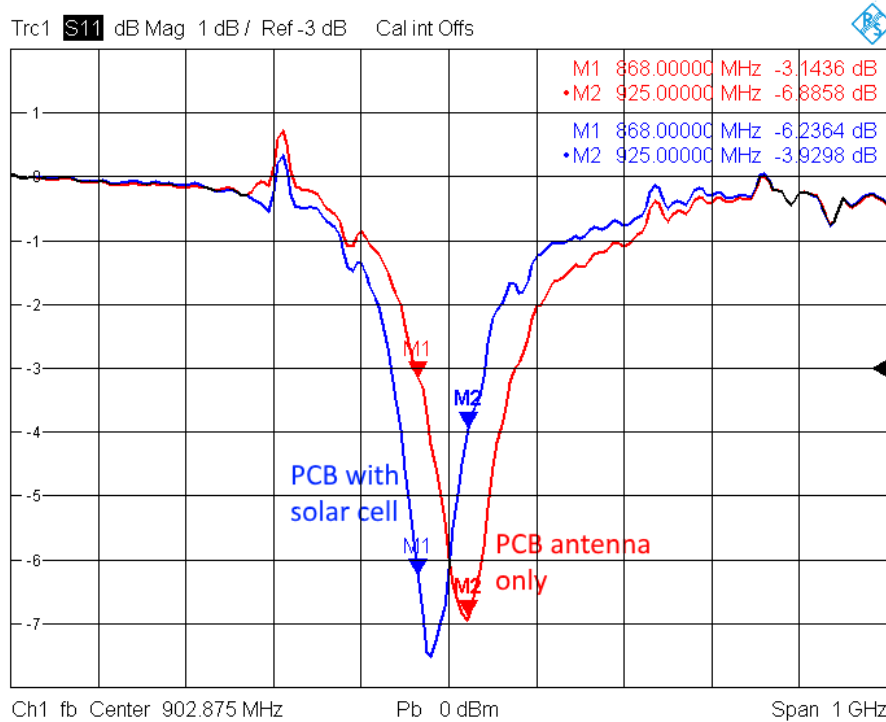
Figure 2.41. Magnitude of the S11 parameter of the integrated PCB antenna measured from the CON7 when the rest of the circuitry is disconnected by removing L29. The measurements are done without a solar cell placed on the bottom side of the PCB (blue line) and with the placed solar (red line). The markers are placed at two different transmit frequencies 868 MHz and 925 MHz respectively.

Should another transmit frequency be needed for the sensor system, apart from changing the radio chip frequency register value, antenna impedance matching can be performed also, based on the above figures. One example of integrated PCB antenna matching component values for the exact 868 MHz frequency is provided in the Figure 2.42. The calculations and simulations shown are done with the Optenni Lab tool.
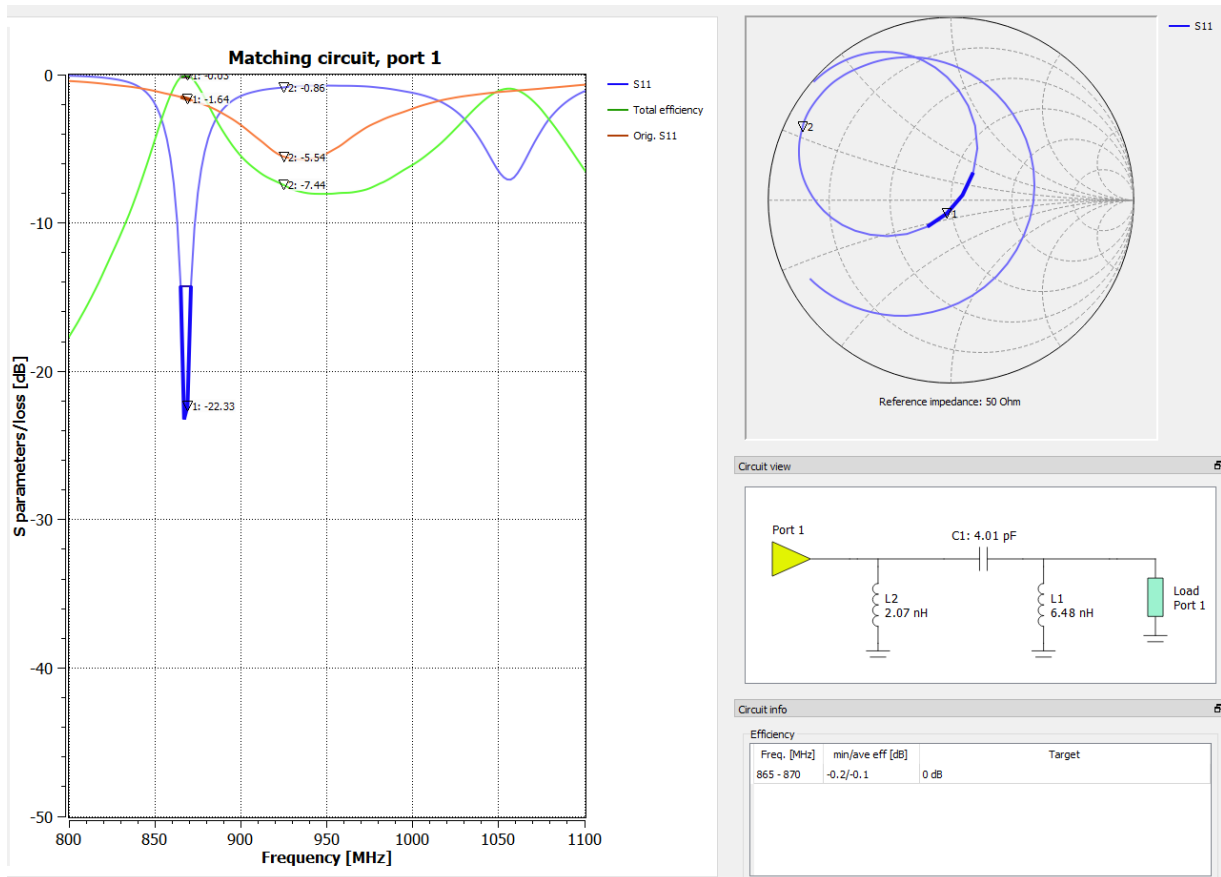
Figure 2.42. Integrated PCB antenna impedance matching for 868 MHz. On the right, the Smith diagram with the matched antenna impedance is shown complete with the matching components. The brown line on the left shows the initial measured S11 parameter. This is done when the solar cell was placed on the bottom side of the PCB antenna.

To achieve full long range potential of the developed sensor system, an external antenna with a higher gain should be used. Different types of external antennas which can be connected to CON7, for both a sensor module and data logger module are given in the Chapter 2.3.2.

Although, range tests at the lake (Chapter 5.2) showed that an 8 km transmission range is achievable even when the integrated PCB antenna is used on the sensor module. The gain of the integrated PCB antenna is -0.1 dBi. Measurement results obtained from the anechoic chamber in the certified measurement laboratory by the two-antenna method [39] are provided in the Table 2.10. The integrated PCB antenna gain is determined by comparing conducted RF power measured on the CON7, with the EIRP from the known substitution antenna.

Table 2.10. Integrated PCB antenna gain measurement values.

Radiated Measurement				Conducted Measurement	Calculated
Receiver reading	Substitution power	Substitution Antenna Gain	E.I.R.P	Antenna Power	Antenna gain
[dBm]	[dBm]	[dBi]	[dBm]	[dBm]	[dBi]
-32.45	14.35	-7.85	6.5	6.6	-0.1

Figure 2.43. Integrated PCB slot antenna. View from the bottom side of the PCB with the attached solar cell.

2.2. Sensor module interfaces

As seen in Figure 2.44 the developed sensor module has three dedicated external communication interfaces, represented by the three external connectors (excluding the external antenna connector). The two connectors at the bottom of the module are used for the two external sensors (Sensor Interface 1 and 2 respectively). The other is a side connector (Host Interface) used for sensor module programming and establishing serial connection with the PC.

Each connector has 10 pins, some of which are signal lines and others power lines, as described in the following chapters.
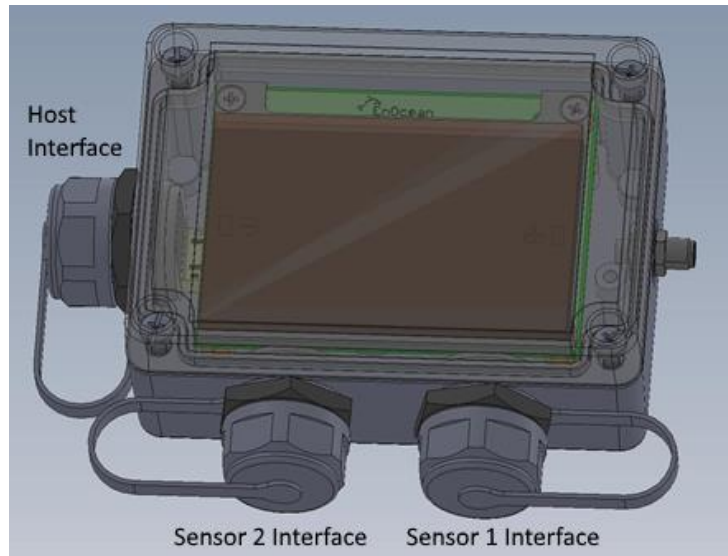
Figure 2.44. Drawing of the developed sensor module placed inside the plastic housing with the marked interfaces.

2.2.1. Host interface

The host interface of the sensor module is primarily intended for debugging purposes and firmware updates, but can also be used to trigger telegram sending, charge the supercapacitor or read stored telegrams from the flash memory. When the developed PCB is used as a data logger module, it is permanently powered via the host interface. The receiving and logging of telegrams on the PC is also done via same interface. In chapter 2.3.1 differences between the sensor module and data logger module PCB assembly are described.

Table 2.11. Types of signals in the host interface.

Data lines	2 Signals (UART RX and UART TX)
Programming lines	2 Signals (Spy-Bi-Wire TCK and TDIO)
Control lines	2 Signals (Inputs Learn and Trigger)
Power Supply	2 Signals (External Positive Supply +3.3 V and Ground)

Table 2.11 shows types of signals present in the host interface, while Table 2.12 summarises pin assignment in the host connector.

Table 2.12. Pin assignment in the Host connector.

Pin 1	VCC	External positive power supply (+3.3 V)
Pin 2	IO 1	Trigger pin to force Data radio telegram sending.
Pin 3	UART TX	UART Tx line
Pin 4	TDIO	Spy-Bi-Wire data line

Pin 5	IO 2	Learn pin to force Teach-in radio telegram sending
Pin 6	TCK	Spy-Bi-Wire programming clock line
Pin 7	UART DET	Signal to detect host cable connected
Pin 8	UART RX	UART Rx line
Pin 9	GND	Ground
Pin 10	GND	Ground

As seen in the tables above, the host interface can be used to provide an auxiliary power supply to the sensor module. This might be beneficial during test in certain indoor situations where charging via the solar cell would be insufficient.

When the host cable is connected, the sensor module recognises this via pin 7. If the sensor module is in the deep sleep mode it will wake up and prepare for the serial communication with the PC via UART lines (Chapter 4).

As seen in Figure 2.45, on pin 7 at the PCB connector side, there is a 30 MΩ resistor (R47) used to minimise the current loss towards ground when the host cable is connected. With the added resistor this current is about 100 nA. Due to this, it becomes irrelevant since the host cable receives a constant supply from the PC. On the same figure, resistor R53 can be seen. Its role is to limit the potential current flowing towards the UART detection pin.

When the same PCB is used as the data logger module (Chapter 2.3) neither of these two resistors are assembled. This is because the data logger module is always in an active mode, and is powered via pin 1 of the host interface. Therefore, additional detection of a host cable plug-in is not needed.

A cable for the host interface is specially designed for the developed sensor system. On one end is the USB plug with the integrated FTDI chip (TTL-232RG-VREG3V3-WE), which is a TTL (Transistor-Transistor Logic) to USB serial converter. It supports +3.3 V based TTL level UART signals and has a +3.3 V / 250 mA rated power output. On the other side of the cable is, depending on the housing (plastic or metal) a plastic RJ-45 plug or a more robust metal pin connector. When the host interface cable is connected to a sensor module or data logger module, the UART communication via a PC virtual COM port will be enabled. Different serial commands can then be executed following the EnOcean Serial Protocol 3 (ESP 3) standard [40]. Using these serial commands, configuration parameters of the sensor module such as frequency, output power, wake up cycle, etc. can be easily changed. This also holds true for the data logger module.
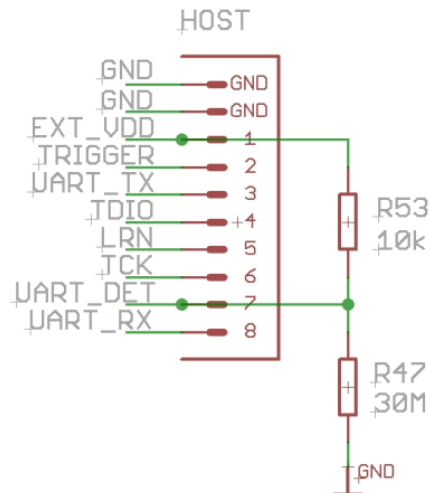
Figure 2.45. Host PCB connector with the assigned pins.

During debug or in test conditions, the host interface can also be used to manually trigger the transmission of both types of telegram; teach-in or data telegram (structure of these telegrams is described in chapter 3.4.) This is done via the signals IO 1 and IO 2 from Table 2.12.

2.2.2. Sensor interface

Two sensor interfaces are used to connect the external sensors to the sensor module and start the system. Without the external sensor connected to either the Sensor 1 or Sensor 2 interface, the entire sensor module circuitry (except charging circuitry) is disconnected from the supercapacitor. This separation point is displayed in Figure 2.4, represented by the non-assembled resistor R44. This implies that during sensor module storage, transport or when the module generally is not in use, the available energy from the supercapacitor is not drained by the rest of the circuitry. The only current drained from the supercapacitor during this time is due to leakage current. However, this can be easily compensated by charging via a solar cell if there is any light present. As previously shown in Figure 2.27, with the supercapacitor voltage decrease of an only 1.5% during 3 years of storage, this mechanism has proved to be very efficient in preserving supercapacitor's charge.

Besides allowing an entire sensor module to start up, the sensor interface contains communication lines towards external sensors. Table 2.13 outlines all the signal types available on the sensor interface.

Table 2.13. Types of signal available on the Sensor interface.

Analog Interface	2 Analog inputs (0 – 2.5 V)
Digital Interface	2 Digital inputs (shared with analog interface)
Serial Interface	I²C lines (SCL and SDA signals)
Power Supply	2 Outputs (permanent and MCU-controlled supply)
	1 Input (supply voltage enable bridge)
Sensor Detection	1 Input (to detect sensor plug-in)

The pin assignment of the sensor interface is defined in Table 2.14.

Table 2.14. Pin assignment in the Sensor interface connector.

Pin 1	ADIO1	Analog or digital input 1
Pin 2	VCC	Permanent positive power supply (3.6 V – 2.5 V)
Pin 3	SDA	I²C data line – SDA
Pin 4	ADIO2	Analog or digital input 2
Pin 5	PWR_CONT	MCU controlled positive power supply (3.6 V)
Pin 6	VDD	Main circuitry supply voltage (3.6 V – 2.5 V)
Pin 7	PRES_DET	Sensor presence detection and sensor recognition
Pin 8	SCL	I²C clock line – SCL
Pin 9	GND	Ground
Pin 10	GND	Ground

From the two tables above, it is evident that different types of sensors can be connected to the sensor interface. Sensors with analog outputs are intended to be connected on pin 1 and pin 4 respectively. One example is the ambient temperature and relative humidity sensor (EE060 from E+E Elektronik). This sensor is adapted to fit the developed sensor module and its external connectors. To pin 1 it delivers an analog value of the ambient temperature, while on the same connector, to pin 4 it delivers an analog value of relative humidity. On the second sensor interface, e.g. adapted soil temperature sensor (DS18B20 from Maxim Integrated) can be connected, which to pin 1 delivers a digital value of soil temperature. More information concerning the type of sensors adaptable to the developed sensor module can be found in Chapter 5.2.1. Following the aforementioned, the state of pin 1 and pin 4, depends on the respective type of sensor connected and detected by the sensor module. Based on this, these pins can be internally reconfigured to accept both analog and digital values.

The type of sensor connected can be detected by the microcontroller via the sensor interface pin 7; the sensor presence detection pin. As seen in Figure 2.46, a 30 MΩ resistor is connected to this pin to form a voltage divider with the resistor, which is contained within the cable of each sensor. The value of these resistors are in mega-ohms to minimise current loss via this pin when a sensor is connected. Only the ambient temperature and relative humidity sensor has no voltage divider resistor. This particular sensor short circuits the sensor presence detection pin with the sensor module supply voltage. When sensor connection is present, current is flowing from the supply voltage through the divider to the ground. The maximum value of this current is 120 nA and is approximately 1/10 of the overall sensor module deep sleep current.

With every microcontroller wake up, the presence detection pin is configured as digital input with the interrupt detection enabled. If a sensor is present, this pin will have a high state and an interrupt flag will be raised. After this, the microcontroller reconfigures this pin as analog and measures the voltage on it. Following (2.2), the microcontroller recognises which type of sensor is connected by comparing the calculated resistor value with those stored in the memory and specific to each sensor. A small margin due to the sensor detection resistor tolerances (±1%) is taken into consideration during calculations.

The remaining pins, besides the I²C lines, are power pins. Pin 2 in the sensor interface is the direct connection to the positive electrode of the supercapacitor and it is used for the previously mentioned bridge connection with pin 6.

When connected, each sensor short circuits pin 2 and pin 6 on the PCB connector as seen in Figure 2.46.

$$R_{sensor}[\text{MΩ}] = \frac{30(V_{cc} - V_{det})}{V_{det}} \qquad (2.2)$$
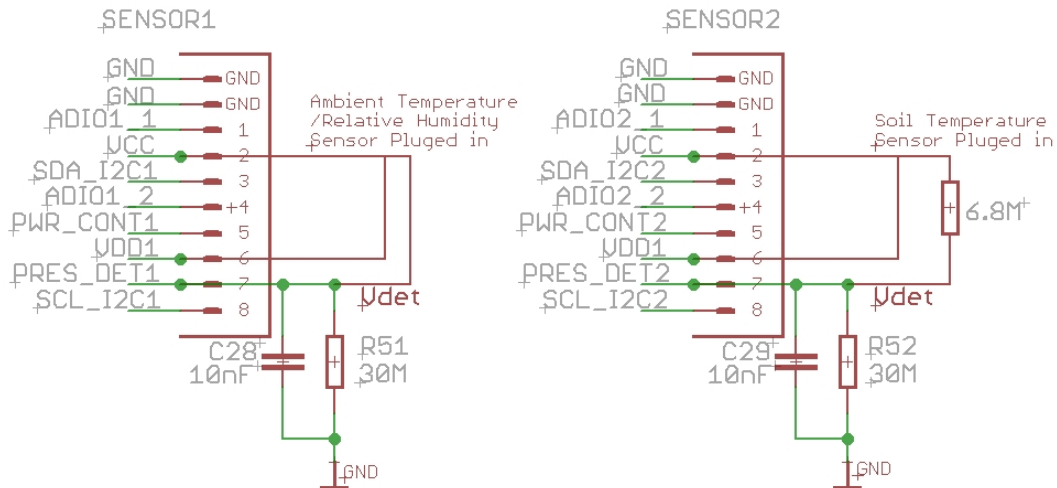
Figure 2.46. Sensor connectors on the PCB side with the 30 MΩ resistors used for external sensor recognition and detection. Examples are given for an ambient temperature and humidity sensor on the sensor connector 1 and a soil temperature sensor on sensor connector 2. The wire connections marked in red are present only when sensors are connected.

All the sensors receive their supply via pin 5, which has a stable 3.6 V output from the step-up converter TLV61220 from Texas Instruments [24]. This converter is enabled/disabled by the microcontroller and is only used when the connected sensor needs to be powered to perform a measurement (Figure 2.47). Resistor R23 is not assembled and is used for test purposes to bridge the step-up converter.

Figure 2.47. Voltage step-up converter to ensure a stable 3.6 V supply for the connected sensors.

Pins 3 and 8 in the sensor interface are the I²C communication lines. Sensors with an I²C digital output can be connected to these pins. An example of this is the ambient illuminance sensor, featuring MAX44009 from Maxim Integrated, which is developed from scratch specially for this sensor module.

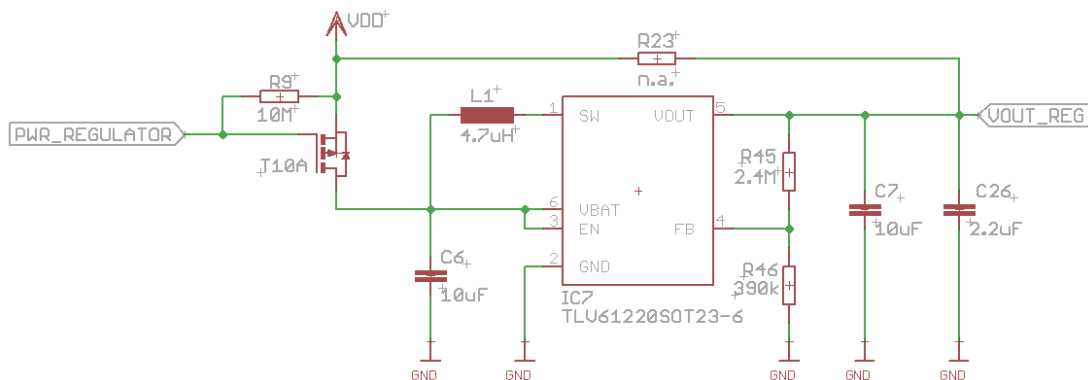Since two sensors of the same type can be connected to the sensor module, if they have same I^2C addresses it will not be possible to communicate with them when they are both powered simultaneously. To overcome this, 2-channel I^2C-bus multiplexer PCA9540B from NXP [41] is integrated on the sensor module PCB. As a standard part of the sensor interface, this component allows the microcontroller to communicate with only one sensor at the time when two sensors are present on the I^2C lines. To keep the same voltage levels on the supply lines and communication lines of the connected sensors, the I^2C-bus multiplexer needs to be powered with the stable voltage. For this purpose, a stable 3.6 V output is used from the above mentioned voltage step-up regulator. Figure 2.48 shows I^2C-bus multiplexer lines towards the sensor interface. Pull-up resistors on these lines have to be contained within connected sensor.
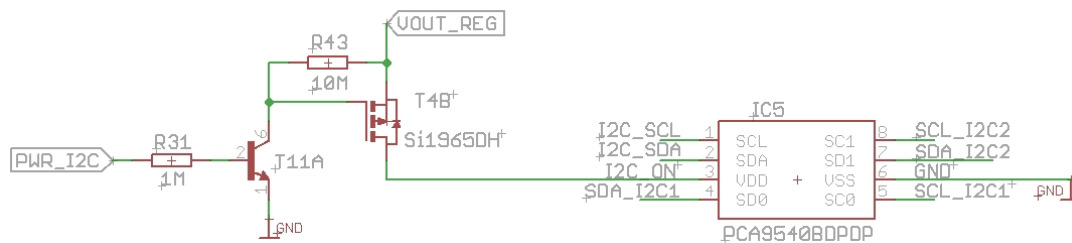
Figure 2.48. 2-channel I^2C-bus multiplexer controlled by the microcontroller and supplied from the voltage step-up converter output.

2.3. *Data logger module hardware architecture*

In parallel with the development of a sensor module, its counterpart, which will be able to receive transmitted telegrams and understand the carried information inside the telegrams, has been developed. Much research focuses only on one end of the communication channel, and it is usually the sensor node (mote) side development [14], [16], [42], while for the receiver, off-the-shelf solution is usually utilised [14]. However, to achieve long range communication, the receiver architecture and it configuration plays a major role. The block diagram of the developed data logger module is depicted in Figure 2.49. Depending on the type of communication mode configured (Chapter 3.3), the data logger module can operate as a transceiver.

Figure 2.49. Data logger module block diagram.

If this block diagram is compared with that of the sensor module shown in Figure 2.2, it is obvious that they share the main parts such as: microcontroller, radio chip, flash chip and crystals. However some sections such as energy management circuitry or sensor connectors are missing. The sensor module and da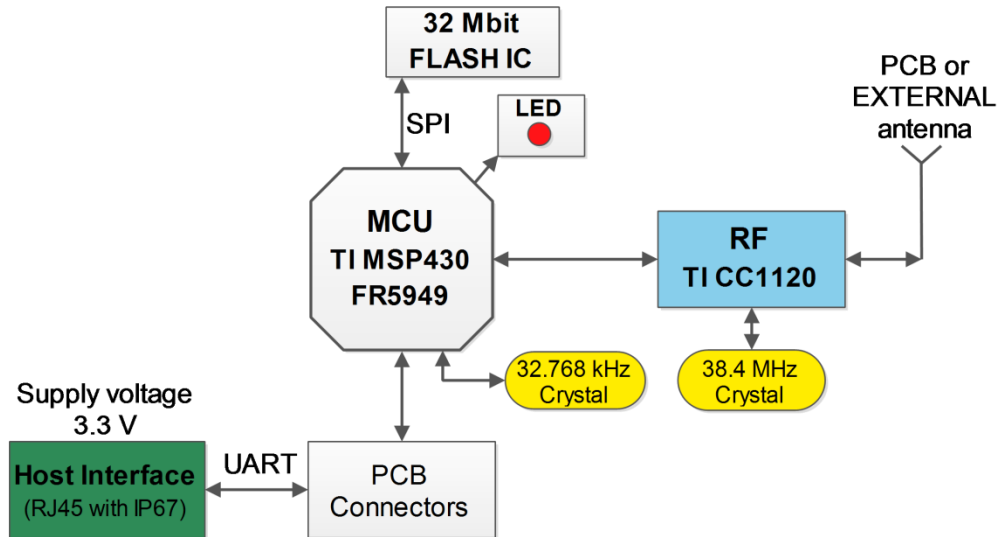ta logger module share the same PCB design; the differentiation arises from the components which are not assembled when the PCB is used as a data logger module.

2.3.1. The difference between the hardware platform of the sensor and data logger module

The major and the most evident difference upon comparing hardware architectures, the omitted complete energy management circuitry and supercapacitor, of the data logger module. The data logger module is permanently powered by the PC via the host interface and the earlier mentioned, accompanying USB cable with the FTDI chip. Any other external voltage source can be used, ensuring that the maximum supply voltage level does not exceed 3.6 V.
The data logger module has also no sensor connectors assembled on the PCB or any other circuitry which is related to the sensor interface described in the previous chapter. The step-up voltage convertor used to power the sensors, and the I^2C-bus multiplexor used to communicate with the sensors or solar cell, are as well not assembled (Figure 2.50).

The main difference in the radio output stage of the two hardware modules is that the data logger module is intended to be constantly used with the external antenna instead of the integrated PCB antenna. Otherwise, long range reception will be compromised.

Having one PCB design for two different hardware modules, reduces costs, test effort, minimises unknowns regarding component behaviour and forms the first step towards an entire sensor system development optimisation.
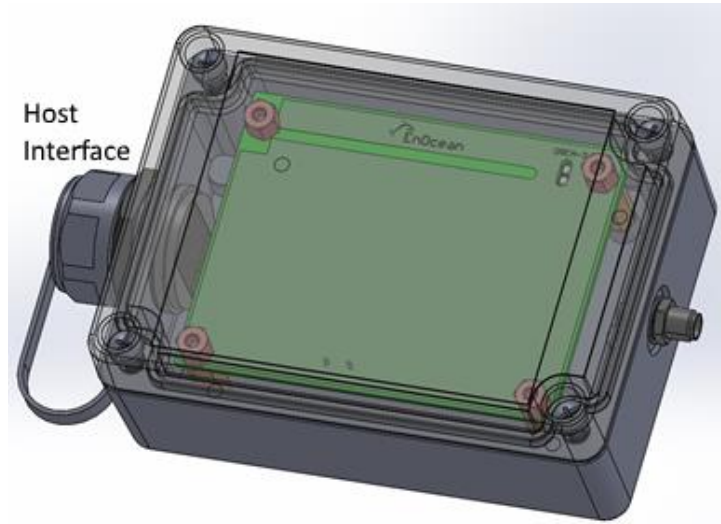
Figure 2.50. Data logger module PCB inside housing (bottom view of the PCB is seen).

2.3.2. External antenna types

Two different types of the external antennas are intended for the data logger module. Small omnidirectional (monopole) antennas with the antenna gain of up to +3 dBi have been investigated. Another type is a high gain panel type antenna (up to +14 dBi) for high performance and truly long range operation. Depending on the type of the antenna used, and not to violate radio norms, the output power of the data logger module needs to be adjusted accordingly (Figure 2.51) [43].
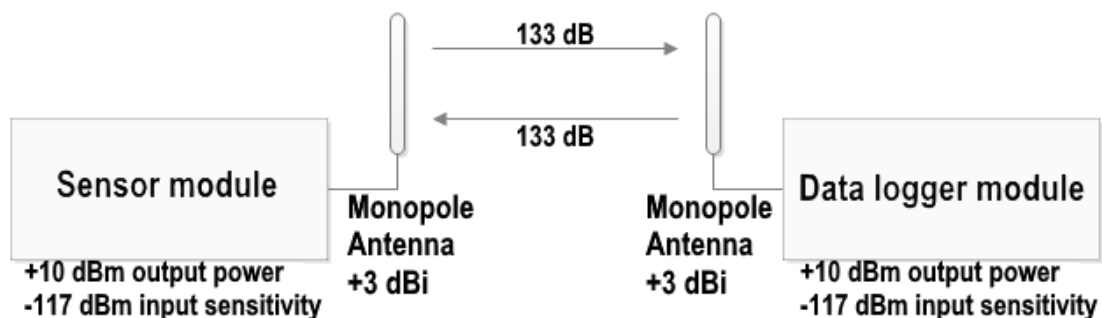
Figure 2.51. Uplink and Downlink budget when the monopole antenna is connected to a data logger module.

Due to this, only the uplink budget for the transmissions from the sensor module towards data logger module can be improved by using a high gain antenna (Figure 2.52). For the downlink

(transmissions from data logger module towards sensor module) the link budget improves only 3 dB, due to the fact that the data logger module output power has been decreased.
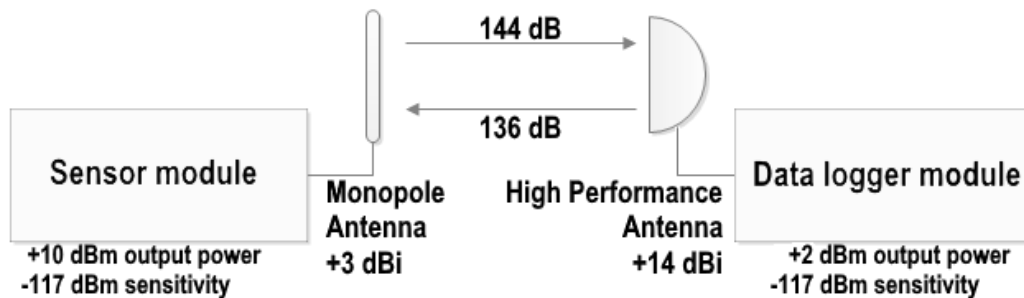
Figure 2.52. Uplink and Downlink budget when the high gain antenna is connected to a data logger module.

To improve the achievable range, the sensor module should also always have a small external omnidirectional antenna connected instead of utilising the integrated PCB antenna.

Four different antennas suitable for both the sensor module and data logger module have been tested and the results are summarised in Table 2.15. The measurement setup for the horizontal and vertical antenna polarization is shown in Figure 2.53 and Figure 2.55 respectively. The radiation patterns of the best performing antenna (Antenna #2) are depicted in Figure 2.54 and Figure 2.56 respectively. All measurements have been performed by connecting the antenna under test to the data logger module, which was emitting special continuous wave (CW) test signal at 925 MHz. The output power at the antenna input was measured to be 7.9 dBm. The antenna gain was determined through a comparison with a tuned precise dipole antenna.

Table 2.15. Test of four different antennas suitable for the use with the data logger or sensor module respectively.

Antenna No.	Antenna #1	Antenna #2	Antenna #3	Antenna #4
Manufacturer Marking	ANT-WP915SMA-Y	W5017	1019-045A	1019-008A
Picture				
Maximum gain horizontal	1.6 dBi	3.4 dBi	2.5 dBi	2.3 dBi
Maximum gain vertical	1.1 dBi	3.3 dBi	2.9 dBi	2.4 dBi
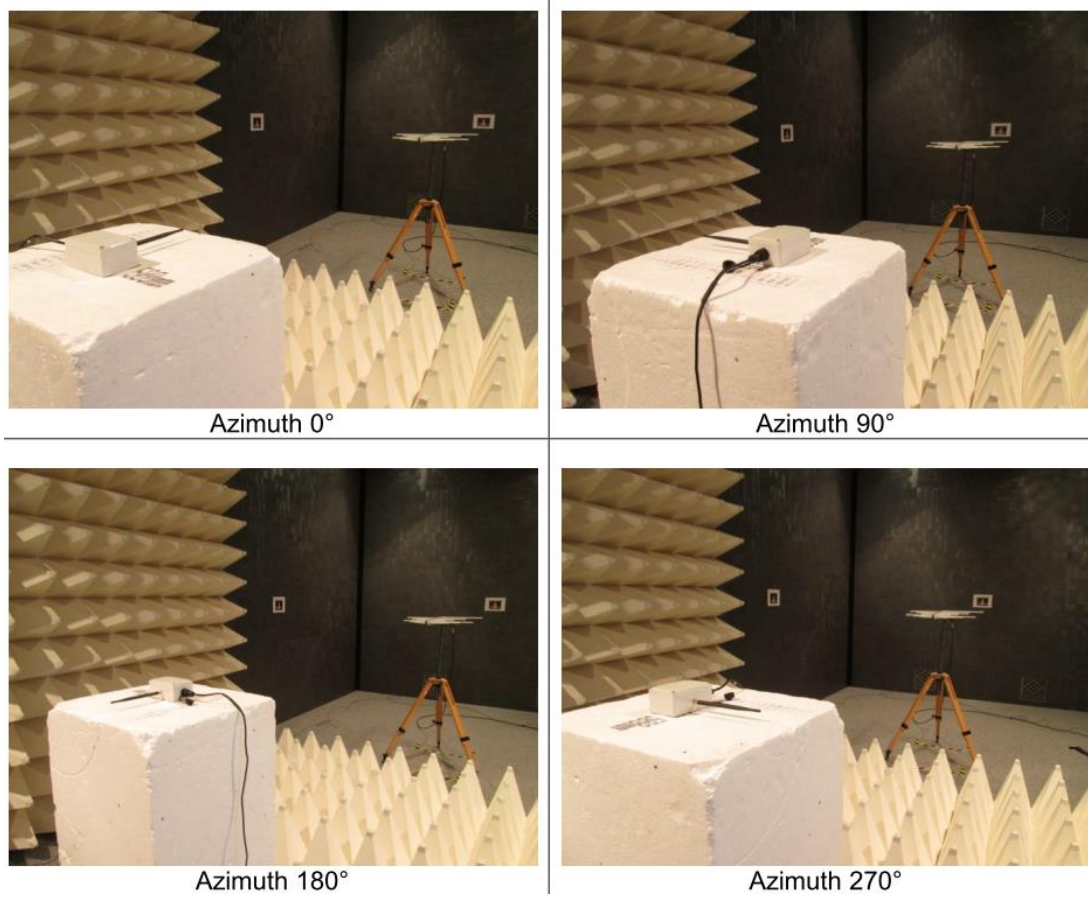
Figure 2.53. Measurement of the radiation pattern for the horizontal antenna polarization.
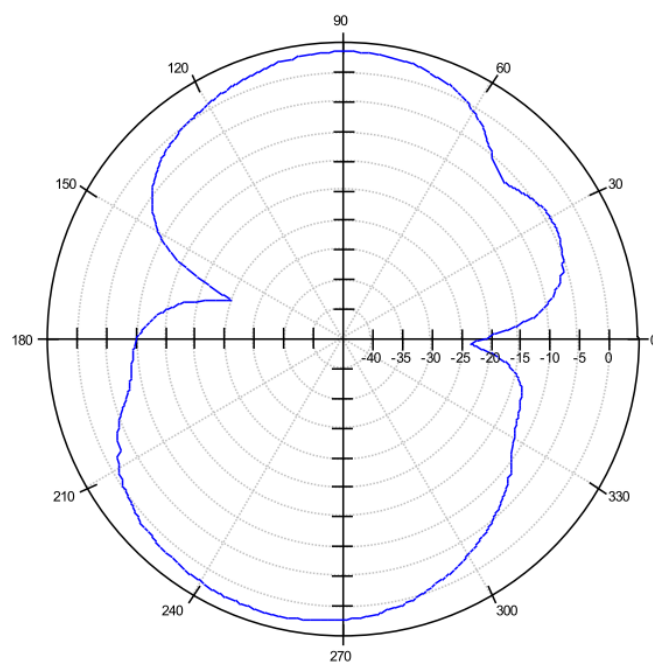
Figure 2.54. Horizontal polarization azimuth chart for antenna #2.
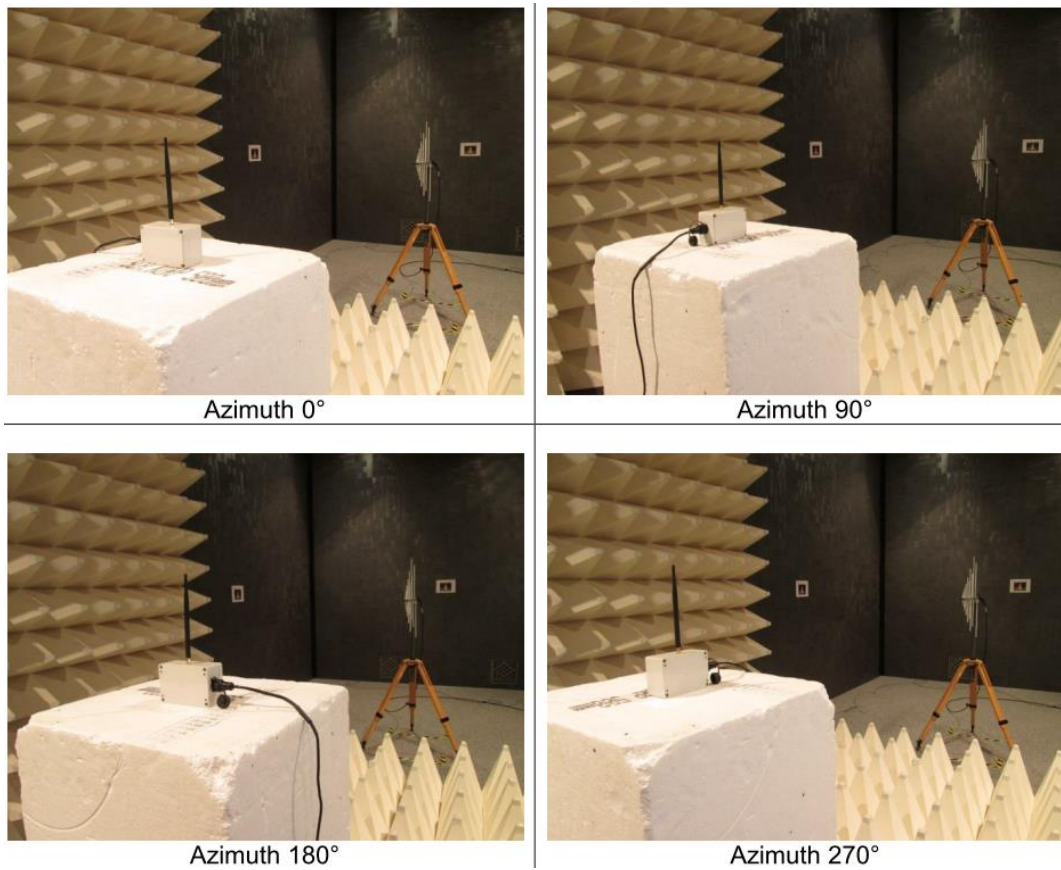
Figure 2.55. Measurement of the radiation pattern for the vertical antenna polarization.
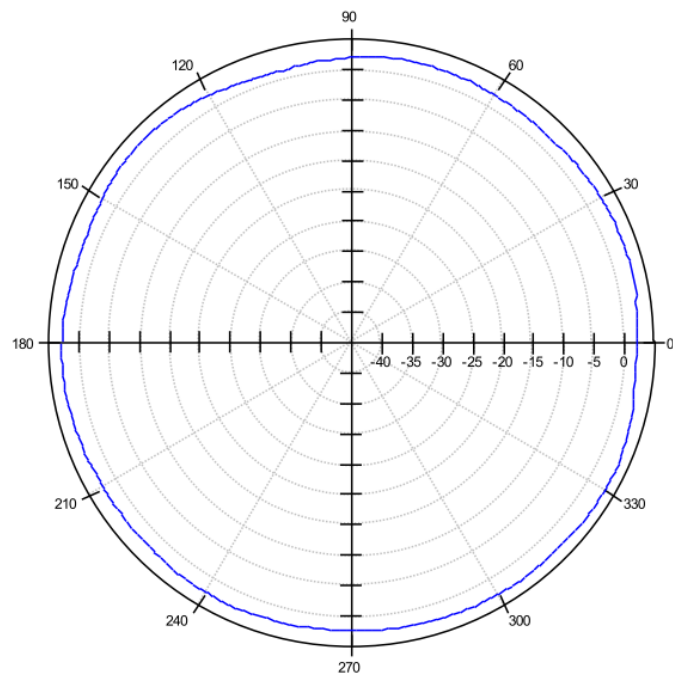
Figure 2.56. Vertical polarization azimuth chart for antenna #2.

The tested high gain antenna is displayed in the Figure 2.57. It is a 900 MHz ARC-IA0913B02 from ARC Wireless, with a measured 12.5 dBi maximum gain.
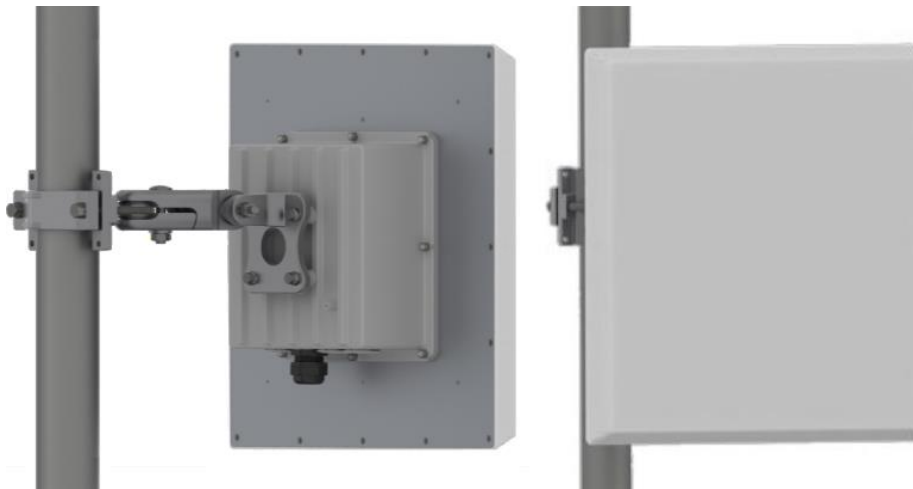
Figure 2.57. A high gain panel type antenna used with a data logger module only.

2.4. One PCB design to support two different wireless modules

To minimize costs, effort and have compact and interoperable sensor system, one PCB design should be shared between a sensor module and a receiver module. This approach has been followed in this thesis. One PCB was designed for a sensor module and data logger module. As mentioned earlier, PCBs will differ after the component assembly. The sensor module has 113 assembled components, while the data logger module has almost half of this, with only 55 components assembled on its PCB.

Both modules use a 2 layer PCB with a total thickness of 1.57 mm, as seen in Figure 2.58 which represents a PCB layer stack. The core of the PCB is standard FR4 (IT-158BS/IT-158TC) material [44].
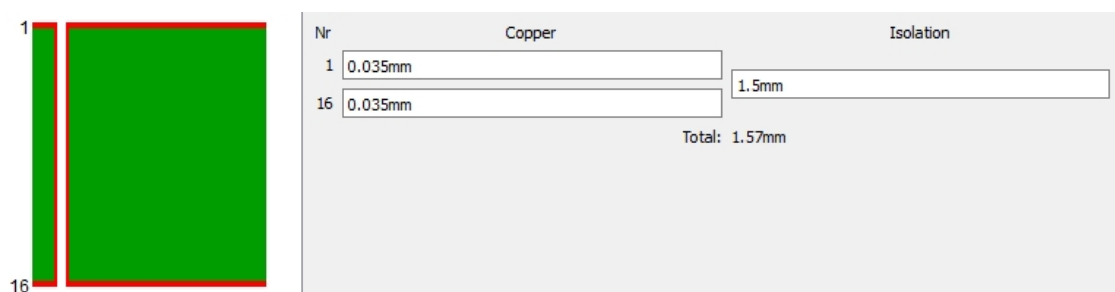
Figure 2.58. PCB stack with the core and copper dimensions.

The dimensions of the PCB are 78 mm x 60 mm. The top and the bottom layer layout, with all the traces can be seen in Figure 2.59 and Figure 2.60 respectively.

Many vias (conductive holes through the PCB layers) have been placed to secure good electrical connection between the top and bottom layer. This forms a solid ground plane and minimises potential noise and its influence on the RF part. The possible source of the unwanted noise on the PCB is the step-up voltage converter [24]. This component is placed in the lower right corner of the PCB (Figure 2.59). This area is diametrically opposite the radio chip and surrounding components which are most susceptible to noise. As seen in Figure 2.59 and Figure 2.60, the step-up voltage converter is isolated from the rest of the copper surface. In both layers it forms a connection with the rest of the surface through only two lines. These lines are the input and output voltage of the step-up converter. Parallel to these lines, in the bottom layer, are two ground lines which connect this isolated island of copper to the rest of the bottom layer surface.
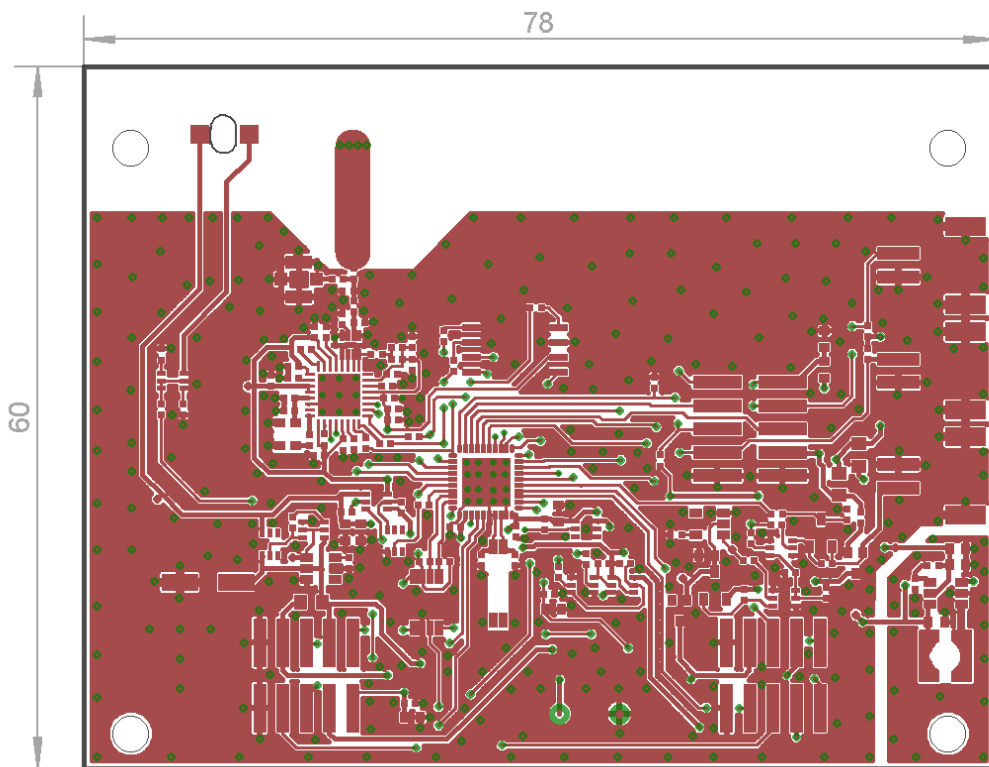
Figure 2.59. PCB top layer with all the copper traces (red) and vias (small green circles) towards the bottom layer.
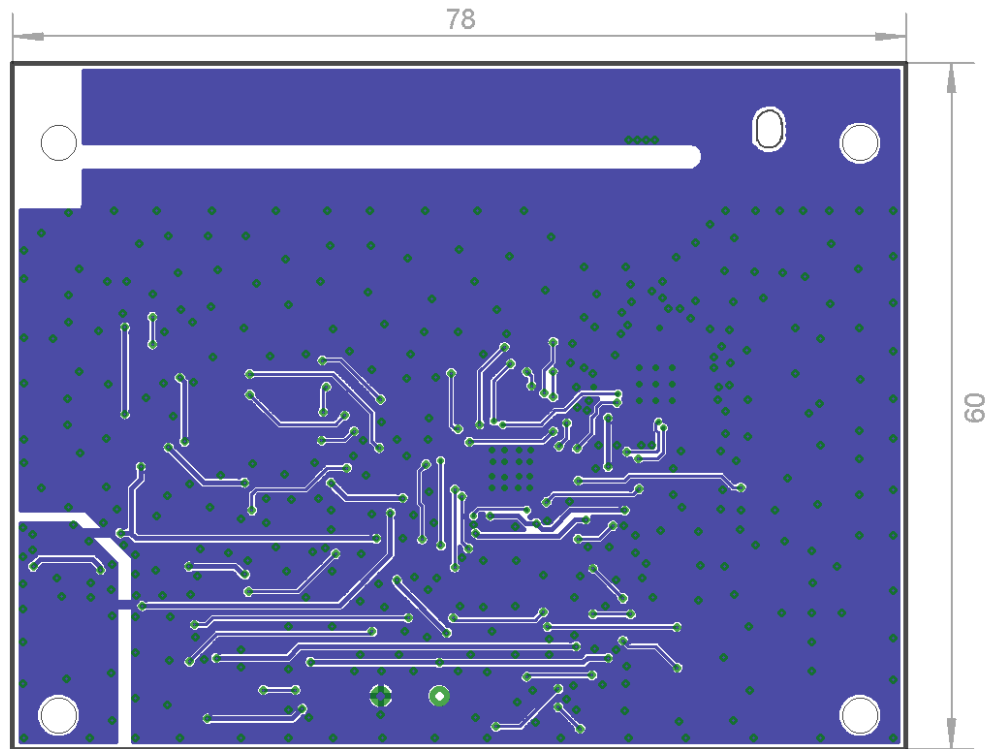
Figure 2.60. PCB bottom layer with all the copper traces (blue) and vias (green circles) towards the top layer.

2.5.   Produced and assembled PCB

In Figure 2.61, the top side of the assembled sensor module PCB with the 40 F supercapacitor can be seen. The component blocks are marked respective to the block diagram described in Chapter 2.1.

In the Figure 2.61 and Figure 2.62, it can be seen that the finished PCB is coated with a special lack (Bectron PL4122-45E BLF FLZ). This is to minimise the potential hazards of the assembled components if there is, for example, high humidity, or in worst case, water intrusion occurs inside the housing due to the insufficient sealing.
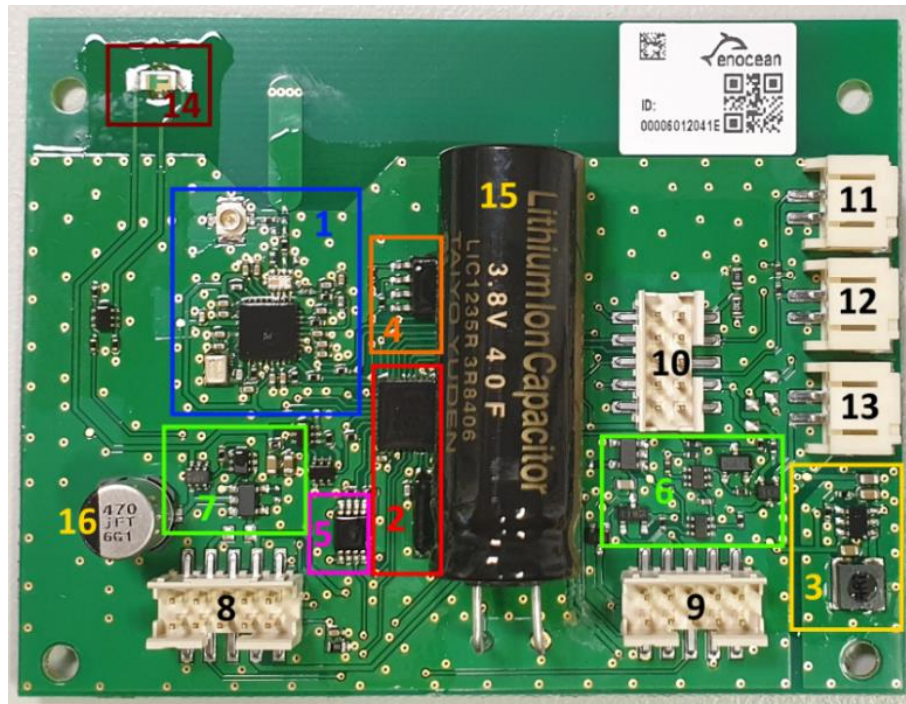
Figure 2.61. Top side of the assembled sensor module PCB with the marked components.
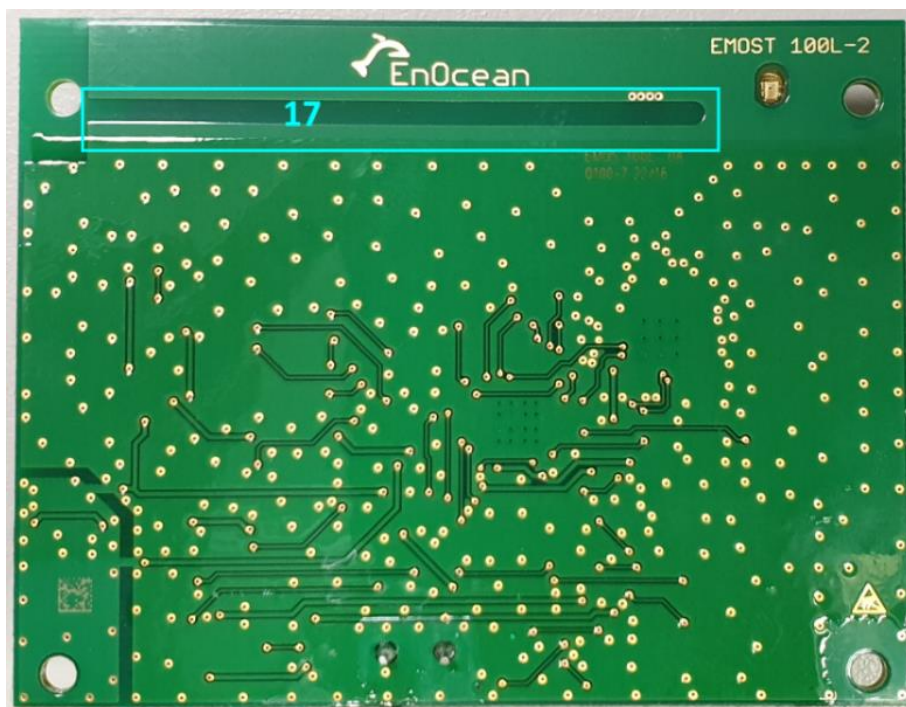
Figure 2.62. Bottom side of the assembled sensor module PCB with the marked integrated PCB slot antenna.

The main components and component blocks in the above figures are marked with numbers and with different colours. These represent the following parts:

1- RF block with the radio chip, TCXO, Balun and external antenna connector and the PCB antenna feed line

2- Microcontroller with the external 32.768 kHz crystal oscillator (tuning fork type)

3- Step-up voltage regulator block with the 4.7 µH power inductor coil (WE 744031004)

4- External flash memory chip

5- I^{2}C multiplexor chip

6- Overvoltage protection block

7- Undervoltage protection block

8- Sensor interface 1 PCB connector

9- Sensor interface 2 PCB connector

10- Host interface PCB connector

11- Learn button connector to trigger Teach-in telegrams (for test purposes only)

12- Trigger button connector to trigger Data telegrams (for test purposes only)

13- Solar cell connector

14- Low power hyper red LED

15- Supercapacitor 40 F

16- Aluminium Electrolytic Capacitor 470 µF for smoother startup on sensor plug-in

17- Integrated slot PCB antenna

Many of these blocks are not assembled when the PCB is used as a data logger module. In Figure 2.63 and Figure 2.64, the top and bottom side of the assembled data logger PCB is given. From all the interface connectors, only the host interface PCB connector is assembled. Since the data logger module does not contain a supercapacitor, the entire overvoltage and the undervoltage protection circuitry is not needed. Through the use of 0 ohm resistor (displayed to the right of the host interface connector in Figure 2.63), the external voltage supply is directly bridged to supply a microcontroller. The bottom side of the PCB remained unchanged when compared to the sensor module assembly. This is because, the bottom side of the PCB does not contain any components.
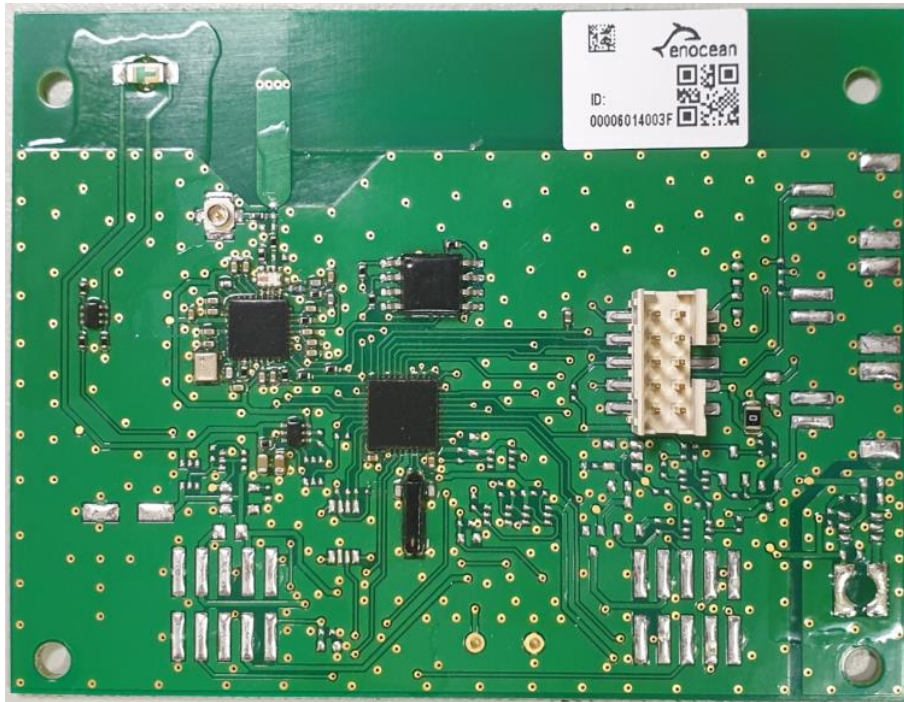
Figure 2.63. Assembled data logger module PCB (top view).

Figure 2.64. Assembled data logger module PCB (bottom view).

3. ENERGY EFFICIENT COMMUNICATION PROTOCOL

To prove that the PCB development was successful and that all the components can successfully interact with each other, an adequate communication protocol is needed.

Keeping in mind some of the base postulates in this thesis:

- The sensor system must support energy harvesting.

- The sensor system should consume the least power possible.

- The measured data must be transmitted over greater distances.

A communication protocol specially designed for energy constrained sensor modules has been developed. Using purely low power electric components is not enough to ensure energy efficiency. Techniques and mechanisms for harvesting and saving energy are implemented in the developed communication protocol. Thus, making it not only functional but also energy efficient. The proposed protocol optimises the way in which information is collected from the environment, packed and transmitted over long distances using minimum energy.

The gathered information is transmitted in a form of two different packet types called Teach-in (TI) and Data telegrams (DT), respectively. Beyond configuring a sensor module or data logger module as a transmitter or receiver, the developed communication protocol allows it to also operate in two different communications modes: unidirectional and bidirectional. The main difference between these two modes lies in how the sent telegrams are acknowledged on the receiving side [8].

Some radio norms can have limitations on the total radio ON time per transmission [43]. If needed, the subtelegrams can be split into shorter parts so that the radio ON time per transmission is shorter. In this case, the subtelegram needs to be merged again on the data logger side. This mechanism is called telegram chaining and it is also part of the developed communication protocol (Chapter 3.6).

From the communication protocol perspective, all the sensor module and data logger module functionalities described in this chapter are enabled through the use of different protocol layers. Following the OSI (Open Systems Interconnection) layer model [45], the specific protocol layer architecture is developed as shown in Figure 3.1.

Layer	Data Unit	Description	Status
7. Application	Data	Generic Profiles coding	Defined
6. Presentation			Not used
5. Session			Not used
4. Transport	Datagram	Telegram chaining	Defined
3. Network	Packet	Subtelegram timing, Carrier sense, Listen Before Talk, Repeater functionality	Defined
2. Data Link	Frame	Subtelegram structure, Hash Algorithms, Header Compression, Acknowledges	Defined
1. Physical	Bit	Frequency, Modulation, Preamble, Sync, Coding, Length	Defined

Figure 3.1. The communication protocol layer architecture.

3.1. Physical layer

The developed sensor system is open for communication in the unlicensed sub-1 GHz frequency band. Limitations can come from the radio chip performance and radio regulation norms. This depends on where the sensor system will be installed and used. Examples of the standard transmission frequencies used include 868 MHz for Europe, 902 MHz for USA and 925 MHz for Japan. Transmitting on higher frequencies would decrease the achieved range due to certain radio signal propagation characteristics [1]. The modulation used is 2GFSK (Gaussian shaped Frequency Shift Keying), in which baseband pulses are first passed through a Gaussian filter with BT (bandwidth-symbol time) product = 0.5, and then modulated. This spectrum shaping feature reduces the adjacent channel power (ACP) value, as well as the occupied bandwidth [46]. A Gaussian filter allows a very narrowband frequency modulated signal with a frequency deviation of just 1.875 kHz. This results in a narrower occupied spectrum which is less susceptible to interferences, allowing transmission over greater distances [1], [47]. Conducted range tests showed that a range greater than 3 km is easily achievable with only 11 dBm of output power.

Other modulation techniques like spectrum spreading [1], [6] have a broad spectrum and require special coding schemes to extract useful signals from the channel noise. Adding redundant bits can make the system more robust but they also increase transmitter ON time. Table 3.1. compares the transmitter ON time of the developed sensor module and the commercial LoRa spread spectrum system, for the same telegram structure and similar data rates.

Table 3.1. Comparison of the narrowband (2GFSK) system transmit time to the spread spectrum system (LoRa®)
for different attached sensor combinations [8].

Sensor type	2GFSK, BT = 0.5, 1.25 kbps	LoRa, SF 10, BW = 125 kHz, 0.98 kbps
	Telegram transmit time [ms]	
Temperature and humidity	160.0	327.53
Illuminance	153.6	327.53

If the developed sensor module would use an identical bit rate as the spread spectrum module, the maximum transmit time would still be around 36% shorter in comparison.

3.2. Receiver sensitivity

When choosing a proper symbol rate there is a trade-off between receiver sensitivity and transmission time. Receiver sensitivity is one of the most important parameters, and at the same time the main limiting factor when designing a long range system. Receiver sensitivity can be defined as a minimal received signal strength ("weakest" signal) from which a receiver can still successfully demodulate and retrieve originally transmitted information. Receiver sensitivity level depends primarily on the receiver architecture noise figure and the receiver channel (filter) bandwidth [46]. Increase of the receiver filter bandwidth is needed to compensate for expected frequency errors (Chapter 2.1.5.1), between a transmitter and a receiver. Thus, the receiver sensitivity will be always below the theoretical Rx noise floor. The theoretical, absolute noise floor ("noise power") at room temperature assumes that the channel capacity is 1 bit per Hz of bandwidth (the required SNR is thus 0 dB). This can be calculated from (3.1) [17].

$$P_{nABS} = 10 \log_{10}(k \times T \times B \times 1000) \ [dBm] \tag{3.1}$$

Where:

P_{nABS} = equivalent noise power (dBm)

K = Boltzmann's Constant (~1.38 x 10^{-23})

T = 293 kelvin ("room temperature")

B = channel bandwidth (Hz)

1000 = scaling factor from watts (W) to milliwatts (mW)

Using (3.1) and the values above, the theoretical noise floor, at room temperature can be simplified and expressed as:

$$P_{nABS} = -174 + 10\log_{10}(B)\ [dBm] \tag{3.2}$$

The current generation of the Sub-GHz FSK transceivers, such as CC1120, have a more realistic noise floor [17], which can be expressed as:

$$P_{nREAL} = -174 + 10\log_{10}(B \times 1.5) + D_{SNR} + NF\ [dBm] \tag{3.3}$$

Where:

    (B x 1.5) = idealised channel bandwidth for GFSK modulation (Hz)

    D_{SNR} = required demodulator E_b/N_0 for coherent FSK (~ 10 dB)

    NF = receiver architecture noise figure (~ 6 dB)

The receiver sensitivity value should always be expressed for certain percentage of the PER (Packet Error Radio). The value of the receiver sensitivity in the developed sensor system is defined at the PER of 1%. This means that in 1000 send subtelegrams by the sensor module, a data logger module is allowed to miss reception of maximum 10 subtelegrams. Data logger module sensitivity was measured for different data rates and the results are compared in Figure 3.2. During each receiver sensitivity test, the data logger module (receiver) was directly connected to the signal generator which outputs test telegrams. Each test telegram has the same structure as the standard data telegram described in Chapter 3.4.2. The only difference is that the telegram data payload was set to 16 bytes. The output power was attenuated from -100 dBm to -120 dBm, in 1 dB increments. Within each increment, 1000 test telegrams have been sent with the telegram length of 120 ms, at the room temperature of +25 °C. Bit length was set to 120 µs. The number of successfully received telegrams in each increment was counted.

Figure 3.2. The data logger module sensitivity for the different data rates. Here, the packet error rate (PER) represents the percentage of non-received subtelegrams.

It can be seen that there is no significant difference in the data logger sensitivity between 0.9375 kbps and 1.250 kbps symbol rate. While using 0.9375 kbps symbol rate prolongs the transmitter and receiver ON time by 33% and reduces the overall sensor module dark time operation by 28%. The achieved range increases by only 7%.

Tests also showed that increasing the transmission rate to 1.875 kbps, increases the overall sensor module dark time operation by 30%, but also reduces the achievable range by 15% percent. Based on this, the used data rate is set to 1.25 kbps. This is considered the best trade-off between transmitter ON time and energy needed per transmission, packet error ratio and achieved range.

If the installation site has stricter requirements regarding energy consumption rather than achievable range, the transmission rate can be easily changed in the software. Figure 3.3 reiterates that mentioned above, how different data rates affect sensor module dark time operation. Test was performed with the sensor module set to a 2 minute wake up cycle and with 11 dBm of radio output power.
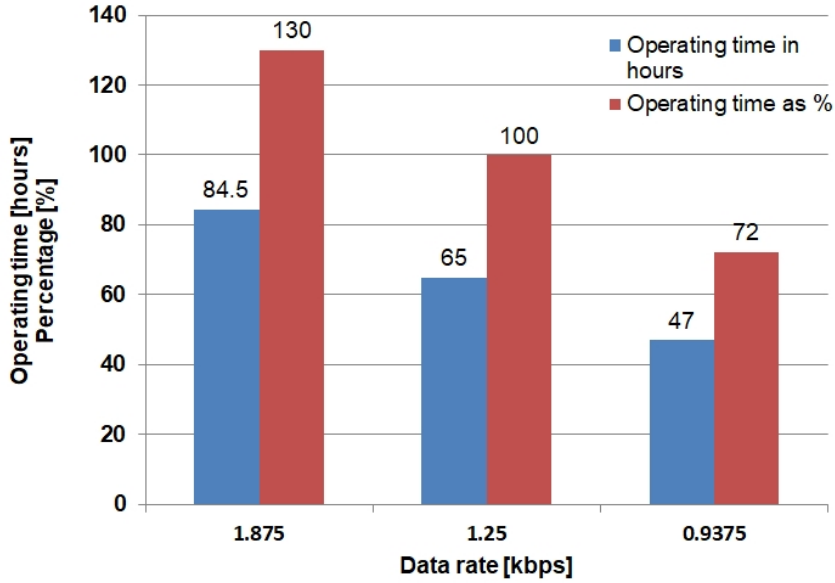
Figure 3.3. Comparison of the dark time operation for different data rates of the sensor module and with 2 minute wake-up cycle. 1.25 kbps is taken as reference and the achieved operating time is expressed as 100% of the dark time operation.

In a classic FSK modulation, for a suitable demodulation of the signal, frequency deviation should be equal or greater than the baud rate [46]. Bits are formatted using the binary NRZ (non-return-to-zero) format. The binary NRZ format has two symbols, one for bit 0 and one for bit 1. In this case baud or symbol rate is the same as a bit rate. The resulting occupied bandwidth, containing 98% of the sideband energy of the modulated signal, can be expressed using Carson's rule [48]:

$$B_M = 2 \cdot f_m \cdot (m + 1) \tag{3.4}$$

where,

$\Delta f - frequency\ deviation$

$f_m - highest\ frequency\ in\ the\ modulating\ signal$

and:

$$modulation\ index\ m = \frac{\Delta f}{f_m} \tag{3.5}$$

By using (3.4) and the values used in the developed sensor module, the resulting transmit signal occupied bandwidth is calculated to be 5 kHz.

Measurements taken with the sensor module confirm that Carson's rule, although originally written for the FM modulation, gives a good estimation for FSK and GFSK modulation [49],

72

[50]. As seen in Table 3.2, thanks to the use of the 2GFSK modulation and the bit shaping, the occupied bandwidth of the transmit signal is smaller than for the pure FSK modulation.

Table 3.2. The measured occupied signal bandwidth (OCBW) vs. calculated OCBW with equation (3.4), for different frequency deviations Δf [8].

Δf [kHz]	bit rate [kbps]	modulation index	OCBW Carson's rule [kHz]	Measured OCBW 2GFSK (BT = 0.5) [kHz]	Measured OCBW FSK [kHz]
0.3125	1.25	0.5	1.875	1.172	1.317
0.625	1.25	1.0	2.500	1.867	2.500
1.250	1.25	2.0	3.750	3.169	3.864
1.875	1.25	3.0	5.000	4.428	5.152

A smaller occupied bandwidth on the transmit side suggests that a smaller receiver filter bandwidth on the receive side is possible. This should improve received Signal-to-Noise ratio (SNR) and thus increase receiver sensitivity. In practice, lowering the frequency deviation Δf under the bit rate value will increase the packet error ratio. This is due to the increased difficulty when decoding the narrower signal on the receiver side as shown in Figure 3.4.
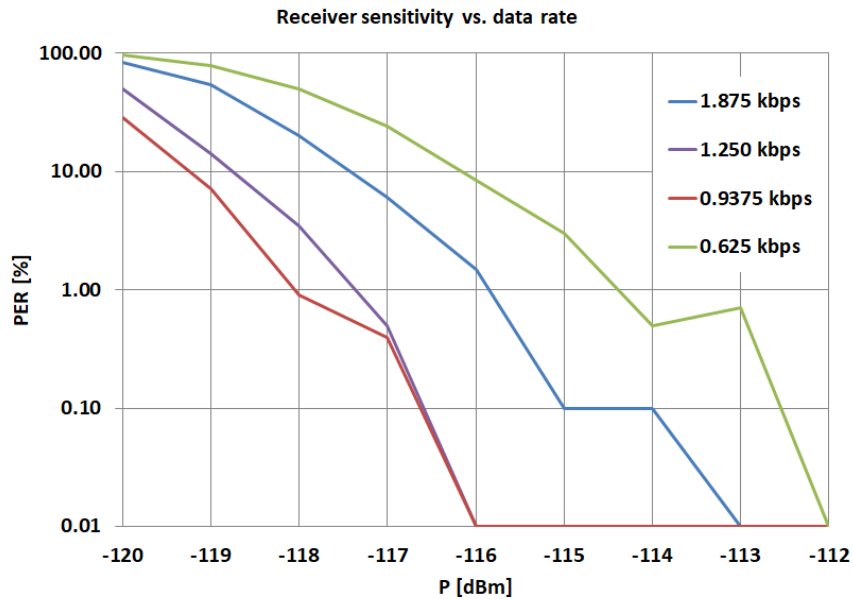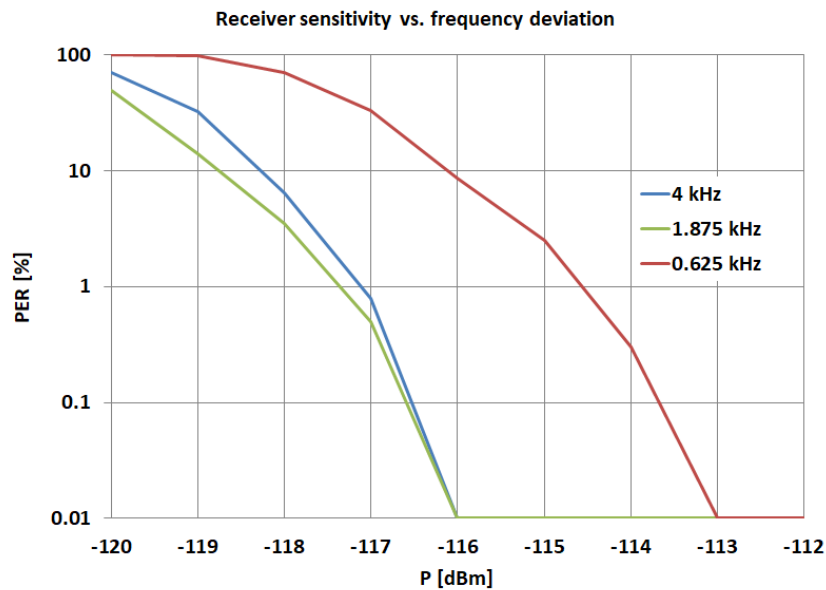

Figure 3.4. The data logger module sensitivity for different frequency deviation values. Here, the packet error rate (PER) represents the percentage of non-received subtelegrams.

As shown in this chapter, receiver sensitivity is a compromise parameter. Bit rate, frequency deviation, receiver filter bandwidth, crystal tolerances all influence receiver sensitivity. An integrated feature of the CC1120 radio chip, which combats the influence of the crystal tolerances on the needed Rx filter bandwidth, is the *Frequency offset correction*,

also known as *Feedback to PLL* (*Phase Locked Loop*). This feature can be enabled in the register FREQOFF_CFG of the radio chip. Based on the user guide of the radio chip [34], by enabling this feature the Rx filter BW increases, while the noise bandwidth remains constant.

Two different values can be stored in the register, 0x30 and 0x34. These values increase the programmed *Rx filter BW* value for ± *(Rx filter BW)/4* and ± *(Rx filter BW)/8* respectively [34].

As an example, the Rx filter BW is set to 33.3 kHz and the FREQOFF_CFG = 0x30. The feedback to PLL increases this filter bandwidth to 50 kHz (although 33.3 kHz is still the noise bandwidth). This effect can be seen in Figure 3.5. A PER is provided for the same receiver when using 50 kHz Rx filter BW and no feedback to PLL, and also for 33 kHz Rx filter BW value, with the feedback to PLL enabled.

Although a smaller Rx filter BW is used, the lower noise floor is obtained for the same offset from the central frequency, thus compensating for the tighter crystal tolerances.
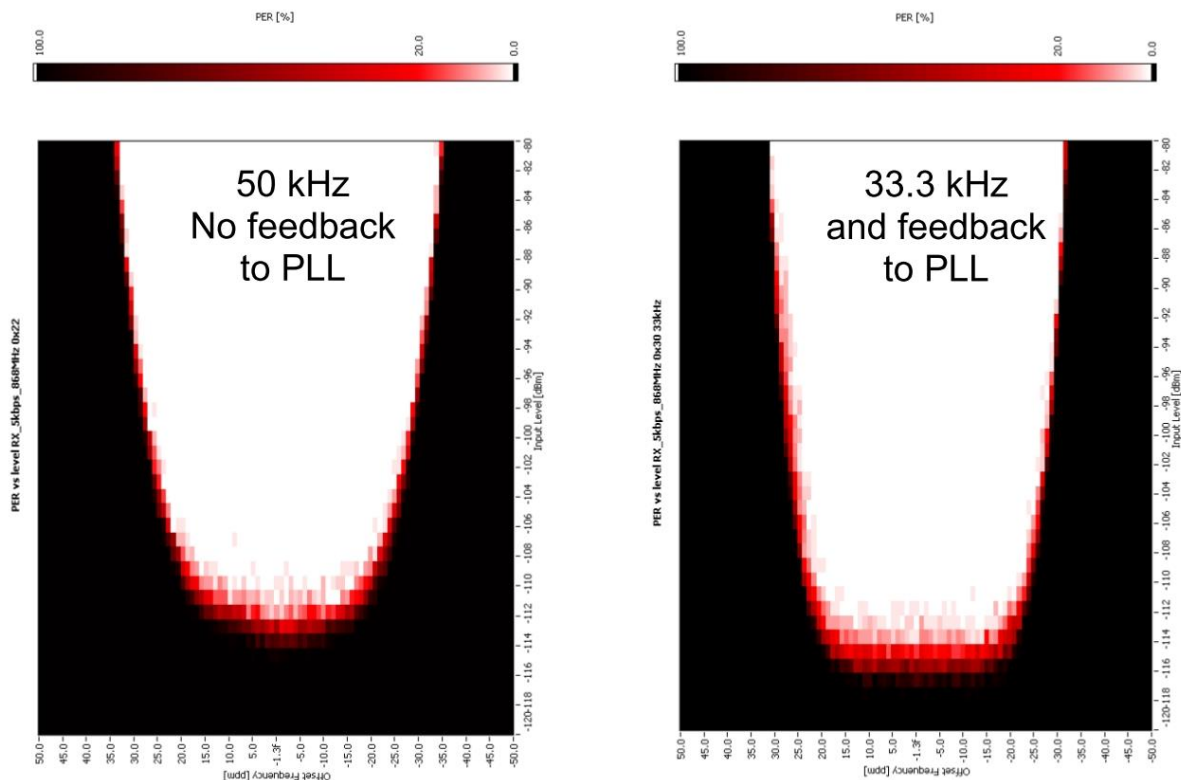
Figure 3.5. Feedback to PLL feature DISABLED (left) and ENABLED (right). With the enabled feature, a smaller Rx filter bandwidth can be used to compensate for the frequency offset due to the external crystal tolerances [34].

The feedback to PLL feature is enabled in the data logger module and different settings were tested. Feedback to PLL can be activated in the frequency synthesiser or it can be used

after the channel filter [34]. Figure 3.6 and Figure 3.8 show the impact on data logger module sensitivity when using different options. Using feedback to PLL at the frequency synthesiser stage has a more positive impact on the data logger sensitivity. Although, settling time is longer; typically 2 – 4 preamble bytes compared to 0 – 1 preamble bytes when feedback to PLL is used after channel filter. Upon detection of a synchronization word, the radio chip will automatically switch to frequency offset correction after the channel filter option [34]. Setting the loop gain factor to the value 1/256 compared to 1/128, will also result in improved sensitivity for the same frequency offset from the central frequency. This is presented in Figure 3.6 and Figure 3.7 respectively.
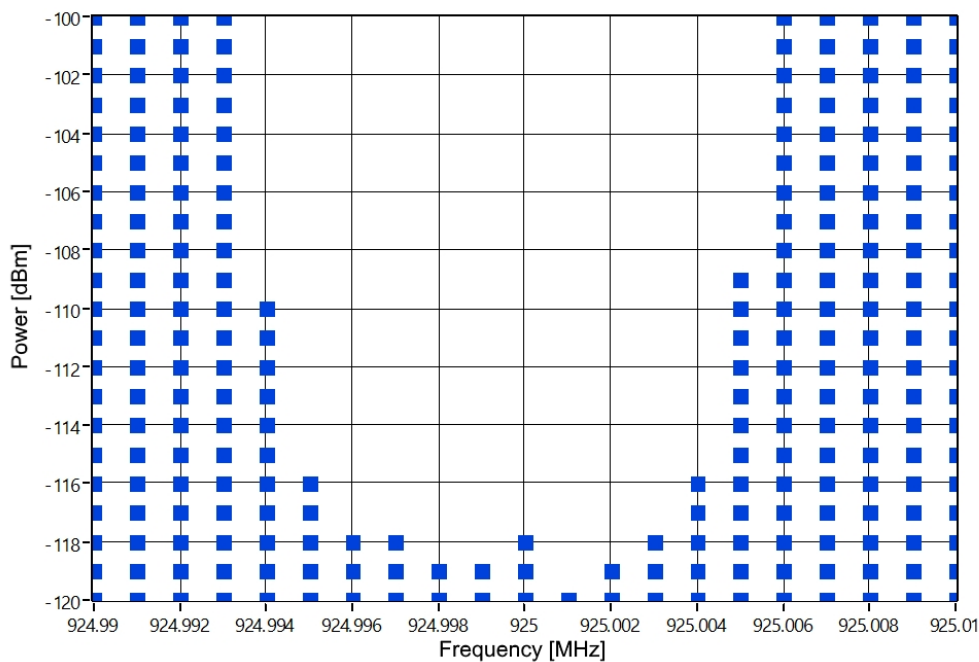
Figure 3.6. Frequency offset correction in the frequency synthesizer is enabled. Loop gain factor is 1/256 and the programmed Rx bandwidth is 10 kHz.
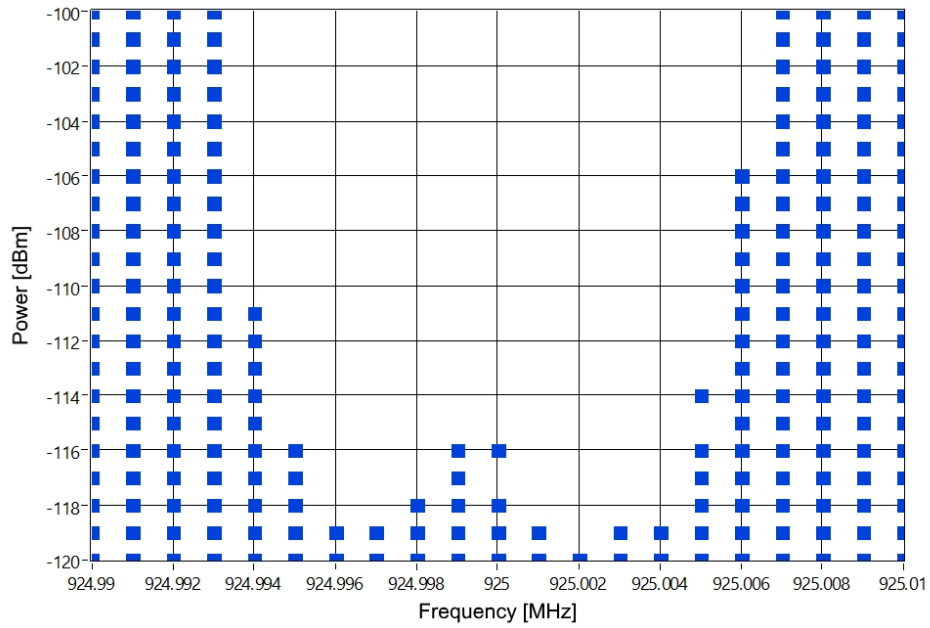
Figure 3.7. Frequency offset correction in the frequency synthesizer is enabled. Loop gain factor is 1/128 and the programmed R_X bandwidth is 10 kHz.
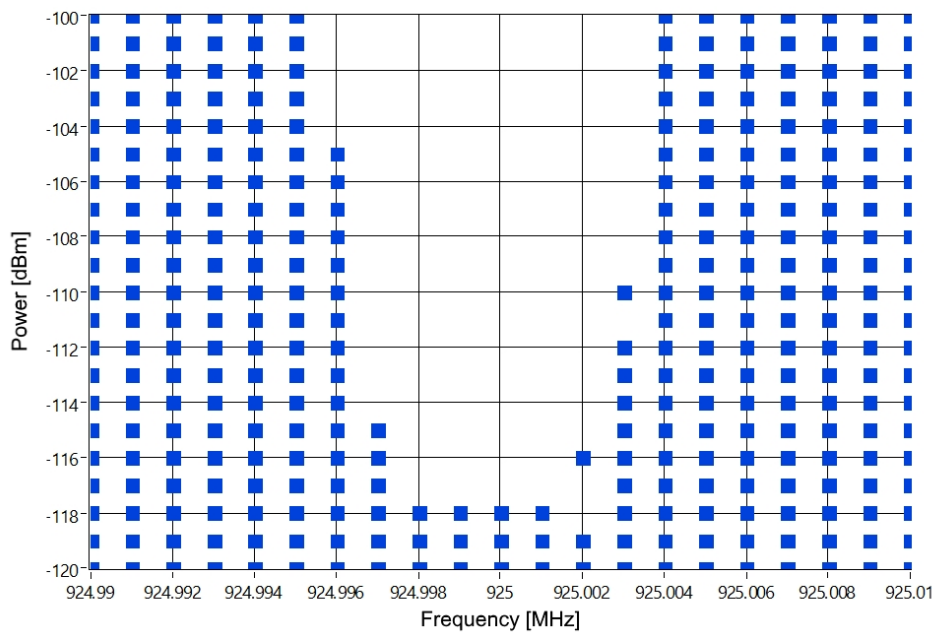
Figure 3.8. Enabled frequency offset correction after the channel filter. Programmed Rx bandwidth is 10 kHz.

Generally, enabled the feedback to PLL feature will not directly increase the receiver sensitivity. However, once enabled, the correct settings must be used otherwise it will degrade receiver sensitivity.

3.2.1. Temperature dependency of the data logger module sensitivity

Comparing different radio modules using the sensitivity values highlighted in their data sheets can often be misleading. This is because these values are usually expressed as the maximum possible achievable values using unique conditions (lowest possible bit rates, small frequency deviation, highest spreading factors, special receiver features enabled, etc.). For example, for the LoRa module, the receiver sensitivity based on the chosen radio settings and modulation parameters, can vary from -137 dBm up to -92 dBm [51]. For the CC1120 radio chip, used in the sensor system this number is advertised as -123 dBm at 1.2 kbps [22]. The achievable usable sensitivity can vary from these figures.

It is clear from Figure 3.2 and Figure 3.4, that around -117 dBm sensitivity is achieved with the developed data logger module at 1.25 kbps. To prove the actual performance of the sensor system in the field, an individual range test should always be performed as discussed in Chapter 5.2. When installed outdoors, the sensor system is subject to temperature oscillations, and these will ultimately reflect on the sensitivity figures. The data logger module was exposed to three different temperatures -20 °C, +25 °C and +60 °C respectively. At each temperature, sensitivity was measured for a 1.25 kbps data rate and ±1.875 kHz frequency deviation. Results are depicted in the figure below.
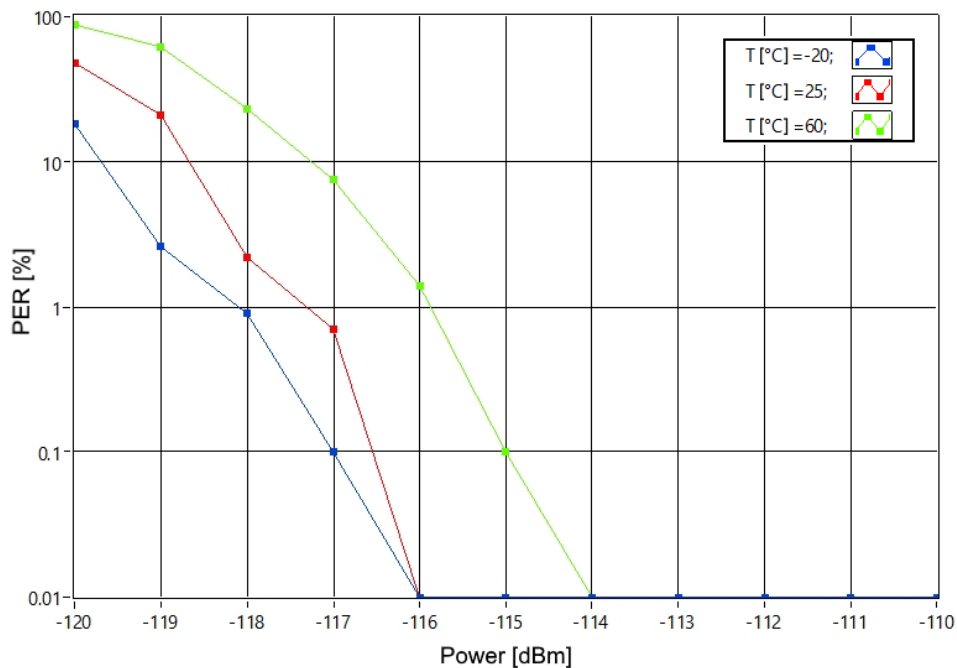
Figure 3.9. Measured data logger module sensitivity at different temperatures.

It is evident that the data logger module performs slightly better at lower temperatures. The packet error ratio at -117 dBm sensitivity is almost 10 times lower compared to the room temperature. With a temperature increase towards +60 °C performance becomes worse by the same factor compared to the room temperature. This behaviour stems directly from the characteristics of the quartz crystal and the radio chip (Chapter 2.1.5).

3.2.2. Preamble and Synchronization Word

A sensor module and a data logger module communicate by wirelessly exchanging radio packets defined in this thesis as long range radio telegrams. As mentioned, these telegrams can be in either the teach-in (TI) or data telegram (DT) format [52]. At the beginning of every long range radio telegram used here, either TI or DT, a 2-byte preamble (0xAAAA) appearing as an alternating bit series of zeros (0) and ones (1), and a 4-byte long synchronization word (0x593CA93C) are sent. These 6 bytes have always assume fixed values and are used to properly set up the amplifier gain of the radio chip front end. They are also used to appropriately synchronize the receiver with the sender, in order to correctly identify the start of the sent subtelegram. Without achieving bit synchronization, the receiver will not be able to extract the clock from the incoming symbols, nor correctly identify the first bit of the synchronization word and the data bytes that follow. As a consequence, the received data will be considered as noise and neglected [53].

During protocol development different preamble lengths were investigated. In older radio chips from Texas Instruments, preamble was also used for bit synchronization together with the synchronization word. In newer chip families, such as the used CC112x, preamble can be only used for the Automatic Gain Control (AGC). This feature adjusts the input signal level of the demodulator [34]. Table 3.3 describes the minimum required preamble length required by the bit synchronization algorithm inside the radio chip. Depending on the timing offset correction value (TOC = 0 or TOC $\neq$ 0), automatic selection between two different bit synchronization algorithms is performed.

Using the low tolerance setting (Algorithm type with TOC = 0) would greatly reduce system settling times and system power consumption. This is because no preamble bits are needed for bit synchronization or frequency offset compensation (4 bits preamble needed for AGC settling only). Since the expected lifetime of the developed sensor system is at minimum 10 years in the outdoor environment, symbol rate offset will eventually occur. This is due to the

quartz crystal tolerances. Therefore, this needs to be taken into consideration. This is why a preamble length between 2 and 4 bytes is set as the minimum requirement.

Table 3.3. Minimum required preamble length to achieve bit synchronization with respect to the symbol rate offset tolerances [34]

Timing Offset Correction value	Symbol rate offset tolerance	Required preamble length
00	< 0.2%	0.5 byte (4 bits)
01	< 2%	2 - 4 bytes
11	< 12%	2 - 4 bytes

Less preamble bytes means shorter radio ON time and more energy preserved per subtelegram transmission. The radio chip has four different preamble words integrated (Table 3.4) and preamble length can be set anywhere between 0.5 bytes (4 bits) and 30 bytes (240 bits). All these can be set in the PREAMBLE_CFG1 register of the radio chip [34].

Table 3.4. Default radio chip preamble word values and the required first 2 least significant bits (LSB) values in the PREAMBLE_CFG1 register for each of the preamble words

2 LSB register values	Preamble word
00	1010 1010 (0xAA)
01	0101 0101 (0x55)
10	0011 0011 (0x33)
11	1100 1100 (0xCC)

Figure 3.10 depicts how different preamble lengths, 16 bits (0xAAAA) versus 32 bits (0xAAAAAAAA) affect the reception of telegrams at different telegram power levels, and for different offsets from the central frequency. As it can be seen, the difference in the data logger module sensitivity (white area in the centre) is neglectable between these two preamble lengths. Since transmitting 2 bytes less saves energy, 2 byte preamble is chosen as the optimal preamble length for the developed sensor system.
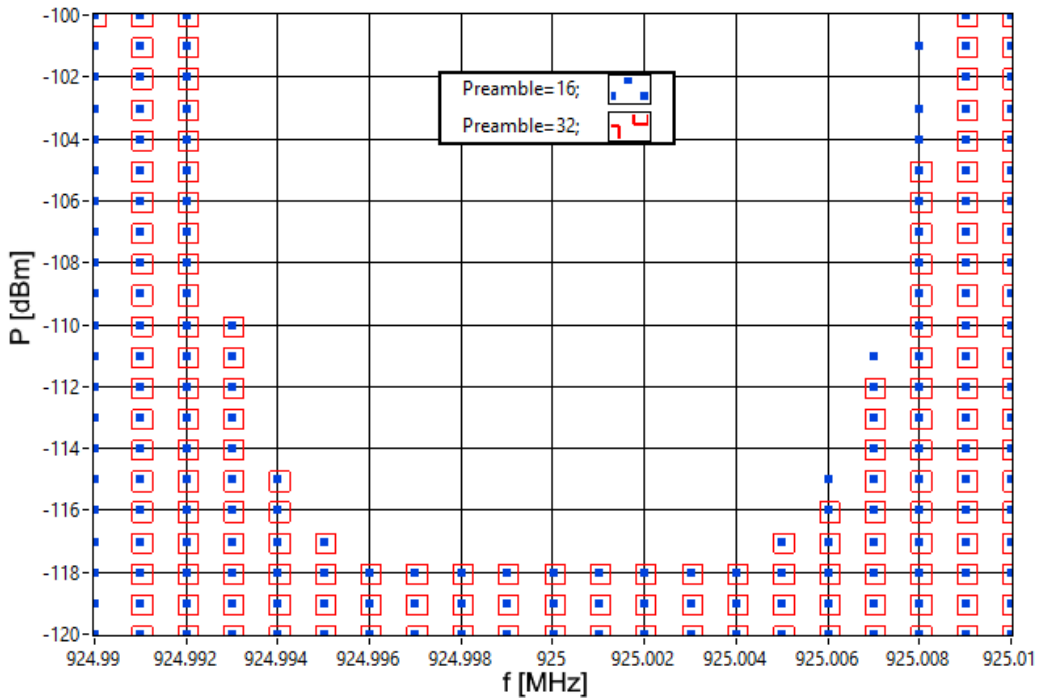
Figure 3.10. Telegram power levels at which they could still be received by the data logger module depending on the offset from the central frequency. Measurements are performed for two different preamble lengths, 16 bit preamble (blue squares) and 32 bit preamble (red squares) respectively.

One of the other reasons why the preamble should be a minimum 2 bytes long, is the possibility of using the Rx sniff mode. This mode would allow the data logger to enter sleep mode when there are no telegrams in the air and preserve energy. This can be a useful feature in the installations where the data logger would not be line powered. Figure 3.11 depicts how the receiver wakes up at such an interval that ensures at least 4 bits of preamble is received. After these 4 bits are detected, the receiver stays in the Rx mode to receive the rest of the telegram.
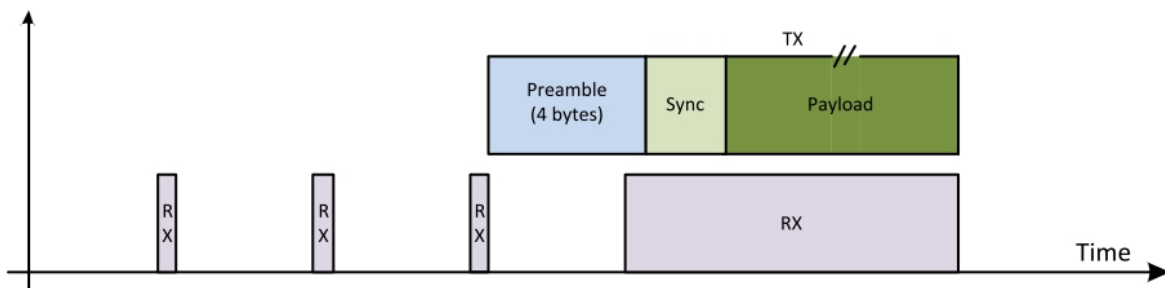
Figure 3.11. Rx Sniff mode and wake up at an interval that ensures that at least 4 bits of preamble is received [34].

Since the developed data logger is constantly powered via a special USB cable and can be surrounded with many sensor modules which transmit telegrams at different times, the Rx sniff mode would not provide any benefit in this case. This is why the ordinary Rx mode is implemented as the standard data logger operation mode (Figure 3.12).
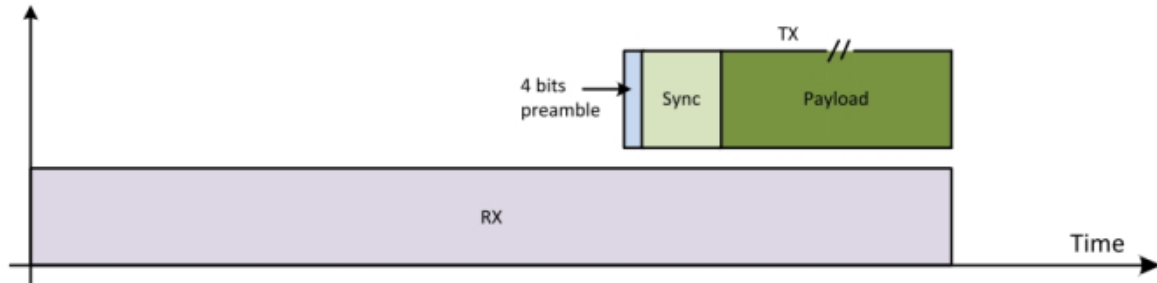
Figure 3.12. Ordinary Rx mode in which the receiver is always ON and ready for the packet reception [34].

The radio chip also supports automatic preamble detection through its high performance preamble detector which is turned ON in the PREAMBLE_CFG0 register. This option is a standard part of the radio chip's built-in hardware support, specifically intended for packet oriented radio protocols [34]. This means that in the transmit mode the radio chip automatically adds preamble and synchronization bytes to the teach-in, data or acknowledge telegram respectively. While in the receive mode it uses the same feature to de-construct the telegram.

A "good" synchronization word is determined by a high density of transitions (from 0 to 1 state), a high probability of byte uniqueness and consequently by good autocorrelation characteristics [46]. To achieve this, a special mathematical algorithm is written using the LabVIEW tool. This algorithm takes all possible 32 bit synchronization words and identifies the best autocorrelation characteristics for each of them. Each synchronization word is then used as the input sequence to the default AutoCorrelation VI available in LabVIEW.
A 1D AutoCorrelation (DBL) block used is depicted in Figure 3.13.
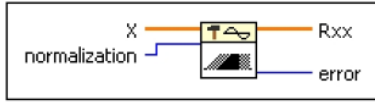
X is the input sequence.

normalization specifies the normalization method to use to compute the autocorrelation of **X**.

0	none (default)
1	unbiased
2	biased

Rxx is the autocorrelation of **X**.

error returns any error or warning from the VI. You can wire **error** to the Error Cluster From Error Code VI to convert the error code or warning into an error cluster.

Figure 3.13. LabVIEW AutoCorrelation VI used to find the "good" synchronization word for the developed sensor system [54].

In the above figure the autocorrelation *Rxx(t)* of a function *x(t)* is defined as:

$$Rxx(t) = x(t) \otimes x(t) = \int_{-\infty}^{+\infty} x(\tau)x(t + \tau)d\tau \qquad (3.6)$$

where the symbol $\otimes$ denotes correlation.

For discrete implementation of the AutoCorrelation VI, let *Y* represent a sequence that can have negative indexing, and let *N* be the number of elements in the input sequence **X**. It is assumed that the indexed elements of **X** that lie outside its range are equal to zero, as shown in the following relationship [54]:

$$x_j = 0, j < 0 \text{ or } j \geq N \qquad (3.7)$$

Then the AutoCorrelation VI obtains the elements of *Y* using the following equation:

$$Y_j = \sum_{k=0}^{N-1} x_k x_{j+k} \qquad (3.8)$$

for, $\qquad j = -(N-1), -(N-2), \dots, -1, 0, 1, \dots, (N-2), (N-1)$

The elements of the output sequence *Rxx* are related to the elements in the sequence *Y* by:

$$Rxx_i = Y_{i-(N-1)}, \text{for } i = 0, 1, 2, \dots, 2N-2 \qquad (3.9)$$

82

Therefore, **Rxx** represents the correlation values that the AutoCorrelation VI shifts N times in indexing [54].

In some situations, in order to make the autocorrelation calculation more accurate, normalization is required. The AutoCorrelation VI from the Figure 3.13 provides biased and unbiased normalization, or no normalization respectively [54]. The default value was used without any additional normalization.

Figure 3.14 depicts the calculated autocorrelation characteristics for the chosen 4 byte synchronization word.
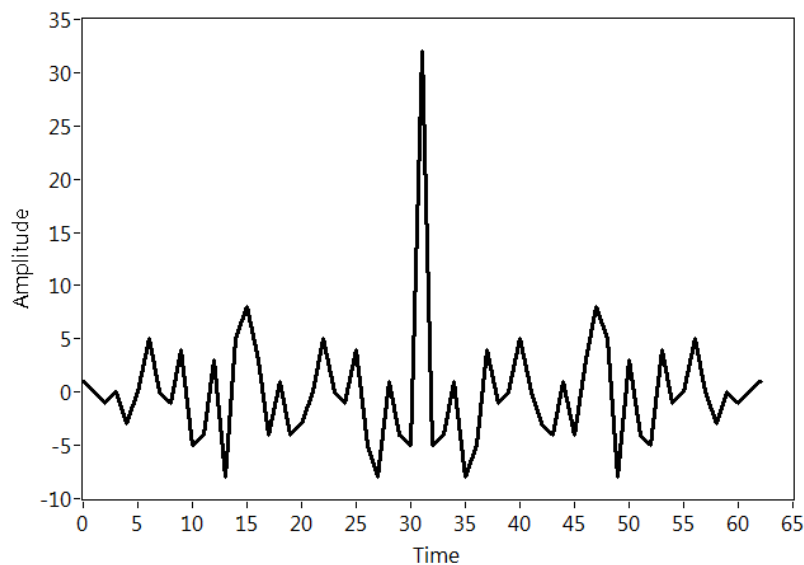
Figure 3.14. The autocorrelation characteristic of 0x593CA93C sync. word obtained with LabVIEW.
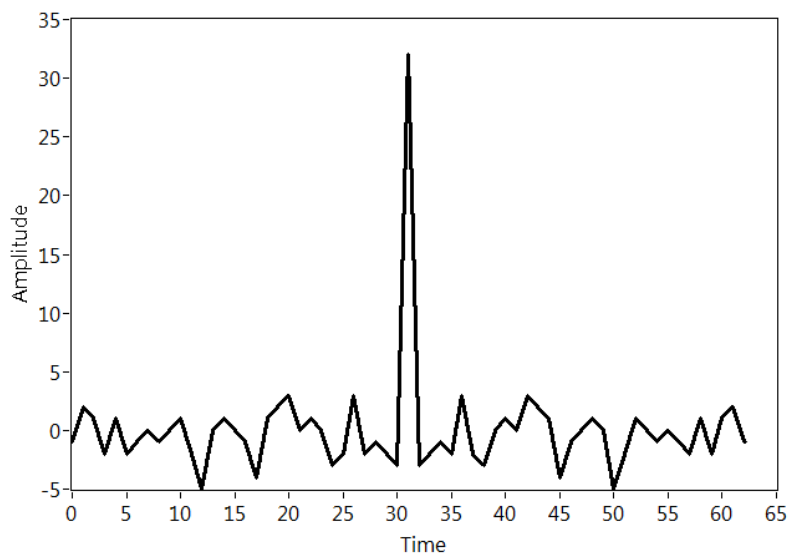
Figure 3.15. The Auto correlation characteristic of the CC1120 default sync. word 0x930B51DE obtained with LabVIEW.

The default synchronization word of the CC1120 radio chip is 0x930B51DE and its autocorrelation characteristic is shown in Figure 3.15.

This sync. word is used in the Texas Instruments radio chips since CC1101 series (released in 2007) [55]. Since the default sync. word has been used in many radio chips so far, it might happen that in the surrounding RF environment there are existing sensor modules with the same sync. word. Due to this, having a unique sync. word in the developed sensor system, but with the autocorrelation characteristic that can match the default one, is required. As it can be seen in Figure 3.16 this is successfully achieved. The red line represents the newly calculated, unique sync. word, while the blue line represents the default sync. word from Texas Instruments. The black line represents all the overlapping values between these two sync. words.
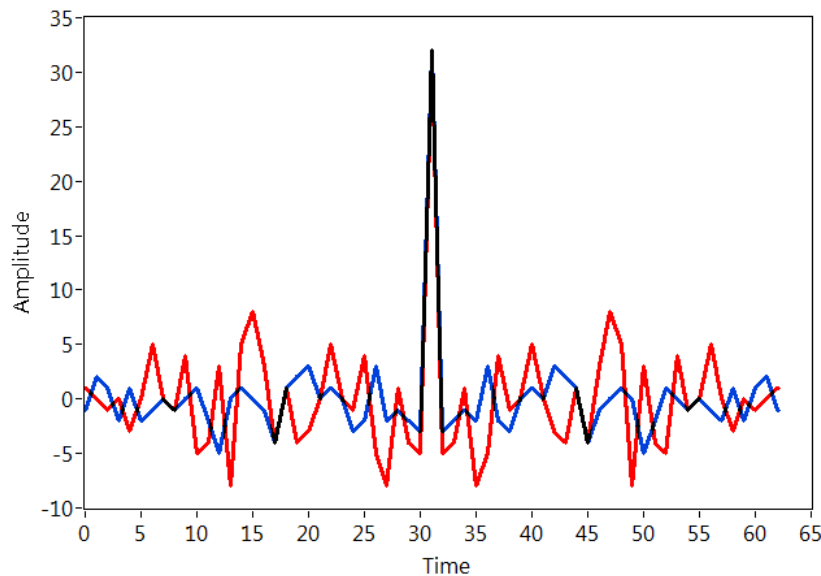
Figure 3.16. Match of autocorrelation characteristics for two 4 byte synchronization words. The red line depicts sensor system sync. word, the blue line is the default sync. word from Texas Instruments, and the black line depicts matched values.

Having a unique sync. word helps the data logger module to immediately eliminate packets from other transmitters containing a Texas Instruments radio chip. They could be operating at a similar frequency and data rate, somewhere in data logger module's proximity. Figure 3.17 shows the degradation of the autocorrelation characteristic, calculated for only the first 2 bytes of the above mentioned sync. words. The peak of the autocorrelation characteristic is halved in amplitude compared to the 4 bytes sync. words shown in Figure 3.16.
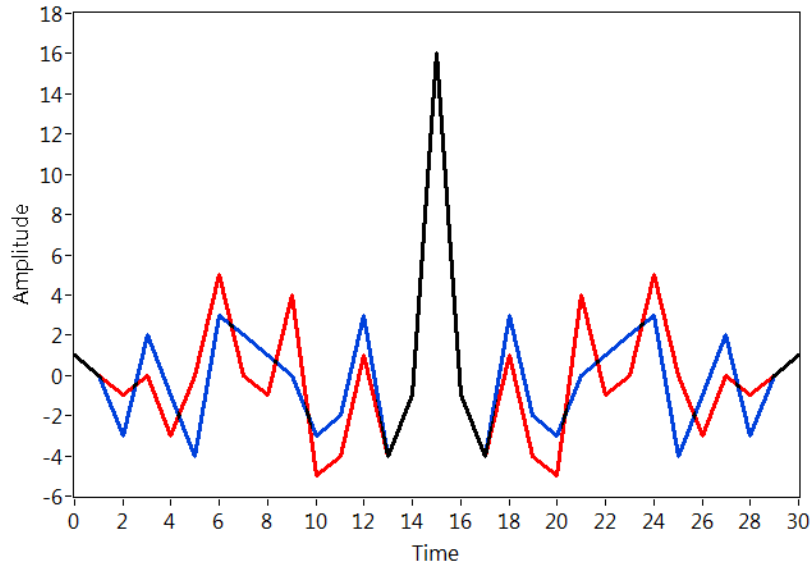
Figure 3.17. Match of autocorrelation characteristics for two 2 byte synchronization words. The red line depicts 0x593C sync. word, the blue line depicts 0x930B sync. word, and the black line depicts matched values.

An example of a "bad" synchronization word, which should be avoided is shown in the Figure 3.18. This graph depicts an autocorrelation characteristic of 0xAAAAAAAA sync. word [55].
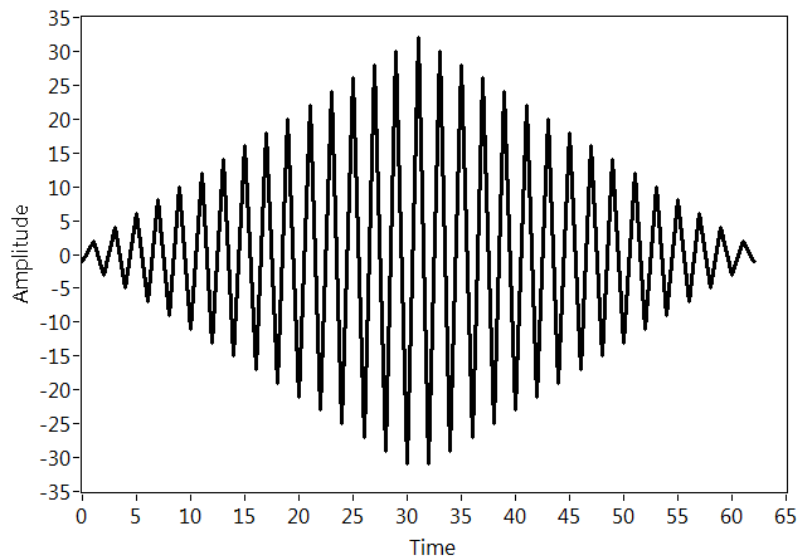
Figure 3.18. Example of 4 byte "bad" synchronization word 0xAAAAAAAA, and its autocorrelation characteristic [55].

Reducing the sync word length to less than 4 bytes and selecting bad sync word will have a negative impact on the packet error rate. When changing from the default radio chip sync. word, proper autocorrelation analysis should be performed as demonstrated in this chapter.

3.3. *Communication modes*

3.3.1. Unidirectional communication mode

In the unidirectional communication mode, the sensor module sends the same packet three times without waiting for the "acknowledged" reception on the receiver side. Each sent iteration is called a subtelegram and is observed as subtelegram 1, subtelegram 2 and subtelegram 3 respectively [52]. The delay between each of the subtelegrams can be fixed or variable. A variable delay is recommended since it will prevent a potential overlap of the subtelegrams sent at the same time from different sensor modules. If the repeating feature (Chapter 3.7) of the data logger module is desired, then it is recommended to keep a fixed time between the subtelegrams as seen in Figure 3.19.
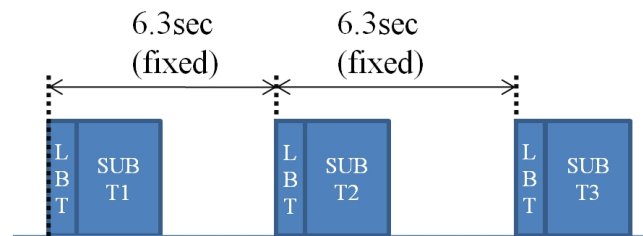
Figure 3.19. Fixed time delay between each of the transmitted subtelegrams.

Due to the same repeating feature, 6.3 seconds is chosen as the fixed delay between each of the subtelegrams. Before each transmission, the sensor module activates a Listen before talk algorithm (LBT) to determine if the radio channel is free for transmission (Chapter 3.5.1). To combat potential interferences between subtelegrams originating from different sensor modules in close proximity, an additional interference avoidance mechanism is implemented. This mechanism randomises the sensor module wake up cycle within the defined fixed interval. This fixed interval can be set by sending a serial command via a host interface of the sensor module. The default wake up and transmission time is each 15 minutes ± 30 seconds. It can be set as low as 2 minutes ± 30 seconds, depending on the sensor type and how often the user would like to perform a measurement and transmit the gathered information. It is not recommended to set the wake up and the transmission cycle to less than a minute, due to the overall startup and initialisation phase of the sensor module and the duration of the transmission of three subtelegrams. If a lower wake up time is needed then the sensor module supports wake up through the interrupt mode used with "always ON" attached sensors.

Figure 3.20 shows how sending times are distributed when a 2 minute ± 30 second wake up and transmission cycle is selected.
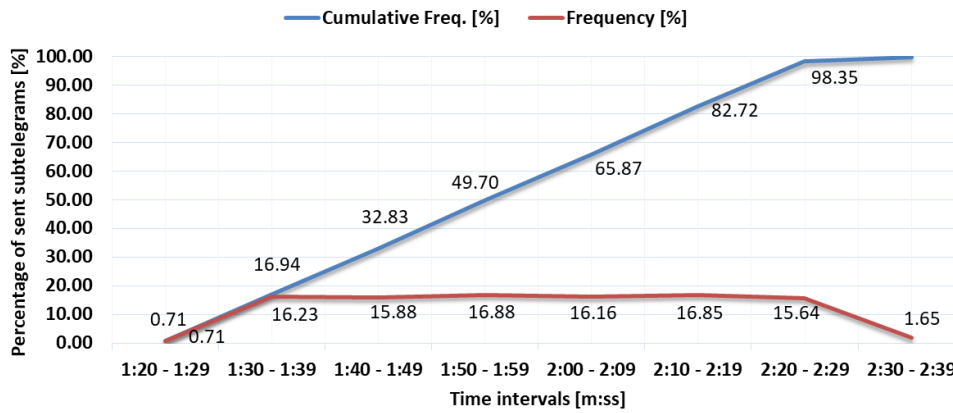
Figure 3.20. Distribution of the random send times within a fixed 2 minute ± 30 second interval (analysed among 3217 received subtelegrams) [8].

In the above figure, the cumulative frequency distribution plot (blue line) as well as the frequency distribution plot (red line) show that sent subtelegrams are evenly distributed within a ± 30 second interval. Initially to obtain values for the ± 30 second interval the random function from the C language was used. However, it did not prove to be random enough when used as part of the control algorithm in the sensor module. One of the reasons for this, is that on the each wake up of the senor module, the code would execute from the beginning and the random function would run as if it was called for the first time.

The solution is to use the random generator inside the CC1120 radio chip [34] which provides timing distributions as seen in Figure 3.20. The 32.768 kHz quartz crystal (Seiko SSP-T7-F) controls wake up of the sensor module from deep sleep mode. Due to its tolerances there is a small percentage of subtelegrams that are sent on the very edge, or a couple of seconds outside of the ± 30 second interval.

Sending the same telegram three times, with fixed or delayed time gaps, increases the probability of successful reception on the receiver side. This is despite potential short disturbances and noise in the communication channel. A similar retransmission approach is presented in the Sigfox protocol [7]. As described in [20] the overall transmission energy per wake up cycle directly depends on the number of retransmissions. In our case this is the number of transmitted subtelegrams. At the same time this is the main drawback of the unidirectional communication mode. Since LPWAN uses low transmission data rates, the subtelegram transmission time can be a couple of hundred milliseconds [6]. While the length

of our subtelegram varies depending on the attached sensor, the longest data telegram sent is around 170 ms. This suggests that the radio channel will be occupied during that time for the other sensor modules in close vicinity. The integrated Clear Channel Assessment (CCA) mechanism in the radio chip together with the LBT algorithm [22] will postpone subtelegram sending in case of an occupied radio channel (Chapter 3.5).

In Figure 3.21 the electrical current profile of the sensor module is shown during transmission of three subtelegrams. A maximum current of 45 mA is drawn from the supercapacitor during this time. In the same figure, it can also be seen that the transmission duration of the second subtelegram is 156 ms. The electrical current profile is recorded indirectly, by measuring a voltage drop across the 1 Ω resistor connected in series with the supercapacitor. The current and energy consumption of the sensor module is described in greater detail in the Chapter 4.
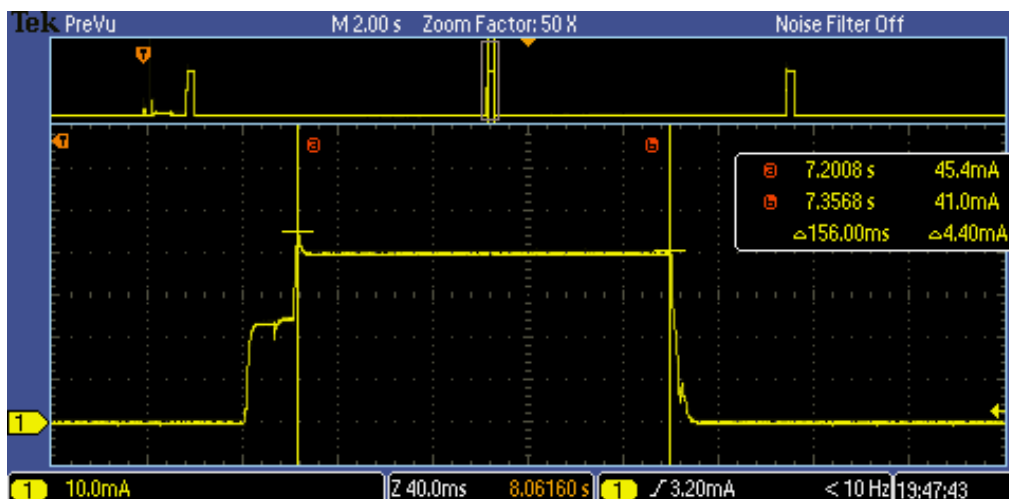
Figure 3.21. Three transmissions shown through overall sensor module current consumption. The second transmission is highlighted to show the peak current. Markers a and b are placed at the beginning and at end of the radio transmission state respectively to show the radio ON time.

3.3.2. Bidirectional communication mode

Another communication mode supported by both the sensor module and data logger module, is the bidirectional communication mode. When set in this mode, both modules operate as transceivers. After sending a teach-in or data subtelegram the sensor module waits for the acknowledge (ACK) telegram from the data logger, as a confirmation of a successful subtelegram reception. When the sensor module receives the acknowledge telegram it does not start transmitting further subtelegrams until the next wake up cycle occurs. A similar

principle is described in [56]. The authors there introduce adaptive and fixed duty cycle in packet transmission.

Waiting for the ACK telegram occurs immediately after subtelegram transmission and has a duration of 200 ms. During this time, the sensor module is in the receive mode with a total current consumption of around 25 mA as seen in Figure 3.22. Transmission of the acknowledge telegram takes around 140 ms, so there is a 60 ms margin added in wait for the ACK telegram time. This can be further optimized. An acknowledge telegram contains the source ID of the data logger as well as the destination ID of the recipient sensor module. It also includes one byte of confirmation represented as "OK" and a sequence number, identical to that in the received subtelegram. Further information about the structure of the acknowledge telegram can be found in Chapter 3.4.3.
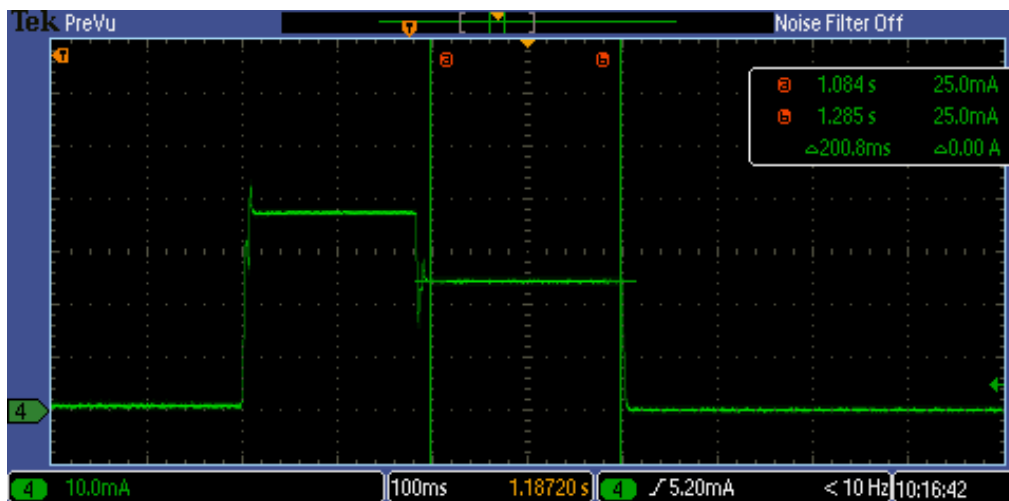
Figure 3.22. The electrical current drawn from the supercapacitor during the bidirectional mode. Consumption during transmission of the subtelegram can be seen together with the consumption while the sensor module waits for the ACK telegram (between markers a and b).

3.3.3. Energy consumption comparison between communication modes

In the bidirectional communication mode, if the first subtelegram is successfully received and acknowledged by the data logger module, no further subtelegram sending is needed in that wakeup cycle and consequently energy is preserved. Figure 3.23 compares the sensor module consumption for two different type of sensors, between the unidirectional and bidirectional mode during active periods.

As long as the radio link is good and the first subtelegram is successfully acknowledged, the sensor module, during active cycle, consumes close to 40% less energy than in unidirectional mode. This is the main advantage of the bidirectional mode over the unidirectional mode.

Figure 3.24 depicts results from the performed dark time tests (solar cell disconnected) for these two communication modes and for two different radio chip output power settings.

A sensor module with a fixed 2 minute wake up cycle operates in the bidirectional mode (blue and purple line in the Figure 3.24), in the best case, 96% longer than in the unidirectional mode (a red and green line in the Figure 3.24). This ratio between communication modes remains roughly constant when the output power increases. During this test the sensor module continued to run with the attached analog sensor and full supercapacitor (3.6 V). Supply voltage was directly measured on the supercapacitor after every wakeup cycle, using an external voltmeter. This was done until the module stopped sending upon reaching 2.5 V. Measurements were then repeated with the same module for different power settings and communication modes.
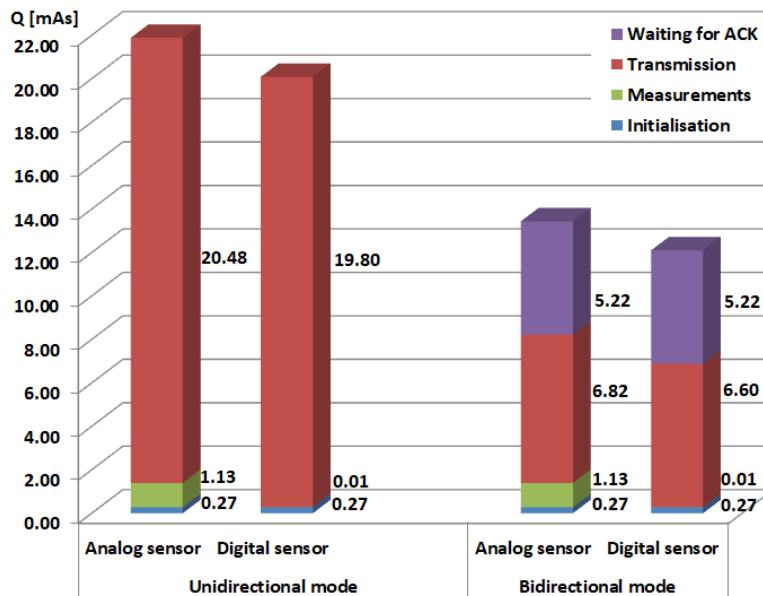
Figure 3.23. The sensor module energy consumption in different active periods for two different communication modes, and for two different types of attached sensors. This is the best case scenario when the ACK telegram is received after the first subtelegram [8].
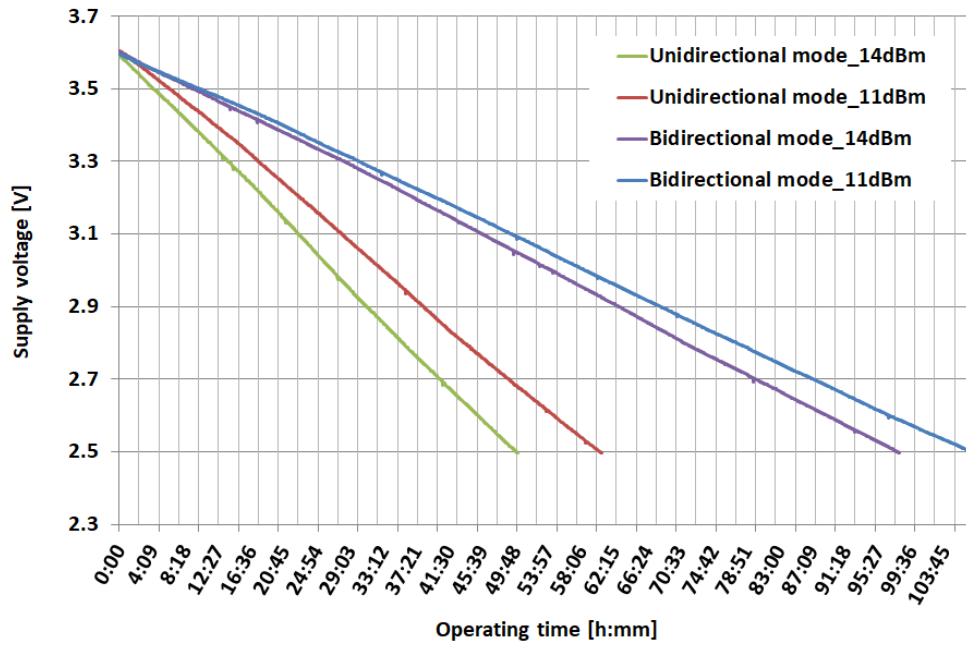
Figure 3.24. Measured operating time without energy harvesting (dark run time) and with a 2 minute wake up cycle. Dark run time is shown for two different communications modes and two different radio power settings. On the Y axis linear decrease of the supercapacitor's voltage can be seen [8].
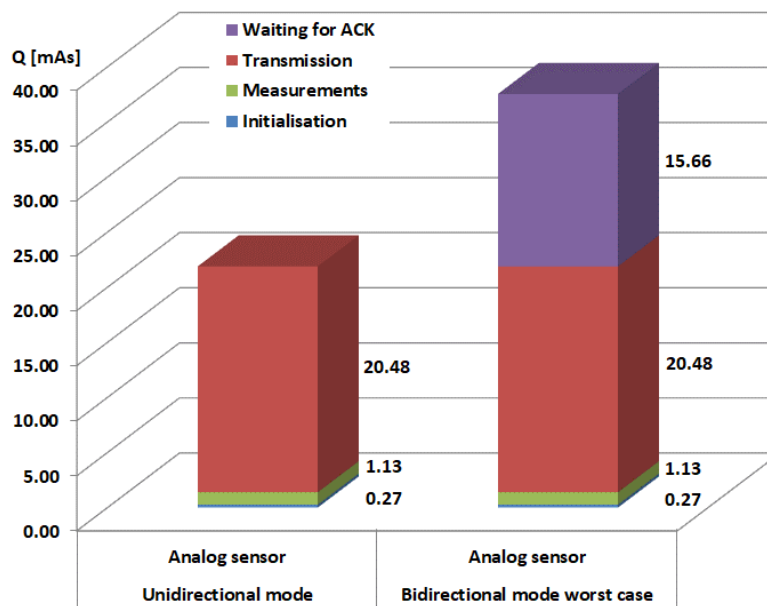
Figure 3.25. The worst case sensor module energy consumption in different active periods for two different communication modes (waiting for the ACK telegram in the bidirectional mode is repeated three times).

The worst case scenario is displayed in Figure 3.25. and this shows a disadvantage of the bidirectional mode. If the sensor module does not receive an acknowledge telegram from the data logger module it will resend the subtelegram until the acknowledge telegram is received,

although no more than 3 times. If after the third time, there is still no acknowledge telegram, the sensor module enters a deep sleep mode until the next wake up cycle. Since every time after sending a subtelegram the sensor module enters receive mode and waits for the ACK, the overall consumption will be larger than in the unidirectional mode.

Another disadvantage is a potential unbalanced radio power link due to the restrictions that arise from the radio regulation norms [43], [57]. In the particular case where a high performance gain antenna is used on the receiver side, the acknowledge telegram transmit power must be reduced accordingly. This is also explained in the Chapter 2.3.2.

3.4. *Radio telegram format*

3.4.1. Teach-in telegram format

Teach-in (TI) is the telegram type sent each time a sensor is plugged into the sensor module. If two sensors are connected to the sensor module and one of them is unplugged, upon unplugging, a TI telegram will be also sent. The role of the TI telegram is to teach the data logger module how to interpret the data telegrams that will follow from the sensor module. A TI telegram is also sent in the form of 3 identical subtelegrams as described in Chapter 3.3.1. The total length of the TI telegram is variable and depends on the number and type of sensors attached to the sensor module. The fixed part, which does not depend on the sensor attached, is 21 bytes long as it can be seen in Figure 3.26.

Physical layer (6 Bytes)		Data link layer (21 Bytes minimum.)						
Preamble 0xAAAA 2 bytes	Sync. Word 0x593CA93C 4 bytes	Length 1 byte	Header 1 byte	Ext. Telegram type 0x05 1 byte	Originator ID 4 bytes	GP Header 2 bytes	Channels description 4 bytes + N bytes + 6 bytes	CRC 1 byte
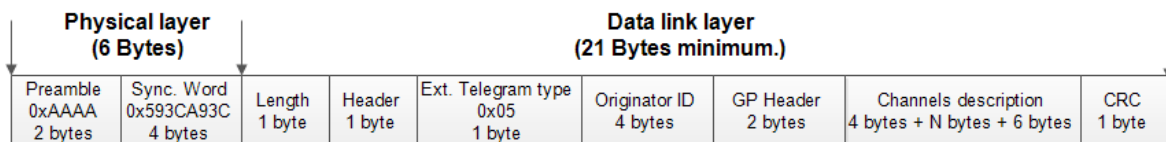
Figure 3.26. Teach-in telegram format.

With the currently supported analog and digital sensors, the minimum length of the TI telegram, including preamble bytes and sync. word, is 41 bytes. The maximum length is 51 bytes, when two sensors are connected to the sensor module. With a transmission rate of 1.25 kbps, the total maximum transmit time for one TI is 326.4 ms.

Some radio norms can have limits on the total radio ON time per transmission [43]. If needed, the TI telegram can be split into shorter parts so that the radio ON time per transmission is shorter. In this case, the TI telegram needs to be merged again on the receiver side, this is known as telegram chaining (Chapter 3.6).

As seen in Figure 3.26, the data link layer of a TI telegram starts with a length byte. This byte tells the data logger module how many data bytes the TI telegram contains. All bytes, from the header byte to inclusively last CRC (Cyclic Redundancy Check) byte, are counted and described in the length byte. Header bytes define how large the originator ID is (24 bit, 32 bit or 48 bit). A standard sensor module (originator) has an ID size of 32 bits. The header also defines the TI telegram as an extended telegram type according to [52]. Whereas in [58] this type of telegram is more precisely defined and called Generic Profiles Teach-in request. Using definitions contained in the header byte, the developed sensor module, with its unique long range protocol, also obeys EnOcean protocols and standards and complies with the EnOcean technology certifying body, EnOcean Alliance.

The 4 bytes that follow after the *Header* and *Telegram type* contain the sensor module ID (*Originator ID*). A *Generic Profiles (GP) Header* contains the manufacturer ID, type of communication (unidirectional or bidirectional) and informs the data logger module that this is a teach-in type of the telegram [58]. Bytes are grouped depending on weather they set up the data logger module to interpret correct energy levels on the sensor module, the charging current, or the types of the attached sensors. The respective values they measure are also grouped into so-called channels [58]. The last three channels in every TI telegram are debug channels. The status of the connected sensors together with the sensor module status is reported in these channels. These three channels are very important since any misbehaviour of the connected sensors or sensor module will be indicated here. Possible status codes which are sent as part of the data telegram are listed in the Chapter 3.4.2.2.

The last transmitted byte is always a CRC-8 byte and it is used to indicate a potential bit corruption in the transmitted TI subtelegram. CRC-8 byte takes into account the complete data link layer content except the length byte. Optionally the radio chip calculates 16 bits CRC (CRC-CCITT) over an entire subtelegram, excluding the preamble and synchronization word [34]. These extra 2 bytes are attached automatically by the radio chip and ensure optional, additional protection against data corruption. In both cases the verification is done by the data logger module. If the verification of the intactness of the received subtelegram fails, the subtelegram is ignored and discarded. The manual CRC-8 algorithm uses the same generator polynomial ($x^8 + x^2 + x + 1$) as the ATM (Asynchronous Transfer Mode) Header Error Control (HEC) described in the ITU-T recommendation I.432.1. [59]. The radio chip uses a CRC 16 algorithm with polynomial $x^{16} + x^{12} + x^5 + 1$ [34].

After the TI telegram is received, the receiver knows how to interpret the data telegrams which will follow. Since all the channels are defined using the TI telegram, data telegrams can be much shorter, with the majority of their content being the sensor's measured values, without a need of repeating channel descriptions.

3.4.1.1. Example of Teach-in telegram coding

To better understand the structure and content of the TI telegram, one example of a transmitted TI telegram when an analog sensor (which measures ambient temperature and relative humidity) is connected to socket 1 of the sensor module. For this purpose, the DolphinView tool from EnOcean is used to depict telegrams received by the data logger module. The telegram log window taken from DolphinView is shown in Figure 3.27. The total length of this TI subtelegram, sent when an analog sensor is connected to the sensor module, is 46 Bytes (6 bytes of physical layer + 40 bytes of data link layer). With a 1.25 kbps data rate, the transmission of one TI subtelegram lasts 294.4 ms.
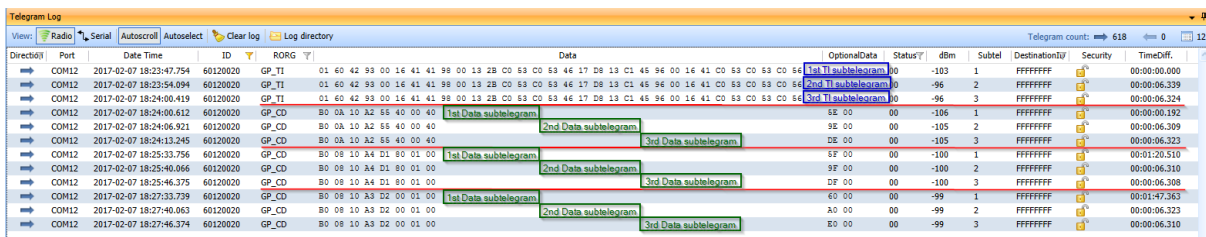
Figure 3.27. Three teach-in subtelegrams received with the data logger module with the 6.3 second time gap between each of them. Teach-in subtelegrams are followed by data subtelegrams. Three sensor module wakeup cycles are depicted.

When a TI telegram is received by the data logger module it is automatically transferred to the data logger host interface and its UART lines. Before forwarding the received bytes to the serial port, the data logger module adds additional bytes to the serial byte stream, according to the EnOcean serial protocol (ESP3) [40]. Table 3.5 shows the bytes added by the serial protocol, before the complete serial byte stream present on the serial port is formed.

Table 3.5. EnOcean serial packet coding according to the ESP3 protocol [40].

Group	Offset	Size	Field	Value hex	Description
-	0	1	Sync. Byte	0x55	Serial synchronization byte; always set to 0x55
Header	1	2	Data Length	0xnnnn	Specifies how many bytes in DATA must be interpreted
	3	1	Optional Length	0xnn	Specifies how many bytes in OPTIONAL_DATA must be interpreted
	4	1	Packet Type	0xnn	Specifies the packet type of DATA, respectively OPTIONAL_DATA
-	5	1	CRC8H	0xnn	CRC8 Header byte; calculated checksum for bytes: DATA_LENGTH, OPTIONAL_LENGTH and TYPE
Data	6	x	... ...	... ...	Contains the actual data payload with topics: - RawData (e.g. 1:1 radio telegram) - Function codes + optional parameters - Return codes + optional parameters - Event codes x = variable length of DATA / byte number
Optional Data	6+x	y	... ...	... ...	Contains additional data that extends the field DATA; y = variable length of OPTIONAL_DATA
-	6+x+y	1	CRC8D	0xnn	CRC8 Data byte; calculated checksum for whole byte groups: DATA and OPTIONAL_DATA

Following the table above, 6 bytes will be added before the initially received data bytes and 3 bytes at the end to form a serial data packet.

For example, when connecting one analog sensor to the sensor module, the 40 received bytes (in hexadecimal format) of the data link layer are:

27 2F 05 60 12 00 20 01 60 42 93 00 16 41 41 98 00 13 2B C0 53 C0 53 46 17 D8 13 C1 45 96 00 16 41 C0 53 C0 53 C0 56 1C.

To this byte stream, excluding the first length byte, serial protocol bytes (marked in red) are added to form the following packet:

55 00 27 02 0A 49 2F 05 60 12 00 20 01 60 42 93 00 16 41 41 98 00 13 2B C0 53 C0 53 46 17 D8 13 C1 45 96 00 16 41 C0 53 C0 53 C0 56 1C 01 67 27.

From Table 3.5 and as depicted in Figure 3.28 the received bytes have following meaning:

0x55 – Serial synchronization byte, always set to 0x55.

0x00 27 – Data length. Specifies how many bytes must be interpreted as part of the radio packet data link layer, not including the length byte. 0x27 = 39 bytes.

0x02 – Length of the optional data added by the serial protocol. 2 bytes are added in this case.

0x0A – Received packet type. 0x0A represents EnOcean Radio Protocol 2 (ERP2) telegram [40].

0x49 – CRC8 serial header byte. Calculated checksum for data length, optional data length and packet type bytes (0x00 27 02 0A).

0x01 67 – Optional data. 0x01 = 1 is the subtelegram number and 0x67 = 103 is the Receive
Signal Strength Indicator (RSSI) value (without the negative sign, the highest value
obtained from all received subtelegrams).

0x27 – CRC8 serial data byte. Calculated checksum for data and optional data bytes (39 data
link bytes and 0x01 67).
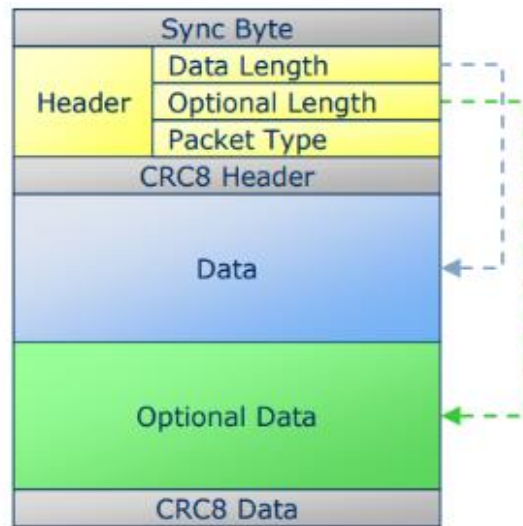
Figure 3.28. Main parts of the EnOcean serial data packet (ESP3) [40].

After decoding bytes added by the serial protocol, remain to decode are 39 bytes of the
raw data payload of the TI telegram data link layer (without the first length byte):

2F 05 60 12 00 20 01 60 42 93 00 16 41 41 98 00 13 2B C0 53 C0 53 46 17 D8 13 C1 45 96
00 16 41 C0 53 C0 53 C0 56 1C.

The first byte of the teach-in telegram's data link layer right after the length byte, is the
Header byte.

Table 3.6. Encoding example of the TI subtelegram header field.

Header (1 byte)		0x2F = 0010 1111$_2$
Bits 7…5	Bit 4	Bits 3…0
001	0	1111
Originator ID size (48, 32, or 24 bits) 001 = 32 bit ID	Is Extended header (1 byte) present or not? 0 = Not present	Is Extended Telegram type (1 byte) field present? 1111 = Present

Table 3.7. Encoding example of the TI subtelegram extended header field.

Extended Telegram type (1 byte)	0x05
0x05: Generic Profiles Teach-in request	

The Extended Telegram type byte is available if bits (3…0) in the Header byte are all set. If not, the telegram type is defined in the header field with the combination of the same 4 bits and the extended telegram type field is not required [52].

Value 0x05 stored in the extended telegram type makes the teach-in telegram compatible with the existing standards defined by EnOcean Alliance in the Generic Profiles (GP) specification [58]. GP specification contains a unique numbering scheme for different EnOcean telegrams based on a R-ORG (*Radio **Org**anization*) value. According to this numbering scheme, the teach-in telegram defined here has an assigned R-ORG value of 0xB0 and it is identified as the *Teach-in request* telegram.

When the data logger module is in bidirectional mode, after it receives a teach-in request telegram, it will immediately send a *Teach-in response* type of telegram, which has R-ORG value 0xB1 [58]. This is a confirmation of the successful TI telegram reception to the sensor module. This is similar to the acknowledge telegram used for the confirmation of a successful data telegram reception. A detailed structure of these two types of telegram is shown in Chapter 3.4.3. and Chapter 3.4.4.

Table 3.8. Encoding example of the TI subtelegram Originator ID field.

Originator ID (4 byte)	0x60 12 00 20
ID of the sensor module which transmitted the teach-in telegram	

Table 3.9. Encoding example of the TI subtelegram Generic Profiles header field.

GP Header (2 bytes)		0x01 60 = 0000 0001 0110 0000$_2$	
Bits 15…5	Bit 4	Bits 3…2	Bits 1…0
0000 0001 011$_2$ = 0x0B	0	00	00
Manufacturer ID 0x0B is code for EnOcean	Communication mode 0 = unidirectional 1 = bidirectional	Purpose of the packet 00 = To teach-in	Not used

After the *GP header*, the *Channel definition data* follows, according to Generic profiles specification. As it can be seen in Table 3.10 each channel definition data is 40 bits long [58].

Table 3.10. Teach-in telegram channel definition data [58].

Channel definition Data							
Channel type	Signal type	Value type	Resolution	Engineering minimum	Scaling minimum	Engineering maximum	Scaling maximum
2 bits	8 bits	2 bits	4 bits	8 bits	4 bits	8 bits	4 bits

Table 3.11. Teach-in telegram channel 0 data definition content example.

Channel 0 description (5 bytes) **Energy level**			0x42 93 00 16 41	
0x42 93 = 0100 0010 1001 0011$_2$				
Bit 39…38	Bits 37 … 30		Bits 29 … 28	Bits 27…24
01	00 0010 10		01	0011
Channel type = Data	Signal type Data = Number		Value type = Current value	ADC parameters = 4 bit resolution
0x00 16 41= 0000 0000 0001 0110 0100 0001$_2$				
Bit 23 … 16	Bits 15 … 12	Bits 11 … 4		Bits 3…0
0000 0000$_2$	0001$_2$	0110 0100$_2$=100$_{10}$		0001$_2$
8 bit Engineering minimum (Eng_{min}) = 0	4 bit Scaling minimum (F_{min}) = 1	8 bit Engineering maximum (Eng_{max}) = 100		4 bit Scaling maximum(F_{max}) = 1

The concluding 3 bytes describe Channel 0 in a way that the data logger module understands how the received value fits within the minimum and maximum range.

The measured energy level minimum and maximum value is 0 and 100 respectively. Both minimum and maximum values can be scaled to different values. In this case, both of these multipliers are set to 1 [58].

Measurement value quantization uses the equations below and the defined maximums and minimums from the Table 3.11 [58].

$$Eng_{min} = \frac{X_{min}}{F_{min}} \qquad (3.10)$$

$$Eng_{max} = \frac{X_{max}}{F_{max}} \qquad (3.11)$$

$$L = 2^N \qquad (3.12)$$

$$n = L \times \frac{x - X_{min}}{X_{max} - X_{min}} \tag{3.13}$$

$$x = \frac{n}{N} \times (X_{max} - X_{min}) + X_{min} \tag{3.14}$$

Where,

x = actual value

X_{min} = actual engineering minimum, X_{max} = actual engineering maximum

Eng_{min} = scaled engineering minimum, Eng_{max} = scaled engineering maximum

$Fmin$ = scaling factor minimum, $Fmin$ = scaling factor maximum

L = number of quantization levels, N = number of ADC resolution bits

n = quantized value

Table 3.12. Teach-in telegram channel 1 data definition content example.

Channel 1 description (5 bytes) **Solar cell charging current**		0x41 98 00 13 2B	
0x41 98= 0100 0001 1001 1000$_2$			
Bit 39…38	Bits 37 … 30	Bits 29 … 28	Bits 27…24
01	00 0001 10	01	1000
Channel type = Data	Signal type Data = Current [A]	Value type = Current value	ADC parameters = 12 bit resolution
0x00 13 2B= 0000 0000 0001 0011 0010 1011$_2$			
Bit 23 … 16	Bits 15 … 12	Bits 11 … 4	Bits 3…0
0000 0000$_2$	0001$_2$	0011 0010$_2$=50$_{10}$	1011$_2$
8 bit Engineering minimum (Eng_{min}) = 0	4 bit Scaling minimum (F_{min}) = 1	8 bit Engineering maximum (Eng_{max}) = 50	4 bit Scaling maximum(F_{max}) = 0.001 = 1e-3

Since Channel 1 data is in amperes, a scaling maximum of x0.001 is used, so that the data logger correctly interprets the received value of charging current in miliamperes. The engineering maximum is set to 50 because the maximum solar cell short circuit current is 41 mA (Chapter 1.2.2.).

The next two Channels are reserved for the sensor module's sensor interface 1 and sensor interface 2 descriptions respectively. Both channels have same description values (0xC0 53) which characterises them as 4 bit Enumerations as seen in Table 3.13.

Each physical sensor that can be connected to one of the sensor interfaces of the sensor module has unique 4 bit identifier as follows:

0 = 0000: No sensor connected

1 = 0001: Ambient air temperature (10 bit, -40...+60°C) and relative

humidity (8 bit, 0...100%) analog sensor

2 = 0010: Illuminance digital sensor (12 bit, 0...100 000 lux)

3 = 0011: Soil moisture analog sensor (8 bit, 0...100%)

4 = 0100: Soil temperature digital sensor (8 bit, -40...+60°C)

5 = 0101: Illuminance and Ambient air temperature and relative humidity sensor

combined on one sensor interface

6 = 0110: Soil temperature and Soil moisture sensor combined on one sensor interface

..... 1110: Reserved

1111: Reserved for sensor configuration extensions

Table 3.13. Sensor interfaces channels description.

Channel 2 description (2 bytes) Sensor Interface 1		0xC0 53 = 1100 0000 0101 0011$_2$	
Channel 3 description (2 bytes) Sensor Interface 2		0xC0 53 = 1100 0000 0101 0011$_2$	
Bits 15…14	Bits 13 … 6	Bits 5…2	Bits 1…0
11	00 0000 01	01	0011
Channel type = Enumeration	Signal type Enumeration = Multipurpose	Value type = Current value	ADC parameters = 4 bit resolution, used for sensor identifier

Teach-in telegram content, rounded with channels 3 and 4, is always fixed. After these bytes, the bytes which depend on the type of the sensor connected follow. Based on this, these channels will have a different number of bytes and this will define the overall TI telegram length. This can be seen in Table 3.14 which contains the description of the connected ambient temperature and relative humidity analog sensor. For this sensor description two channels are used, each containing 5 bytes. If only an illuminance sensor is connected to the

sensor module, the TI subtelegram would be 5 bytes shorter. This is due to the fact that only one measurement unit (illuminance) is reported by this sensor.

Table 3.14. Ambient temperature and relative humidity sensor channels description.

Channel 4 description (5 bytes) Ambient temperature		0x46 17 D8 13 C1		
0x46 17= 0100 0110 0001 0111$_2$				
Bit 39…38		Bits 37 … 30	Bits 29 … 28	Bits 27…24
01		00 0110 00	01	0111
Channel type = Data		Signal type Data = Temperature [°C]	Value type = Current value	ADC parameters = 10 bit resolution
0xD8 13 C1= 1101 1000 0001 0011 1100 0001$_2$				
Bit 23 … 16	Bits 15 … 12		Bits 11 … 4	Bits 3…0
1101 1000 $_2$ 2s Complement	0001$_2$		0011 1100$_2$=60$_{10}$	0001$_2$
8 bit Engineering minimum (Eng_{min}) = -40	4 bit Scaling minimum (F_{min}) = 1		8 bit Engineering maximum (Eng_{max}) = 60	4 bit Scaling maximum(F_{max}) = 1
Channel 5 description (5 bytes) Realtive humidity		0x45 96 00 16 41		
0x45 96= 0100 0101 1001 0110$_2$				
Bit 39…38		Bits 37 … 30	Bits 29 … 28	Bits 27…24
01		00 0101 10	01	0110
Channel type = Data		Signal type Data = Relative humidity [%]	Value type = Current value	ADC parameters = 8 bit resolution
0x00 16 41= 0000 0000 0001 0110 0100 0001$_2$				
Bit 23 … 16	Bits 15 … 12		Bits 11 … 4	Bits 3…0
0000 0000 $_2$	0001$_2$		0110 0100$_2$=100$_{10}$	0001$_2$
8 bit Engineering minimum (Eng_{min}) = 0	4 bit Scaling minimum (F_{min}) = 1		8 bit Engineering maximum (Eng_{max}) = 100	4 bit Scaling maximum(F_{max}) = 1

After the connected sensor channels, the following 6 bytes contain the fixed content enumeration channels. In these 3 channels with 2 byte content each, sensor 1 status, sensor 2 status and the sensor module status respectively will be reported.

Table 3.15. Description of the connected sensors status.

Channel 6 description (2 bytes) Sensor Interface 1 Status		0xC0 53 = 1100 0000 0101 0011$_2$	
Channel 7 description (2 bytes) Sensor Interface 2 Status		0xC0 53 = 1100 0000 0101 0011$_2$	
Bits 15…14	Bits 13 … 6	Bits 5…2	Bits 1…0
11	00 0000 01	01	0011
Channel type = Enumeration	Signal type Enumeration = Multipurpose	Value type = Current value	ADC parameters = 4 bit resolution, used for sensor status

Table 3.16. Description of the sensor module status.

Channel 8 description (2 bytes) Sensor Interface 1		0xC0 56 = 1100 0000 0101 0110$_2$	
Bits 15…14	Bits 13 … 6	Bits 5…2	Bits 1…0
11	00 0000 01	01	0011
Channel type = Enumeration	Signal type Enumeration = Multipurpose	Value type = Current value	ADC parameters = 8 bit resolution, used for sensor module status codes

In order to check that a TI subtelegram has arrived intact, a hash of the TI subtelegram is calculated before transmission and it is attached as the last data byte of the Data link layer (Figure 3.26), the CRC byte. In this example, the value of this calculated CRC byte is 0x1C. The entire TI subtelegram (without preamble and synchronization word) can be additionally protected by the radio chip and its 16 bit CRC calculator.

If a second sensor were to be plugged in, e.g. illuminance sensor, 3 new TI subtelegrams would be sent. As previously mentioned, each TI subtelegram would now be 5 bytes longer and the transmission time would increase by 32 ms, to 326.4 ms per subtelegram. Based on

the coding scheme demonstrated in this chapter, the content of the TI telegram for a two sensor combination attached to the sensor module is shown in Table 3.17.

Table 3.17. Teach-in telegram content when two sensors which measure three different parameters (illuminance, ambient temperature and relative humidity) are connected to the sensor module.

Parameter	Hex Value	Description
Length	2C	In this example the length of the following data is 44 bytes
Header	2F	Originator-ID 32 bit, no Destination-ID, extended header not available, extended telegram type
Ext. Telegram type	05	Generic Profiles Teach-In Request
Originator ID 32 bits	60 12 00 20	MSB LSB
Generic Profiles Teach-In Request Header	01 60	Manufacturer is EnOcean ID = 0x0B, unidirectional communication enabled, purpose of the telegram is teach-in
Channel 0 definition: Energy Storage level	42 93 00 16 41	Channel type = Data Channel, Signal type = Number Current value, Resolution 4 bit, 8 bit Engineering minimum is 0 4 bit Scaling minimum is 1, 8 bit Engineering maximum is 100, 4 bit Scaling maximum is 1
Channel 1 definition: Charging current	41 98 00 13 2B	Channel type = Data Channel, Signal type = Current in Amperes Current value, Resolution 12 bit, 8 bit Engineering minimum is 0 4 bit Scaling minimum is 1, 8 bit Engineering maximum is 50 4 bit Scaling maximum is 0.001 → 50 mA
Channel 2 definition: Sensor module Port 1	C0 53	Enum Channel, Multipurpose 4 bit
Channel 3 definition: Sensor module Port 2	C0 53	Enum Channel, Multipurpose 4 bit
Channel 4 definition: Sensor module Port 1: Illuminance	43 D8 00 16 44	Data Channel, Illuminance intensity, Current value, Resolution 12 bit, Eng.min 0, Scaling min 1, Eng.max 100 Scaling max 1.000 → 100.000 lux
Channel 5 definition: Sensor module Port 2: Temperature	46 17 D8 13 C1	Data Channel, Temperature, Current value, Resolution 10 bit, Eng.min -40, Scaling min 1, Eng.max 60 Scaling max 1 → -40...+60°C
Channel 6 definition: Sensor module Port 2: Relative Humidity	45 96 00 16 41	Data Channel, Relative Humidity, Current value, Resolution 8 bit, Eng.min -0, Scaling min 1, Eng.max 100 Scaling max 1 → 100%RH
Channel 7 definition: Sensor Port 1 Status	C0 53	Enum Channel, Multipurpose 4 bit
Channel 8 definition Sensor Port 2 Status	C0 53	Enum Channel, Multipurpose 4 bit
Channel 9 definition: Sensor module status	C0 56	Enum Channel, Multipurpose 8 bit
CRC	07	CRC

3.4.2. Data telegram format

A data telegram (DT) has a similar structure as the TI telegram. A preamble (0xAAAA) and a sync. word (0x593CA93C) are followed by the length byte. This informs the receiver how many following bytes to consider as payload of the data link layer (Figure 3.29).
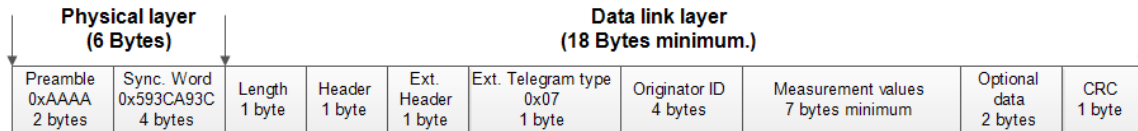

Figure 3.29. The Data telegram format.

The total length of the data telegram also varies depending on the type of sensors connected to a sensor module. When only an ambient temperature and humidity sensor is connected, the total length of the data telegram, not including optional CRC bytes added by the radio chip, is 25 bytes (including a preamble and a sync. word). When a second, e.g. illuminance sensor is connected, only one additional byte is added to a data telegram (26 bytes in total). This is almost half the length of the teach-in telegram for the same sensor combination (51 bytes). If only one illuminance sensor is plugged in, then a total data telegram length is 24 bytes. Transferring a data telegram using a 1.25 kbps data rate, the total sensor module ON air time for different combinations of sensors is as follows:

- *Illuminance digital sensor*: 153.6 ms (24 bytes) + 12.8 ms (2 byte Radio CRC)
- *Ambient temperature and humidity analog sensor*: 160 ms (25 bytes) + 12.8 ms (2 byte Radio CRC)
- *Both analog and digital sensors connected*: 166.4 ms (26 bytes) + 12.8 ms (2 byte Radio CRC)
- *Soil moisture analog sensor*: 140.8 ms (22 bytes) + 12.8 ms (2 byte Radio CRC)
- *Soil temperature digital sensor*: 140.8 ms (22 bytes) + 12.8 ms (2 byte Radio CRC)
- *Both soil moisture and soil temperature sensors connected*: 147.2 ms (23 bytes) + 12.8 ms (2 byte Radio CRC)

If the radio calculated CRC-16 option is enabled, to the timings listed above, an additional 12.8 ms would be added by the radio chip. A 2 byte CRC checksum, computed over the data link layer of the data telegram, is also part of the packet handling hardware support integrated into the CC1120 radio chip. This feature can be easily enabled or disabled in the PKT_CFG1

radio chip register [34]. Table 3.18 shows which options can be chosen regarding the CRC configuration.

Table 3.18. All possible radio chip automatic CRC configurations in the PKT_CFG1 register (bits 3:2) [34].

00	CRC disabled for TX and RX
01	CRC calculation in TX mode and CRC check in RX mode enabled. $CRC16(X^{16}+X^{15}+X^{2}+1)$. Initialized to 0xFFFF
10	CRC calculation in TX mode and CRC check in RX mode enabled. $CRC16(X^{16}+X^{12}+X^{5}+1)$. Initialized to 0x0000
11	Reserved

Value (10_2) is used in the developed sensor system which allows the radio chip to calculate a 2 byte CRC and add this to the end of either the teach-in or data telegram. During telegram reception, the radio chip automatically checks the content of these 2 bytes and determines whether the telegram arrived unchanged. Since CRC-16 provides greater protection against packet corruption than CRC-8, its use is recommended. CRC-8 is also used as a standard part of a developed protocol but it could be ignored for optimisation purposes. The current implementation of the sensor system actively utilises both mechanisms.

As in the teach-in telegram, the *Header* byte describes how large the sensor module ID is (24 bit, 32 bit, or 48 bit), and also describes if a specific destination ID is defined [58].

The data telegram, unlike a teach-in telegram, contains a one byte long *Extended header*. In this one byte, the length of the optional data is defined (two bytes in this case) as well as if the data telegram is the "original" or a repetition.

The "original" data telegram means that it comes directly from a sensor module and that it has not been previously received by the receiver set in the repeating mode and retransmitted. The repeater mode is one of the developed functionalities integrated into the protocol. It allows transmission over longer distances, by forwarding the previously received telegram. More about repeating can be found in the Chapter 3.7.

The extended header byte is followed by the *Extended telegram type* byte, again to ensure compatibility with the EnOcean Alliance Generic profiles specification. The fixed value (0x07) stored in this byte defines the used data telegram as a Generic Profiles Complete data telegram [58]. The *Originator ID* is followed with the real measurement values. To maximise energy efficiency, different physical values are not separated into each byte, but rather "compressed". This is done so that one byte can contain bits which carry information about the energy level and also bits which describe the charging current of the solar cell. An

example of the transmitted bytes when an ambient temperature and humidity analog sensor is connected to sensor interface 1 of the sensor module, is given in the chapter that follows.

At the end of the data telegram there are two bytes of *Optional data* and one byte for the data integrity confirmation (*CRC byte*). Optional data bytes are very important since they contain sequence numbers of the transmitted telegrams, as well as the subtelegram number identifier. Table 3.27 demonstrates optional data field encoding.

Optional data bytes also carry information about the traffic in the used radio channel. With the use of the Clear Channel Assessment (CCA) mechanism, each subtelegram informs a data logger module from which attempt the transmission of a previous subtelegram succeeded. If some subtelegrams have not been received by a data logger module, it is then possible to verify the reason for the missed reception in the used radio channel. More about the CCA mechanism can be found in the Chapter 3.5.1.

Upon comparison with other protocols, even with the above mentioned mechanisms integrated, here described protocol can still be considered light weight. The Sigfox protocol [7], which is considered lightweight, uses a total 26 bytes to transfer 12 bytes of data, with a 2 second over-the-air transmission. However, in contrast, the developed protocol uses 25 bytes to transfer 8 bytes of data, with an over-the-air transmission of only 160 ms (e.g. ambient temperature and humidity analog sensor).

3.4.2.1.   Example of Data telegram coding

To better understand the structure and content of the data telegram, one example of transmitted data telegram is shown when an analog sensor (which measures ambient temperature and relative humidity), is connected to the sensor module's sensor interface 1. This example continues from the teach-in telegram structure explanation given in chapter 3.4.1.1. The 3 data subtelegrams which follow the 3 teach-in subtelegrams can already been seen in the Figure 3.27. The total length of the depicted data subtelegram sent in the air, when an analog sensor is connected to the sensor module, is 25 bytes (6 bytes of physical layer + 19 bytes of a data link layer). With a 1.25 kbps data rate, the transmission time of this data subtelegram is 160 ms.

The 19 received bytes (in hexadecimal format) of the data link layer are as follows:

12 3F 02 07 60 12 00 20 B0 0A 10 A2 55 40 00 40 5E 00 83

Following Table 3.5, excluding the first length byte, serial protocol bytes (marked in red) are added to this byte stream to form the following serial packet:

55 00 12 02 0A 68 3F 02 07 60 12 00 20 B0 0A 10 A2 55 40 00 40 5E 00 83 01 6A 04

Where:

0x55 – Serial synchronisation byte, always set to 0x55.

0x00 12 – Data length. Specifies how many bytes must be interpreted as part of the radio packet data link layer, excluding the length byte. 0x12 = 18 bytes.

0x02 – Length of the optional data added by the serial protocol. 2 bytes are added in this case.

0x0A –Received packet type. 0x0A represents EnOcean Radio Protocol 2 (ERP2) telegram [40].

0x68 – CRC8 serial header byte. Calculated checksum for data length, optional data length and packet type bytes (0x00 12 02 0A).

0x01 6A – Optional data. 0x01 = 1 is the subtelegram number and 0x6A = 106 is the Receive Signal Strength Indicator (RSSI) value (without the negative sign, the highest value obtained from all received subtelegrams).

0x04 – CRC8 serial data byte. Calculated checksum for data and optional data bytes (18 data link bytes and 0x01 6A).

After decoding the bytes added by the serial protocol, 18 bytes of the raw data payload from the data telegram data link layer (without the first length byte) remain to decode:

3F 02 07 60 12 00 20 B0 0A 10 A2 55 40 00 40 5E 00 83

The first byte of the data telegram data link layer following the length byte is the *Header* byte.

Table 3.19. Encoding example of the data telegram Header field.

Header (1 byte)		0x3F = 0011 1111$_2$
Bits 7…5	Bit 4	Bits 3…0
001	1	1111
ID size (48, 32, or 24 bits) 001 = 32 bit Originator ID = No Destination ID	Is Extended header (1 byte) present or not? 1 = Present	Telegram type 1111 = Extended telegram type field present (1 byte)

The difference between the teach-in telegram header byte (Table 3.6) and the header byte of a data telegram (table above) is in bit 4. In the data telegram this bit informs a data logger module that the following byte is the extended header byte. This is not present in the teach-in telegram.

Table 3.20. Encoding example of the data telegram Extended header field

Extended header (1 byte)	$0x02 = 0000\ 0010_2$
Bits 7…4	Bits 3…0
0000	0010
Repeater counter 0000 = Original telegram	The length of the optional data 0010 = 2 bytes of the optional data present

The *Extended telegram type* byte is also available, as bits 0 to 3 in the header byte are all set (Table 3.19).

As seen in Table 3.21 the content of the *Extended telegram type* for the data telegram is always set to the value (0x07). This value defines the data telegram as *Generic Profiles Complete data* [52] and maintains compatibility with the Generic profiles specification from EnOcean alliance. This type of telegram is known as GP_CD (Complete Data) with an assigned R-ORG value of 0xB2 [58].

Table 3.21. Encoding example of the data telegram extended telegram type field.

Extended Telegram type (1 byte)	0x07
0x07: Generic Profiles Complete data	

The Originator ID filed contains the sensor module ID. If the telegram is repeated, it will still contain the originator ID and not the ID of the repeating device [52].

Table 3.22. Encoding example of the data telegram originator ID field.

Originator ID (4 byte)	0x60 12 00 20
ID of the sensor module which transmitted the data telegram	

8 bytes (64 bits) of sensor configuration and measurement data respectively follow the sensor module ID bytes. These bytes contain information about the sensors connected to the sensor module, as well as measurement values obtained from these sensors. These bytes are organised into previously defined data channels by the teach-in telegram.

Table 3.23. Measurement data obtained by the sensor module.

$0xB0\ 0A = 10110000\ 00001010_2$	
Channel 0 (4 bits) **Supercapacitor energy level**	Min. = 0 (0x0)... Max. = 100% (0xF) Received value: $1011_2 = 11_{10}$
[(11)/15]*100=73.33%	

Channel 1 (12 bits) Solar cell charging current value	Min. = 0 (0x000)... Max. = 50 mA (0xFFF) Received value: $0000\ 0000\ 1010_2 = 10_{10}$
$\left(\dfrac{10}{4095}\right) * 50 = 0.12210$ mA	

Table 3.24. Attached sensor configuration example.

0x10= $0001\ 0000_2$	
Channel 3 (4 bits) **Sensor Interface 1 configuration**	Received value: 0001_2
Currently existing coding values: 0000: No sensor connected **0001: Air temperature (10 bit, -40...+60°C) and Air humidity sensor (8 bit, 0...100%)** 0010: Illuminance sensor (12 bit, 0...100.000 lux) 0011: Soil moisture sensor (8 bit, 0...100%) 0100: Soil temperature sensor (8 bit, -40...+60 °C) 0101: Illuminance sensor together with the Air Temperature and Air Humidity sensor 0110: Soil Temperature sensor together with the Soil Moisture sensor xxxx: All other combinations are reserved for future sensors	
Channel 4 (4 bits) **Sensor Interface 2 configuration**	Received value: 0000_2
0000: No sensor connected	

Table 3.25. Obtained sensor values.

0xA2 55 40= $\underline{1010\ 0010\ 0101\ 0101\ 01}00\ 0000_2$	
Channel 5 (18 bits) **Sensor 1 measured values** **(10 bits, Air temperature)**	Received value: $1010\ 0010\ 01_2 = 649_{10}$
$\left[\left(\dfrac{649}{1023}\right) * (60 + 40)\right] - 40 = 23.44\ °C$	
Sensor 1 measured values **(8 bits, Air humidity)**	Received value: $01\ 0101\ 01_2 = 85_{10}$
$\left(\dfrac{85}{255}\right) * 100 = 33.33\%$	
Channel 6 (4 bits)	Received value: $00\ 00_2$

Sensor 1 status	
0000_2 : No issues with reading from the sensor connected to the Sensor Interface 1 (Chapter 0)	
Channel 7 (4 bits) **Sensor 2 status**	Received value: 00_2 and 2 first bits from the following byte seen in Table 3.26.
0000_2: Although sensor 2 is not connected 0000_2 is transmitted as part of the status byte.	

Table 3.26. Sensor module status byte encoding.

0x00 40 = ~~0000 0000 01~~00 0000	
Channel 8 (8 bits) **Sensor module status**	$00\ 0000\ 01_2$
0x01: Sensor module woke up by a power reset. This is the normal mode when an external sensor is connected for the first time and the sensor module starts operation (Chapter 3.4.2.2).	

The remaining 6 zeros in the table above are used to round the information to a byte size. Depending on the sensor configuration, fewer bits might be needed to fill a byte size.

In the data telegram packet structure, 2 bytes of the *Optional data* and a 1 *CRC*-8 byte, remain.

Table 3.27. Optional data bytes encoding.

Optional data (2 bytes)		Received value: 0x5E 00 = $0101\ 1110\ 0000\ 0000_2$		
Bits 15…14	Bits 13 … 8	Bits 7…6	Bits 5…0
01_2	$01\ 1110_2 = 30_{10}$	00_2	$00\ 0000_2$
Subtelegram number 00_2: Reserved **01_2: Subtelegram number 1** 10_2: Subtelegram number 2 11_2: Subtelegram number 3	Telegram Sequence number is 30_{10}	CCA status **00_2 = OK at 1st attempt** 01_2 = OK at 2nd attempt 10_2 = OK at 3rd attempt	Reserved

A telegram sequence number, displayed in Table 3.27, is an identifier of a group of the same 3 subtelegrams. When a data logger module receives 3 consecutive subtelegrams, based on the sequence number, it can recognise that they are transmitted during the same sensor

module wake up cycle. Subtelegrams with the same sequence number always carry identical measurement values. The sequence number as part of optional data bytes is highlighted in Figure 3.27. The telegram sequence number is especially important when a sensor module is used in the bidirectional mode (Chapter 3.3.2). In this mode, each subtelegram received by the data logger has to be acknowledged. This information is then returned to the sensor module in the form of an *acknowladge telegram*. The main information contained in the acknowledge telegram is the acknowledged subtelegram sequence number (Table 3.30).

The CCA (Clear Channel Assessment) status describes from which attempt the previously received subtelegram was sent. This means that each received subtelegram carries information about the radio environment just before the time it was sent. The CCA mechanism is described in greater detail in the Chapter 3.4.3.

In order to check that a data subtelegram has arrived intact, the same checksum calculation as in a teach-in telegram is performed (Chapter 3.4.1). The checksum calculation is executed over all the bytes in the data telegram starting from the header byte to optional data inclusively. In the example provided, the calculated and transmitted value of the CRC-8 byte within a subtelegram is 0x83.

3F 02 07 60 12 00 20 B0 0A 10 A2 55 40 00 40 5E 00 **83**

If an additional sensor were to be plugged into the sensor interface 2, e.g. illuminance sensor, only 1 additional byte would be sent within each subtelegram. The first 3 data channels would not change (Table 3.23 and Table 3.24) but data channel 4 would now carry information that the illuminance sensor is connected. One additional channel would be added which would contain a 12 bit measurement value of the illuminance.

3.4.2.2.   Status and error codes integrated into data telegram

As outlined in *Table 3.25* and Table 3.26 respectively, different sensor and sensor module status codes are a standard part of the transmitted data telegram. Any misbehaviour of the attached sensors or of the sensor module itself will be reported through these status codes. The list of the status codes is given in the table below.

Table 3.28. Status and error codes of the sensor module and its sensor interfaces.

Sensor interface status	Description	Sensor module status	Description
0x0	SUCCESS	0x00	UNDEFIEND
0x1	FAILURE	0x01	POWER RESET
0x2	WRONG PARAMETER	0x02	WATCHDOG TIMER RESET
0x3	NOT USED	0x03	ERROR RESET
0x4	SENSOR CALIBRATION ERROR	0x04	RTC ALARM
0x5	SENSOR CONNECTION ERROR	0x05	UART RX
0x6	SENSOR MEASURING ERROR	0x06	UART CONNECTED
0x7	SENSOR GENERIC ERROR	0x07	UART DISCONNECTED
0x8	SENSOR RECOGNITION ERROR	0x08	SENSOR CONNECTED/ DISCONNECTED
0x9 ::: 0xF	RESERVED FOR FUTURE USE	0x09	LRN BUTTON PRESSED
		0x0A	TRIGGER BUTTON PRESSED
		0x0B … 0xFF	RESERVED FOR FUTURE USE

3.4.3. Acknowledge telegram format

When both, the sensor module and data logger module are set in the bidirectional communication mode (Chapter 3.3.2), a new type of telegram will be present in the sensor system, called Acknowledge (ACK) telegram. Only data telegrams are acknowledged, while an answer to the received teach-in telegram is called Teach-in telegram response.

The ACK telegram is 13 bytes long (not including preamble and sync. word.); its structure is provided in Figure 3.30. After receiving a subtelegram the data logger module immediately sends an acknowledge telegram. As shown in Figure 3.22, the sensor module waits 200 ms after sending a subtelegram to receive the acknowledge telegram. If no acknowledge was received, the next sub telegram is sent. After 3 attempts without receiving an ACK the communication attempt is considered as failure. The data logger module can also filter sensor modules by their ID, in order to distinguish which devices should be acknowledged.

Physical layer (6 Bytes)		Data link layer (13 Bytes)					
Preamble 0xAAAA 2 bytes	Sync. Word 0x593CA93C 4 bytes	Length 1 byte	Header 1 byte	Originator ID 4 bytes	Destination ID 4 bytes	Acknowledge 2 bytes	CRC 1 byte
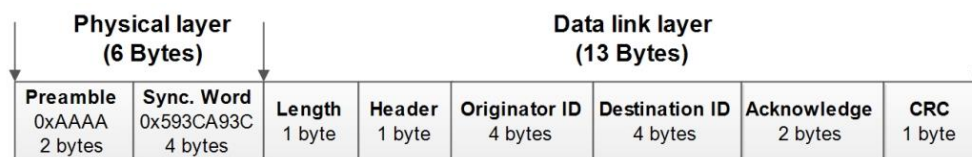
Figure 3.30. Acknowledge telegram structure.

3.4.3.1. Example of an Acknowledge telegram coding

An example of acknowledge telegram content is presented below. The following data link layer bytes are received by a sensor module set in the bidirectional mode:

0C 4B 60 11 10 32 60 12 00 20 00 02 9F

The coding scheme is the same as for a standard data telegram. The *Length* byte ($0x0C = 12_{10}$) informs the sensor module how many of the following bytes to interpret as data payload. This length byte is followed by the *Header* byte, which defines ID lengths and telegram type, as evident in the Table 3.29.

Table 3.29. Encoding example of the acknowledge telegram Header field.

Header (1 byte)		$0x4B = 0100\ 1011_2$
Bits 7…5	Bit 4	Bits 3…0
010	0	1011
ID size (48, 32, or 24 bits) 010 = 32 bit Originator ID = 32 bit Destination ID	Is Extended header (1 byte) present or not? 0 = Not present	Telegram type 1011 = Acknowledge telegram

The next 4 bytes after the header byte, is the ID of the data logger module (0x60 11 10 32) which is sending an ACK telegram. This is then followed by a 4 byte sensor module ID (0x60 12 00 20) which originally sent the data telegram.

As shown in Table 3.30, the acknowledge field consists of 2 bytes of data. These bytes contain the sequence number of the acknowledged telegram and the confirmation of successful acknowledgment.

Table 3.30. Encoding example of the acknowledge telegram Acknowledge field.

Acknowledge (2 bytes)	0x00 02
Byte 1	Byte 0
0x00	0x02
0x00 = Acknowledge OK	Sequence number is 2_{10}

At the end of the acknowledge telegram, there is 1 byte of CRC-8 (0x9F). This is calculated over the entire data link layer, excluding the length byte.

3.4.4. Teach-in Response telegram format

Upon receiving the teach-in telegram, the data logger module, when set in the bidirectional mode, will respond with the *Teach-in Response* telegram. The teach-in response telegram has a similar structure to the teach-in telegram (Figure 3.26), with the exception of not containing data channels bytes, and having an optional data byte. A teach-in response telegram is 17 bytes long and its structure is depicted in the Figure 3.31.
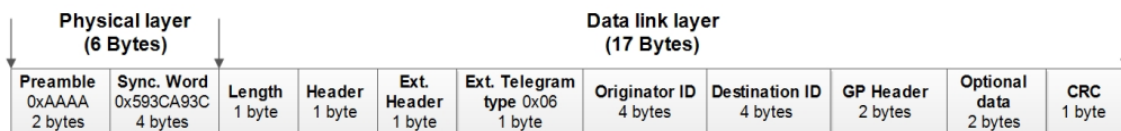
Figure 3.31. Teach-in Response telegram format.

3.4.4.1. Example of a Teach-in Response telegram format

As an example, the teach-in response bytes received by the sensor module, which previously sent a teach-in telegram, are analysed. The received bytes (hexadecimal) are as follows:

10 5F 02 06 60 14 02 59 60 12 04 2F 01 68 43 01 EE.

The header encoding field is provided in Table 3.31. The only difference compared to the header byte of a teach-in telegram (Table 3.6), is the indication that a *Destination ID* is available as well. This is the ID of the sensor module which originally sent the teach-in telegram.

Table 3.31. Encoding of a teach-in response header byte.

Header (1 byte)		0x5F = 0101 1111$_2$
Bits 7…5	Bit 4	Bits 3…0
010	1	1111
ID size (48, 32, or 24 bits) 010 = 32 bit Originator ID = 32 bit Destination ID	Is Extended header (1 byte) present or not? 1 = Present	Telegram type 1111 = Extended telegram type field present (1 byte)

The extended header byte is available and it is identical to the data telegram (Table 3.20). It describes that this is an original telegram, and that there are 2 bytes of optional data available in the teach-in response telegram.

The extended telegram type byte has a value 0x06, compared to 0x05 in a teach-in telegram. As previously mentioned, the value 0x06 identifies this type of telegram, according to GP specification, as *Teach-in response* telegram [58].

The following 8 bytes, is the data logger module ID (0x60 14 02 59) and the sensor module ID (0x60 12 04 2F).

The generic profiles header contains the manufacturer ID and confirms the outcome of the teach-in procedure.

Table 3.32. Encoding example of the Generic Profiles Header field of the Teach-in Response telegram.

GP Header (2 bytes)		0x01 68 = 0000 0001 0110 1000$_2$
Bits 15…5	Bits 4..3	Bits 2…0
0000 0001 011$_2$ = 0x0B	01	000
Manufacturer ID 0x0B is code for EnOcean	Result 01 = teach-in successful	Not used

The 2 bytes following the GP Header are *Optional data* bytes (0x43 01). Table 3.33 outlines the encoding of these 2 bytes. The last byte in the teach-in response telegram is the calculated CRC-8 byte (0xEE in this example).

Table 3.33. Optional data bytes encoding of the Teach-in Response telegram.

Optional data (2 bytes)	Received value: 0x43 01 = 0100 0011 0000 0001$_2$

Bits 15…14	Bits 13 … 8	Bits 7…6	Bits 5…0
01_2	$00\ 0011_2 = 3_{10}$	00_2	$00\ 0001_2$
Subtelegram number 01_2: Subtelegram number 1	Telegram Sequence number is 3_{10}	CCA status **00_2 = OK at 1st attempt** 01_2 = OK at 2nd attempt 10_2 = OK at 3rd attempt	Reserved

How the DolphinView tool from EnOcean interprets the above teach-in response telegram is depicted in the figure below.

Figure 3.32. Teach-in response telegram interpreted by DolphinView tool from EnOcean.

3.5. *Additionally integrated pre telegram sending features*

3.5.1. Clear Channel Assessment mechanism

As previously stated, at the very end of the data telegram there are two bytes called optional data. The second byte of the optional data contains information about radio link occupancy. This information is obtained through the radio chip's integrated mechanism called Clear Channel Assessment (CCA). This mechanism is activated before sending each subtelegram, and during this time, the radio channel is observed for noise. The radio chip is in the receiver mode and consumes around 25 mA at 3.6 V.

To minimise sensor module energy consumption, it is important to keep the clear channel sense time as low as possible. In radio norms, this listening time is known as LBT (Listen before talk) time. Depending on different radio norms, the request on the minimum LBT time can vary from 128 μs [43] to 160 μs [57]. By altering the number of analysed RSSI input samples in the AGC_CFGO register of the radio chip [34], the LBT time will change also.

Table 3.34 shows how the clear channel sense time varies with different radio register settings. It also indicates how this reflects on the overall energy consumption per subtelegram transmission. From this it is clear that the CCA mechanism can consume up to 2.5% of the overall energy needed for subtelegram transmission, if 9 RSSI input samples are used to obtain a RSSI value. The test suggested that taking only 3 input RSSI samples is sufficient to obtain a correct RSSI value. By selecting this setting, the CCA mechanism consumes only 1.1% of the overall energy needed for one subtelegram transmission. Analysing less than 3 samples is not recommended since it will most frequently result in the incorrect RSSI value.

Table 3.34. Measured duration of the CCA mechanism, depending on the number of analysed samples and the respective correlation with the consumed energy [8].

No. of the RSSI samples	Measured CCA duration [ms]	Consumed energy by the CCA mechanism [µJ]	Percentage in overall subtelegram transmit energy [%]
2	2.54	228.6	0.88
3	3.24	291.6	1.13
5	4.56	410.4	1.58
9	7.18	646.2	2.49

If the radio channel is busy (signals stronger than the threshold set in the AGC_CS_THR register [34] are present in the air), the sending of a subtelegram will be postponed. In the developed protocol it is designed that after 150 ms, the second CCA is triggered. If this also fails, the third one will be executed 350 ms later (500 ms total delay from first CCA check). The value of timing is related to an average telegram transmit time. This allows any transmission already in progress from other sensor modules to finish, before the channel is checked for clearance again. If all three CCA attempts fail, the subtelegram sending will be completely cancelled until the next wake up cycle, due to the busy channel. When the receiver misses the receipt of the three subtelegrams, optional data can then be used to determine if the reason for missed reception was due to a congested radio channel. In Figure 3.33 the complete CCA algorithm integrated into the communication protocol is provided.
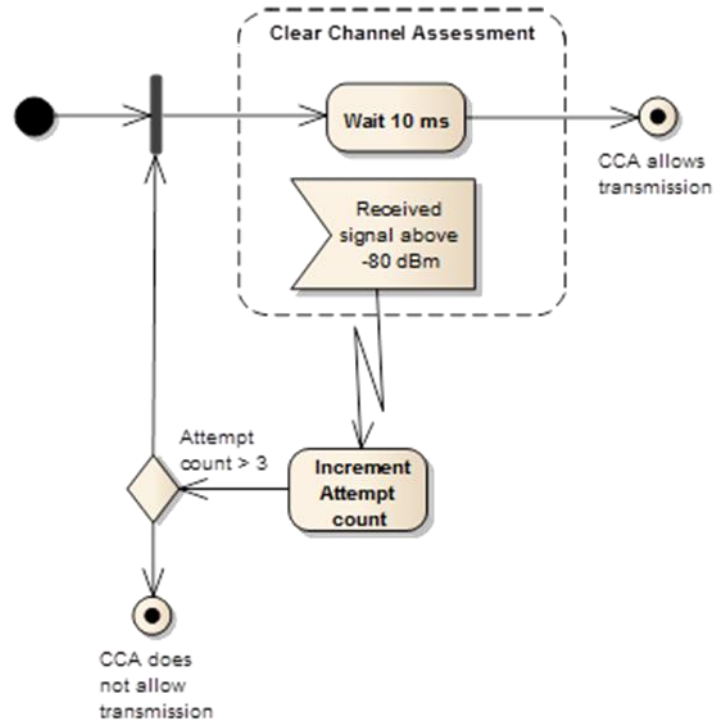
Figure 3.33. The CCA algorithm integrated into the communication protocol.

3.5.2. Data whitening mechanism

One of the packet handling hardware support features integrated into the radio chip is called *Data Whitening*. From a radio perspective, the ideal over the air data is random and free of DC components. This results in the smoothest power distribution over the occupied bandwidth. This also allows uniform operation conditions of the regulation loops in the receiver, without any data dependencies [34].

Real data often contains long sequences of zeros and ones making it difficult to track the data bits. In these cases, performance can be improved by whitening the data before transmitting, and de-whitening the data in the receiver. With the CC1120, this can be done automatically. By setting the value of WHITE_DATA to 1 in the register PKT_CFG1, all data, except the preamble and the synchronization word will be XORed with a 9-bit pseudo-random (PN9) sequence, before being transmitted [34].

Data whitening is applied to each telegram sent by the developed sensor system. How this mechanism improves the sensor system performance is evident from the figures below. These figures depict data logger module sensitivity, without (Figure 3.34) and with (Figure 3.35) the data whitening mechanism enabled. By enabling data whitening, an additional 2 dB is gained in the data logger module sensitivity at the central transmit frequency.
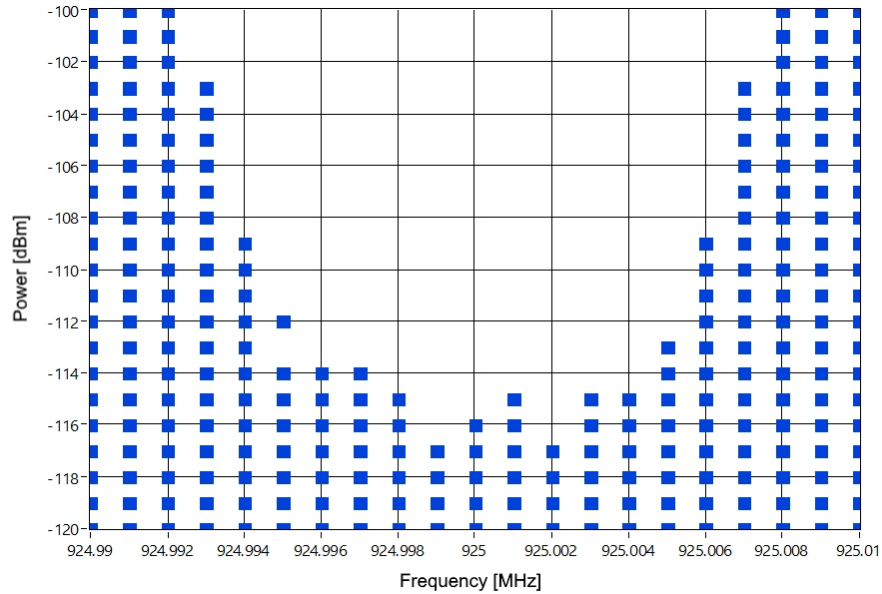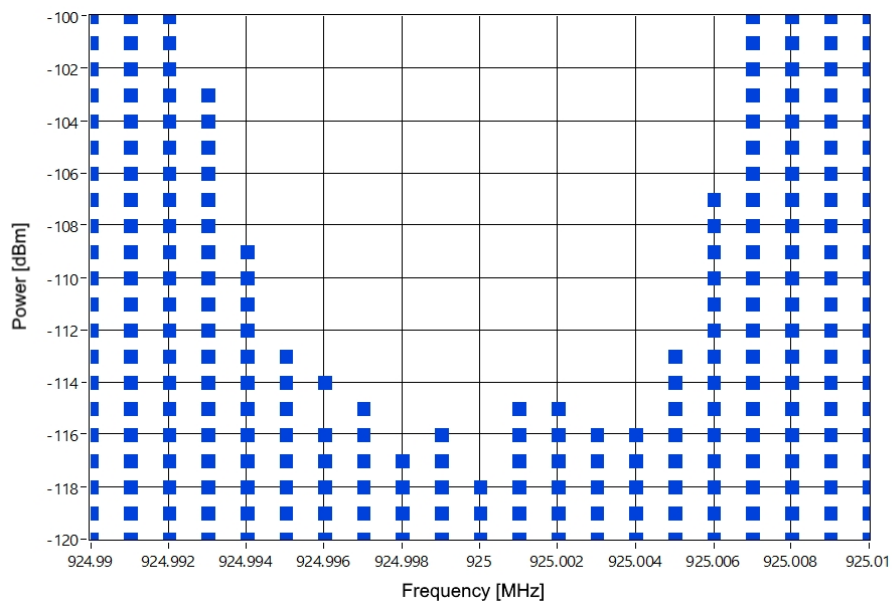
Figure 3.34. Measured data logger module sensitivity at the central transmit frequency and within ± 10 kHz from the central frequency. Data whitening is DISABLED. Receiver Channel bandwidth filter (CHAN_BW) is set to 16 kHz.

Figure 3.35. Measured data logger module sensitivity at the central transmit frequency and within ± 10 kHz from the central frequency. Data whitening is ENABLED. Receiver Channel bandwidth filter (CHAN_BW) is set to 16 kHz.

3.6. Radio telegram chaining

Some radio norms, like Japanese ARIB limit the maximum transmission time. According to one of the ARIB standards STD-T108, the maximum allowed transmission duration time is 200 ms, after which, a pause of minimum 5 ms is needed [43]. Since the intention to one day

119

bring the developed sensor system to the market, limitations like this need to be taken into consideration. Transmission duration of the described teach-in telegram in Chapter 3.4.1.1 would be longer than 200 ms, it would last 294.4 ms. Therefore a tech-in telegram needs to be split and transmitted into smaller parts. This mechanism, as a standard part of the described communication protocol, is called *Radio telegram chaining.*

When a chained subtelegram is received by a data logger module operating in a "normal" mode, it is automatically merged into a single subtelegram. In this form it is available at the serial interface. Figure 3.36 shows a chained teach-in telegram captured by a data logger module set in the "sniffer" mode. The "Sniffer" mode means subtelegrams are displayed exactly as they are transmitted over the air.

Figure 3.36. Parts of the chained teach-in telegram.

An original message and a first split part are provided below.

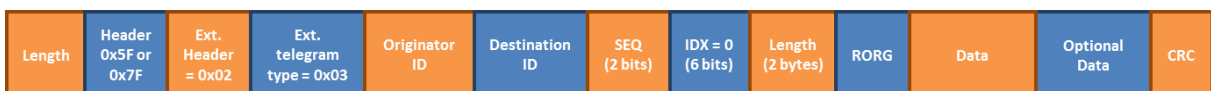*Figure 3.37. Original message (e.g. teach-in telegram)*

Figure 3.38. First split part of the main message.

Each message can be split into multiple parts. The first split part differs slightly compared to the other split parts which are identical in their structure. The first split part contains two additional *Length* bytes and a R-ORG value. For coding the fields shown in Figure 3.38 the following rules apply:

- The first *Length* byte represents the number of bytes in the 1st split part.
- Since a teach-in telegram is a non-addressed message, the *Header* byte field indicates that the 48 bit Originator ID is present, and that there is no Destination ID present in the sent telegram (value 0x7F). A 48 bit Originator ID is transmitted only once due to the ARIB regulation request [43].

120

- The *Header* byte field indicates that the *Extended header* is available**.**

- The *Header* byte field indicates that the *Extended telegram type* is available.

- The *Extended header* with the value 0x02 indicates that the two bytes of *Optional data* are present in the 1st split part. The *Optional data* bytes are removed from the merged telegram.

- The *Extended telegram type* is always set to the value 0x03, which indicates *Chained data message* [52] with the R-ORG value of 0x40 [58].

- *Sequence* (*SEQ*) indicates the current sequence number of the chained message. The sensor module increments this number after sending the complete chained message. Every split part of the original telegram belonging to the same chained message has the same sequence number.

- *Index* (*IDX*) is an index of the split part of the telegram. The first split part has IDX = 0, the second IDX = 1 and so on...

- The 2nd *Length* field is the length, in bytes of the *Payload* from the *Data Link Layer* of the original message. *Payload* includes the *Generic Profiles Header* and the *Channels description* bytes for a teach-in telegram (Figure 3.26). *Payload* for a data telegram includes *Measurement* data (Figure 3.29).

- R-ORG value is evaluated based on the *Telegram type* and the *Extended telegram type* fields of the original message. For a teach-in request telegram this value is set to 0xB0

- *Optional data* does not contain the *Optional data bytes* from the original message. *Optional data* from each split part has the same subtelegram number. The CCA attempt value can vary, while the sequence number corresponds to the internal counter of the sensor module. This counter is increased by 1 for each transmitted content (data telegram or the split part of the chained teach-in telegram respectively).

Content of the second and each subsequent split part slightly differs from the first split part of the chained telegram. It does not contain a *Payload Length* field or a R-ORG field. Currently, each teach-in telegram sent by the sensor module is split into 3 chained parts, but in some future applications the number of splits can be even higher. As seen in Figure 3.39, the content of the 2nd and further split parts is displayed.
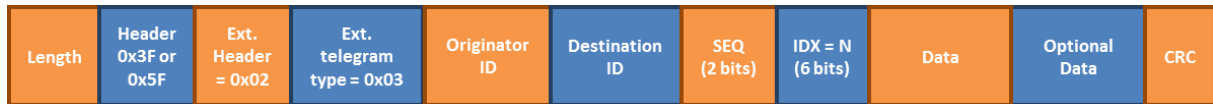
Figure 3.39. The content of the second and each further split parts of the chained telegram.

At the data logger module, all the split parts will be merged again into one message, and the content of this message for a teach-in telegram will be identical as shown in Figure 3.26. Data telegrams are not split currently, but if needed, the same rules as described in this chapter would be followed.

During the merging process the following rules apply:

- The *Length* byte is now indicating the number of bytes in the data link layer of the merged telegram, not the number of bytes in the split parts.

- In case of an addressed message, the *Header* is set to indicate that a 32 bit Originator ID is present, together with the 32 bit Destination-ID (value 010_2). In standard use case of a non-addressed message, the *Header* field indicates that the 32 bit Originator-ID is present, and that there is no Destination-ID present in the sent telegram (value 001_2) [52].

- The Header field always indicates that there is no *Extended header* field.

- The Header field, depending on the R-ORG value, indicates whether the *Extended telegram type* is available or not.

- The *Extended telegram type* is set based on the R-ORG value.

- Content and length of the *Payload* is exactly the same as before the splitting and chaining process.

3.6.1. Example of Teach-in Telegram chaining

Each teach-in telegram sent by the sensor module is actually a chained telegram. This is already seen in Figure 3.36. In this example, a 40 byte long tech-in telegram is split into 3 parts with a length of 25, 25, 23 bytes respectively.

The content (hexadecimal) of the merged teach-in telegram is:

28 2F 05 60 12 04 2F *01 70 42 93 00 16 41 41 98 00 13 2B C0 53 C0 53 46 17 D8 13 C1 45 96 00 16 41 C0 53 C0 53 C0 56* 3D

These bytes are transmitted over the air as outlined in Table 3.35.

Table 3.35. Split teach-in telegram parts content (hexadecimal) example.

| **1st Split part , 25 bytes long, SEQUENCE = 2, INDEX = 0** |
| **19** 7F 02 03 00 00 60 12 04 2F 80 00 20 B0 <u>01 70 42 93 00 16 41 41</u> 75 00 20 |
| **2nd Split part , 25 bytes long, SEQUENCE = 2, INDEX = 1** |
| **19** 3F 02 03 60 12 04 2F 81 <u>98 00 13 2B C0 53 C0 53 46 17 D8 13 C1</u> 76 00 34 |
| **3rd Split part , 23 bytes long, SEQUENCE = 2, INDEX = 2** |
| **17** 3F 02 03 60 12 04 2F 82 <u>45 96 00 16 41 C0 53 C0 53 C0 56</u> 77 00 07 |

Field	Value	Meaning
Length	19	25 bytes long is the first split part
	19	25 bytes long is the second split part
	17	23 bytes long is the third split part
Header	7F	48 bit Originator ID, no destination ID
		Extended header available
		Extended telegram type available
	3F	32 bit Originator ID, no destination ID
		Extended header available
	3F	Extended telegram type available
Extended Header	02	Original telegram, not a repeated one
	02	2 bytes of Optional data are present
	02	
Extended Telegram Type	03	Chained data message
	03	
	03	
48 bit Originator ID	00 00 60 12 04 2F	48 bit Sensor module ID
	60 12 04 2F	32 bit Sensor module ID
	60 12 04 2F	
Sequence and Index	80	Sequence number of the chained telegram is 2
		Index number of the split part is 0
	81	Sequence number of the chained telegram is 2
		Index number of the split part is 1

	82	Sequence number of the chained telegram is 2 Index number of the split part is 2
Payload Length	00 20	Merged telegram will have 32 bytes of data Payload
	Not present field	
	Not present field	
R-ORG	B0	Merged telegram will be Generic profiles Teach-in Request
	Not present field	
	Not present field	
Optional data	75 00	Subtelegram number 1 Transmitted content sequence number is 53 CCA was OK at 1st attempt
	76 00	Subtelegram number 1 Transmitted content sequence number is 54 CCA was OK at 1st attempt
	77 00	Subtelegram number 1 Transmitted content sequence number is 55 CCA was OK at 1st attempt
CRC-8	20	Calculated CRC-8 byte over entire data content except first length part for each split part.
	34	
	07	

3.7. Radio telegram repeating

The data logger module is capable of retransmitting received telegrams. This function is called radio telegram repeating [60]. By using radio telegram repeating, a received telegram can be forwarded once to the next data logger module in the sensor network. Through this, the transmission range can be expended. Particular rules apply when this telegram repeating mode is enabled in the data logger module. The repeated subtelegrams are sent at specific times defined in the Table 3.36. The time slot calculation starts after receiving the first original

subtelegram, while the other original subtelegrams (2nd and 3rd respectively) will not be repeated.

Table 3.36. Timings of the repeated subtelegrams.

1st repeated subtelegram	2nd repeated subtelegram	3rd repeated subtelegram
2.1 seconds	8.4 seconds	14.7 seconds

Before sending repeated subtelegrams, the data logger will trigger the CCA mechanism to check for a clear radio channel. The repeated telegrams will not be acknowledged by any data logger module in the sensor network. The repeated telegrams differ from the original telegrams by the timing at which they are received by the data logger module, but also by the extended header byte. The bits in this byte define whether the received subtelegram is a repetition or the original. Before it is included in the repeated subtelegram, the extended header byte is modified by the data logger set in the repeater mode. Table 3.37 shows the possible encoding of the extended header byte [52]. Since teach-in telegrams do not have an extended header field, they are not intended to be repeated.

Table 3.37. All possible encodings of the Extended header field.

Extended header (1 byte)	
Bits 7…4	Bits 3…0
Repeater counter 0000 = Original telegram 0001 … 1110 = Repeated telegram level 1111 = Original telegram which is not allowed to be repeated.	The length of the optional data 0000 = No optional data bytes Other = Number of optional data bytes

Enabling repeating in a data logger module is done by sending a serial command via the host interface. It is possible to enable filter and allow the repetition of subtelegrams which arrive only from a specific sensor module. This is achieved by storing that sensor module ID into the data logger module memory, also by sending a specific serial command (Figure 3.40).
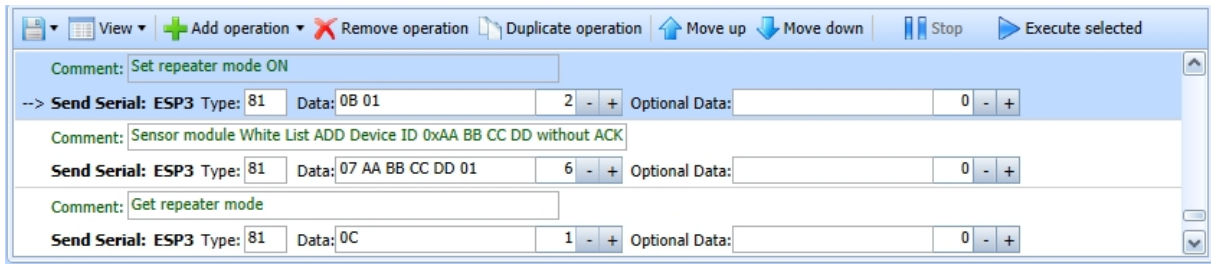
Figure 3.40. Serial commands used to enable repeater mode at the data logger module sent via DolphinView tool.

3.7.1. Test of repeater functionality

A test of repeater functionality was carried out indoors. The floor plan of the building together with the positions of the sensor modules and data logger modules is portrayed in Figure 3.41.
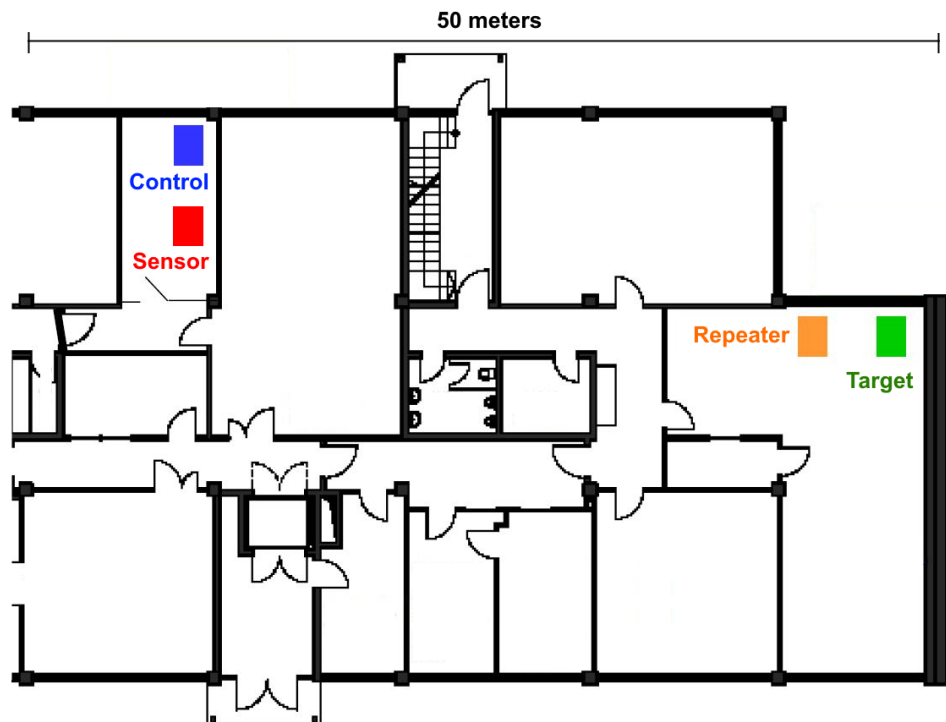

Figure 3.41. Floor plan and module positions for the repeater functionality tests.

The repeater test was conducted using the following procedure. A stable communication between the sensor module and target data logger was first established. The received subtelegrams RSSI value over a distance of around 40 meters and 4 thick concrete walls was approximately -100 dBm. After this, the target data logger module was contained within a shielded box, and an additional 40 dB of attenuation was added to the external antenna. In this setup, the target data logger module could no longer receive subtelegrams sent from the same

sensor module. Two additional data logger modules were introduced into the test. One was set in the repeater mode and placed 1 meter from the target data logger module. The other, a control data logger module, was placed in the same room as the sensor module. The repeater data logger had a stable radio link connection with all modules in the test, the sensor module, the control data logger module and also with the target data logger module in the shielded box.

The sensor module continued transmitting subtelegrams every 15 minutes. The target data logger module was now able to receive these telegrams due to the repeater data logger positioned in its proximity. When the repeater data logger was turned off, the target data logger module could not receive any subtelegrams. These results are clearly displayed in Figure 3.42 and Figure 3.43 respectively. Figure 3.42 depicts the telegram log obtained from the control data logger module. This control data logger module was receiving all the sent subtelegrams from the sensor module as well as repeated telegrams sent from the repeater data logger module. All the "original" subtelegrams are identified as subtelegram 1, subtelegram 2, and subtelegram 3 respectively. The repeated telegrams are identified as subtelgram 4, subtelgram 5 and subtelegram 6 respectively. Figure 3.43 depicts the telegram log obtained from the target data logger module. During the time when the repeater data logger module was shut down, the target data logger module could not receive any telegrams. After a period of one and a half hours, the repeater data logger module was turned on again, and the target data logger module began receiving subtelegrams again.

Figure 3.42. The telegram log from the "control" data logger module placed in the same room as the sensor module. Marked in the green box are the received repeated subtelegrams, while marked in the yellow box are the original telegrams received when the repeater was shut down.

Figure 3.43. The telegram log from the "target" data logger module. Marked in the red box is the first subtelegram received after the "repeater" data logger module was turned on again.

4. OPERATION FLOWCHART AND ENERGY USAGE CONTROL ALGORITHM

Energy efficiency of the sensor module relies on its ability to function in different operation modes, which continuously execute a defined operation cycle, while also maintaining 100% (or close to 100%) of the available energy. If the sensor module constantly remains in the active mode with continuous energy consumption, it would be difficult to achieve any energy efficiency. The sensor module needs to operate in at least two modes: active mode and sleeping mode. The sensor module should spend the majority of operation time in sleep mode. At defined moments, it should wake up, shortly enter active mode to execute needed operations such as collection of data from the attached sensors, data processing and data transmission. Then it should enter sleep mode once again. Based on these assumptions, the sensor module's operation flowchart is designed as depicted in Figure 4.1.
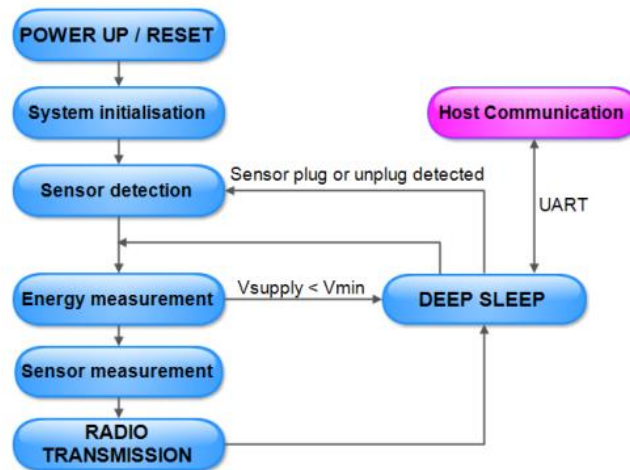
Figure 4.1. Operation flowchart of a sensor module.

In each of the steps shown, the sensor module can enter sleep mode to save additional energy before reaching its true low power state; the deep sleep mode. Entering deep sleep mode between the operation steps is avoided, since this mode requires re-initialisation of microcontroller's peripherals. Thus doing this, would be less energy efficient than just entering sleep mode. Based on this, the sensor module is always in one these three modes: active mode, sleep mode or deep sleep mode. Aside from these three operating modes, there is a non-operating mode, when the sensor module is shut down. This occurs when there is no external sensors connected to the sensor module, or when the supercapacitor's undervoltage protection circuitry is active (Chapter 2.1.1.4). In this case, the sensor module's

microcontroller is physically disconnected from the supercapacitor or, has a "weak" connection through the reversely polarised diode. The complete sensor module shutdown mode is useful when a sensor module is stored and not in use, or during transportation to installation location.

Upon sensor plug-in the microcontroller becomes powered and the programmed sensor module's algorithm starts executing tasks from the flowchart in Figure 4.1. During each wake-up, the sensor module can transmit either teach-in subtelegrams together with data subtelegrams (teach-in transmit cycle), or only data subtelegrams (data transmit cycle).

One complete teach-in transmit cycle, recorded upon analog ambient temperature and humidity sensor connection, can be seen in Figure 4.2. The shown case is for a sensor module operating in the default unidirectional communication mode (Chapter 3.3.1.). A teach-in transmit cycle will be carried out each time one of the following scenarios occurs:

1. When a sensor is plugged in for the first time.
2. When a second sensor is connected.
3. When there are two sensors connected to the sensor module and one of them is disconnected.
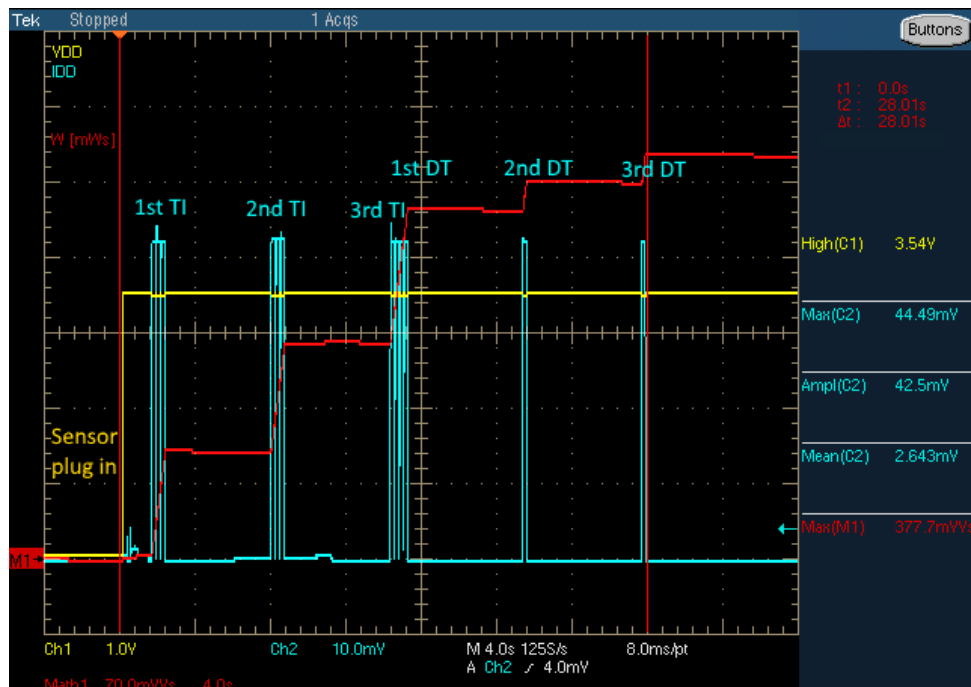
Figure 4.2. Oscillogram of a teach-in transmit cycle. Transmission of 3 chained teach-in subtelegrams is followed by 3 data subtelegrams. The blue curve represents a voltage drop measured across 1 Ohm shunt resistor used on the main power supply line. The blue curve and the associated values represent current drawn [mA] by sensor module during the entire cycle. The yellow curve (VDD) is the microcontroller supply voltage

and the red curve (W) represents the total consumed energy during one teach-in transmit cycle. The red curve is obtained by enabling a mathematical integral function over the product of the two input channels; supply voltage (VDD) and supply current (IDD).

As clear from Figure 4.2, the total duration of one teach-in transmit cycle is 28 seconds and the total consumed energy during this time is around 378 mWs. During these 28 seconds, between each transmission, the sensor module is in the lowest energy consuming state; the deep sleep mode. This state occurs 4 times and lasts a total of 25 seconds, or 90% of the teach-in transmit cycle. The rest of the time (9.5%) the microcontroller is in the sleep mode while other peripherals such as the radio chip, or sensors can be active. During one wake-up cycle the microcontroller is in its active mode only 0.5% of the time.

The highest energy consumption occurs during the radio transmission state. In Figure 4.2 this state is indicated by the steepest slopes of the consumed energy curve (red line).

After a 3rd data subtelegram is sent, the entire sensor module re-enters deep sleep mode for predefined time (15 minutes is the default). Upon the next wake up cycle, if the sensor configuration did not change, the sensor module will execute the data transmit cycle shown in Figure 4.3. As seen in the figure, the total duration of one data transmit cycle is approximately 14 seconds and at 3.5 V of supply voltage, a total 88 mWs of energy is consumed during this time. This is 77% less energy consumption compared to the teach-in transmit cycle shown in Figure 4.2. If the sensor configuration does not change (i.e. the sensor module remains installed at the same location with the same type of sensor), this will be the energy consumption for each sensor module wake-up cycle. This is also one of the energy efficiency guarantees of the developed communication protocol and the supporting operating algorithm.

In the following chapters, the tasks performed at each operating state are explained and a closer look is given to the energy consumption at each of these states.
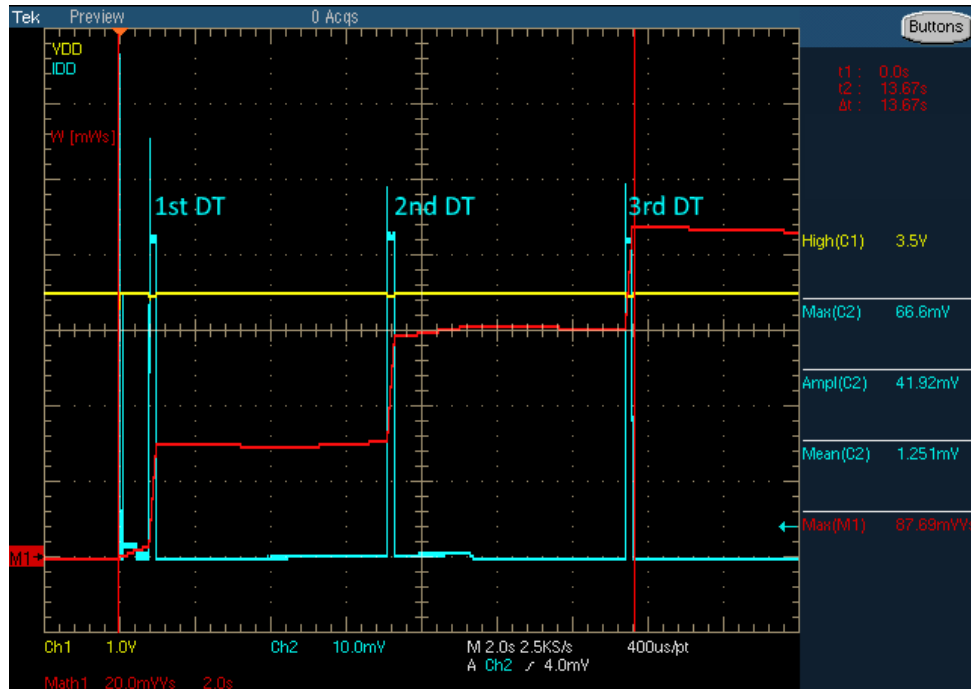
Figure 4.3. Oscillogram of a data transmit cycle. 3 data subtelegrams transmissions upon regular sensor module wake-up. The blue curve represents voltage drop measured across 1 Ohm shunt resistor used on the main power supply line. The blue curve and the associated values represent current drawn [mA] by sensor module during the entire cycle. The yellow curve (VDD) is the microcontroller supply voltage and the red curve (W) represents the total consumed energy during one data transmit cycle. The red curve is obtained by enabling a mathematical integral function over the product of two input channels; supply voltage (VDD) and supply current (IDD).

4.1. Power-up and Reset state

As mentioned earlier, when an external sensor is connected for the first time, the sensor module powers up, since a physical connection is established between the supercapacitor and microcontroller. The highest current peaks, approximately 80 mA, can be observed during this power-up (Figure 4.4). This is due to the many capacitors becoming charged for the first time. For example, on the main power supply line there are two 10 µF ceramic capacitors and one 4.7 µF ceramic capacitor. After the power-up, it takes around 10 ms before the internal clocks and voltages are stabilised and the system initialisation phase begins. During the power-up phase, between the first two current peaks (Figure 4.4) around 0.2 mWs of energy is consumed. 0.5 mWs is consumed during initialisation phase, which follows immediately after. This phase has a duration of approximately 70 ms.
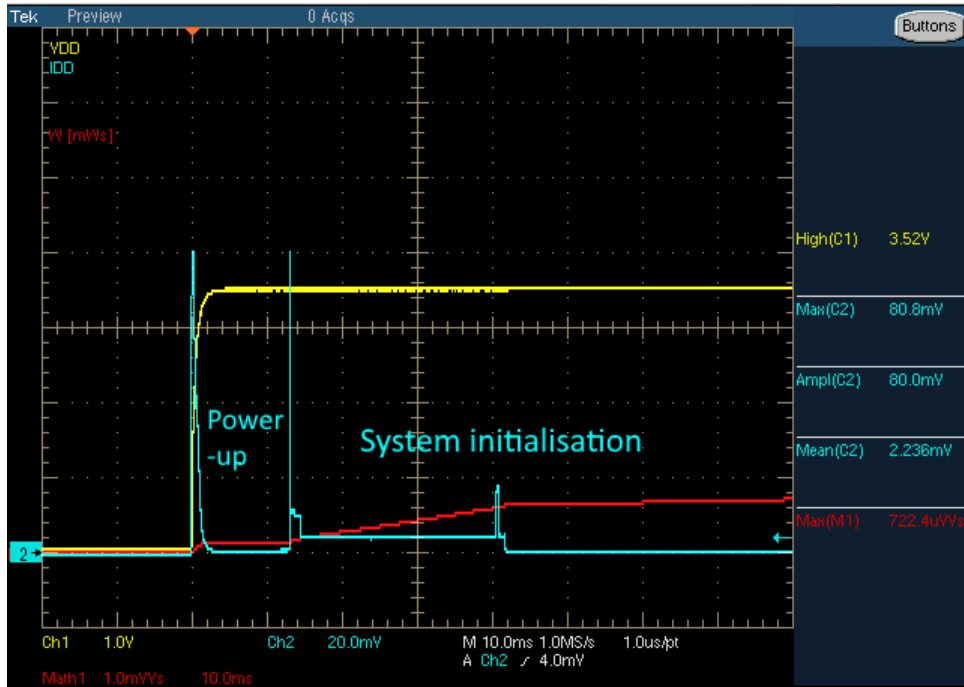
Figure 4.4. The current peaks upon sensor's first plug in. The sensor plug in moment is represented with the increase of supply voltage VDD (yellow curve) from 0 V to 3.52 V. A current peak of approximately 80 mA is observed during this moment. The second current peak occurs at the start of the system initialisation phase. The third current peak, close to 20 mA, occurs upon enabling the radio and flash chip for the initialisation.

The microcontroller does not start executing code until the supply voltage reaches V_{SVSH+}. This is controlled by the microcontroller Supply Voltage Supervisor (SVS), whose limits are given in the table below [21].

Table 4.1. Microcontroller Supply voltage supervisor (SVS) parameters [21].

	PARAMETER	TEST CONDITIONS	MIN	TYP	MAX	UNIT
$I_{SVSH,LPM}$	SVS_H current consumption, low power modes			170	300	nA
V_{SVSH-}	SVS_H power-down level		1.75	1.80	1.85	V
V_{SVSH+}	SVS_H power-up level		1.77	1.88	1.99	V
V_{SVSH_hys}	SVS_H hysteresis		40		120	mV
$t_{PD,SVSH, AM}$	SVS_H propagation delay, active mode	$dV_{Vcc}/dt = -10$ mV/µs			10	µs

To reset the sensor module, all of the external sensors must be unplugged. If only one sensor is disconnected while the other remains plugged in, the sensor module will undergo the sensor detection state (Chapter 4.3) to identify which sensor is still connected.

4.2. System initialisation state

During the sensor module's initialisation phase (Figure 4.4) the following actions are executed:

- Cause of wake up is identified.

- Peripherals (GPIOs, ADC) and interrupts are initialised.

- The radio and flash module are initialised.

- The watchdog timer is set up.

After the cause of the sensor module wakeup is identified, it is logged and included in the sensor module status bytes. These are transmitted as part of the data telegram (Chapter 3.4.2.2).

Table 4.2 displays the estimated duration of the tasks performed and the energy consumed by the sensor module during the initialisation phase. The values regarding energy consumption are obtained from the component data sheets, while the duration of tasks is estimated from the software code.

Table 4.2. Duration and energy consumption of the tasks performed during the initialisation phase. Red highlights current consumption values above 0.5 mA and yellow represents current consumption values between 0.5 μA and 0.5 mA.

Initialisation Phase	Time duration	MCU	Radio	Flash	Other	Charge (mAs)	Energy (mWs)
Basic/IO Part 1	1.6 ms	0.80 mA			0.80 μA	0.063423 mAs	0.228324 mWs
ADC Energy Threshold (Voltage)	2.0 ms	0.80 mA			0.80 μA		
Basic/IO Part 2	1.0 ms	0.80 mA			0.80 μA		
Flash	12.0 ms	0.80 mA	1.3 mA	9.0 mA	0.80 μA		
Radio	21.0 ms	0.80 mA	1.3 mA	50.00 μA	0.80 μA	0.045167 mAs	0.162600 mWs
Timer	28.0 ms	0.80 mA	0.50 μA	1.00 μA	0.80 μA	0.022464 mAs	0.080872 mWs
Basic/IO Part 3	4.0 ms	0.80 mA			0.80 μA	0.003203 mAs	0.011532 mWs
	69.6 ms					0.134258 mAs	**0.483327 mWs**

The energy consumption of the initialisation phase is estimated to be approximately 0.48 mWs. This corresponds to the measured value of approximately 0.5 mWs (Figure 4.4).

The system initialisation state is a very low energy consuming state and it only occurs upon sensor connection for the first time. This state contributes to only 0.1% of the overall energy consumption of one teach-in transmit cycle.

4.3. Sensor detection state

At this step, the sensor module checks what type of sensor is connected to the sensor interface 1 and sensor interface 2 respectively. To be able to detect sensor presence on any of these interfaces a presence detection pin is used (Chapter 2.2.2.). The state of this pin will be altered from digital input (for interrupt detection when a sensor is connected), to an analog input, when voltage across the voltage divider, created upon sensor detection, is measured. After this, the state of the pin is altered back to digital input.

The presence of a sensor with an I^{2}C interface (e.g. digital illuminance sensor) can be detected by triggering the I^{2}C communication and waiting for the acknowledgment from the sensor. In this case, the I^{2}C address of the sensor should be known. This is an alternative, digital method of detecting sensor presence, compared to an analog detection via the resistor and voltage divider. The algorithm execution for sensor detection via the I^{2}C lines is shown below.

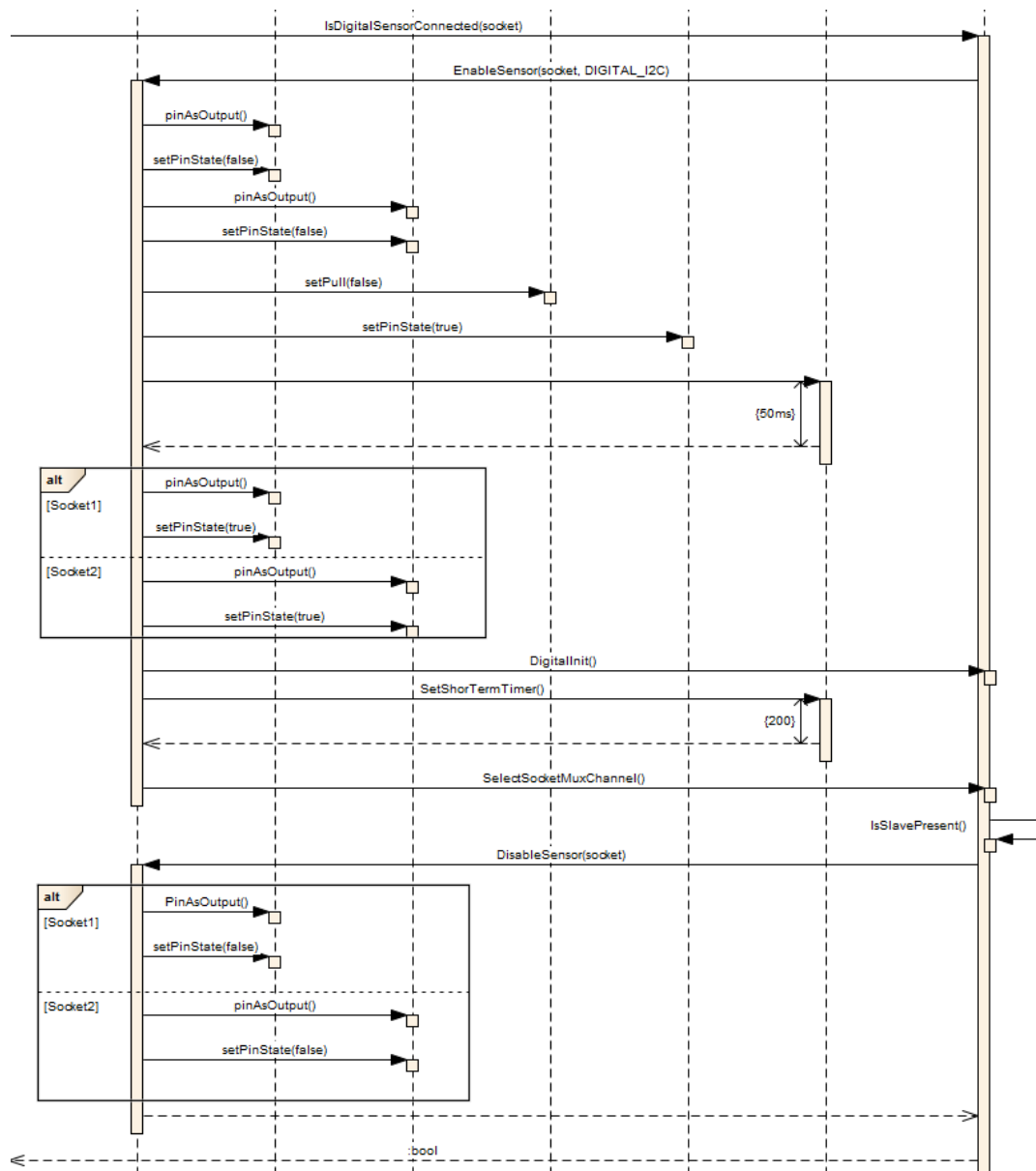*Figure 4.5. Algorithm for detection of an I^{2}C sensor connected to the sensor module.*

To detect sensor presence via the I^{2}C lines, the I^{2}C multiplexor chip needs to be enabled and the I^{2}C interface initialised. After initialisation, each of the sensor sockets (Sensor Interface 1 and 2 respectively) must be enabled to deliver power to the sensor supply pin. After this, the

I^2C communication is triggered towards both sensor sockets, while simultaneously waiting for the acknowledgment from the connected sensors. If the acknowledgment is not received, the algorithm assumes there are no digital sensors present on the I^2C lines. When the acknowledgment is detected, this confirmation will be returned to the main program and used later in the sensor measurement state.

In the future, more digital I^2C sensors are intended to be used with the sensor module. Therefore, this detection algorithm will be preferred over an analog approach, which uses the resistor voltage divider.

The sensor detection state either comes after the initialisation state, or after wake up from the deep sleep state upon sensor plug/unplug. When a sensor module wakes up the conventional way, by the real time clock timer, it skips the sensor detection state and it goes directly to the energy measurement state. This is due to the fact that no interrupts regarding sensor change have been detected.

4.4. Energy measurement state

In this state, the sensor module will decide if there is sufficient energy stored in the supercapacitor to continue executing further operation states. If there is not enough energy in the supercapacitor, the operation algorithm will put the sensor module in the deep sleep mode until the next wake up cycle. During this deep sleep mode, the supercapacitor recharges further. This continues until the voltage on the supercapacitor exceeds the programmed threshold. In order to make a decision, the microcontroller supply voltage needs to be measured and compared to the threshold value stored in the microcontroller memory. The threshold value is set to 2.5 V and is selected based on the performed undervoltage protection circuitry characterisation (Chapter 2.1.1.4). This value can be easily altered in the microcontroller memory by sending a dedicated serial command via the host interface. The microcontroller supply voltage is measured indirectly with the use of an internally generated reference voltage.

There are 3 different reference voltage values available in the microcontroller; 1.2 V, 2.0 V and 2.5 V [61]. A reference voltage of 2.0 V is used because it can cover the full supply voltage range from 2.5 V to 3.6 V. To determine the microcontroller supply voltage, half of its value is passed to the internal bandgap reference and used as the input channel of the ADC. This is set in the register ADC12CTL3 of the microcontroller [61]. If the 1.2 V reference is used it would allow a maximum of 2.4 V to be measured, which is insufficient in this case.

Preference is given to the 2.0 V voltage reference compared to 2.5 V, as it allows a better resolution of the ADC conversion. For a 12-bit ADC, 2.0 V voltage reference allows 0.488 mV resolution, compared to 0.610 mV allowed by the 2.5 V voltage reference.

The ADC value of microcontroller supply voltage is calculated from (4.1) and then scaled to the 3.6 V to 2.5 V voltage range.

$$ADC_{value} = \frac{VDD}{2} \times \frac{2^{12}}{V_{REF}} \tag{4.1}$$

When the stored energy on the supercapacitor is sufficient, the control algorithm in the sensor module allows the execution of the next operation state; sensor measurement.

If the sensor module supply voltage, during normal, outdoor operation, drops below the programmed threshold, this could be a serious indicator that something is wrong with the sensor module. For example, a potential short circuit caused by water intrusion due to damaged housing or assembly failure.

4.5. Sensor measurement state

In this state, the control algorithm powers the external sensors, by enabling the step-up converter to deliver a stable 3.6 V to the connected sensors (Chapter 2.2.2.). Depending on the sensor type, sensors can be powered for a shorter, or longer time. For example, the specific analog sensor which measures ambient temperature and humidity, must be powered for a minimum of 600 ms, compared to the minimum 200 ms for the specific digital illuminance sensor. In addition, depending on the type of the sensor, either ADC must be enabled, or the I²C multiplexor respectively. Sensors are enabled individually, and when the measurement value is obtained, the sensor is shut down. Then, the second sensor (if existing) is enabled, and after the measurement is complete and a value obtained, it is also shut down.

Each sensor should be evaluated individually, taking into consideration parameters such as minimum startup or warm up time before triggering measurements. These timings give an initial insight into system performance and the existing limiting factors. Furthermore, this is a step toward into overall system energy consumption optimisation.

In Figure 4.6 and Figure 4.7 recorded oscillograms displaying the sensor measurement state are shown. The measurements are obtained using the same setup used to measure energy consumption of the system initialisation state. In the given example, an analog sensor, which consumes much more energy than a digital sensor, is connected to the sensor module.

Before the sensor is powered, two of tasks must be executed; the ADC module of the microcontroller must be set up (measurements on two different analog pins in this case), and the supply voltage and selected voltage reference must become stable. These initial steps, before the sensor is enabled, are depicted in Figure 4.6. The duration of these tasks is approximately 30 ms and during this time 0.5 mWs of energy is consumed. The moment when the voltage step-up converter is enabled, is represented by the high current peak, reaching close to 70 mA, in Figure 4.6. This current peak is a result of the electrical current passing through the 4.7 µH inductor L1, and charging the 10 µF capacitor C6 in the input stage of the step-up converter (Chapter 2.2.2). After 50 ms wait time for the output voltage of the step-up converter to become stable, the analog sensor is enabled. This moment can be seen in Figure 4.6, as the second highest current peak (35 mA). The time taken to enable both the step-up converter and the analog sensor is extremely short. Although current peaks are high, the consumed energy during this time is quite low; around 0.2 mWs.

Figure 4.6. Transmission of the 3 data subtelegrams (upper section) and below, a zoomed-in picture of the operations performed before the transmission of the 1ˢᵗ data subtelegram. The two large current peaks (bottom blue lines) represent the enabling of the step-up converter (~70 mA) and the analog sensor (~35 mA) respectively.

After the sensor is enabled it starts to measure. Depending on the type of the sensor this measurement time can vary. This value is usually stated in the data sheet, or expressed through the sensor's minimum settling time. As seen in Figure 4.7, for the analog sensor used,

this measurement time is close to 400 ms. During this time almost 2 mWs of energy is consumed. After the measurement is complete, the measured values are received by the microcontroller and further processed. Meanwhile, the sensor is shut down, together with the step-up converter. In Figure 4.8 all the operation states executed before the 1st subtelegram transmission are provided. The operation steps executed before sending the 2nd and 3rd subtelegram are different. This is because these subtelegrams are only iterations of the 1st subtelegram. The information they carry is obtained before the 1st subtelegram is sent. The energy consumption curve (red line in Figure 4.8) is also given. The total execution time of the here mentioned operations is close to 800 ms and the energy consumed is around 3 mWs. This represents 3.4% of the overall energy consumed during the data transmission cycle.
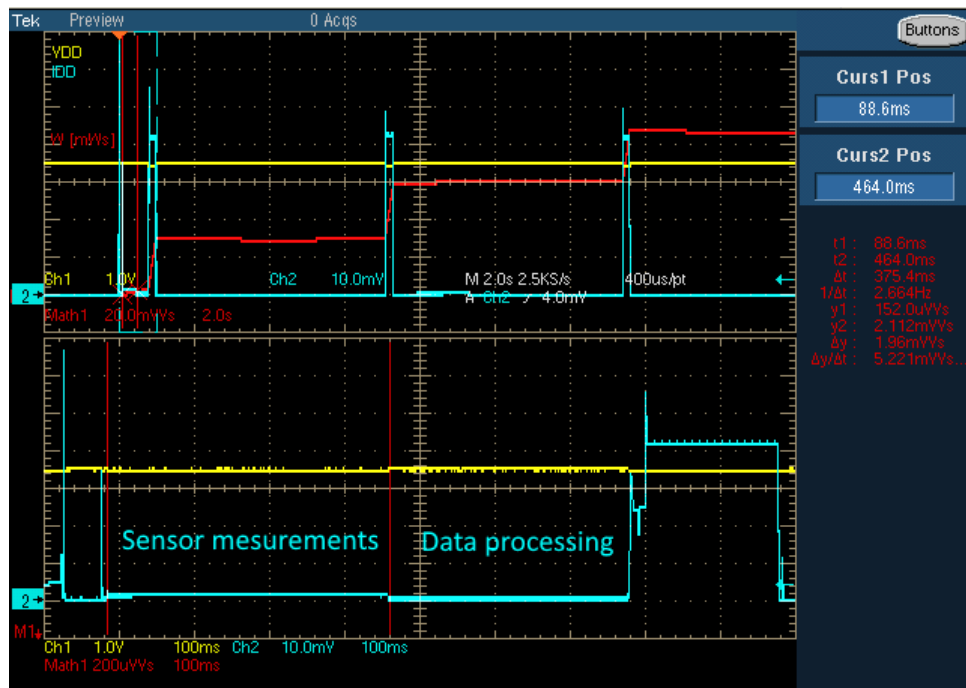

Figure 4.7. Execution of measurements after powering the sensor and processing of the obtained data.

Figure 4.8. Operations executed before the 1ˢᵗ data subtelegram transmission and the energy consumed during this time. The total time between the two red markers is 779.2 ms and the energy consumed during this time is 3 mWs. After the second red marker, the red curve starts to quickly ascend, representing the beginning of the 1ˢᵗ subtelegram transmission.

4.6. Radio transmission state

In this state, the obtained and processed measurement values are ready to be packed into a data telegram and transmitted. Whether, teach-in or data telegram they are formed in this state and before they are transmitted, they are also stored in the external flash memory via SPI lines. The difference between storing and transmitting the first (chained) teach-in telegram and data telegram can be seen in **Figure 4.9** and Figure 4.10 respectively.

In Figure 4.10, the time taken to store the first data subtelegram in the flash memory can be observed. The duration of this task depends on the type of sensor connected, but the average value of 20 ms can be taken as a reference. From a software perspective, the teach-in and the data telegram preparation are identical operations. This implies they share the same core functionalities such as, transmission of the radio telegrams, control of the timing between subtelegrams, and checking for the acknowledge telegrams in the bidirectional mode. Between each of these activities the microcontroller enters sleep mode (LPM3).
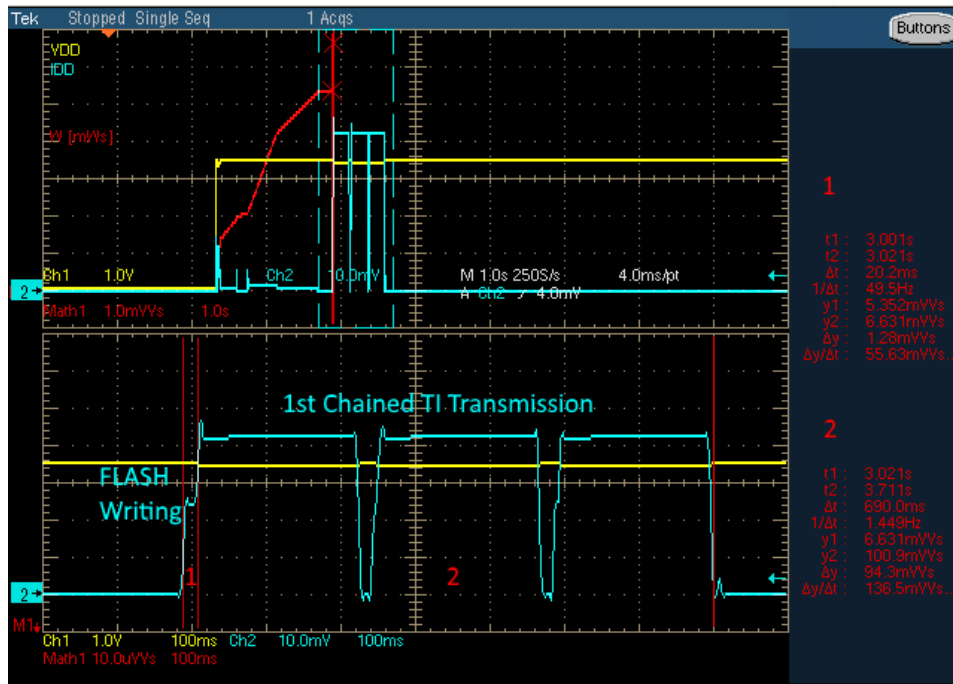
Figure 4.9. Before the 1st teach-in subtelegram is transmitted, a copy of its data is stored in the flash memory (not the entire teach-in telegram structure). This action lasts around 20 ms for an analog sensor and consumes around 1.3 mWs of energy. During this time, both the flash chip and radio chip are powered, resulting in current peaks of up to 30 mA. After this, the 1st teach-in subtelegram is transmitted as a chained telegram. Between the chained parts, there is a small pause where the radio chip shuts down due to limitations of the regulatory norms. The transmission of one chained TI subtelegram lasts around 690 ms for an analog sensor (46 bytes + 2 bytes radio added CRC). The energy consumed during this is approximately 94 mWs.
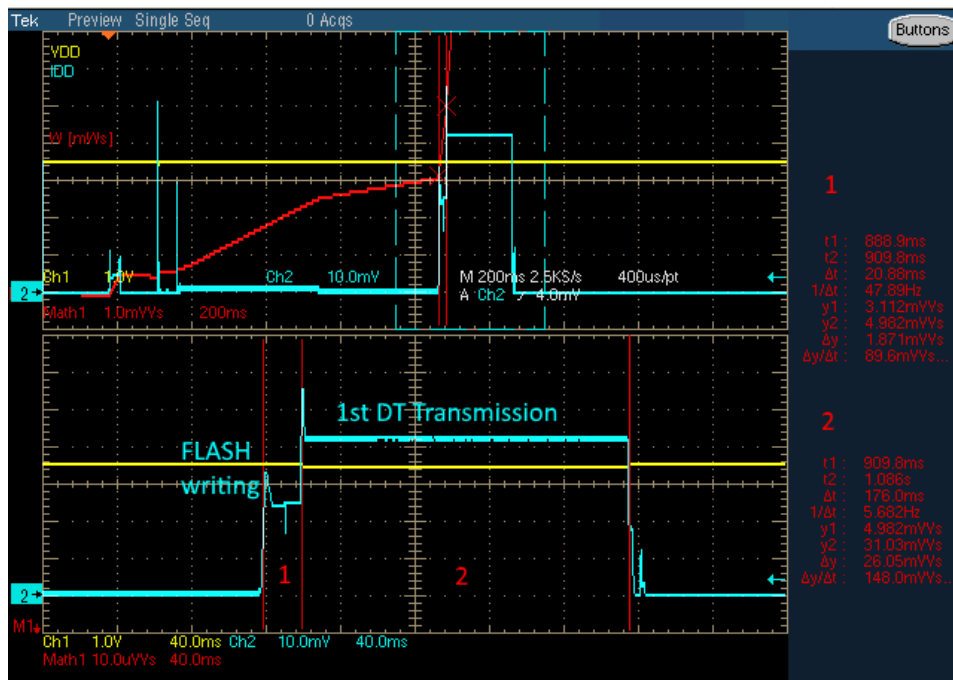

Figure 4.10. Before the 1st data subtelegram is transmitted, a copy of its data is stored in the flash memory. This action lasts around 21 ms for an analog sensor and consumes around 1.9 mWs of energy.

141

During this time, both the flash chip and radio chip are powered, resulting in current peaks of up to 30 mA. After this, the 1st data subtelegram is transmitted. This task has a duration of approximately 176 ms for an analog sensor (25 bytes + 2 bytes radio added CRC). The energy consumed during the transmission is 26 mWs.

When in sleep mode, one of the following "fire and go" interrupts can wake up the microcontroller, causing the algorithm to continue executing operations. Among these interrupts are:

- Real-time clock alarm event, every 15 minutes
- LRN pin event (1 to 0 edge)
- Data pin event (1 to 0 edge)
- Sensor connected or disconnected event
- RTC ready flag event (every second)
- Rx UART byte received
- 5 second time-out checking for UART connection

Since the flash memory and radio chip share the same SPI lines and supply voltage enable pin, these components are turn on, and shut down at the same time. To save energy, after the data is stored in the flash chip, it enters the sleep state while the radio is in the active state and vice versa. Since transmission of telegrams also occurs here, this is the most energy consuming state. As evident from Figure 4.10, around 91% of the overall energy consumption during one wake up and data transmit cycle, occurs when in this state.

The completion of telegram transmission is immediately signalled to the microcontroller via the interrupt line. This causes the running algorithm to shut down the flash and radio chip, and sends the sensor module into the deep sleep mode for further energy preservation.

4.7. Deep sleep state

This is the state in which the sensor module spends 90% of its operating time during one full operation cycle (wake-up, measure, transmit 3 data subtelegrams). 100% of the time between each operation cycle is also spent in this state. When in this state, the I/O pins of the microcontroller are configured individually for the minimum sensor module current consumption. After this, the microcontroller enters, the LPM3.5 mode [61].

Once in the LPM3.5 mode, the microcontroller can wake up through any of the following events:

- Real-time clock alarm event, every 15 minutes
- LRN pin event (1 to 0 edge)

- Data pin event (1 to 0 edge)

- Sensor connected or disconnected

- UART connected

- Brown-out

- Reset pin activation

In the deep sleep state, all the peripherals are disconnected from the supply voltage with the use of MOSFET transistors. Only the real-time clock remains running in order to wake up the microcontroller after the scheduled interval expires. This timing is controlled by the external low power quartz oscillator. The energy consumed in the deep sleep state depends on the duration of the deep sleep. The default programmed value between two full operating cycles is 15 minutes. At 3.6 V, the total electrical current drawn from the supercapacitor is around 1 µA. During the 15 minutes of deep sleep, the consumed energy is 3.2 mWs. If this energy is added to the energy consumption of one data transmit cycle (around 88 mWs), it would contribute to 3.5% of the overall energy consumption.

Unlike the short-lasting transmission state with higher current levels, the deep sleep state is long-lasting with the lowest current levels. This is ultimately the main driving force behind the control algorithm: keep the sensor module in the high and low energy consuming states, for as little and as long as possible respectively.

5. EXPERIMENTAL RESULTS

It is evident through this thesis, that in order to demonstrate the capabilities of the developed sensor system, many tests have been conducted, to characterise its indoor and outdoor performance. As the title of this thesis indicates, the developed sensor system incorporates energy harvesting, long range, and low power capabilities simultaneously. To prove this premise, three main outdoor field measurements are summarised in this chapter:

- Energy harvesting measurements
- Long range measurements
- Long term operation measurements

All three measurements are conducted separately and combined with measurements performed at various long term field installations which are still running in test sites in Japan and Germany. Besides important measurements, many application use cases are also presented in this chapter.

5.1. Energy harvesting initial tests

To prove energy harvesting capabilities and evaluate outdoor charging performance, short term outdoor tests have been conducted. Sensor modules with different supercapacitor voltage levels are left in the sun and the time before the first wake-up and telegram transmission is observed. These are initial tests to prove that the sensor module can be successfully charged and operational in outdoor conditions. Figure 5.1 illustrates a sun charging test using a sensor module with illuminance sensor attached to measure light intensity. Additionally, ambient temperature and humidity sensor has been attached to the sensor module and a reference light meter (Voltcraft LX-1108) was used for measurement result control.

The initial voltage of the supercapacitor was 2.2 V. For a sensor module to be able to send a telegram this voltage level needs to reach a minimum 2.5 V. It is clear from Figure 5.2 this occurred 10 minutes after the start of sun exposure (11:04). 10 minutes after the initial subtelegrams were received, 3 new data subtelegrams arrived (11:15). After this, the sensor module entered a regular wake up cycle each 15 minutes. When waking up for the first time from low voltage, RTC can trigger wake up earlier if the sensor module has entered the reset state due to the low energy. However, the timer stabilises after the second transmission. Full capacity was reached 50 minutes after the test began and this level was maintained during the next one hour, with sensor module continuously sending telegrams every 15 minutes.

Figure 5.1. A sensor module placed on the roof during sun charging tests. Digital illuminance sensor (white box), reference light meter with the sensing element (black box) and an analog ambient temperature and humidity sensor are displayed.

After 2 hours, the voltage level measured at the supercapacitor was 3.65 V. In Figure 5.3, illuminance values obtained with the sensor module are provided. Initial illuminance at the start of the test was around 70 000 lx and 20 mA charge current was recorded. At maximum illuminance of 79 000 lx, the recorded charge current was 44 mA.
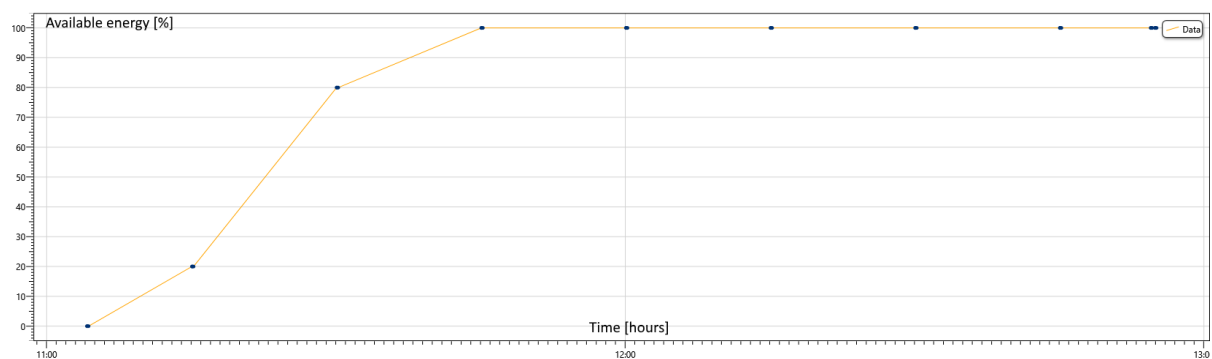

Figure 5.2. Supercapacitor charged by solar energy. 80% of the available energy (3.38 V) is reached within 40 minutes after the test start. Initial voltage at the supercapacitor was 2.2 V.
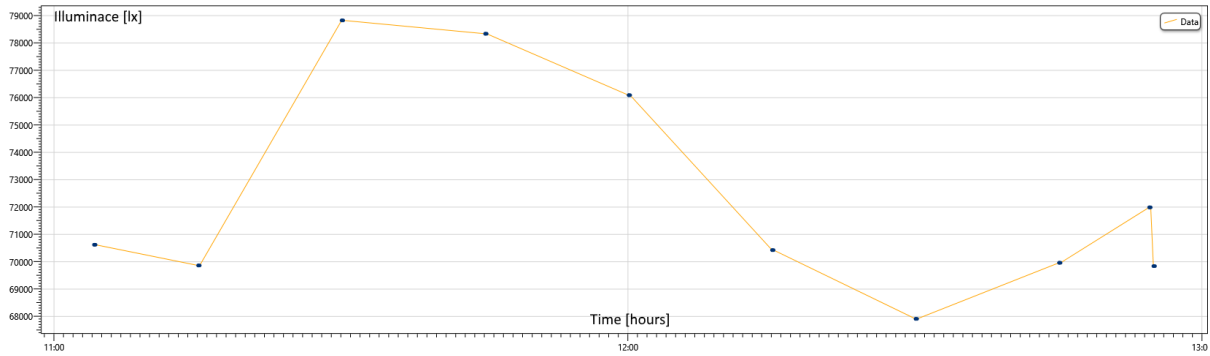
Figure 5.3. Illuminance levels during supercapacitor charging via solar energy.

The same test is executed during very cloudy and rainy conditions. At the start of the test the measured illuminance value was approximately 5000 lx. During the test, illuminance levels remained below 11 000 lx, while for the last two observed hours, values did not rise above 5000 lx (Figure 5.4). With these illuminance levels, recharging of the supercapacitor was much slower compared to the previous test. It took 1 hour for the sensor module to send the first teach-in telegram and after that it continued sending in 15 minutes intervals while continuously recharging. In these conditions, as clear from Figure 5.5, 89% of the capacity (3.48 V on the supercapacitor) is reached 7 hours after the start of the test.
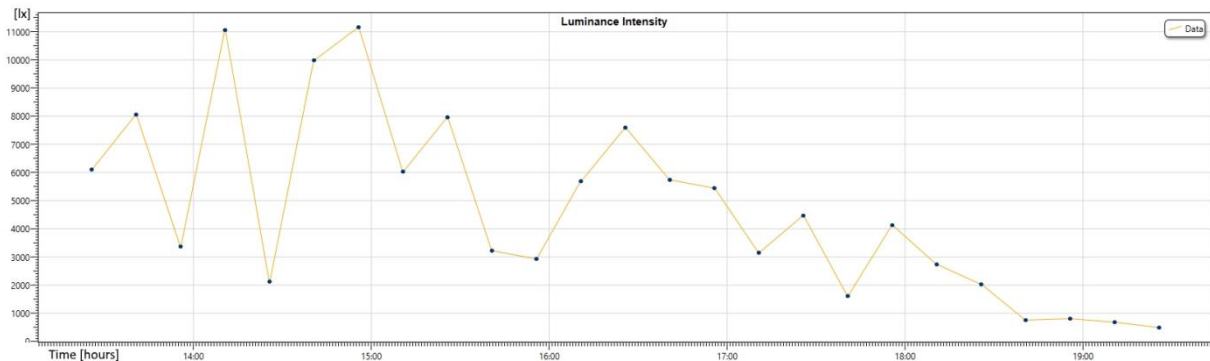

Figure 5.4. Illuminance levels during solar charging test in cloudy and rainy conditions. Illuminance levels are observed each 15 minutes and transmitted as part of the data telegrams.
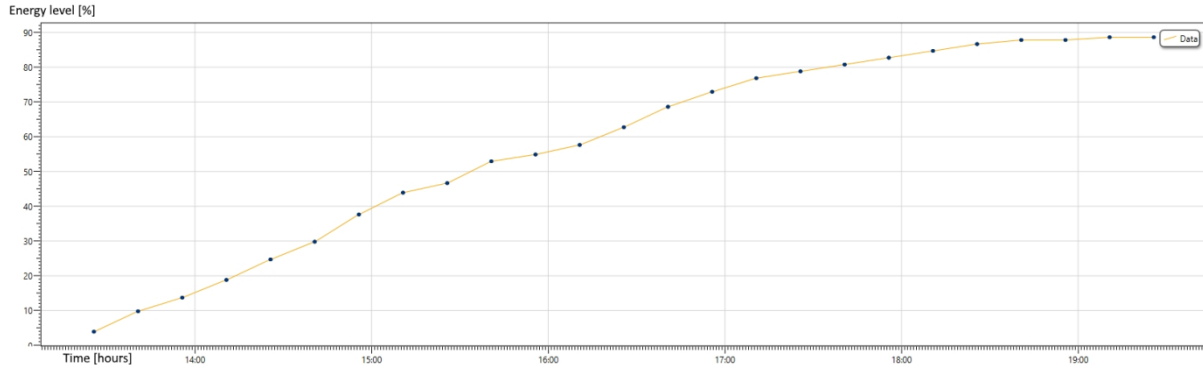
Figure 5.5. Energy level of the supercapacitor during recharge in the cloudy and rainy conditions. Charging began at 12:20 and the first teach-in telegram was received at 13:25. Two hours later with continuous operation and wake up each 15 minutes, the sensor module reported an energy level of 50%. Six hours later the energy level reached 89%.

5.2.   Range testing

Through the range tests in Germany, different radio chip settings as mentioned in chapter 3.1 have been investigated. The results given in this chapter are obtained with a chosen optimal 1.25 kbps data transmission rate. In the first test at lake Ammersee in south Germany, an +11 dBm output power setting and 925 MHz transmission frequency (suitable to be used in Japan) have been utilised. With these settings, tests showed an achievable line-of-sight transmission range of almost 8 km, as evident in the Figure 5.6.

During this range test, the sensor module was moved along one side of the lake shore and positioned on a 2 m high pole. As mentioned previously, the transmit power was set to +11 dBm. The data logger module was stationed on the other side of the lake shore also on a 2 m high pole. During the test, two different external antennas were used on the data logger module side: the high gain antenna (+12.5 dBi) and a monopole antenna (+2.5 dBi), as depicted to the right in Figure 5.6. With the high gain antenna, the achieved transmission range was close to 8 km, and with the monopole antenna attached to the data logger module, telegrams were successfully received from almost 3.5 km.

The unique aspect of the tests at lake Ammersee is that, no external antenna was connected to the sensor module, but rather an integrated PCB antenna with 0 dBi gain was used, as described in Chapter 2.1.6. This test proved effective long range functionality, even with the integrated PCB antenna. Although, the external monopole antenna (with +2.5 dBi gain) is used as the default sensor module antenna in all later installations and tests.

Figure 5.6. Range tests at lake Ammersee (south Germany) with the ~ 8 km achieved transmission range. The data logger module was equipped with the high gain antenna shown on the right (+12.5 dBi) and the sensor module (shown on left) with the integrated PCB antenna (~ 0 dBi).

The range test in Japan was performed in a rural area surrounded by fields, farms and forests as shown in Figure 5.7. The same type of antennas tested at lake Ammersee in Germany, have also been used in Japan. The difference was with the sensor module; the external monopole antenna was used instead of the integrated PCB antenna, which was disconnected. Also, the communication between the modules was no longer in line-of-sight, since the terrain contained of valleys and forests. However, even in this environment and with a not very high installed receiver, long range capabilities of the sensor module have been confirmed. The sensor module was moved along the path before it was installed at the fixed location in one of the farmer's fields. From the different points along the way, the received telegrams RSSI level was measured. At 600 m, with the directional antenna, a huge RSSI level margin (14 dB) is still preserved, compared to the defined receiver sensitivity of -118 dBm. With the monopole antenna attached to the data logger module, this available margin drops to only 3 dB. Based on this range test, the use of the directional antenna and the small monopole antenna on the data logger and sensor module sides respectively, became standard setup for further installation. This is because, it guarantees the best sensor system performance, regarding transmission range, in non-line-of-sight conditions.
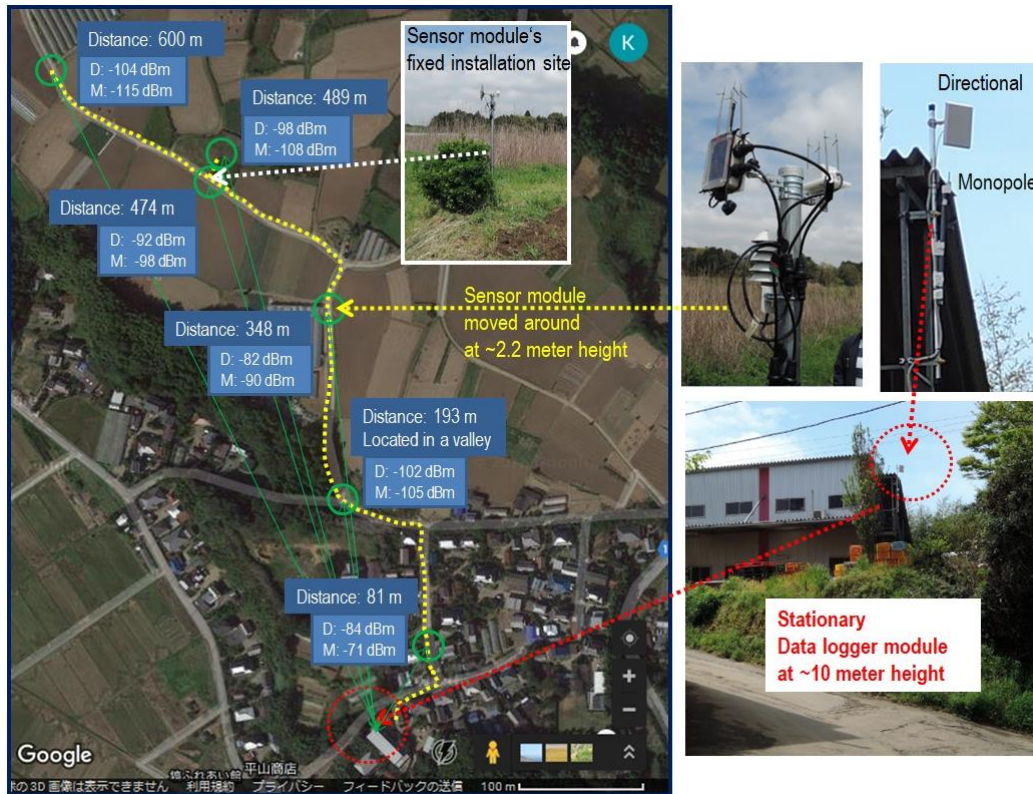
Figure 5.7. Range test in a rural area in Japan. Two different types of the antennas have been used at the stationary data logger module. A monopole (M) with 2.5 dBi gain and a directional (D) antenna with 12.5 dBi gain respectively. The sensor module was moved around before it was installed at the fixed location. Telegrams RSSI values have been measured for both types of the receiving antennas, obtained from different measuring points (green circles) along the way.

Another range test has been performed in a moderately urban environment in the suburbs of Munich, Germany. In these conditions a transmission range close to 3.5 km is achieved (Figure 5.8). During this range test, the receiver with the small monopole antenna was placed on a 1.5 m high pole and stationed on a small hill. The sensor module with the same antenna, was attached to a 1.25 m high pole and moved along the route. The sensor module was maintained, on average, 10 meters below the elevation level of the receiver. As evident from Figure 5.8, at a distance of approximately 3.2 km from the data logger (red line), the received telegram RSSI level was -112 dBm. Beyond this distance, the communication between the modules became unreliable.
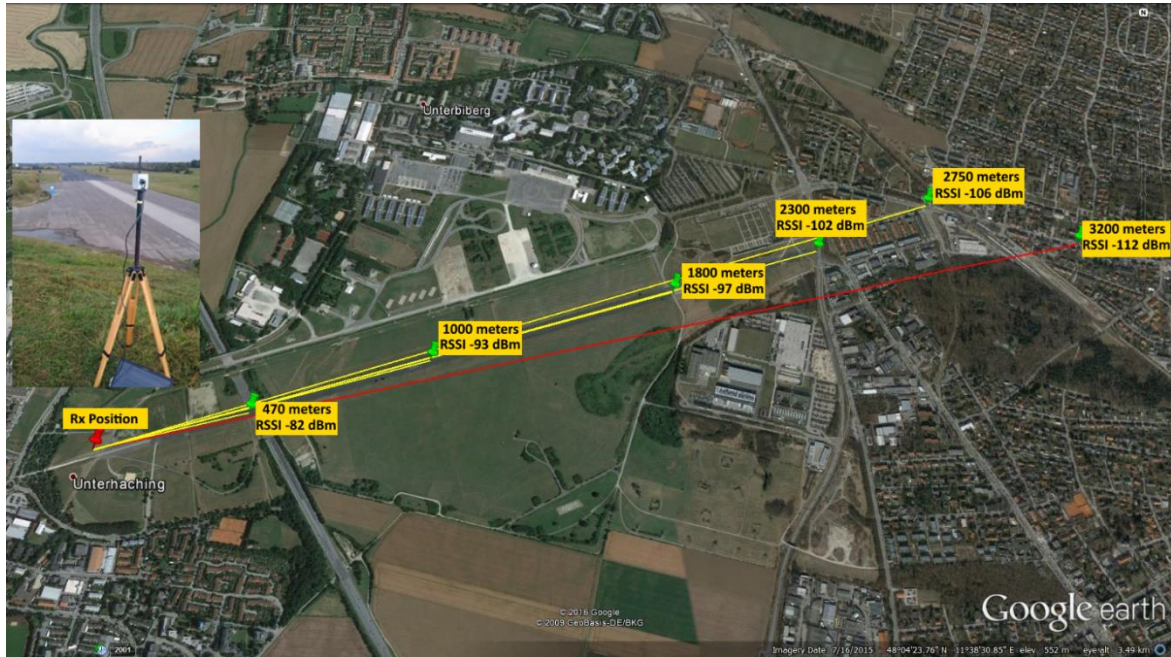
Figure 5.8. Range tests at the airfield and moderately urban area, with an achieved transmission range of more than 3 km. Both data logger and sensor module were equipped with the same type monopole antenna (+2.5 dBi) during test.

The results presented in this chapter are comparable with the achieved range described in e.g. [19], within which the LoRa radio module was used for river monitoring in Dublin, Ireland. The authors mention an achieved range of 3 km to 12.5 km. However, this was obtained with +17 dBm of output power and a 580 meter elevation difference between the sender and receiver [19].

A direct comparison between the developed sensor module and the LoRa radio module currently available on the market (Microchip RN2483 module with the Semtech SX1276 radio chip inside) has been made during the range test displayed in Figure 5.8.

For test purposes, a LoRa module was integrated on a PCB identical to that which is developed in this thesis; the radio chip CC1120 together with its RF environment was replaced with the Microchip LoRa module. LoRa radio modules use special wideband, spread spectrum LoRa modulation. This allows the extraction of the transmitted signal even when the power levels fall below the receiver noise floor [17]. Currently on the market, LoRa modulation and the Semtech radio chips [6] which support this type of modulation are the synonym for long range communication and low power operation. Therefore, a direct comparison between the developed sensor module and technology like LoRa gives a valid estimation regarding the achieved sensor module performance. Table 5.1 compares these two

systems based on their respective transmission range and received signal strength measured at certain points.

Table 5.1. Comparison of received signal strength values over different transmission distances for two different long range technologies. Wideband spread spectrum modulation (LoRa) and ultra-narrowband modulation (sensor module).

Distance from the receiver [m]	Elevation difference between Rx and Tx [m]	LoRa module 868.1 MHz 0.97656 kpbs SF 10 BW 125 kHz 14 dBm		Sensor module 868 MHz 1.25 kbps 11 dBm	Sensor module 925 MHz 1.25 kbps 11 dBm
		SNR [dB]	RSSI [dBm]	RSSI [dBm]	RSSI [dBm]
470	7	6	-87	-82	-90
1000	8	1	-95	-93	-98
1800	10	-2	-101	-97	-103
2300	11	-3	-105	-102	-108
2750	8	-4	-110	-106	-112

Since LoRa modules use a different type of modulation, radio settings also differ. However, the values are chosen in such a way that the transmission data rate, frequency and output power are approximately identical. The most important LoRa modulation parameter is the Spreading Factor (SF). The value of 10 is used which produces the maximum signal to noise ratio (SNR) of -15 dB [6]. It also ensures an equivalent data rate of 0.97656 kpbs which is comparable to the sensor module's 1.25 kbps. The other settings used in the LoRa module are given in Figure 5.9. These are obtained using the theoretical LoRa modem calculator tool. The results in Table 5.1 show that at 2.75 km, both the LoRa and developed sensor module have around 10 dB remaining margin before reaching the limiting values of receiver sensitivity. For the LoRa module the practical threshold is around -15 dB SNR (SF=10,
BW = 125 kHz) which translates to approximately -122 dBm. The limiting value for receiver sensitivity for the developed data logger module device was measured as approximately -118 dBm.

The advertised long range potential of the LoRa module is achieved when the module is used as part of LoRaWAN network. This requires certain infrastructure to be build, e.g. base stations supporting LoRaWAN, receivers high above ground and gateways. When point to point communication is concerned, which the developed sensor system is primarily intended

for, the range measurements prove similar and in some cases a better performance, compared to those from LoRa modules.
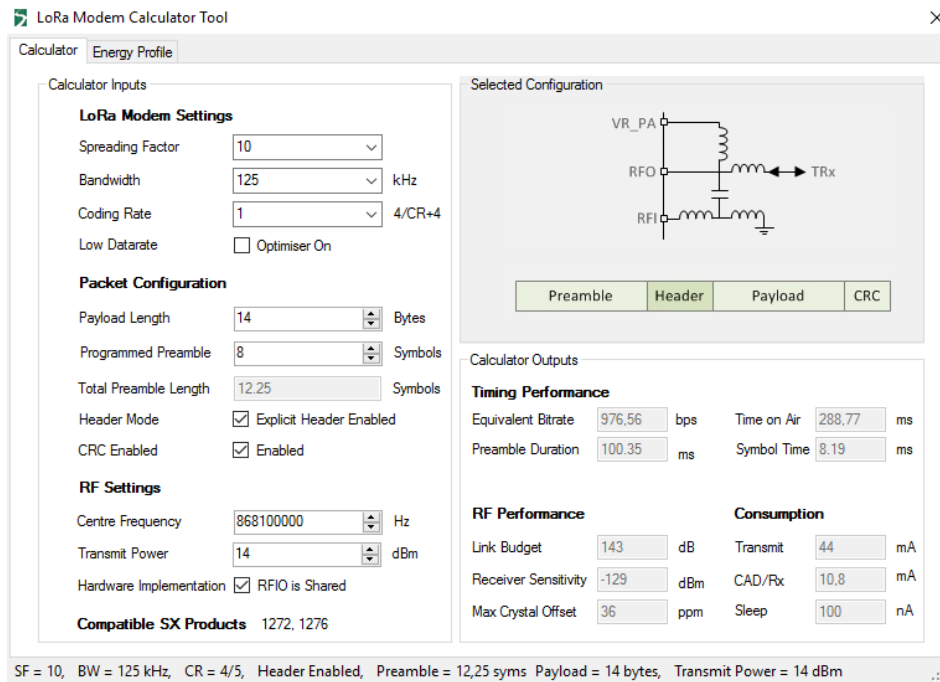

Figure 5.9. LoRa modem parameters used during the direct range test comparison with the developed sensor module.

5.1. Long term operation

During a one year period, uninterrupted operation has been achieved at the different test sites in Germany and Japan (Figure 5.10 and Figure 5.11 respectively).

In Figure 5.10 four sensor modules in two variations of plastic housings are depicted. To each sensor module two external sensors are attached. One is a digital sensor which measures outdoor illuminance and the other one is an analog combined sensor which measures air temperature and relative humidity. The analog sensor is placed inside a special metal housing (in the form of a collection of wedge–shaped plates) which allows air circulation and prevents sensor exposure to direct sunlight or rain. Each sensor module has a small integrated solar cell for energy harvesting and a small external monopole antenna attached. Figure 5.11 shows the developed sensor modules deployed in the two different environments in Chiba, Japan; an outdoor field and a greenhouse. The same type of sensors used in Germany are also used at the test site in Japan. In the southernmost part of Japan, on the island Miyakojima, functionality and robustness of the developed sensor module in the compact metal housing was also successfully tested.

Figure 5.10. Four test devices deployed in a small bush at the test site in south Germany.

Figure 5.11. A sensor module with illuminance and ambient air temperature and humidity sensors attached, at the Chiba and Niigata test sites in Japan. Left is the outdoor installation in an onion field (Chiba) and on the right is the installation in a greenhouse used to grow strawberries (Niigata).

The developed sensor module withstood inclement weather in south Germany, as well as the typhoon season in south Japan, while, for the majority of time, maintaining an energy supply level of 100%. This is illustrated in Figure 5.12. As evident from this figure, the sensor module was deployed with a low energy level and left to recharge in the available outdoor conditions. The test started at the end of November when the sun is relatively low on the horizon, with the only 13.3% of energy available from the supercapacitor. Despite the winter season and recording quite low illuminance values at the test site, within a week of constant operation and the 15 minute wake up interval, the supercapacitor successfully recharged to a 100%.
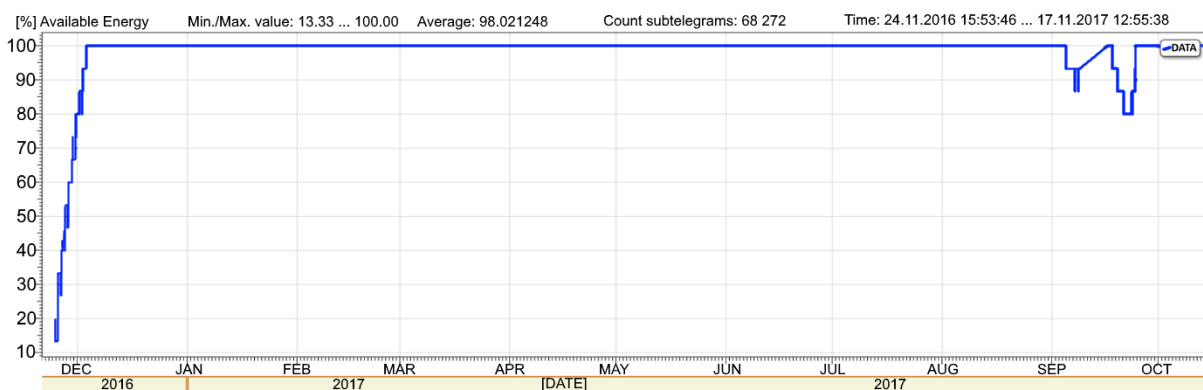

Figure 5.12. Percentage of available energy from the supercapacitor during one year of outdoor operation (test site Germany). Results obtained using the EnOcean DolphinView tool.

Illuminance at the test site within the first week of deployment is provided in Figure 5.13. These values were obtained using a digital illuminance sensor connected to one of the sensor modules from Figure 5.10. It is clear that the measured maximum in the bush was only 13 200 lx, while the remaining days within this first week did not exceed 10 000 lx.
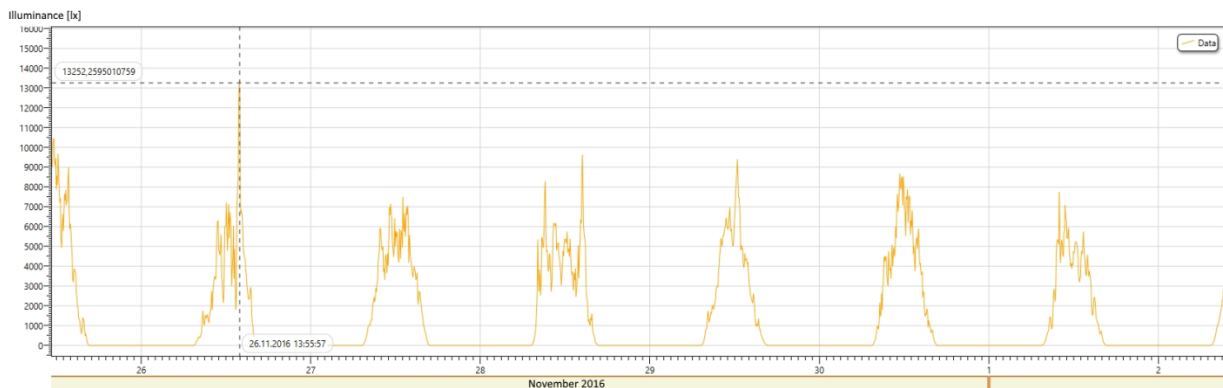

Figure 5.13. Illuminance in the bush at the test site in south Germany. Results obtained with a sensor module and a digital illuminance sensor connected. The maximum value of 13 252 lx is highlighted.

After almost one year of constant operation, a small drop to 80% of the energy available on the supercapacitor is observed (Figure 5.12). This was due to fallen wet leaves partially covering the sensor module's solar cell. After these leaves were removed, the supercapacitor quickly recharged to 100% available energy as evident in the same figure.

In addition, long term operation with "always ON" sensors has also been tested. Limitations of these type of sensors primarily concern the supply voltage (ideally up to 5 V), peak currents (above 10 mA, successfully tested up to 100 mA), standby currents (up to 100 µA) and startup times (up to 500 ms). An example is the infrared sensor (Optex VXI-R) which was adapted to the developed sensor module, and successfully tested as an occupancy detection sensor. When movement is detected the sensor triggers an interrupt. This wakes up the microcontroller in the sensor module and information about the change of state is immediately transmitted. This sensor constantly drains 10 µA of current, while peak currents reach 20 mA. Dark time run tests conducted with this sensor show an uninterrupted operation time of 10 days with data transmission each 15 minutes and occupancy check every 2 minutes. The outdoor tests consisted of continuous monitoring of a parking spot for 50 days, using the occupancy sensor attached to the developed sensor module as pictured in the figure below.

Figure 5.14. "Always ON" infrared sensor for parking occupancy monitoring. Sensor is attached to the left of the parking sign and connected to a sensor module placed on a pole in the background with the solar cell facing towards building. Another infrared sensor can also be seen on the pole above, together with some other sensors. This is the second test site in south Germany.

Analysis of 34 519 received telegrams showed that the sensor module's energy level never dropped below 86% (Figure 5.15). The average transmission rate here, was one subtelegram every 2 minutes. Furthermore, 98.41% of the received subtelegrams reported a fully charged supercapacitor.
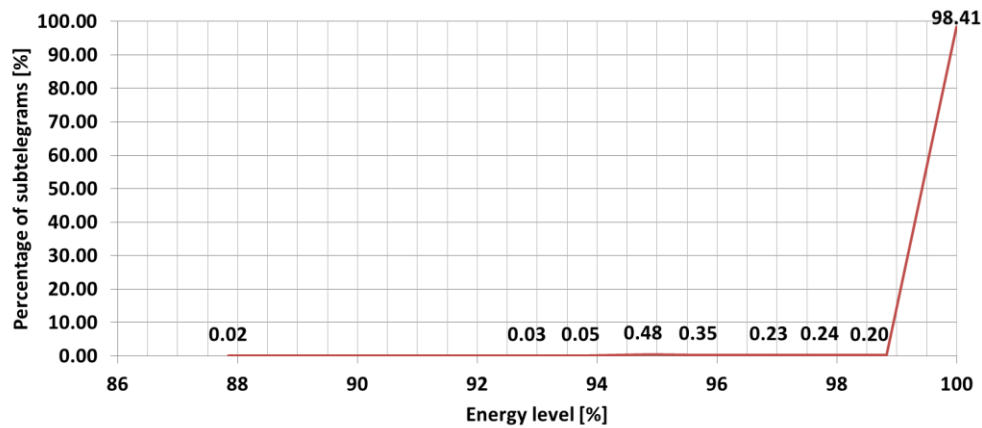

Figure 5.15. A CDF (Cumulative distribution function) plot of the sensor module's energy level during 50 days of telegram transmission. The vertical axis represents the percentage of subtelegrams (34 519 analysed) carrying information about this particular sensor module's energy level.

The plot in Figure 5.15 illustrates how the sensor module behaves when pushed to its limits ("alaways ON" sensor, transmission and measurement every 2 minutes, installation in non-direct sunlight, peak current of minimum 20 mA, constant sensor sleep current of minimum 10 μA).

Another type of sensor with higher peak currents, close to 100 mA have been tested. These are ultrasonic sensors MB7046 and MB7383 respectively from MaxBotix. During the ranging phase and emission of ultrasonic pulses, current consumption of these sensors increases to up to 100 mA. Sensor MB7046 has also been running in the outdoor test environment pictured in Figure 5.14. After 10 months of operation, 100% energy is still maintained at the sensor module's supercapacitor.

It is clear from the long term operation tests, that with the currently supported sensors, the energy margin is huge. Connecting the most consuming "switch ON" analog sensor (5 mA peak current), or "always ON" sensors (peak currents from 20 mA to 100 mA respectively) the sensor module's energy level remains above 85%.

5.2.   Sensor types and an application use cases

Depending on the type of sensor connected to the sensor module, different sensor system applications can be realised. The initial application was for agriculture, with the intention to maximise crops yields by observing different environmental parameters like air temperature and humidity, soil moisture and humidity, illuminance, CO_2 levels, etc. With further sensor development such as ultrasonic and infrared sensors, application can be extended to parking place and river level monitoring in smart cities. Potential applications do not stop here; further sensors can be developed, or already existing sensors on the market can be easily adapted to the developed sensor system. Therefore, wherever there is need to observe environmental parameters or detect movement with the use of inexpensive infrastructure, the developed sensor system can be applied. It is useful, considering that no wiring or maintenance is required and that a long range data transmission is secured.

5.2.1. Developed sensor types

The current pallet of sensors includes:

- Ambient air temperature and humidity sensor (E+E EE060)

- Illuminance sensor (Maxim Integrated MAX44009)

- Soil moisture sensor (Decagon Devices EC-5)

- Soil temperature sensor (Maxim Integrated DS18B20)

- Infrared occupancy sensor (Optex VXI-R)

- Ultrasonic distance sensor (MaxBotix MB7383)

The illuminance sensor is developed from scratch, while the other types of sensors are taken from the market and adapted to the developed sensor module. In Figure 5.16 the typical supported sensor architecture is given, complete with the interfaces and an example connector to the sensor module.

Sensor adaption sometimes consisted of creating a small PCB to support the connection from the sensor module to the sensing element (e.g. Figure 5.16). More commonly, modifications were made directly to the sensor cable by simply adding resistors for sensor type recognition and wiring the sensor pins to match the sensor module sensor interfaces (Chapter 2.2.2.).

An overview of the currently developed sensors to be used with the sensor module is provided in Figure 5.17.
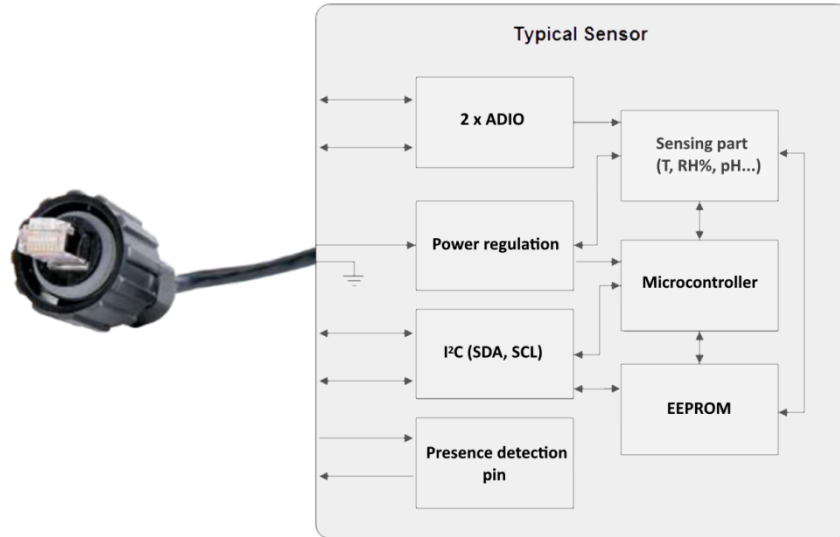
Figure 5.16. Typical external sensor architecture with the interfaces towards the sensor module. Sometimes an additional PCB containing the electronic components shown above needs to be built to support the sensing element operation.

Air temperature and humidity sensor -40 … 60 °C 0 … 100% RH	Soil moisture sensor 0 … 100%	Soil temperature sensor -55 … +125 °C
Illuminance sensor 0 … 100 000 lx	Presence detection sensor 0 … 10 meters	Ultrasonic sensor 0 … 10 meters

Figure 5.17. Currently developed sensor module's accompanying sensors.

5.2.2. Application use cases

The majority of trial installation sites are located in Japan since Japanese partners were the first to recognise the need for a developed sensor system and its applicability in agriculture and smart cities. One of the first trial installation sites was in two farms in the Chiba prefecture in Japan. An air temperature and humidity sensor together with an illuminance sensor was used to monitor environmental conditions in the outdoor onion production fields. A transmission range of 1 km was easily achieved as evident in Figure 5.18, with the sensor and data logger module equipped with small monopole antennas.
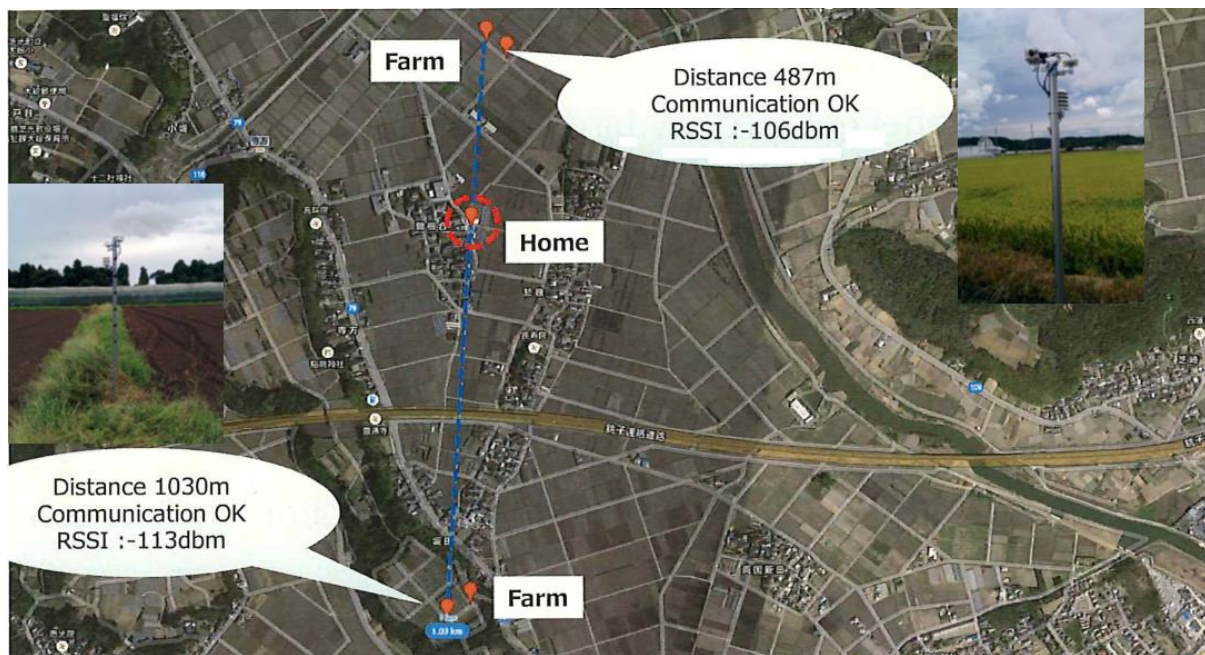
Figure 5.18. One of the first trial field installations of the developed sensor system in the Chiba prefecture, Japan.

Another installation site on Miyako Island (one of Japan's southernmost islands), was used to prove sensor system robustness and track harsh weather conditions (Figure 5.19). Multiple sensor modules with air temperature and humidity, and illuminance sensors connected, have been installed around the island. Two data logger modules with monopole antennas, have been placed inside a small building and connected to an internet gateway. This allows the received data to be easily transferred further to the internet cloud.
A similar installation pictured in Figure 5.20, has been also installed in Japan's northernmost island, Hokkaido.
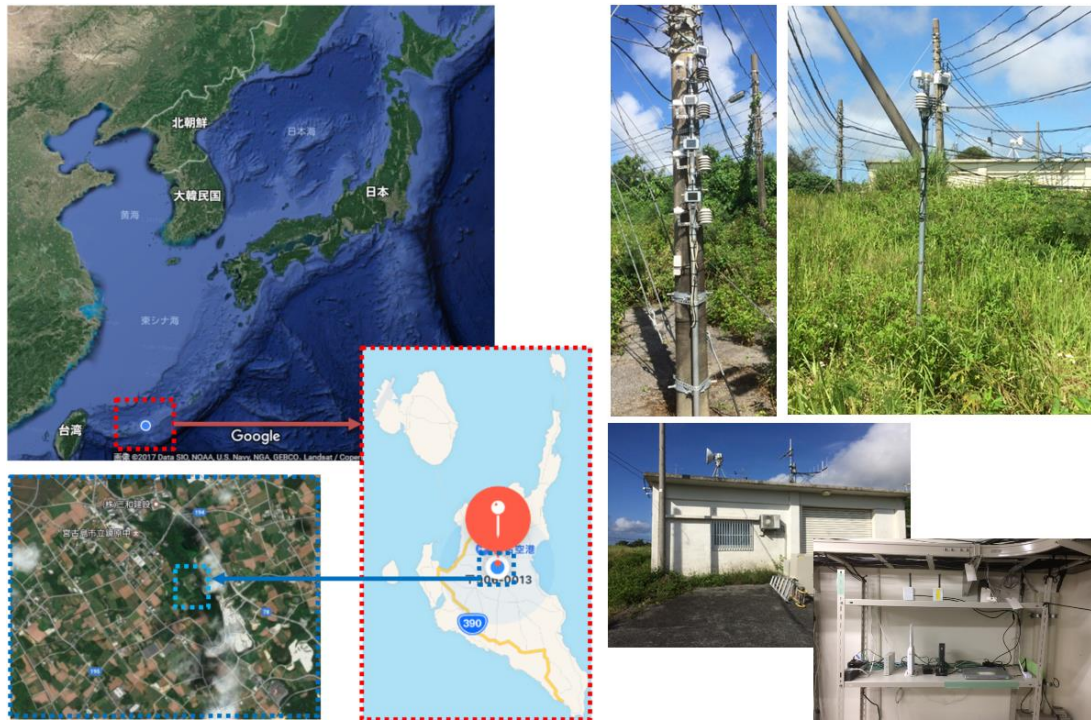
Figure 5.19. Test site on the Miyako Island in Japan. Harsh island environment, especially during typhoon season was observed with the developed sensor system.

Figure 5.20. Sensor modules installed in the northernmost Japanese island Hokkaido.

The developed sensor system was successfully installed and deployed inside greenhouses used for growing strawberries, tomatoes and grapes. These installations can be seen in the following figures.

Figure 5.21. A sensor module installed in a greenhouse to monitor conditions during strawberry growth.

Figure 5.22. A sensor module used to monitor environmental conditions during grape production.

Figure 5.23. Sensor modules installed in a greenhouse to monitor conditions during tomato growth. The sensor module hanging on the left (zoomed down) has soil moisture and soil temperature sensors attached, while the sensor module on the right (zoomed up) has illuminance and air temperature and humidity sensor attached.

In the greenhouse seen in Figure 5.23, information about soil temperature obtained from the two installed sensor modules, was directly used to control the soil heater installed in the ground, as illustrated in Figure 5.24.
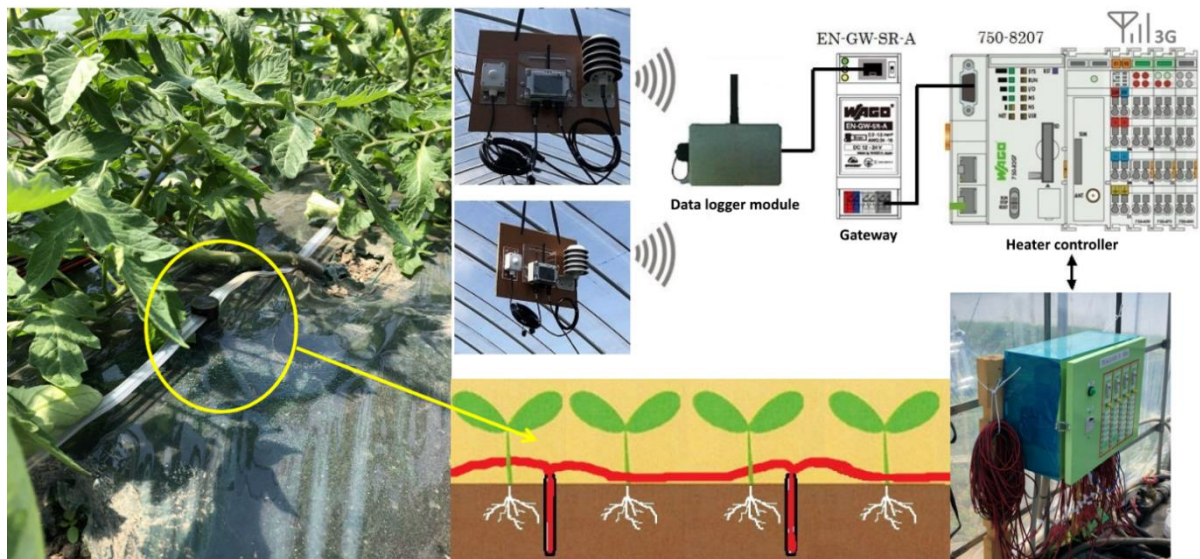
Figure 5.24. Installed soil heaters controlled by the Wago system which receives soil temperature values from the developed sensor modules installed in the greenhouse.

During tomato growth, soil temperature was observed along two rows. One row with an installed and controlled heater, and the other without. The first month after planting is the most important time period in root growth. If the soil temperature is below 10 °C root necrosis might occur, therefore, the heater would turn ON. Results obtained during a 4 month growth period from May to September have been plotted in the figure below.
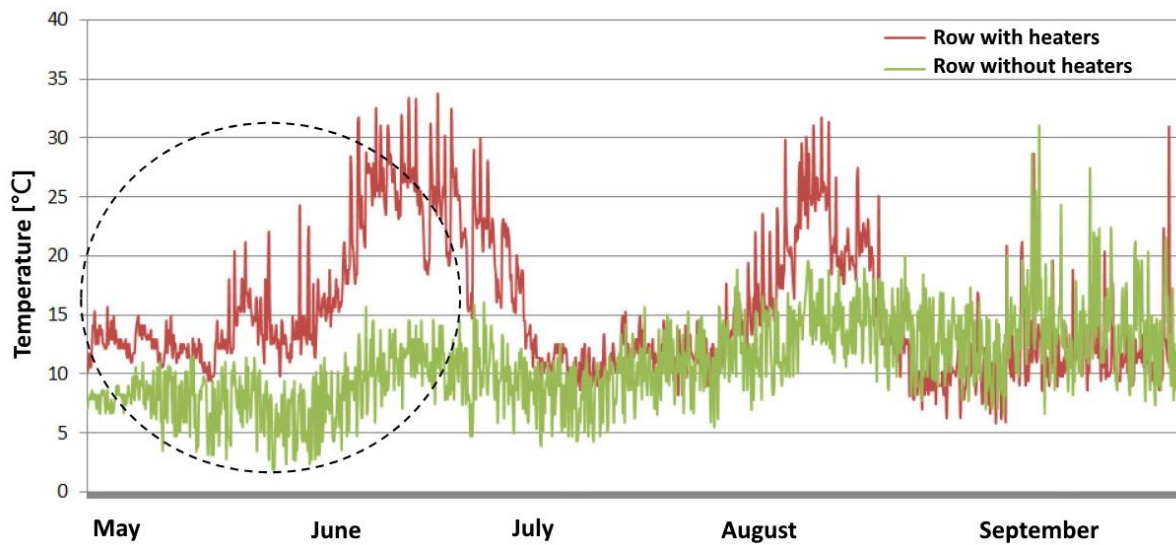
Figure 5.25. Soil temperature monitoring in the greenhouse during tomato growth. Marked in the circle are the temperature values during the critical growth period within the first month. The red and green lines represent soil temperature of the row with and without the heater installed respectively.

After the tomatoes have been harvested, the roots have been obtained from both rows for comparison. As evident in Figure 5.26, the row with the installed heater (marked A in the figure) contained thicker and longer tomato plant roots. These roots are more capable of absorbing water, compared to the thin and bushy roots from the row without a soil heater (marked B in the figure).

Figure 5.26. Comparison of the tomato plant roots after the harvest. Row A on the left with the installed soil heater contained longer and thicker roots, compared to the row B without the soil heater which contained thinner and bushier roots. The two black cables from the soil moisture sensors connected to the sensor module located above can be identified also.

One of the test applications besides agriculture is river water level monitoring. For this purpose, a sensor module with an ultrasonic sensor attached has been installed. Installation is pictured in Figure 5.27.

Different monitoring modes have been tested; water level can be measured every 2 or 10 minutes respectively. Depending on the change in water level, information can be immediately transmitted or transmission can be skipped and energy saved. In the next measurement cycle, again depending on the water level, a new decision can be made regarding transmission.

With this implementation, an early flood detection warning system can be realised.

Figure 5.27. Ultrasonic sensor attached to a sensor module used for river water level monitoring.

CONCLUSIONS

The development of a low power, energy harvesting sensor module requires not only optimisation of the system hardware but also of the way the sensor modules communicate. With an advanced energy storage system even a very small solar cell can be efficiently used to maintain full charge of the sensor module and allow long term operation. All of the advantages of a supercapacitor as an energy storage device have been exploited, allowing full control of the harvested energy in the sensor module. The applied supercapacitor from Taiyo Yuden has been proved as a high quality energy storage which, when used properly, can maintain stored energy for years. In the future, assuming a price reductions of supercapacitors, it can become an energy storage standard for low power energy harvesting sensor modules.

Radio transmissions drain most of the sensor module's available energy and thus needs to be considered as one of the most important parameters in system optimisation. The component pair (MSP430FRxx and CC112x) has many low power features integrated. If used properly, it can propel hardware design in a low power direction. However, selecting the low power microcontroller and the radio chip itself is not enough to ensure low power consumption of the entire sensor system. Thus, the development focus has to be also on the communication protocol.

Focusing on the physical layer is as important as directing focus to the data and application layer. Receiver sensitivity is identified as one of the most important parameters when securing long range transmission. Therefore, much effort is spent optimising this parameter. Choosing a 2GFSK modulation technique instead of the FSK, and optimising the data rate and frequency deviation, affects the occupied signal bandwidth. This consequently allows a very narrow transmit signal as well as receiver bandwidth. Advanced coding of preamble and the synchronization word increases sensor system robustness as well. This allows fast detection within the receiver, and the correct identification of both the telegram and the information it carries.

Implementation of the two different communication modes expands the sensor system applicability to different environments. Thus, allowing balance between longer transmission range and lower energy consumption. Enabling the bidirectional communication mode can increase dark run operating time by 96% compared to the unidirectional mode. With both communication modes, two different types of data packets (Teach-in and Data telegrams) are

integrated into the developed protocol. This concept conserves energy by wirelessly informing the receiver about sensor configuration only when the attached sensors on the transmitter side have been changed. The rest of the time, only measurement data is transferred.

Additionally, implemented and enabled features, such as, optimisation of the Carrier Sense time duration can achieve up to 15% saving in the consumed energy per transmission. Furthermore, radio telegram repeating is very practical and useful feature implemented as standard part of the developed communication protocol. By sending an adequate serial command, the data logger module can be easily configured as a repeater and then a network of data logger modules can be established, which in turn extends the possible transmission range.

Combining all these ideas with a proven RF design, counters what are normally two opposite requests: long range and low power consumption. This ultimately leads to the development of a fully functional, long range, low power, energy harvesting sensor module with a unique communication protocol.

The demonstrated applications and test sites are just a small insight into the possibilities of the developed sensor system. With each new sensor developed for the sensor module, its application field will be expanded. The current sensors are easily recognised by the resistor embedded inside the connection cables. In the future, when the number of different types of sensors increases, this sensor identification approach may become a limiting factor. Therefore, focus should be given to the identification of the sensor type via I^2C lines. This approach is successfully demonstrated and may ultimately lead to the transformation of current and future analog sensors into digital ones. These sensors will communicate with the sensor module exclusively via digital I^2C lines. This would require the implementation of a small microcontroller on the sensor side acting as a mediator between the sensor element and the sensor module. This would pave a way for the development of a completely generic sensor interface.

REFERENCES

[1] J. P. Bardyn, T. Melly, O. Seller and N. Sornin, "IoT: The Era of LPWAN is starting now," in *42nd European Solid-State Circuits Conference (ESSCIRC)*, Lausanne, Switzerland, 2016.

[2] K. Mekki, E. Bajic, F. Chaxel and F. Meyer, "A comparative study of LPWAN technologies for large-scale IoT deployment," *ICT Express,* 2018.

[3] M. Keshtgary and A. Deljoo, "An Efficient Wireless Sensor Network for Precision Agriculture," *Canadian Journal on Multimedia and Wireless Networks,* vol. 3, no. 1, 2012.

[4] N. Wang, N. Zhang and M. Whang, "Wireless sensors in agriculture and food industry - Recent development and future perspective," *Computers and Electronics in Agriculture,* vol. 50, pp. 1-14, 2006.

[5] É. Morin, M. Maman, R. Guizzetti and A. Duda, "Comparison of the device lifetime in wireless networks for the Internet of Things," *IEEE Access,* vol. 5, pp. 7097-7114, 2017.

[6] Semtech, "AN1200.13, SX1272/3/6/7/8 LoRa Modem, Designer's Guide," [Online]. Available: https://www.semtech.com/uploads/documents/LoraDesignGuide_STD.pdf. [Accessed September 2018].

[7] "Sigfox Technology," [Online]. Available: https://www.sigfox.com/en/sigfox-iot-technology-overview. [Accessed July 2018].

[8] D. Purkovic, M. Hoensch and T. R. M. K. Meyer, "An Energy Efficient Communication Protocol for Low Power, Energy Harvesting Sensor Modules," *IEEE Sensors Journal,* vol. 19, no. 2, 2018.

[9] S. Beeby and N. White, Energy Harvesting for Autonomous Systems, Norwood, MA, USA: Artech House, 2010.

[10] A. M. v. Voorden, L. M. R. Elizondo, G. C. Paap, J. Verboomen and L. v. d. Sluis, "The Application of Super Capacitors to relieve Battery-storage systems in Autonomous Renewable Energy Systems," in *IEEE Lausanne Power Tech*, Lausanne, 2007.

[11] F. Simjee and P. H. Chou, "Everlast: Long-life, Supercapacitor-operated Wireless Sensor Node," in *ISLPED*, Tegernsee, Germany, 2006.

[12] P. D. e. al., "Trio: enabling sustainable and scalable outdoor wireless sensor network

deployments," in *5th International Conference on Information processing in sensor networks*, Nashvile, TN, USA, 2006.

[13] Moteiv Corporation, "Telos Ultra low power IEEE 802.15.4 compliant wireless sensor module," May 2004. [Online]. Available: http://www2.ece.ohio-state.edu/~bibyk/ee582/telosMote.pdf. [Accessed March 2019].

[14] P. Gupta, R. N. Shukla and P. Lohia, "A ZigBee based Smart Wireless Sensor Network for Monitoring an Agricultural Environment," *IJSRD - International Journal for Scientific Research & Development,* vol. 2, no. 7, 2014.

[15] G. R. Mendez, M. A. M. Yunus and S. C. Mukhopadhyay, "A WiFi based Smart Wireless Sensor Network for Monitoring an Agricultural Environment," in *IEEE International Instrumentation and Measurement Technology Conference. (I2MTC)*, Graz, Austria, 2012.

[16] A. L. Diedrichs, G. Tabacchi, G. Grünwaldt, M. Pecchia, G. Mercado and F. G. Antivilo, "Low-power wireless sensor network for frost monitoring in agriculture research," in *IEEE Biennial Congress of Argentina (ARGENCON)*, Bariloche, Argentina, 2014.

[17] Semtech, "AN1200.22 LoRa™ Modulation Basics," May 2015. [Online]. Available: https://www.semtech.com/uploads/documents/an1200.22.pdf. [Accessed March 2019].

[18] G. Vellidis, M. Tucker, C. Perry, C. Kvien and C. Bednarz, "A real-time wireless smart sensor array for scheduling irrigation," *Computers and Electronics in Agricalcture,* vol. 6, no. 1, pp. 44-50, 2008.

[19] W. Guibene, J. Nowack, N. Chalikias, K. Fitzgibbon and M. Kelly, "Evaluation of LPWAN technologies for smart cities: River monitoring use-case," in *IEEE Wireless Communications and Networking Conference (WCNC)*, San Francisco, CA, 2017.

[20] B. Martinez, M. Montón, I. Vilajosana and J. D. Prades, "The power of models: Modeling power consumption for IoT devices," *IEEE Sensors Journal,* vol. 15, no. 10, p. 5777–5789, 2015.

[21] "Texas Instruments MSP 430FR59XX Family of Microcontrollers Data Sheet," October 2012. [Online]. Available: http://www.ti.com/lit/ds/symlink/msp430fr5949.pdf. [Accessed February 2019].

[22] "Texas Instruments CC1120 Radio Chip Data Sheet," June 2011. [Online]. Available: http://www.ti.com/lit/gpn/cc1120. [Accessed February 2019].

[23] "Adesto Technologies AT45DB321E Data Sheet," August 2012. [Online]. Available: https://www.adestotech.com/wp-content/uploads/doc8784.pdf. [Accessed February 2019].

[24] "Texas Instruments TLV61220 Low-Input Voltage Step-Up Converter in Thin SOT-23 Package," May 2012. [Online]. Available: http://www.ti.com/lit/gpn/tlv61220. [Accessed February 2019].

[25] "Seiko Instruments Inc. SSP-T7-F," February 2014. [Online]. Available: https://www.sii.co.jp/en/quartz/files/2014/02/SSP-T7-F_Leaflet_e20151217.pdf. [Accessed February 2019].

[26] "Ablic S-1009 Series," January 2018. [Online]. Available: https://www.ablic.com/en/doc/datasheet/voltage_detector/S1009_E.pdf. [Accessed February 2019].

[27] "Taiyo Yuden Cylinder Type Lithium Ion Capacitors," October 2018. [Online]. Available: https://ds.yuden.co.jp/TYCOMPAS/or/download?pn=LIC1235RS3R8406&fileType=CS. [Accessed February 2019].

[28] L.-O. Varga, G. Romaniello, M. Vucinic, M. Favre and A. Banciu, "GreenNet: An energy-harvesting IP-enabled wireless sensor network," *IEEE Internet of Things Journal,* vol. 2, no. 5, pp. 412-426, 2015.

[29] A. Wagner, Photovoltaik Engineering: Handbuch für Planung, Entwicklung und Anwendung, Berlin: Springer-Verlag, 2006.

[30] M. Chegaar, A. Hamzaoui, A. Namoda, P. Petit, M. Aillerie and A. Herguth, "Effect of illumination intensity on solar cells parameters," in *Energy Procedia*, Beirut, Lebanon, 2013.

[31] Huahui Energy, "Super Li-ion Battery," December 2017. [Online]. Available: https://www.amec-gmbh.de/wp-content/uploads/2017/12/Huahui-Energy-Super-LI-Ion-Battery-2.pdf. [Accessed March 2019].

[32] TAIYO YUDEN, "TAIYO YUDEN Lithium Ion Capacitors: An Effective EDLC Replacement," [Online]. Available: https://www.yuden.co.jp/include/english/solutions/lic/LIC_White_Paper_Final.pdf. [Accessed February 2019].

[33] H. Medu, "Energy Comparison of Cypress F-RAM and EEPROM," October 2017. [Online]. Available: https://www.cypress.com/file/46746/download. [Accessed February 2019].

[34] Texas Instruments, "CC112X/CC1175 Low-Power High Performance Sub-1 GHz RF Transceivers/Transmitter, User's Guide," September 2013. [Online]. Available: http://www.ti.com/lit/ug/swru295e/swru295e.pdf. [Accessed Febraury 2019].

[35] Texas Instruments, "CC1120EM 868/915 MHz Reference Design," 2013. [Online]. Available: http://www.ti.com/lit/df/tidr240/tidr240.pdf. [Accessed February 2019].

[36] Johanson Technology, "High Frequency Ceramic Solutions P/N 0900PC15J0013," January 2013. [Online]. Available: https://www.johansontechnology.com/datasheets/0900PC15J0013/0900PC15J0013.pdf. [Accessed February 2019].

[37] NDK, "Crystal Oscilator Application Note," [Online]. Available: https://www.ndk.com/catalog/AN-CO_GG_e.pdf. [Accessed February 2019].

[38] Peternann-Technik GmbH, "SMD-TCXO OSCILLATOR SPECIFICATION TXO2520-18-0.5-W-38.4M-1-CSW," Peternann-Technik GmbH, Landsberg am Lech, Germany, 2014.

[39] C. A. Balanis, Antenna Theory: Analysis and Design, John Wiley & Sons, Inc., 1987.

[40] EnOcean GmbH, "EnOcean Serial Protocol 3 (ESP3)," September 2018. [Online]. Available: https://www.enocean.com/esp. [Accessed February 2019].

[41] NXP, "PCA9540B Data sheet," January 2018. [Online]. Available: https://www.nxp.com/docs/en/data-sheet/PCA9540B.pdf. [Accessed February 2019].

[42] I. Aziz, M. Hasan, M. J. Ismail, M. Mehat and N. S. Haron, "Remote Monitoring in Agricultural Greenhouse Using Wireless Sensor and Short Message Service (SMS)," *International Journal of Engineering & Technology IJET,* vol. 9, no. 9, 2009.

[43] ARIB, "ARIB Standard, ARIB STD-T108 Version 1.0.," February 2012. [Online]. Available: https://www.arib.or.jp/english/html/overview/doc/5-STD-T108v1_0-E1.pdf. [Accessed February 2019].

[44] ITEQ, "Multifunctional Filled Epoxy Resin and Phenolic-Cured Lead Free Laminate & Prepreg," 2012. [Online]. Available: http://www.eurotronics.be/documents/Iteq_IT_158_data_sheet.pdf.

[Accessed February 2019].

[45] ITU, "Recommendation X.200: Information technology - Open Systems Interconnection - Basic Reference Model: The basic model," July 1994. [Online]. Available: https://www.itu.int/rec/T-REC-X.200-199407-I. [Accessed February 2019].

[46] M. Schwartz, W. R. Bennett and S. Stein, Communication Systems and Techniques, Hoboken, NJ, USA: Wiley, 1995.

[47] T. Lassen, "Long-range RF communication: Why narrowband is the de facto standard.," Texas Instruments, White Paper SWRY006, Dallas, TX, USA, 2014.

[48] J. R. Carson, "Notes on the theory of modulation," *Proceedings of the institute of radio engineers,* vol. 10, no. 1, pp. 57-64, 1922.

[49] E. McCune, Practical Digital Wireless Signals, Cambridge, UK.: Cambridge University Press, 2010.

[50] J. Dunlop and D. G. Smith, Telecommunications Engineering, 3rd edition, Boca Raton, FL, USA: CRC Press, 1994.

[51] Semtech Corporation, "Semtech SX1272/73 Transceiver Data Sheet," January 2019. [Online]. Available: https://www.semtech.com/uploads/documents/SX1272_DS_V4.pdf. [Accessed April 2019].

[52] EnOcean GmbH, "EnOcean Radio Protocol 2 (ERP2)," September 2013. [Online]. Available: https://www.enocean.com/fileadmin/redaktion/pdf/tec_docs/EnOceanRadioProtocol2.pdf. [Accessed March 2019].

[53] Y.-L. Foo and H. Morikawa, "On the use of manchester violation test in detecting collision," in *International Conference on Information Networking (ICOIN 2007)*, Estoril, Portugal, 2007.

[54] National Instruments, "LabVIEW 2018 Help," March 2018. [Online]. Available: http://zone.ni.com/reference/en-XX/help/371361R-01/lvanls/autocorrelation/. [Accessed February 2019].

[55] Texas Instruments, "CC13x0 Proprietary RF User's Guide," 2016. [Online]. Available: http://dev.ti.com/tirex/content/simplelink_cc13x0_sdk_1_00_00_13/docs/proprietary-rf/html/rf-proprietary/packet-format.html#preamble. [Accessed April 2019].

[56] T. v. D. a. K. G. Langendoen, "An adaptive energy-efficient MAC protocol for wireless

sensor networks," in *1st international conference on Embedded networked sensor systems*, New York, NY, USA, 2003.

[57] ETSI, "European Standard EN 300 220-1, Part 1: Technical Characteristics and Methods of Measurement," ETSI, February 2017.

[58] EnOcean Alliance, "Generic Profiles Version 1.0," EnOcean Alliance, San Ramon, CA, USA, 2013.

[59] ITU-T, " B-ISDN User-Network Interface—Physical Layer Specification: General Characteristics, document ITU-T I.432.1," 1999.

[60] EnOcean GmbH, "EnOcean Radio Protocol 1 (ERP1)," September 2013. [Online]. Available:

https://www.enocean.com/fileadmin/redaktion/pdf/tec_docs/EnOceanRadioProtocol1.pdf. [Accessed March 2019].

[61] "SLAU367F, MSP430FR59xx Family User's Guide," October 2012. [Online]. Available: http://www.ti.com/lit/ug/slau367o/slau367o.pdf. [Accessed February 2019].

BIOGRAPHY

Dalibor Purkovic was born in Doboj, Bosnia and Herzegovina, in 1986. He finished primary school and Electrotechnical secondary school in Bjelovar, Croatia.

He received the B.S. and M.S. degrees in electrical engineering and information technology from the Faculty of Electrical Engineering and Computing, University of Zagreb, Zagreb, Croatia, in 2008 and 2010, respectively, where he is currently pursuing a part-time Ph.D. degree in electrical engineering with the Department of Wireless Communications.

From 2010 to 2014, he was a Research Assistant and a Lecturer in Electrical and Electronic engineering at the study program Mechatronics with the Technical College in Bjelovar, Bjelovar, Croatia. Since 2014, he has been a Hardware Engineer and a Project Lead with the R&D Department, EnOcean GmbH, Oberhaching, Germany.

He has authored several papers in international journals and three conference proceedings. His research interests include energy harvesting sensor systems, low power microcontrollers and RF chips, sensor development, and efficient wireless data transfers over greater distances. He speaks fluent English and German language.

PUBLICATIONS

Peer-reviewed journal articles:

1. D. Purkovic, M. Hönsch and T. R. M. K. Meyer, "An Energy Efficient Communication Protocol for Low Power, Energy Harvesting Sensor Modules," in *IEEE Sensors Journal*, vol. 19, no. 2, pp. 701-714, 15 Jan.15, 2019.
   doi: 10.1109/JSEN.2018.2876746

2. I. Petrović; D. Purković and N. Maleš, "The Comparison of the Measured Clearness Index for Different Locations in the Moderate Continental Climate Region," in Przeglad Elektrotechniczny, vol. 14, no. 3, pp. 128-131, 3/2014; 2014.
   doi: 10.12915/pe.2014.03.27

Conference papers:

1. D. Purkovic, L. Coates, M. Hönsch, D. Lumbeck and F. Schmidt, "Smart river monitoring and early flood detection system in Japan developed with the EnOcean

long range sensor technology," SMAGRIMET 2019 - Second International Colloquium on Smart Grid Metrology, Split, Croatia, April 9-12, 2019, pp. 78-93, ISBN: 978-953-184-245-7

2. D. Purković and Z. Šipuš, "Using RFID technology for sensor purposes," ICECom 2013 – 21st International Conference on Applied Electromagnetics and Communications, Dubrovnik, Croatia, October 14-16, 2013, pp. 1-5, doi: 10.1109/ICECom.2013.6684755

Book chapters:

1. D. Purkovic, "Supercapacitors as Guarantors for Energy Sustainability in Low-Power Energy Harvesting Sensor Modules," IntechOpen, 2019, doi: 10.5772/intechopen.88007

ŽIVOTOPIS

Dalibor Purković rođen je u Doboju u Bosni i Hercegovini, 1986. godine. Osnovnu i srednju Elektrotehničku školu završio je u Bjelovaru u Hrvatskoj.

Diplomu sveučilišnog prvostupnika (baccalaureus) te magistra inženjera Elektrotehnike i informacijske tehnologije stekao je na Fakultetu elektrotehnike računarstva u Zagrebu, 2008., odnosno 2010. godine. Na istom fakultetu, na Zavodu za Radiokomunikacije, trenutno privodi kraju doktorski studij.

Od 2010. do 2014. godine radio je na Visokoj tehničkoj školi u Bjelovaru (danas Veleučilište u Bjelovaru) na studiju Mehatronike, prvo kao asistent, a potom i kao predavač za područje tehničkih znanosti, grana Elektronika.

Od 2014. godine radi kao hardvere inženjer i voditelj projekata u odjelu za istraživanje i razvoj u firmi EnOcean GmbH, iz Oberhachinga u Bavarskoj, Njemačka.

Autor je i koautor više članaka objavljenih u međunarodnim i domaćim časopisima te je prezentirao radove na tri međunarodne konferencije.

Područje interesa su mu senzorski sustavi s mogućnošću „žetve" energije, mikrokontroleri i radio čipovi niske potrošnje energije, razvoj senzora, te općenito senzorski sustavi za bežični prijenos informacija na veće udaljenosti. Govori tečno engleski i njemački jezik.